THE UNIVERSITY OF HULL

PORPHYRIN-NANOSENSOR CONJUGATES: NOVEL TOOLS FOR THE STUDY OF CELLULAR RESPONSE TO OXIDATIVE STRESS

being a Thesis submitted for the Degree of Doctor of Philosophy

in the University of Hull

by

Leanne B. Josefsen, MChem (Hons)

May 2007

ACKNOWLEDGEMENTS

I would like to thank my supervisor Dr. Ross W. Boyle for his support and valued guidance over the past three years. Special gratitude goes to Prof. Chris Peers, Drs. John Boyle and Andy Beeby for their advice and collaborative efforts and to Philip Warburton for his technical assistance. I thank Dr. Jonathan W. Aylott for his input in the design and preliminary investigations into the Project.

Finally, I would like to thank my family and close friends to whom I am indebted: for without their continued patience and support (emotional and financial) over the past seven years the completion of this Thesis would not have been possible. I couldn't have done it without you, many thanks - *a posse ad esse!*

ABSTRACT

The cellular environment is heterogeneous in nature and home to a multitude of species and reactions. If the labyrinth behind these reactions and signaling pathways (along with those leading to cell death) can be decoded it may be possible to identify mal-functioning and apoptotic signaling pathways. The particular interest for this Project is the correlation between reactive oxygen species (ROS) and altered calcium homeostasis. Oxidative stress has been linked to a number of disease states, including heart and Alzheimer's disease; although the exact mechanism(s) of induction are not fully understood. If the relationship between ROS and calcium perturbations can be elucidated further there is the potential to unravel disease "fingerprints".

Conventional spectroscopic techniques have over the years provided insight into intracellular signaling events. However, limitations have been encountered with their toxicity and the difficulties associated with controlling their sub-cellular localisation and relative concentrations at these sites. Therefore, the aim is to create a more reliable tool which is capable of observing/monitoring a biologically relevant intracellular species; more specifically, tracking the intracellular response to oxidative stress *via* luminescent detection of the major signaling ion calcium.

The strategy for achieving such a system/tool is based on the hybridisation of photosensitiser chemistry and polymeric nanoscience. A major advantage of this type of system/tool is the entrapment of a fluorescence species within an inert matrix of low toxicity and the *in situ* generation of ROS.

The nanosensing component of the target system was successfully afforded by a free-radical emulsion polymerisation technique and conjugated (*via* a thiourea bond) to a water-soluble porphyrin. The ability of the target system to generate ROS and any transfer of energy between the two component chromophores was evaluated *via* time-correlated single photon counting (TCSPC). The potential of the system/tool to effect

oxidative stress and chelate free intracellular calcium ions was assessed in human neuroblastoma and human embryonic cell-lines.

Findings from the investigations suggested that the target porphyrin-nanosensor system is capable of generating singlet oxygen (in solution) and detecting free calcium ions (in solution and *in vitro*).

SYMBOLS AND ABBREVIATIONS

$^1O_2$	Singlet Oxygen
$^3O_2$	Molecular Oxygen
γ	Interfacial Tension
$^1\Delta_g$	Lowest Energy-State of Singlet Oxygen
$^1\Sigma_g$	Highest Energy-State of Singlet Oxygen
$^3\Sigma_g$	Ground State Molecular Oxygen
$\Delta\Psi_m$	Mitochondrial Transmembrane Potential
$\lambda_{max.}$	Maximal Absorption
τ	Luminescence Lifetime
Φ	Quantum Yield
ADAPT	Antibody Directed Abzyme Prodrug Therapy
ADC	Analogue to Digital Converter
ADEPT	Antibody Directed Enzyme Prodrug Therapy
ADP	Adenosine Diphosphate
AFM	Atomic Force Microscopy
AIBN	Azoisobutylnitride
AIDS	Acquired Immune Deficiency Syndrome
AIF	Apoptosis Inducing Factor
ANT	Inner Membrane Adenylate Translocator
AOT	Sodium Bis-(2-ethylhexyl) Sulfosuccinate
Apaf-1	Cytosolic Apoptotic Protease Activating Factor-1
APS	Ammonium Persulphate
ATP	Adenosine Triphosphate
BODIPY	4,4-Difluoro-4-bors-3a,4a-diaza-*s*-indacence
Brij 30	Polyethylene Glycol Dodecyl Ether
BSA	Bovine Serum Albumin
cADPR	Cyclic ADP Ribose
CD95	Cell Surface Receptor (Fas)
CI	Configurational Interaction

CLSM	Confocal Laser Scanning Microscopy
c.m.c	Critical Micelle Concentration
COSY	Correlation Spectroscopy
D_2O	Deuterated Water
DCTB	T-2-(3-(4-t-butyl-phenyl)-2-methyl-2-propenylidene)-Malononitrile
DDAB	Dimethyldioctadecylammonium Bromide
DEPT	Distortionless Enhancement by Polarisation Transfer
DLS	Dynamic Light Scattering
DMF	Dimethylformamide
DMSO	Dimethylsulphoxide
DNA	Deoxyribonucleic Acid
E. coli	*Escherichia coli*
EDTA	Ethylenediaminetetra-acetic Acid
em.	Emission
ER	Endoplasmic Reticulum
E_T	Energy Transfer
ex.	Excitation
Fas-L	Fas Ligand
FDA	Food and Drug Administration
FITC	Fluorescein Isothiocyanate
Fl.	Fluorescence
FRET	Förster/Fluorescence Resonance Energy Transfer
GDEPT	Gene Directed Enzyme Prodrug Therapy
HEK	Human Embryonic Kidney Cells
HpD	Haematoporphyrin Derivative
HPLC	High Performance Liquid Chromatography
i	Intracellular
IC	Internal Conversion
IP_3	Inositol-1,4,5-triphosphate
ISC	Intersystem Crossing
K_d	Affinity Constant

LDL	Low Density Lipoprotein
LED	Light Emitting Diode
MALDI	Matrix Assisted Laser Desorption Ionisation
MCU	Mitochondrial Calcium Uniporter
MeOD	Deuterated Methanol
MMP	Mitochondrial Membrane Permeability
MRI	Magnetic Resonance Imaging
NCE	Sodium-Calcium Exchanger
Nd:YAG	Neodymium-Doped Yttrium Aluminum Garnet
NHS	N-hydroxysuccinimide
NMR	Nuclear Magnetic Resonance
NOSEY	Nuclear Overhauser Enhancement Spectroscopy
nr	Non-radiative
o/w	Oil-in-water
OMM	Outer Mitochondrial Membrane
ORMOSIL	Organically Modified Silica
oxi.	Oxidised
P	Phosphorescence
PC	Personal Computer
PCS	Photocorrelation Spectroscopy
PDMA	Polydecylmethacrylate
PDT	Photodynamic Therapy
PEG	Polyethylene Glycol
PET	Positron Emission Tomography
PMCA	Plasma Membrane ATPases
PMT	Photomultiplier Tube
POE	Polyoxyethyl Alcohol
ppm	Parts Per Million
Psen	Photosensitiser
PTH	Parathyroid Hormone
QELS	Quasi-Elastic Light Scattering

r	Radiative
R_f	Retention Factor
RDS	Rate Determining Step
RES	Reticuloendothelial Uptake System
R_h	Hydrodynamic Radius
ROS	Reactive Oxygen Species
rpm	Revolutions Per Minute
S	Singlet
SDS	Sodium Dodecylsulphate
SEM	Scanning Electron Microscope
SERCA	Sarcoplasmic/Endoplasmic Calcium-ATPases
SHSY5Y	Human Neuroblastoma Cell-Line
SPCA	Secretory Pathway ATPases
Subs	Substrate
T	Triplet
TAT	Tyrosine Aminotransferase
TCSPC	Time-Correlated Single Photon Counting
TDP	1,1'-Thiocarbonyldi-2,2'-pyridone
TEM	Transmission Electron Microscope
TEMED	*N,N,N',N'*-Tetramethylethane-1,2-diamine
Tim	Inner Mitochondrial Membrane Protein Transporter
TLC	Thin Layer Chromatography
TMS	Tetramethylsilane
TNF	Tumour Necrosis Factor
Tom	Outer Mitochondrial Membrane Protein Transporter
TPP	Tetraphenylporphyrin
t_R	Retention Time
TRP	Transient Receptor Channels
UPR	Unfolded Protein Response Pathway
UV-vis.	Ultra-violet Visible
VDAC	Voltage Dependent Anion Channel

VOCC	Voltage-Operated Calcium Channel
w/o	Water-in-oil
w/o/o	Water-in-oil-in-oil
w/o/w	Water-in-oil-in-water
$z_{ave.}$	Average Size (Nanospecies)

CONTENTS

CHAPTER 1 INTRODUCTION

1.1 PORPHYRINS

1.1.1 Porphyrin Structure

Porphyrins are a group of naturally occurring and intensely coloured compounds, whose name is drawn from the Greek word *porphura*, the Greek for purple.[1,2] These molecules are known to be involved in a number of biologically important roles, including oxygen transport and photosynthesis, and have applications in a number of fields, ranging from fluorescence imaging to medicine.[3,4,5,6] Porphyrins are classified as tetrapyrrolic molecules with the heart of the skeleton a heterocyclic macrocycle, known as a porphine. The fundamental porphine frame consists of four pyrrolic sub-units linked on opposing sides (α-positions, numbered 1, 4, 6, 9, 11, 14, 16 and 19, figure 1) through four methine (CH) bridges (5, 10, 15 and 20), known as the *meso* carbon atoms/positions (figure 1). The resulting conjugated planar macrocycle may be substituted at the *meso* and/or *β*-positions (2, 3, 7, 8, 12, 13, 17 and 18); if a single hydrogen atom is attached to each of the *meso* and *β*-carbons and two of the inner nitrogen atoms (pyrrolenines) are protonated, the compound becomes known as a free-base porphine. If, on the other hand, the *meso* and *β*-hydrogens are substituted with non-hydrogen atoms or groups, the resulting compounds are known as porphyrins.

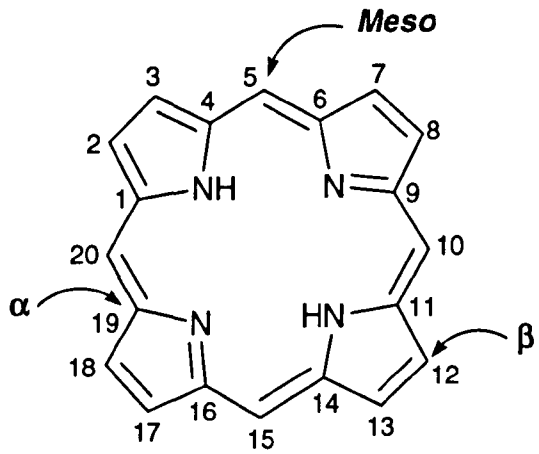

Figure 1 – Porphine Macrocycle

1.1.2 Porphyrin Aromaticity

The porphyrin macrocycle is an aromatic system with 22 π–electrons obeying Hückels rule of aromaticity ((4n + 2) π-electrons, where n = 5). The π–electrons delocalise over the macrocycle forming the π–electron "clouds" present above and below the plane of the skeleton. A number of closed conjugated pathways may be drawn for the free-base porphyrin shell, suggesting two main delocalisation pathways consisting of 16 or 18 carbon/nitrogen atoms. Studies undertaken (X-ray crystallographic data and theoretical calculations) propose that the delocalisation pathway in **free-base** porphyrins is actually composed of **18 atoms**, with a smaller **16 atom** pathway identified in **metalloporphyrins** (bold lines, figure 2).[2,5,7,8,9] However, it is known that the highest degree of bond length equalisation is achieved through those pathways exhibiting the greatest degree of conjugation and that the steric effect of the inner hydrogen atoms (of free-base porphyrins), responsible for forcing the inner protons out of the plane of the macrocycle, contributes to the disfavoured involvement of the non-bonding pyrrolenine electrons in the conjugation pathway present in the system; thus, the less symmetric aromatic pathway of 18 π-atoms is favoured.[7]

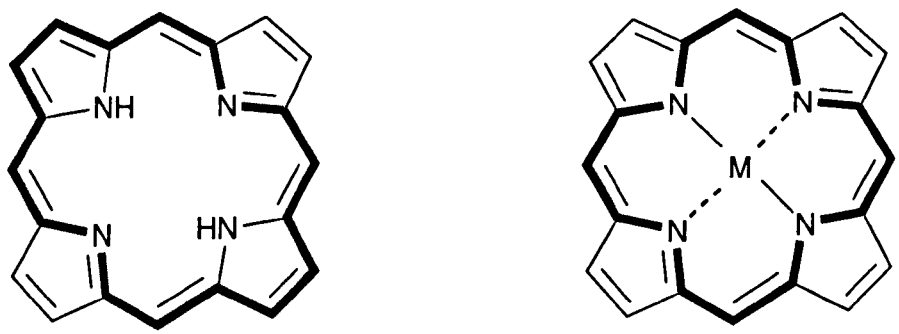

Figure 2 – 18 and 16 Atom Porphyrin Delocalisation Pathways

1.1.3 Porphyrin Spectroscopy

The aromaticity of porphyrin molecules has been directly observed through visible and nuclear magnetic resonance (NMR) spectroscopy, with the planarity of free-base porphyrins demonstrated by X-ray crystallography.[2,5,8,10] It is this planarity which allows efficient overlap between the macrocycle's *p* orbitals; a prerequisite for a molecule to be aromatic.

1.1.3.1 Porphyrin NMR Spectroscopy

In an external magnetic field the delocalised porphyrin π-electrons rotate around the macrocyclic skeleton generating a diamagnetic ring current. Diamagnetism is the result of changes in the orbital motion of electrons when a substance is subject to an externally applied magnetic field. This ring current in turn creates an induced magnetic field which strongly opposes the applied field within the macrocycle, whilst simultaneously assisting the applied field outside the macrocycle (figure 3).

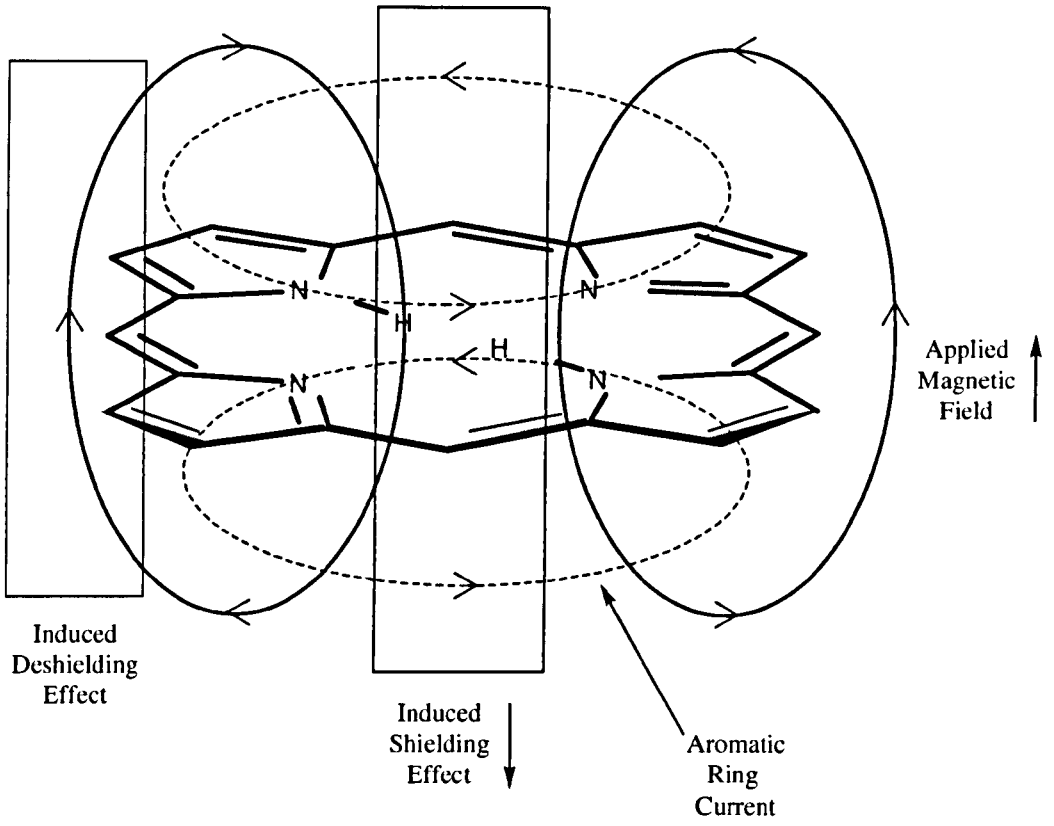

Figure 3 – Aromatic Shielding Effect

The most notable feature of a free base porphyrin proton NMR (^{1}H NMR) spectrum is the presence of a signal with a **negative** chemical shift relative to a zero standard (figure 4). A peak at around – 2 parts per million (ppm) should be always observed and represents the two highly shielded inner macrocyclic protons. These protons are bonded to the inner pyrrolic nitrogens and are effectively **shielded** by the powerful aromatic ring current present in the system; a result of π-electron delocalisation observed in the macrocycle. A second distinctive feature of the spectrum is the striking **low field** proton signals present at around 9 and 10 ppm; these are a result of the diamagnetic ring current **deshielding** the external β and *meso*-protons. The *meso*-protons are affected to an even greater extent than the β-protons and are consequently observed to resonate at values further downfield than 9 ppm.

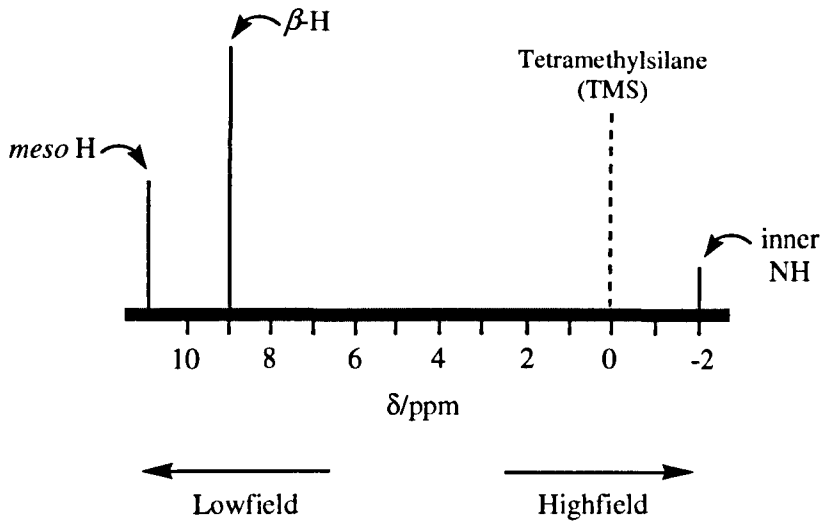

Figure 4 – Simplified Porphyrin ^{1}H NMR Spectrum

1.1.3.2 Ultra-Violet Visible Spectroscopy

On account of their highly conjugated skeleton, porphyrins have a characteristic ultra-violet visible (uv-vis.) spectrum (figure 5). The spectrum typically consists of an intense, narrow absorption band ($\varepsilon > 200{,}000$ l mol^{-1} cm^{-1}) at around 400 nm, known as the Soret or B band, followed by four longer wavelength (450 - 700 nm), weaker absorptions ($\varepsilon >$ 20,000 l mol^{-1} cm^{-1} (free-base porphyrins)) referred to as the Q bands.[1,5,7,11,12]

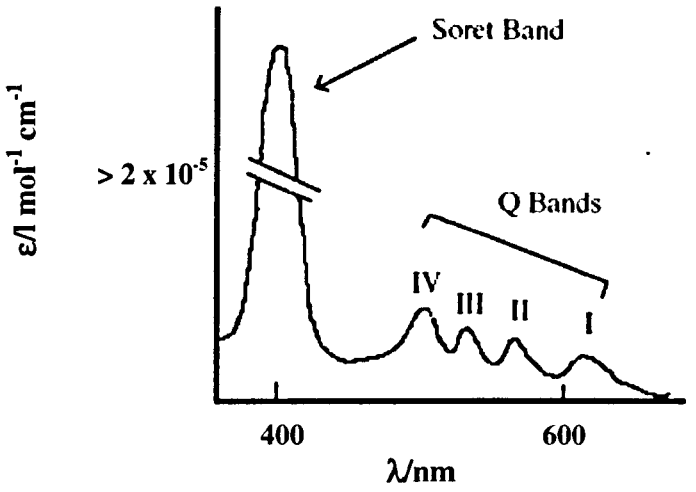

Figure 5 – Typical Porphyrin Absorption Spectrum[10(modified)]

The Soret band arises from a **strong** electronic transition from the (porphyrin) ground state to the second excited singlet state ($S_0 \rightarrow S_2$, figure 6), whereas the Q band is a result of a **weak** transition to the first excited singlet state ($S_0 \rightarrow S_1$). The dissipation of energy *via* internal conversion (IC, see section 1.1.6) is so rapid that fluorescence is only observed from depopulation of the first excited singlet state to the lower-energy ground state ($S_1 \rightarrow S_0$).

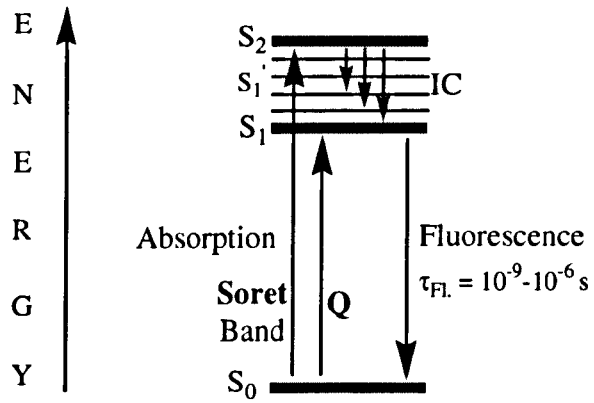

Figure 6 – Modified Jablonski Energy Diagram

The energy gap separating the Q band absorptions allows the Q bands to be attributed to different vibrational components of the same electronic transition, for example Q_y (0 – 0) and Q_x (0 – 1), with Q_x and Q_y denoting the electronic transition where the (transition) dipole lies along the *x* or *y* molecular axis (figure 7). The transition dipole moments experienced by free base porphyrins in the *x* and *y* directions are different, whereas, those present in more symmetric porphyrins (for example, porphyrins where the inner two nitrogens (bearing lone pairs of electrons) are protonated or where a metal is inserted into the macrocycle cavity) are identical (figure 7). Hence, the dipole transitions in more symmetric porphyrins have the same energy and consequently overlap; thus, reducing the number of Q bands and the intensity of the Soret band observed on a porphyrin absorption spectrum.[1,7] Variation of the peripheral substituents on the porphyrin macrocycle also often results in minor changes in the relative intensities and positions at which these absorptions occur.[2,3,7,8,10]

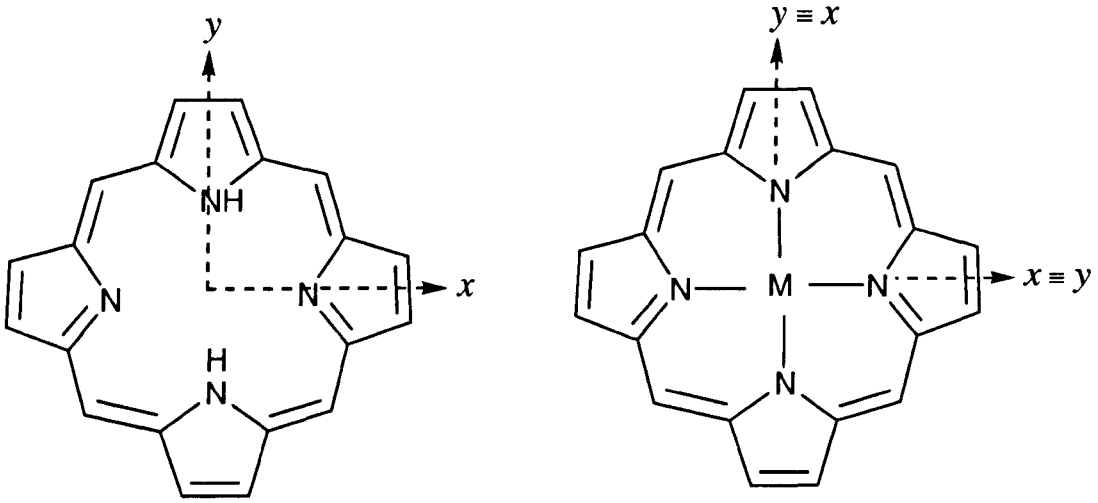

Figure 7 – Porphyrin Symmetry

1.1.3.2.1 Gouterman Four-Orbital Theory

The π to π* transitions giving rise to the Soret and Q bands may be further explained by considering the four frontier orbitals of the porphyrin macrocycle (Gouterman four orbital model): the two π-orbitals (a_{1u}/b_1 and a_{2u}/b_2) and the degenerate pair of π*-orbitals

(e_{gx}/c_1 and e_{gy}/c_2). Although the two highest occupied π-orbitals (c_1 and c_2) have almost equal energies this does not transfer/lead to almost coincidental Q bands. Instead the two transitions ($b_1 \rightarrow c_1$ and $b_2 \rightarrow c_2$) are mixed together (figure 8) *via* configurational interaction (CI), giving rise to two sets of absorption bands of different intensities and wavelengths; the Soret and Q bands. The lower wavelength, more intense Soret band, is a result of constructive interference, with the less intense longer wavelength Q bands a result of destructive combinations (figure 8). Since free-base porphyrins are not symmetric and the *x* and *y* axis (dipole transitions) are perpendicular to one another, each component (*x* and *y*) has two associated transitions, *i.e.* for a free-base porphyrin four Q bands can be observed on its characteristic absorption spectrum. Alternatively, porphyrins with increased symmetry, such as metalloporphyrins, have b_1/b_2 levels of almost equal energies and therefore only two Q bands are present on their absorption spectra.[1,2,7,13]

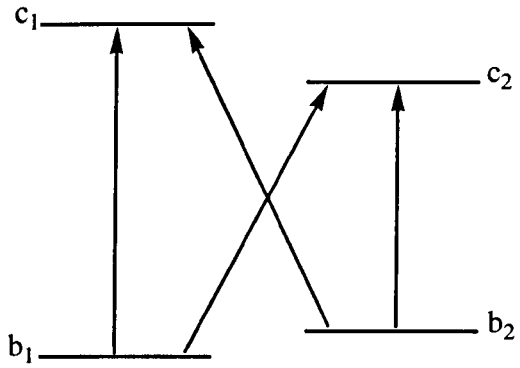

Figure 8 – Simplified Gouterman Diagram of the Four Orbital Model

Porphyrin macrocycles are known to be highly stable towards concentrated acids, such as sulphuric acid and are known to act as both acids and bases. The inner two protons of a free-base porphyrin can be removed by strong bases like alkoxides, forming a dianionic molecule; conversely, the inner two pyrrolenine nitrogens can be protonated with acids such as trifluoroacetic acid affording a cationic intermediate (figure 9).[5] Porphyrins are also known to have good thermal stability, with decomposition occurring above 300°C.

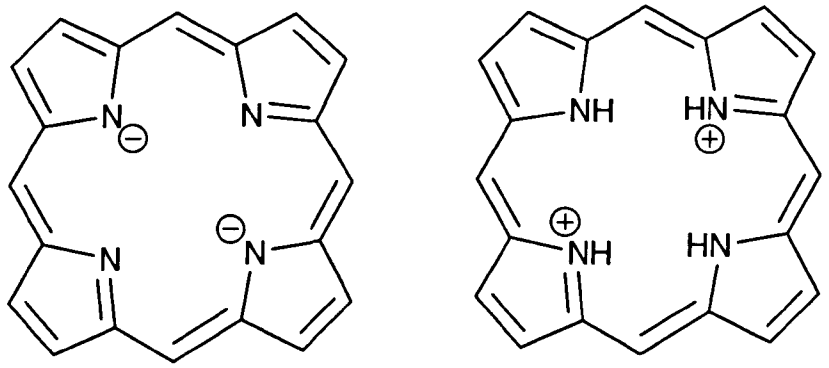

Figure 9 – Porphyrin Dianionic and Dicationic Species

1.1.4 Porphyrin Synthesis I

There are two general approaches used to achieve the porphyrin macrocycle of choice:-

- Modification of naturally occurring porphyrins, for example haem, and
- Total (direct) synthesis.

There are however, a number of limitations in modifying the peripheral substituents of naturally occurring porphyrins, sometimes making the total synthesis methodology more advantageous. It is therefore the latter method which will be covered in more detail in the following discussion.

1.1.4.1 Total Synthesis

Two of the more common total synthesis methods include (i) refluxing pyrrole sub-units (bearing the substituents of choice) with an aldehyde in propionic acid for half an hour, open to the air, followed by chromatographic purification (Rothemund or Adler synthesis, route A, yields ≤20%, scheme 1, see section 1.1.13); and (ii) reacting pyrrole with an aldehyde under acid catalysis at room temperature (under inert conditions), followed by addition of a chemical oxidant and then chromatographic purification to

afford the desired porphyrin in yields of 30-40% (Lindsey synthesis, route **B**, scheme 1, see section 1.1.13).[2,8,14,15,16,17]

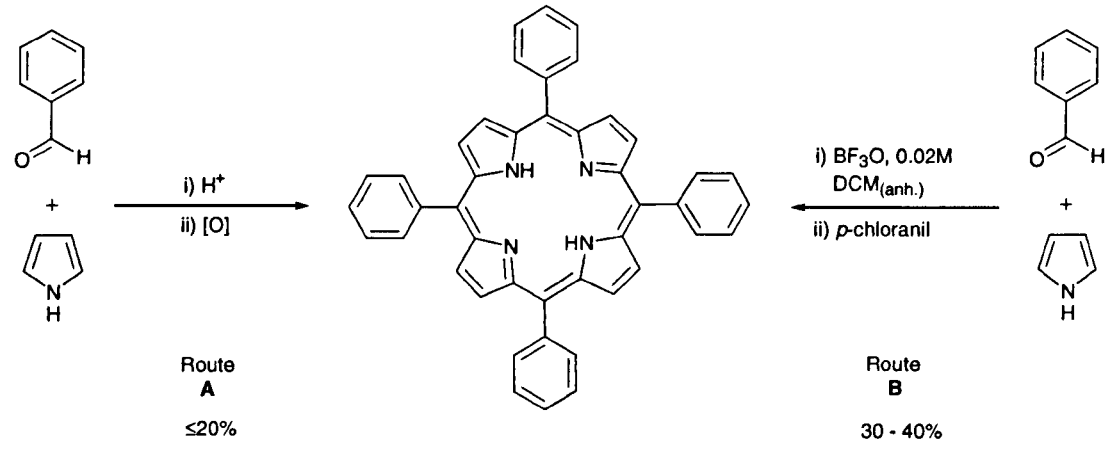

Scheme 1 – Total Synthesis of Tetraphenyl Porphyrin (TPP)

Porphyrins may also be synthesised from dipyrromethanes, dipyrromethenes or dipyrrylketones (figure 10) by the condensation of two dipyrrolic intermediates. These types of reactions are more commonly known as "2+2" condensations (MacDonald synthesis, see section 1.1.13).[2,8,15]

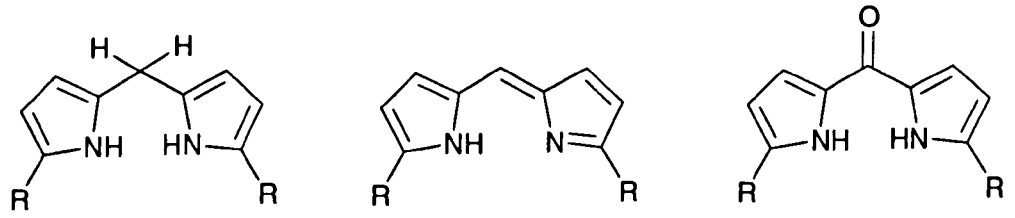

Figure 10 – Structures of Dipyrromethanes, Dipyrromethenes and Dipyrrylketones

1.1.4.2 Porphyrin Reactions

Porphyrins can undergo a number of chemical reactions typical of aromatic compounds, including electrophilic substitution at the *meso* and *β*-pyrrolic carbon positions.[5] For example, in porphyrin chemistry halogens, such as chlorine and bromine, do not simply add across the double bonds (as one would expect in olefins) but instead displace one of the "*-ene*" hydrogen atoms to give a substituted porphyrin (scheme 2).[2]

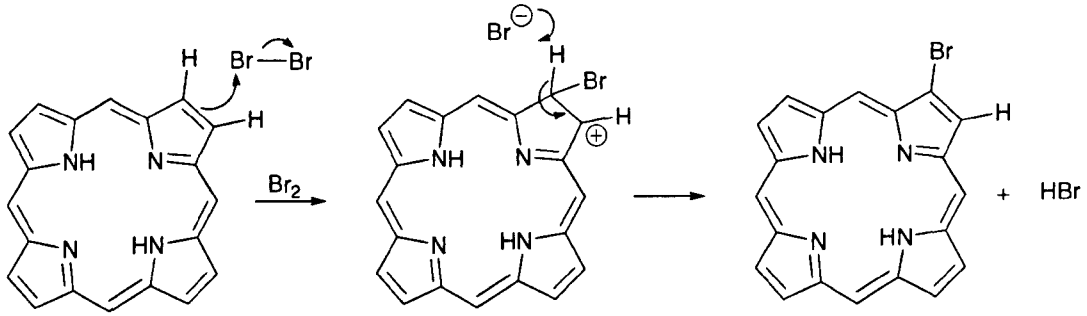

Scheme 2 – Bromination of a Porphyrin

Porphyrins also hold the ability to be metallated and demetallated by the coordination or removal of an appropriate metal ion into the central porphyrin cavity (~ 4.02 Å) using metal salts (metallation) or by applying acids of various strengths to the complex (demetallation, figure 11).[5,18] The most commonly used metals include zinc, palladium, copper, nickel and iron, and it is these brightly coloured compounds which constitute the active sites of some key biological processes.

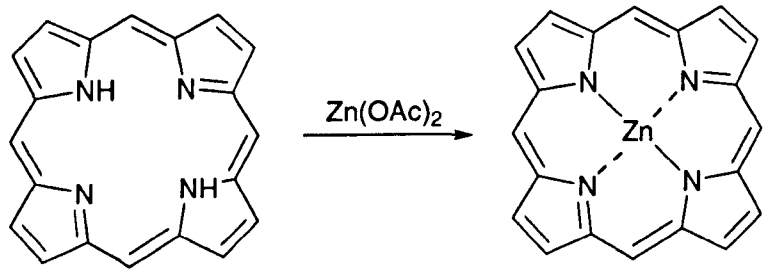

Figure 11 – Porphyrin Metallation

For instance, chlorophyll (the green pigments involved in photosynthesis work by absorbing light energy and transforming it into chemical energy) are an example of a magnesium-metallated reduced porphyrin (figure 12); conversely, haem is an iron-containing porphyrin associated with the transport and storage of oxygen in the bloodstream.[2,7,9]

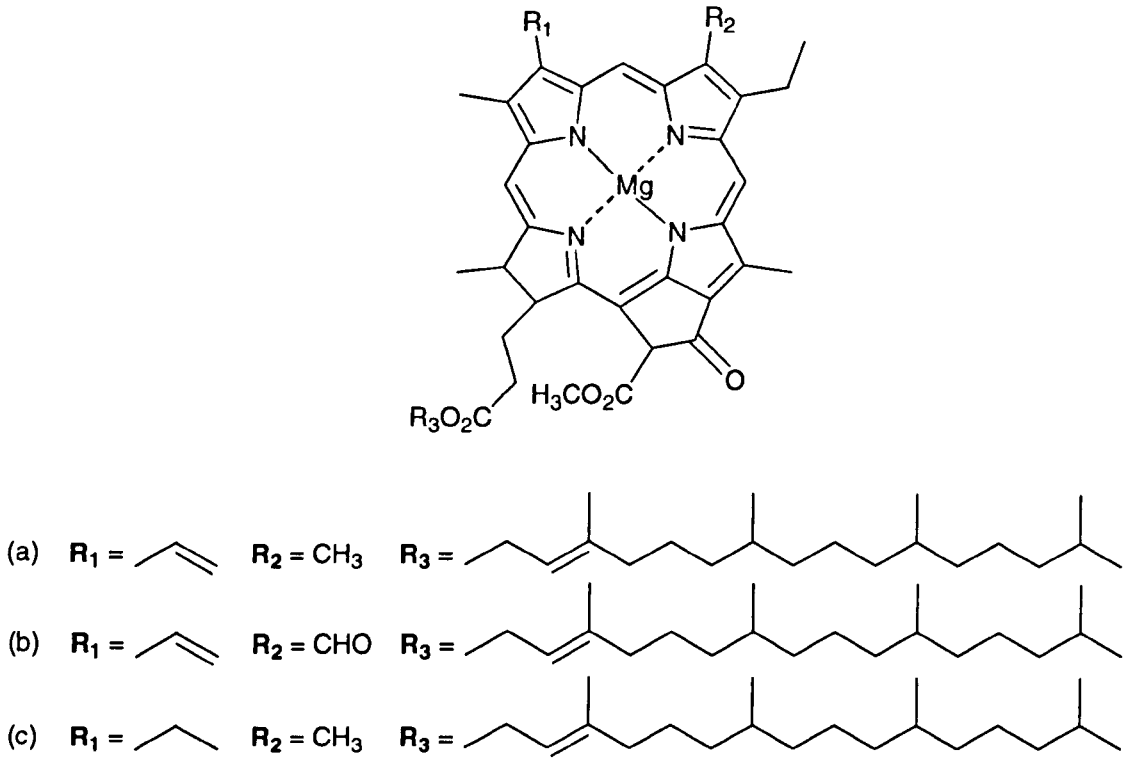

Figure 12 – Chlorophyll *a* (a), *b* (b) and *c* (c)

1.1.5 Porphyrin Chromophores and Photosensitisers

Porphyrin molecules are good examples of fluorophores and photosensitisers. A fluorophore is generally a molecule capable of absorbing light energy when irradiated at a specific wavelength and emitting the energy at longer wavelengths. A photosensitiser is a molecule, which when excited by light energy (and in the presence of molecular oxygen) can utilise the energy to induce photochemical reactions producing lethal cytotoxic agents; these ultimately result in cell death and tissue destruction (figure 13 and see section 1.1.6).[4,5,19] Photosensitisers are absorbed into cells all over the body and alone

are harmless, *i.e.* in the absence of light and oxygen they have no effect on healthy or abnormal tissue, it is only when they become activated that they have the toxic effect. Ideally, they should be retained by diseased tissue, particularly tumour neo-vasculature, for longer periods of time in comparison to healthy tissue; thus, it is important to carefully time light exposure and ensure that activation only occurs once the ratio of photosensitiser in diseased tissue is greater than that present in healthy tissue; thereby minimising unwanted healthy cell damage.[20,21]

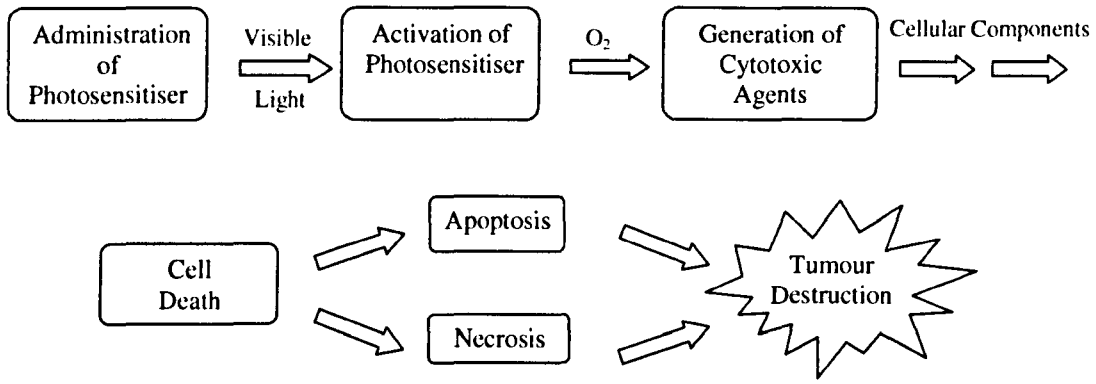

Figure 13 – Porphyrin Initiated Cell Death

It is worthy to note that photosensitisers also have alternative applications. They have been employed in the sterilisation of blood plasma and water in order to remove blood-borne viruses and microbes and have been considered for agricultural uses, including herbicides and insecticides.[4,22,23]

1.1.5.1 Photochemical Processes

Only when a porphyrin is in its excited state ($^3Psen^*$) can it interact with molecular oxygen ($^3O_2$) to produce reactive oxygen species (ROS). The reactive species included singlet oxygen ($^1O_2$), hydroxyl radicals ($^{\bullet}OH$) and superoxide (O_2^{-}). These toxic species interact with cellular components including, unsaturated lipids; amino acid residues and nucleic acids; with ensuing oxidative damage potentially resulting in apoptotic or

necrotic forms of death in the target cells (only within the immediate area of light illumination, see section 1.1.6).

1.1.6 Photochemistry

1.1.6.1 Photochemical Mechanisms

When a chromophore, such as porphyrin molecule, absorbs a photon of electromagnetic radiation in the form of light energy, an electron is promoted into a higher-energy molecular orbital; hence, the chromophore is elevated from the ground state (S_0) into a short-lived, electronically excited state (S_n) composed of a number of vibrational sub-levels (S_n'). The excited chromophore can lose energy by rapidly decaying through these sub-levels *via* internal conversion (IC) to populate the first excited singlet state (S_1), before quickly relaxing back to the ground state (figure 14).

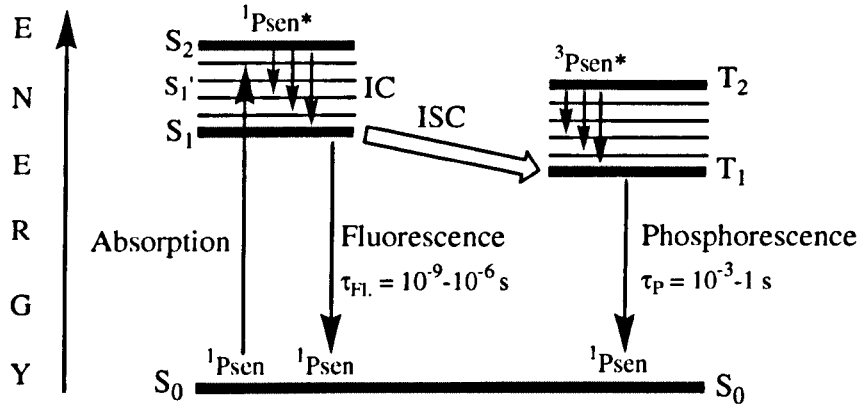

Figure 14 – Modified Jablonski Energy Diagram

The excited electron can depopulate the excited singlet state (S_1) and return back to the ground state (S_0) by losing the absorbed energy *via* **fluorescence ($S_1 \rightarrow S_0$)**. Singlet state lifetimes of excited fluorophores are very short ($\tau_{fl.} = 10^{-9} - 10^{-6}$ seconds) since transitions between the same spin states (S $\rightarrow$ S or T $\rightarrow$ T) conserve the spin multiplicity (spin) of the electron and are considered "allowed" transitions according to the Spin

Selection Rules.[21,24] Alternatively, an excited singlet state electron (S_1) can undergo spin inversion and populate the lower-energy first excited triplet state (T_1) *via* intersystem crossing (ISC), a spin-forbidden process, since the spin of the electron is no longer conserved.[25-28] The excited electron can then undergo a second spin-forbidden inversion and depopulate the excited triplet state (T_1) by decaying back to the ground state (S_0) *via* **phosphorescence ($T_1 \rightarrow S_0$).**[25-28] Owing to the spin-forbidden triplet to singlet transition, the lifetime of phosphorescence ($\tau_P = 10^{-3} - 1$ second) is considerably longer than that of fluorescence.

1.1.6.2 Photosensitisers and Photochemistry

Excited state porphyrins ($^1Psen^*$, $S_{>0}$ or $^3Psen^*$, $T_{>0}$) are relatively efficient at undergoing intersystem crossing and can have a high triplet-state (quantum) yield (Φ_T 0.62 (tetraphenylporphyrin (TPP), methanol), 0.75 (TPP, liposome, D_2O) and 0.71 (tetrasulphonated TPP, D_2O).[24,29,30] This longer lifetime is sufficient to allow the excited triplet state photosensitiser to interact with surrounding bio-molecules, including cell membrane constituents (see below).[4,5]

Excited triplet-state photosensitisers can react in two ways defined as Type I and Type II processes. Type I processes involve the excited triplet photosensitiser ($^3Psen^*$, T_1) interacting with readily oxidisable or reducable substrates; whereas, Type II processes involve the interaction of the excited triplet photosensitiser ($^3Psen^*$, T_1) with molecular oxygen ($^3O_2$, $^3\Sigma_g$).[4,5,9,12,20,21,21-33]

Type I processes can be divided into two further mechanisms; Type I (i) and Type I (ii). The first of these mechanisms (i) involves the transfer of an electron (oxidation) from a substrate molecule to the excited triplet state photosensitiser ($^3Psen^*$), generating a photosensitiser radical anion ($^3Psen^{\bullet-}$) and a substrate radical cation ($Subs^{\bullet+}$). The photosensitiser radical anion can react instantaneously with molecular oxygen ($^3O_2$) to generate a superoxide radical anion ($O_2^{\bullet-}$), which can go on to produce the highly

reactive hydroxyl radical ($OH^{\bullet}$, figure 15), initiating a cascade of cytotoxic free radicals; common in the oxidative damage of fatty acids and other lipids.[5,9]

$$^{3}Psen^{*} + Subs \rightarrow {}^{3}Psen^{\bullet-} + Subs^{\bullet+}{}_{oxi}$$
$$^{3}Psen^{\bullet-} + O_2 \rightarrow Psen + O_2^{\bullet-}$$
$$^{3}Psen^{*} + O_2 \rightarrow Psen^{\bullet+} + O_2^{\bullet-}$$

Figure 15 – Type I Process (i)

The second Type I process (ii) involves the transfer of a hydrogen atom (reduction) to the excited triplet state photosensitiser ($^{3}Psen^{*}$). This generates free radicals capable of rapidly reacting with molecular oxygen and creating a complex mixture of reactive oxygen intermediates including reactive peroxides (figure 16). Again this triggers a cascade of cytotoxic events culminating in cell damage and death.

$$^{3}Psen^{*} + RH \rightarrow Psen\text{-}H^{\bullet} + R^{\bullet}{}_{red}$$
$$R^{\bullet} + O_2 \rightarrow RO_2^{\bullet}$$
$$RO_2^{\bullet} + R\text{-}H \rightarrow RO_2H + R^{\bullet}$$

Figure 16 – Type I process (ii)

On the other hand, Type II processes involve the direct interaction of the excited triplet state photosensitiser ($^{3}Psen^{*}$) with ground state molecular oxygen ($^{3}O_2$, $^{3}\Sigma_g$, figure 17); a spin allowed transition, since the excited state photosensitiser and ground state molecular oxygen are of the same spin state (T).

$$^{3}Psen + {}^{3}O_2 \rightarrow {}^{1}Psen + {}^{1}O_2$$
$$^{1}O_2 + Substrate \rightarrow Oxidative\ damage$$

Figure 17 – Type II Process

When the excited photosensitiser collides with a molecule of molecular oxygen, a process of triplet-triplet annihilation takes place ($^3Psen^* \rightarrow {}^1Psen$: $T_1 \rightarrow S_0$ and $^3O_2 \rightarrow {}^1O_2$: $T_0 \rightarrow S_1$), inverting the spin of one of molecular oxygen's ($^3O_2$) outermost antibonding electrons, generating two forms of singlet oxygen ($^1\Delta_g$ and $^1\Sigma_g$, figure 18), while simultaneously depopulating the photosensitiser's excited triplet state ($T_1 \rightarrow S_0$, figure 19). The higher-energy singlet oxygen state ($^1\Sigma_g$, 157 kJ mol^{-1} > $^3\Sigma_g$) is very short-lived ($^1\Sigma_g$ ≤0.33 ms (methanol, undetectable in H_20/D_20) and rapidly relaxes to the lower energy excited state ($^1\Delta_g$, 94 kJ mol^{-1} > $^3\Sigma_g$).[30] It is therefore this lower-energy form of singlet oxygen ($^1\Delta_g$) which is implicated in cell injury and death.[34]

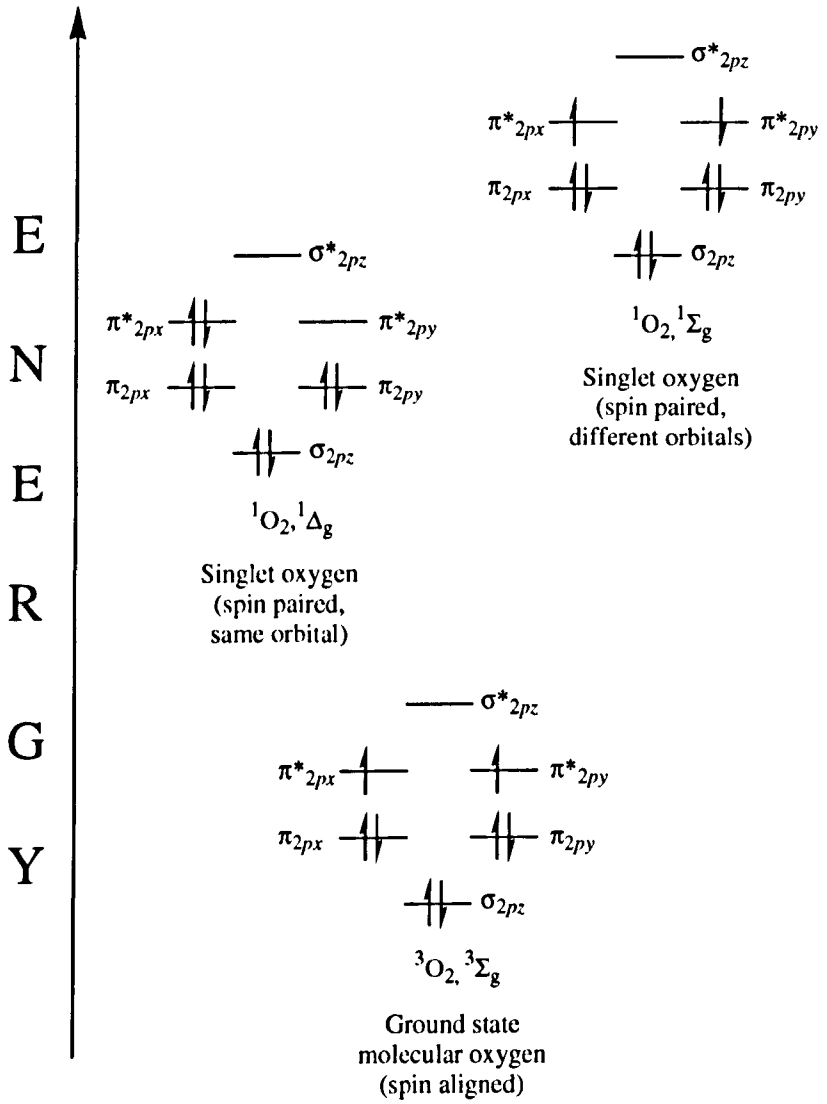

Figure 18 – Molecular Orbital Diagram of Oxygen ($^3\Sigma_g$, $^1\Delta_g$ and $^1\Sigma_g$)

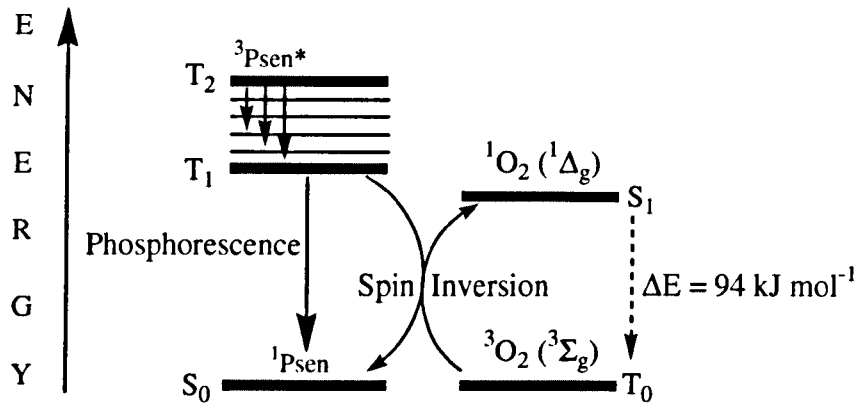

Figure 19 – Modified Jablonski Energy Diagram Showing Type II Process

The highly-reactive oxygen species ($^1O_2$) produced *via* the Type II process act near to their site of generation and within a radius of action of approximately 20 nm, with a typical lifetime of approximately 40 ns in biological systems.[3,5,32] Singlet oxygen can theoretically only interact with proximal molecules and structures within this radius.[5] ROS are known to initiate a large number of reactions with biomolecules, including amino acid residues in proteins, such as tryptophan; unsaturated lipids like cholesterol and nucleic acid bases, particularly guanosine and guanine derivatives, with the latter base more susceptible to ROS.[3-6,9,21,24,30,35-37] These interactions cause damage and potential destruction to cellular membranes and enzyme deactivation, culminating in cell death.[24]

Singlet molecular oxygen is known to react with systems by adding across electron rich double bonds, in an "*–ene*" type reaction to form peroxides or hydroperoxides (figure 20).[37]

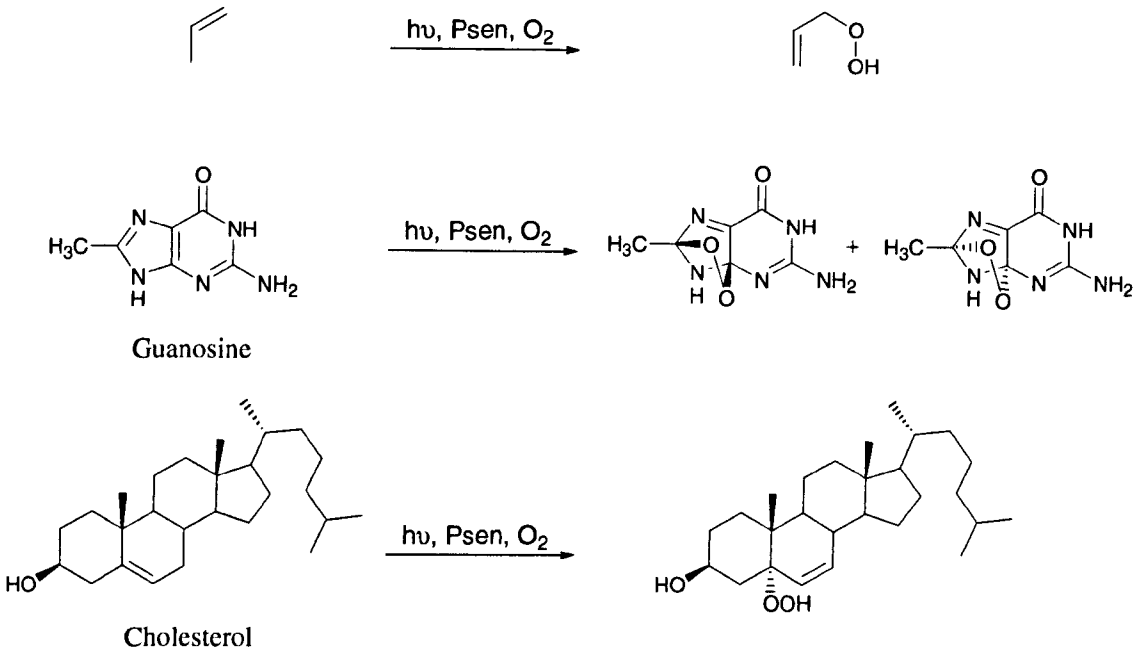

Figure 20 – Examples of Typical Singlet Oxygen Reactions

It is highly probable that in the presence of molecular oxygen, both Type I and II pathways play a pivotal role in disrupting both cellular mechanisms and cellular structure as a direct result of the photo-irradiation of the porphyrin molecule. Nevertheless, there is considerable evidence to suggest that the Type II photo-oxygenation process predominates in the role of cell damage, a consequence of the interaction between the irradiated photosensitiser and molecular oxygen.[3,4,9,24,35,38] It has however, been suggested that cells *in vitro* are partially protected against the effects of photodynamic therapy by the presence of singlet oxygen scavengers, such as histidine, and that certain skin cells are somewhat resistant to photodynamic therapy in the absence of molecular oxygen; further supporting the proposal that the Type II process is at the heart of photo-initiated cell death.[5,35,39,40]

The efficiency of Type II processes is dependent upon the triplet state lifetime (τ_T) and the triplet quantum yield (Φ_T) of the photosensitiser. Both of these parameters have been implicated in the effectiveness of a photosensitiser in phototherapeutic medicine; further supporting the distinction between Type I and Type II mechanisms. However, it is

worthy to note that the success of a photosensitiser is not exclusively dependent upon a Type II process taking place. There are a number of photosensitisers whose excited triplet lifetimes are too short to permit a Type II process to occur. For example, the copper metallated octaethylbenzochlorin photosensitiser (figure 21) has a triplet state lifetime of less than 20 nanoseconds and is still deemed to be an efficient photodynamic agent.[35]

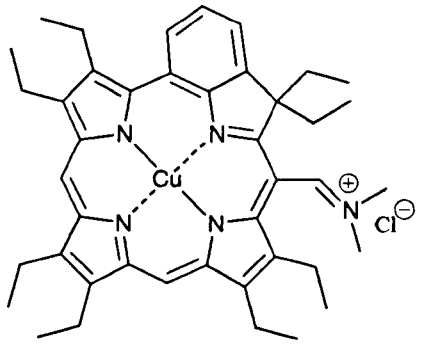

Figure 21 – A Copper Metallated Photosensitiser

1.1.7 Photosensitisers

1.1.7.1 Ideal Photosensitisers

Although a number of different photosensitising compounds, such as methylene blue, rose bengal and acridine (figure 22), are known to be efficient singlet oxygen generators (and therefore potential photodynamic therapy agents) a large number of photosensitisers are actually based around cyclic tetrapyrroles; in particular porphyrin, chlorin and bacteriochlorins derivatives (figure 23). This is possibly because they have an inherent similarity to the naturally occurring porphyrins present in living matter - they have no or little toxicity in the absence of light and, over the years, porphyrin chemistry has been well developed.[3-5,9,20,21,30,36,41]

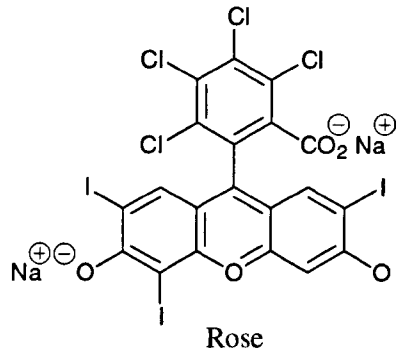

Rose Bengal

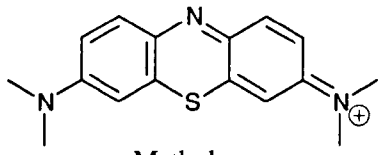

Methylene Blue

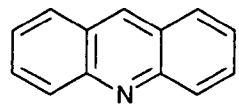

Acridine

Figure 22 – Examples of Non-Porphyrinic Photosensitisers

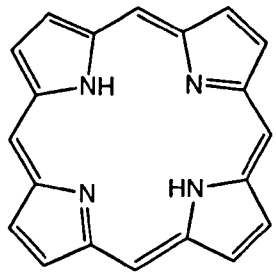

Porphine

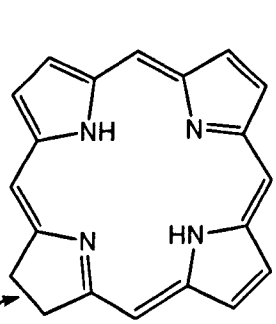

reduced exocyclic bond

Chlorin

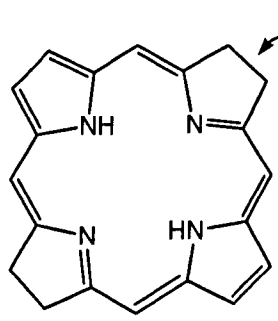

2^{nd} reduced exocyclic bond

Bacteriochlorin

Figure 23 – Porphine, Chlorin and Bacteriochlorin

1.1.7.2 Ideal Photosensitiser Properties

The key characteristic of any photosensitiser is its ability to preferentially accumulate in diseased tissue and *via* the generation of cytotoxic species, induce a desired biological effect. In particular, a good photosensitiser should adhere to the following criteria:-

- Have strong absorption with a high extinction coefficient (ε 20,000 – 30,000 M^{-1} cm^{-1}) in the red region of the electromagnetic spectrum (>650 and <850 nm); thus, allowing deeper tissue penetration.[4,5,12,21,20,32] However, absorption wavelengths should not be too long as the energy required for singlet oxygen formation ($^3Psen^*/T_1 \leftrightarrow {}^3O_2/T_0 \geq 94.1$ kJ mol^{-1}) may not be achieved.[9,30,35] Hence, an optimum window of tissue penetration depth exists between 600 and 800 nm.
- Have suitable photophysical characteristics: high quantum yield of triplet formation ($\Phi_T \geq 0.5$); high singlet oxygen quantum yield ($\Phi_\Delta \geq 0.5$); relatively long triplet state lifetime (τ_T, microseconds); and high triplet-state energy ($\Delta E_T \geq \Delta E_\Delta = 94$ KJ mol^{-1}).[9,21,24,30,42] To date the parameters $\Phi_T = 0.83$ and $\Phi_\Delta = 0.65$ (haematoporphyrin); $\Phi_T = 0.83$ and $\Phi_\Delta = 0.72$ (etiopurpurin); and $\Phi_T = 0.96$ and $\Phi_\Delta = 0.82$ (tin etiopurpurin) have been achieved.[3,21,30]
- Be effective generators of singlet oxygen and other ROS.
- Have negligible toxicity in the absence of light.
- Must exhibit specific retention in diseased tissue over healthy tissue, particularly skin; general skin sensitisation must be avoided - rapid sensitisation and desensitisation of the skin is most desirable.
- Present rapid clearance from the body.[4]
- Be single well characterised compounds, with a simple and stable drug formulation.
- Have a facile synthesis from readily available starting materials with easy translation into multi-kilogram scales/reactions.

- Have the option for facile (side-chain) derivatisation; potentially enhancing the above properties.
- Be soluble in biological media, allowing direct intravenous administration and transport to the intended target. Failing this, a hydrophilic delivery system should be sought enabling efficient and effective transportation of the photosensitiser to the target site *via* the bloodstream.

1.1.8 Photodynamic Therapy

1.1.8.1 Background

The use of light in the treatment of disease has been known for many centuries and can be traced back over 4,000 years to the ancient Egyptians. The Egyptian people used a combination of the orally ingested Amni Majus plant and sunlight to successfully manage vitilago; a skin disorder of unknown cause, involving loss of pigmentation in patches of otherwise normal skin. The active ingredient of this plant (psoralen, figure 24) is now successfully employed in the worldwide treatment of psoriasis.[3,21,43,44]

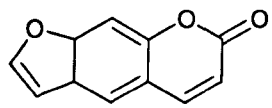

Figure 24 – Structure of Psoralen

A number of different terms have been used in conjunction with photodynamic therapy (PDT) over the years. For the purpose of clarity, the main/key terms are highlighted and defined in the following paragraph.

Phototherapy is a term used to describe the treatment of disease by a series of (photo)chemical processes initiated by light (see section 1.1.6). The treatment of disease with a combination of a chemical substance and light has become known as photochemotherapy. The use of light and a chemical substance (more specifically a

photosensitiser) used in conjunction with molecular oxygen to elicit cell death, is more commonly recognised as photodynamic therapy; a term first used by the scientist von Tappeiner.[9]

Photodynamic therapy is more explicitly a selective treatment modality for the local destruction of diseased cells and tissue. The selectivity is based on the ability of the photosensitiser to preferentially accumulate in the diseased tissue and efficiently generate singlet oxygen, inducing target cell death.

The principle of photodynamic therapy is based on a multi-stage process (figure 25). The first of these stages ((i)) sees the administration of a photosensitiser with negligible dark toxicity, either systemically or topically, in the absence of light. When the optimum ratio of photosensitiser in diseased *versus* healthy tissue is achieved, the photosensitiser is ((iii)) activated by exposure to a carefully regulated dose of light which is shone directly onto the diseased tissue for a specified length of time. The light dose is regulated in order to allow a large enough dose to be delivered to activate the photosensitiser, but at the same time be small enough to minimise damage incurred by the neighbouring healthy tissue. It is the activated form of the photosensitiser which evokes a toxic response in the tissue, resulting in cell death. The success of photodynamic therapy lies in the prolonged accumulation of the photosensitiser in diseased tissue, relative to the more rapid clearance from normal tissue cells.

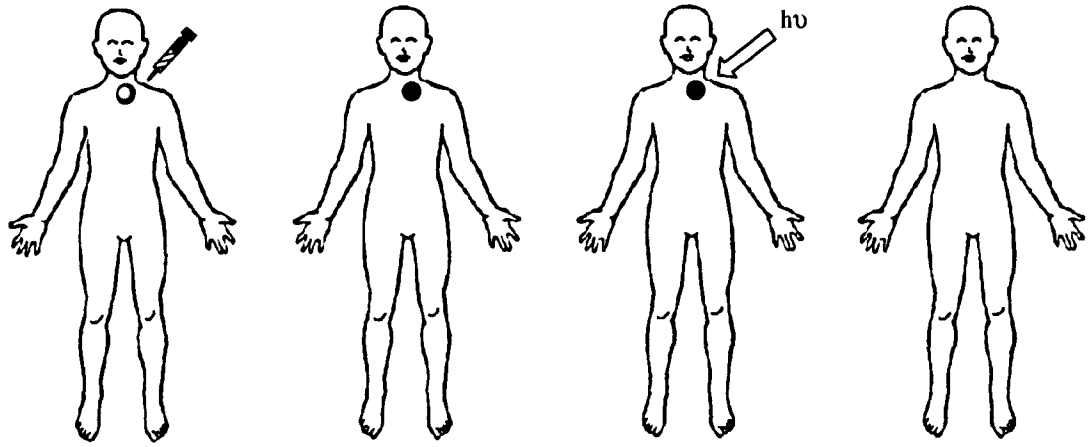

Figure 25 – Photosensitiser Administration

Photodynamic therapy is commonly practiced in the treatment of a number of cancers, including those present in the head and neck, the lungs, bladder and particular skin cancers. It has also been successfully used in the treatment of non-cancerous conditions such as, age related macular degeneration, psoriasis, atherosclerosis and has shown some efficacy in anti-viral treatments, including herpes.[3-5,9,12,20,21,32,33,45]

The nature of photodynamic therapy requires the efficient localisation of a photosensitiser in the target tissue in order to achieve a satisfactory response. Photodynamic therapy can offer an enhanced therapeutic effect *via* preferential uptake of the photosensitiser by: the target tissue; specific illumination of target tissue; strategic timing of the applied light dose; topical application of the photosensitiser and (*via* the ability of the chemist) "control" over the photosensitiser structure.

Photodynamic therapy carries advantages for both the patient and the physician; the need for delicate surgery and lengthy recuperation periods is minimised, along with minimum formation of scar tissue and disfigurement. However, photodynamic therapy is not

without its drawbacks; a major limitation is the associated general photosensitisation of skin tissue.

1.1.8.2 History of Photodynamic Therapy

Reports of contemporary photodynamic therapy came first in the scientific investigations led by Finsen in the late nineteenth century. Finsen successfully demonstrated phototherapy by employing heat-filtered light from a carbon-arc lamp (the "Finsen lamp") in the treatment of a tubercular condition of the skin known as *lupus vulgaris*, for which he won the Nobel Prize in Physiology or Medicine in 1903. But it was not until the early twentieth century that reports of photodynamic therapy for the treatment of cancer patients with solid tumours were made by von Tappeiner's group in Munich.[3,12,33,44,46] In 1913 another German scientist, Meyer-Betz, described the major stumbling block of photodynamic therapy after injecting himself with haematoporphyrin (a photosensitiser). He swiftly experienced a general skin sensitivity upon exposure to sunlight; a problem still persistent with many of today's photosensitisers.[3,9,21,32]

Further studies investigating the accumulation of haematoporphyrin and the purified haematoporphyrin derivative (HpD) in tumours culminated in the late 1980's with the photosensitiser Photofrin® (figure 26). A photosensitiser which, after further purification, was given approval in 1995 by the Food and Drug Administration (FDA) in the USA (and later in Canada, Japan and parts of Europe) for use against certain cancers of the esophagus and non-small cell lung cancer.[4,5,9,12,21,32,44,47,48] Photofrin® was far from ideal and carried with it the disadvantages of prolonged patient photosensitivity and weak long-wavelength of absorption (630 nm, see section 1.1.7).[12,32,47] This led to the development of improved (second generation) photosensitisers, including Verteporfin ((Visudyne®), a benzoporphyrin derivative) and more recently third generation photosensitisers based around targeting strategies (see section 1.1.10).[4,9,20,32,44,49,50]

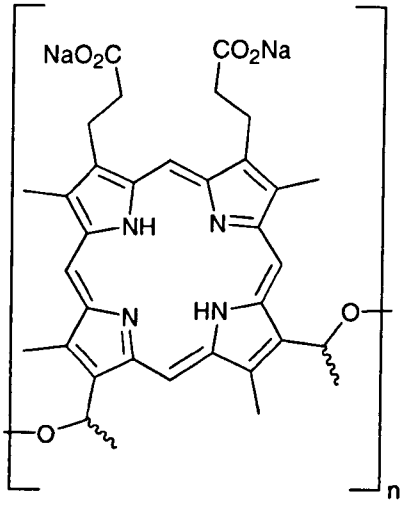

Figure 26 – Structure of Photofrin®, n = 1-9

1.1.8.3 Photosensitiser Distribution/Localisation and Biological Response

The localisation of photosensitisers within tissues and cells can play a significant role in the mechanisms and efficacy of cell death; crucial for effective photodynamic therapy.[5] Photodynamic therapy works by inducing the formation of cytotoxic agents which readily attack neoplastic cells, a response known to be affected *in vivo* by the complexity of biological systems.[4,32] Any number of subcellular targets can be attacked during photodynamic therapy, including mitochondria, lysosomes, plasma membranes and nuclei, and the exact subcellular target can govern whether cell death occurs *via* apoptosis or necrosis (see section 1.2.1).[4,6,12,29,32,41,51] ROS have a short half-life and act close to their site of generation (see section 1.1.6), it is therefore thought that the type of photodamage incurred in irradiated photosensitiser-loaded cells does depend upon the exact subcellular localisation of the photosensitiser.[5,32,36] Consequently, it is of utmost importance to study the distribution patterns of differently substituted photosensitisers in order to gain further insight into this area. Unfortunately, to date there are no clear-cut protocols to do this, either *in vitro* or *in vivo*; though a number of suggestions have been put forward in relation to photosensitiser biodistribution, these will be accordingly outlined in the following discussion.[4,32]

1.1.8.3.1 Intracellular/Subcellular Distribution

Transport mechanisms for systemically administered photosensitisers involve various plasma components, proteins and lipoproteins, depending upon the hydrophobicity of the photosensitising compound. The processes by which photosensitiser localisation occurs are not well understood but a number of hypotheses have been considered.[24]

Macroscopic damage appears to occur *via* three pathways: (i) direct damage to diseased cells; (ii) damage to endothelial cells; and (iii) macrophage-mediated infiltration of the diseased tissue.[24] In addition to this, there seems to be three main structural features relating to the photosensitiser which are of importance: (i) the net ionic charge, ranging from – 4 (anionic) to + 4 (cationic); (ii) the degree of hydrophobicity; and (iii) the degree of asymmetry present in the photosensitiser.[5,36,41,47,51] Hydrophobic photosensitisers with two or less negative charges are able to traverse the plasma membrane and then relocate to other intracellular membranes. Conversely, hydrophilic photosensitisers with two or more negative charges appear to be too polar to diffuse across the plasma membrane and are therefore taken up *via* endocytosis.[5,36]

It has been mentioned previously that the modes of photosensitiser absorption and distribution have proven evasive; although, it has been proposed that the hydrophilicity/hydrophobicity of the photosensitiser plays an important role in the processes of absorption and distribution. Photosensitisers which exhibit sufficient lipophilicity have demonstrated their ability to cross the lipid cell membrane, with absorption the result of passive diffusion.[3,35,41] These photosensitisers can generally be identified in: the cytoplasm; around the nuclear membrane; or around the cellular membrane. Whereas, more polar molecules have demonstrated a preference for endocytotic uptake and lysosomal localisation.[33,36,51]

It has also been reported that certain photosensitisers preferentially localise within the endoplasmic reticulum (ER) and the Golgi apparatus, and although very uncommon, some may even localise in the plasma membrane.[5,12,36]

Particular attention will be paid to lysosomal and mitochondrial localisation in the following paragraphs.

1.1.8.3.2 Subcellular Localisation

Since singlet oxygen can migrate less than 20 nm after its formation, sites of initial photodamage are thought to be related to the photosensitiser's primary localisation point at the time of irradiation. As a result, many researchers have chosen to examine subcellular sites of photodynamic-induced alterations rather than to search for sites of photosensitiser binding.[32] Since most photodynamic photosensitisers do not accumulate in the cell nuclei, photodynamic therapy generally offers a low potential for causing DNA damage, mutations and carcinogenesis; whereas, photosensitisers that localise in mitochondria are likely to induce apoptosis and those localised in the plasma membrane are likely to initiate necrosis once they have been activated.[32] This leads to the question, "will a single subcellular "death" target prove advantageous in all "positively" induced cell death circumstances?" This is a very complex quandary for which no single answer currently exists; although more recent work is now beginning to hypothesise that it may be possible to initiate apoptosis (the preferred form of cell death) through non-mitochondrial targeted photosensitisers. This is a promising potential for new photosensitisers and photodynamic therapy; however, this question largely remains unanswered and the subject of intense research.[32,52]

1.1.8.3.3 Lysosomal Localisation

Initially, it was thought that lysosomes (vacuoles widely dispersed in the cytoplasm) were an important intracellular target in the localisation of the photosensitiser. Subsequent investigations have suggested that the relative efficacy of cell death (upon irradiation of photosensitiser-loaded lysosomes) is significantly lower than that which is observed with the free form of the photosensitiser and that which is localised within the mitochondria and other organelles. This may be a consequence of those photosensitisers which display greater degrees of aggregation and tend to selectively accumulate in lysosomes.[5,32] Other studies have also pointed to mitochondrial localisation of photosensitisers bearing net

cationic character, while those with a net anionic character have appeared to preferentially localise in the lysosomes.[5,12,32,53] Photosensitisers, initially localised within the lysosomes, may redistribute after a small amount of light has been delivered due to the photodynamic action.[5,32,36,41,51] This behaviour can be attributed to the photodynamic permeabilisation of the lysosomal membrane, which allows small molecules, including the photosensitiser, to leak out of the lysosomes and into the cytoplasm.[5,32,36,41,54]

It has been suggested that certain photosensitisers, for example mono-aspartyl chlorin e6, the di- and tetrasulphonated *meso*-tetraphenylporphyrins (figure 27) and the tri- and tetrasulphonated phthalocyanines, are taken up into cells *via* endocytosis and consequently found inside lysosomes.[47,51,55] A common feature shared by the above mentioned photosensitisers is their anionic charge - a feature already mentioned. This confers susceptibility towards endocytosis and lysosomal localisation of photosensitisers with a negative charge of -2 or more.[5,33,51] However, there are reports that tetrasulphonated porphyrins may preferentially localise within mitochondria.[36]

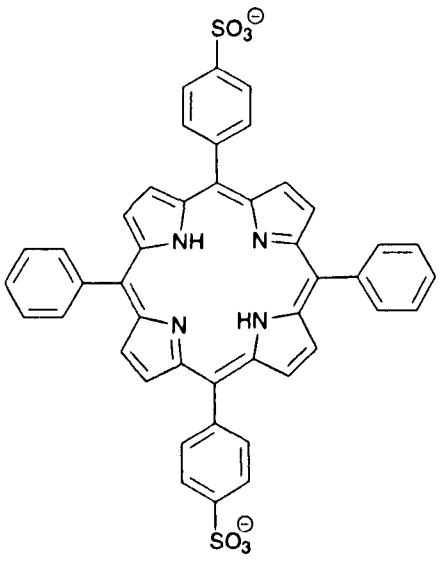

Disulphonated *meso*-Tetraphenylporphyrin

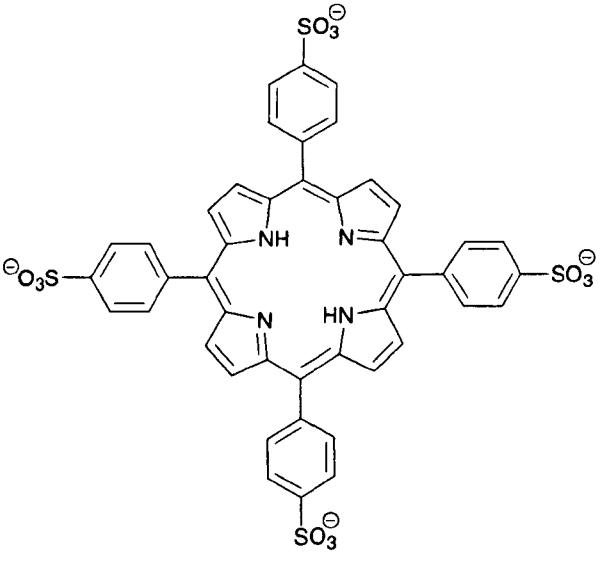

Tetrasulphonated *meso*-Tetraphenylporphyrin

Figure 27 – Sulphonated Porphyrins

Conversely, cationic photosensitisers substituted with quaternised pyridyl groups at the *meso*-positions of the porphyrin macrocycle (figure 28) have demonstrated distribution within the cytoplasm, suggesting lysosomal uptake. It has been suggested that less polar compounds, such as the monosulphonated tetraphenylporphyrin, exhibit a more even distribution throughout the cytoplasm and may diffuse across the cell membrane rather than entering the cell *via* endocytosis.[36]

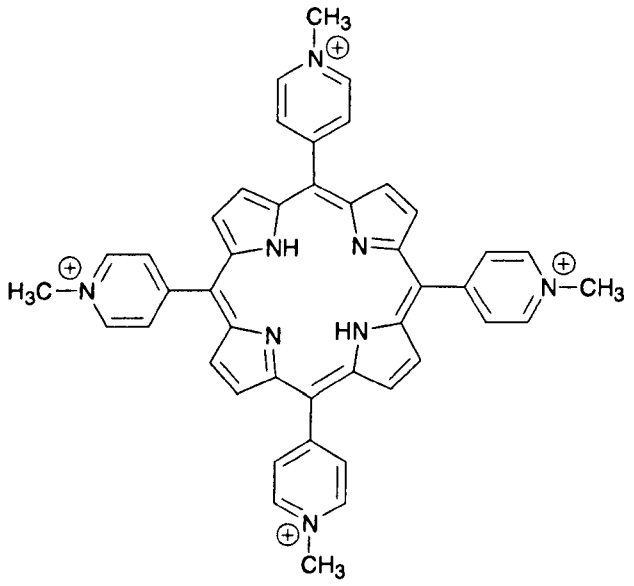

Figure 28 – Cationic *N*-alkyl-pyridiniumyl Porphyrin

1.1.8.3.4 Mitochondria

Mitochondria have been found to be very important subcellular targets for a number of photosensitisers. It is thought that this is related to the tendency of many of the photosensitisers available to promote post-irradiation apoptotic cell death *via* mitochondrial damage. Hydrophobic photosensitisers bearing net cationic charges are also believed to locate preferentially in the mitochondria. This is believed to be a result of the negative membrane potential ($\Delta\psi_m$) associated with the mitochondria, as well as the lipid membrane bilayers.[5,12,32,36,41,51,53,56]

Preferential mitochondrial localisation may be a result of specific binding of the photosensitiser to proteins through an increased affinity for particular lipids including: cardiolipin or phosphatidyl glycerol, which are present in the inner mitochondrial membrane; or as a consequence of non-specific uptake based on the hydrophobicity of the photosensitiser. The delivery route/vehicle may also influence uptake, with some evidence suggesting that the affinity the photosensitiser displays towards the delivery vehicle and towards plasma components may be instrumental in changing its pharmacokinetics.[6,41]

Mitochondria are known to be polarised across their membranes (see section 1.2.2), with the inner membrane negatively charged to a greater degree relative to the outer membrane. This is a consequence of the membrane potential and pH gradient formed by the proton pump. This polarisation and the presence of specific ligands means that cationic photosensitisers may be able to utilise their charge to localise along the mitochondrial membrane gradient and within the organelle.[41,53] It is important to point out that most cationic photosensitisers appear to show rapid tissue clearance.[12] The degree of photosensitiser aggregation is also thought to affect localisation, with monomeric photosensitisers preferentially localising within the mitochondria. However, anionic photosensitisers have been found to localise within mitochondria, as opposed to the inner membrane lipid bilayers. This is thought to be a result of binding receptors, such as the benzodiazepine receptor, present on the surface of the outer mitochondrial membrane.[5,12,33,41,57-60]

1.1.8.3.5 Tumour Localising Ability of Photosensitisers

The degree to which a photosensitiser can preferentially localise in tumourous tissues can be measured in terms of a tumour to peritumoural tissue ratio. It is important to try and quantify the generalised photosensitisation of the photosensitiser by means of investigating tumour to skin cells; tumour to liver cells; and tumour to muscle cell ratios. It is difficult to compare tumour localisation for different photosensitisers due to the number of variables inherent with each system; for example, the chemical nature of the photosensitiser; cell line/animal species; mode of delivery; drug to light interval; total

light incidence and the light fluence rate. However, suggestions have been made regarding the tumour localising ability of photosensitisers and some of these ideas will be addressed in the following passage.

Hydrophobic photosensitisers, differing only in the polarity of the attached substituents have been investigated with proposals that the more hydrophobic a photosensitiser is, the higher the tumour to normal cell ratio achieved, typically between 7:1 and 8:1, with their hydrophilic counterparts much lower (2:1).[61] This doesn't however mean that hydrophobic photosensitisers will be more efficient than their hydrophilic counterparts in every case; there are a large number of variables affecting the uptake of a photosensitiser other than its polarity.

It is much easier to compare different hydrophilic photosensitisers, since they have increased solubility in aqueous media and are capable of being delivered to the disease site *via* the blood system, circumventing the need for an alternative delivery method. It is common practice to substitute high molecular weight, covalently bound hydrophobic molecules with anionic substituents such as sulphonic or carboxyl groups to increase a molecule's hydrophilicity. For example, aluminium phthalocyanines have been investigated and results suggest that the photosensitiser tumour to peritumoural ratio, twenty four hours post-intravenous administration, was 28:1 (tetrasulphonated derivative); 15:1 (trisulphonated); 10:1 (disulphonated) with the monosulphonated derivative undetectable. These polar anionic compounds have also demonstrated selective localising properties varying in relation to the number of sulphonate groups present on the tetrapyrrolic molecule ($S_1 \rightarrow S_4$, where $S = SO_3^-$). It has been postulated that the less hydrophilic monosulphonated derivatives localise to a greater extent intracellularly than their tetrasulphonated counterparts, which appear to localise within close proximity to the plasma membrane.[12,51,62,63] Sulphonated phthalocyanines have also demonstrated similar behaviour with monosulphonated aluminium phthalocyanines selectively localising within tumour cells; whilst its more hydrophilic relatives show selective extracellular localisation within fatty tissues and blood vessels surrounding the tumour.[35,41,54]

The disulphonated porphyrin (figure 29) and phthalocyanine analogues (with "adjacent" sulphonated substituted groups), appear to demonstrate greater photodynamic activity in comparison to their di- (symmetric, figure 29), mono-, tri- and tetrasulphonated counterparts, respectively. The disulphonated analogues have been found to accumulate in the highest concentration *in vitro*, exhibiting greater affinities for lipoproteins.[5,9,21,24,55]

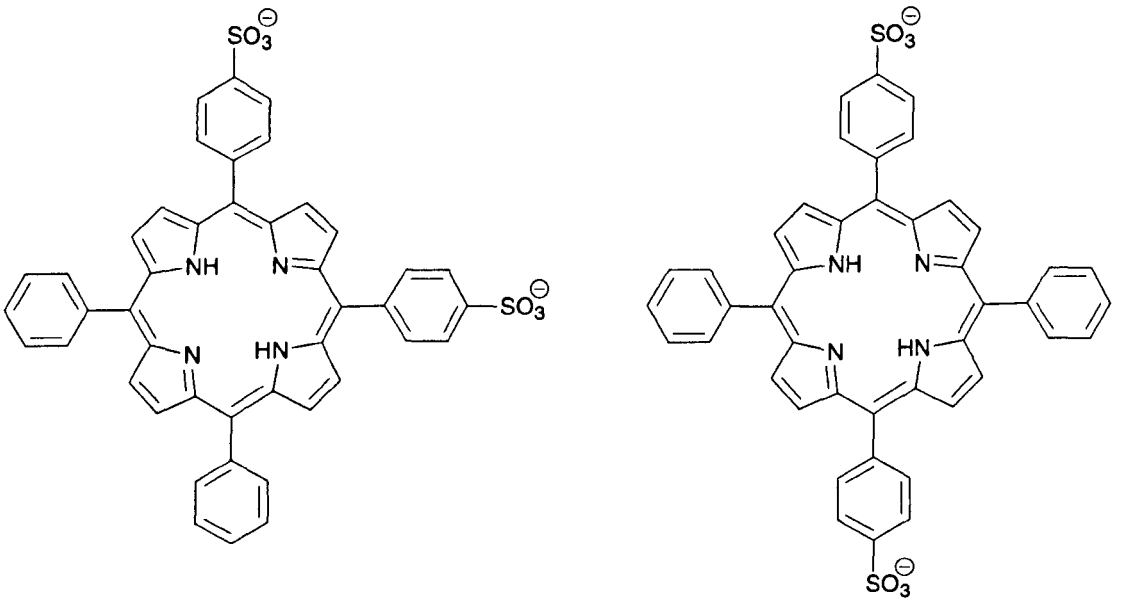

Figure 29 - Disulphonated Tetraphenyl porphyrins

Lipoproteins are species composed of a hydrophobic lipid core, encased by an outer shell of phospholipids and apoproteins. These amphipilic species act to solubilise highly hydrophobic lipids and regulate the movement of specific lipids in and out of target cells and tissue. Lipoproteins can be internalised *via* endocytosis and release their cargos within the cell, after which the lipoprotein returns to the plasma membrane unchanged. Hence, compounds which show a greater affinity for lipoproteins may be selectively targeted towards intracellular delivery/localisation.

It is important to note that although the above mentioned sulphonated tetrapyrrolic compounds have been found to demonstrate good photodynamic activity *in vitro*, they exhibit neurotoxic effects towards humans, hence their use is somewhat restricted.[12,24,33]

1.1.8.3.6 Mechanisms of Tumour Localisation and Destruction

Although, it has been possible to observe a high tumour to normal tissue ratio *in vivo*, it has been demonstrated that isolated tumour cells are unable to significantly accumulate higher levels of photosensitiser in comparison to their neoplastic counterparts. To answer this anomaly a number of potential hypotheses have been suggested, including:

- Lipophilic photosensitisers (frequently associated with lipoproteins in the blood system) may be recognised and taken into the cell by means of lipoprotein receptors present on the cell surface. It has also been suggested that rapidly dividing tumour cells may have an increased demand for cholesterol and subsequently have an increased number of receptors on their cell membranes.[64]
- Reduced lymphatic drainage and abnormal tumour vasculature may encourage the build up of photosensitiser in the interstitial space.[65]
- The large number of macrophages associated with tumours have been found to contain nine times the concentration of photosensitiser compared to the tumour cell, leading to suggestions macrophages may be the major mechanism of photosensitiser uptake in tumours.[66,67]
- It is thought endothelial cell damage to tumour vasculature may result in tumour photonecrosis and lead to suffocation and/or starvation of the tumour.[67]

1.1.9 Light Delivery/Sources

Over the years a variety of light sources have been used to generate the "activating" light needed to initiate photodynamic therapy. Sources have included arc lamps, fluorescent light sources and lasers, and it is these light sources which contribute to the efficacy of photodynamic therapy.[3,9]

The wavelength of light required to generate the therapeutic effect depends upon the photosensitiser chosen and the optical properties of the tissue.[5,9,32] Normally, the longest photosensitiser absorption wavelength is chosen in order to achieve maximum tissue penetration (figure 30); it is known for some photosensitisers that the penetration depth can be nearly doubled by using longer excitation wavelengths.[5,6] It has also been reported that pulsed light may be more effective than using continuous illumination. One possible explanation is the penetration depth of light. Light may penetrate more deeply into the tissue as a result of initial photobleaching of the photosensitiser; the first pulse may excite the photosensitiser into higher and less absorbing levels, reducing the absorbance from the next pulse. Although, on occasion a superficial therapeutic effect is often more appropriate and a shorter wavelength light source may be sought; for example, in avoiding rupture of the tissue wall.[9,32]

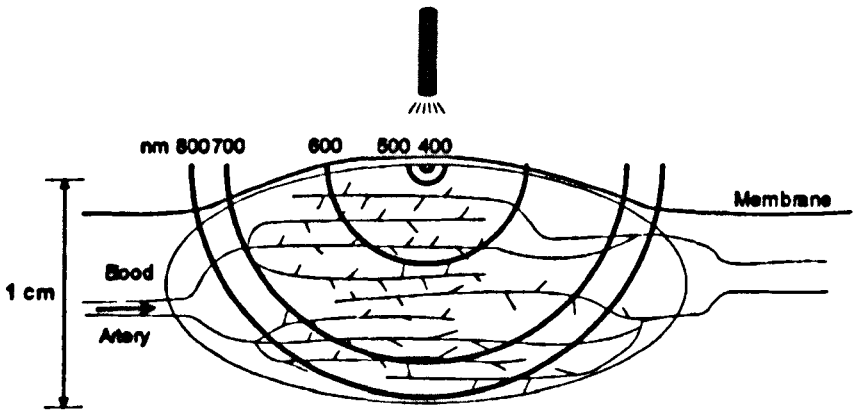

Figure 30 – Light Penetration Depths[13]

The fluence rate (rate of total radiant energy of all wavelengths passing from all directions through an infinitely small sphere) of the light applied in photodynamic therapy, as well as the total light fluence, is thought to affect the efficiency of the photoactivation process, since the fluence rate decreases exponentially with depth.[12] The light dose (fluence) typically required for clinical photodynamic therapy ranges from 50 – 500 J cm^{-2} (Photofrin), although the dose can actually be as low as 10 J cm^{-2} (Foscan). However, care must be taken not to use too high a fluence rate since photodamage to the photosensitiser can be incurred.[4,5,9,32] This photodestruction process is more commonly

termed photobleaching (see section 1.1.11) and is thought to take place when singlet oxygen, or other ROS produced during irradiation, react with the photosensitiser in such a manner that the efficiency of further photosensitisation processes is reduced.[6]

1.1.9.2 Ideal Light Sources

The ideal light source should be capable of exciting the photosensitiser in order to convey the desired effect. Theoretically, a normal white light source should be capable of achieving this, but in practice it has proven more efficient to employ a monochromatic light source, chosen with a porphyrin absorption-peak wavelength in mind. Typically, this is accomplished by employing lasers. The argon ion laser for example has a number of lasing wavelengths ("lines") in the blue and green region of the electromagnetic spectrum, including 457.9, 476.5, 488.0, 514.5 and 528.7 nm, whereas the gold vapour laser emits at 627.8 nm, all within the porphyrin Q band absorption range (450 - 650 nm). It is worthy to note here lasers are not used, as one would normally expect, for their ability to achieve a high power, for strong heating or tissue incision, but instead to exclusively activate the photosensitiser by utilising their highly monochromatic light.[9]

An ideal light source would allow the incidence light to be aimed directly towards the diseased tissue, minimising the area of healthy tissue destroyed, whilst maximising the amount of light received by the diseased tissue. The use of endoscopes (instruments based on optical fibres that are capable of delivering light to the site of treatment) are one solution to this criterion. By efficiently channeling the highly coherent monochromatic laser light into quartz fibres, an ideal photodynamic therapy light delivery system is made available. The endoscope fibres may be tipped with a variety of lenses and diffusers to allow optimal illumination of the tissues to be treated. For example, hollow spherical organs such as the bladder, can be illuminated with cylindrical diffuser fibres of varying lengths. Thin fibre optic cables may be fed directly through existing channels in bronchoscopes and endoscopes, eliminating the need for more complicated surgical procedures.[68,69]

There are drawbacks to using lasers which should be noted. Lasers are expensive, complicated and dangerous devices requiring trained operatives. In addition, they are often rather large and have noisy power sources and cooling apparatus. They are not readily transportable from one place to another, be it around the patient or from one clinic to a second.[9]

The development of a variety of portable and cheaper light emitting diode (LED) systems, along with solid state diode lasers, are now showing improvements of coherent light sources at wavelengths down to 633 nm (Omnilux), with the development of lower wavelength diode systems currently under investigation.[1,3,5,9,20,32,44,69,70] It may be possible, in the future, to see the development of light patches capable of illuminating surfaces even more effectively than the sources which are currently available to the clinician.

1.1.10 Photosensitiser Delivery

The poor solubility of many photosensitisers in aqueous media, particularly at physiological pH, prevents their intravenous delivery directly into the bloodstream. It would therefore, be advantageous if a delivery model could be conceived which would allow the transportation of these (otherwise potentially useful) photosensitisers to the site of diseased tissue.

Work has recently focused on designing systems to effect greater selectivity and specificity on the photosensitiser in order to enhance cellular uptake.[32,33] A number of possible delivery strategies have been suggested, ranging from the use of oil-in-water (o/w) emulsions to liposomes and nanoparticles as potential carrier vehicles.[6,9,30,32,71,72] There is concern however, that although the use of these systems may increase the therapeutic effect observed as a result of photodynamic therapy, the carrier system may inadvertently decrease the singlet oxygen quantum yield (Φ_Δ) of the encapsulated photosensitiser.[9]

1.1.10.1 Delivery Vehicles

1.1.10.1.1 Emulsions

Emulsions are liquid systems where one liquid is dispersed in a second immiscible liquid (with or without emulsifiers), usually forming droplets in which hydrophobic substrates can be embedded, thereby indirectly increasing the solubility of the cargo (photosensitiser).[32,72,73]

Polyethylene glycol (PEG) and Cremophor EL are two of the more common systems used for the emulsification process, although a number of other agents have been investigated.[12,32,47,48,55] Cremophor, moleculsol and γ-cyclodextrin have all been compared against one another for the effective delivery of a hydrophobic porphyrin derivative, tin etiopurpurin, a potent photosensitiser commercially known as Purlytin™.[3, 4,9,12,21,32,47,55] The three emulsifying agents (administered in an aqueous ethanolic solution) all exhibited a greater degree of intracellular localisation relative to that of the "free" ethanolic solution. Results suggested that a lower intracellular concentration of the photosensitiser was required to effect cell death when an emulsifying agent was used, rather than with the ethanolic solution alone; a consequence of more effective photosensitiser accumulation.

1.1.10.1.2 Liposomal Encapsulation

Liposomes are microscopic, spherical, or ellipsoidal structures composed of amphiphilic phospholipids and cholesterol, which self-assembly into one or several bilayers forming hydrophobic and hydrophilic regions; typically encapsulating an aqueous interior.[9,30,72,74] Lipophilic photosensitisers may be encapsulated within the inner hydrophobic region, while the outer hydrophilic layer (soluble in aqueous media), allows transportation of the photosensitiser towards the target site.[32,71] Tin-etiopurpurin, benzoporphyrin derivatives and zinc phthalocyanines have all been successfully encapsulated in order to demonstrate this technique.[4,32,55] Liposome associated photosensitisers have exhibited greater efficiency and selectivity of tumour targeting (demonstrated by improved accumulation

of the photosensitiser in tumour cells) compared with the same photosensitiser administered in a homogeneous (aqueous) solution.[9,32] This improved uptake is thought to be the result of the low density lipoprotein (LDL) receptor mechanism.[9]

1.1.10.1.3 Nanoparticle Carriers

Nanoparticle carriers work on a similar principle to liposomes: they can be composed of an outer hydrophilic and inner hydrophobic region (capable of encapsulating hydrophobic photosensitisers within their inner matrix); thus, facilitating the transportation of photosensitisers in biological environments. They have been developed as an alternative carrier system to liposomes in an attempt to overcome a number of disadvantages associated with liposomal formulations. It has been suggested that only a small fraction of the chosen photosensitiser can be effectively incorporated into liposomes and that the limited lifetimes associated with liposomes results in their structural degradation over time.[74]

It has also been hypothesised, that the type of vehicle used in photosensitiser delivery can influence the distribution of the photosensitiser within the serum. Thus, the transport mechanisms and kinetics of the photosensitiser to the target tissue, as well as the subcellular distribution of the photosensitiser are affected. It would appear delivery *via* lipid-based vehicles shows enhanced binding of the porphyrin (photosensitiser) to the lipoproteins, in particular, orienting towards LDL, possibly resulting in the selective release of the photosensitiser into neoplastic tissue.[32]

1.1.10.1.4 Targeting Strategies

Hypotheses have been reported that suggest accumulation of photosensitisers in the mitochondria efficiently triggers apoptosis. Therefore, the efficacy of a photosensitiser could be potentially improved by mitochondrial targeting. The nucleus is the cellular organelle that is most sensitive to phototherapy damage, hence nuclear damage can lead very quickly to cell death. This implicates the nucleus as a desirable photosensitiser "target".[9,32,52,56]

The intracellular localisation of a photosensitiser is not a static process and may change during irradiation. For example, as a result of photoinduced lysosomal damage the lysosomes can rupture releasing lysomsomally localised photosensitiser into the cytoplasm. In addition, photosensitisers are generally non-site specific drugs, *i.e.* they do not target specific substrates or sites in their "free-state", highlighting the need for site-specific/selective photosensitisers and the development of targeting strategies.[5,9,12,20,41,51,75]

The efficacy of phototherapy could be increased by selectively targeting the photosensitiser towards the diseased tissue, with a two-fold advantage: (i) less photosensitiser would be required to effect cell death; hence (ii) general skin sensitivity would be reduced.[9,32] This has been observed over the last few years where there has been a shift in research away from the development of structural characteristics (to aid better specific localisation) and towards the development of a number of targeting strategies. One such example being the photosensitiser bioconjugates which contain a receptor-targeting moiety (and a photosensitiser): a move that is in line with the "magic bullet" suggested in the early twentieth century by Paul Ehrlich.[76]

Ehrlich's notion of, "a compound which would have a specific attraction to disease-causing microorganisms by seeking them out and destroying them (whilst avoiding other organisms and having minimal undesired/harmful effects on the patient)", could be theoretically achieved using antibody conjugates.[76] By using antibodies (one of the most accurate means of cell recognition) loaded with an agent capable of evoking the desired effect of attacking and destroying a specific target, with minimal impact on healthy tissue, Ehrlich's idea can be brought one step closer to reality.[32,77,78]

1.1.10.1.4.1 Targeting Moieties

A number of small biologically active molecules have been successfully conjugated to porphyrins, for example steroids and other lipids, peptides and antibodies.[3,12,32] Antibodies have been used in a range of techniques such as: (i) antibody directed enzyme prodrug therapy (ADEPT);[79,80] the use of a deactivated toxin or prodrug which can be

converted into its active form by an enzyme covalently bound to a suitable monoclonal antibody, directing the species to the target cells; (ii) antibody directed abzyme prodrug therapy (ADAPT).[81-83] This is similar to ADEPT with the exception that ADAPT uses catalytic antibodies or abzymes, which can be engineered to catalyse the activation of the prodrug like ADEPT, but minimise the immune response. Finally, (iii) gene directed enzyme prodrug therapy (GDEPT) which differs from ADEPT in that the activating enzyme in GDEPT is not conjugated to the directing antibody.[84-86] Instead, a gene encoding this enzyme is used which, upon entry to the cell, can generate localised concentrations of the enzyme. This enzyme in turn activates a systemically administered prodrug in the same manner used in ADEPT. GDEPT requires alternative methods of gene delivery since the targeting ability associated with antibodies is lost. One possibility is the use of viruses to deliver the gene *via* local injection, a technique known as virus directed prodrug therapy (VDEPT).[87-90]

Other targeting or localising biomolecules can also be employed in "targeting therapy" to achieve the "magic bullet" notion, these include: serum albumin; LDL; peptides; sugars; and nucleotides. Serum albumin is the most abundant blood protein and is synthesised by the liver hepatocytes. Serum albumin is a multi-functional protein whose general purpose is to transport metabolites and drugs around the body and it plays a key role in buffering and maintaining the osmolality of blood. It is also an effective antioxidant and a source of nutrition in the form of vitamins, steroids, amino acid, copper (II) and zinc (II) for healthy cells distant from the vasculature. Albumin is present in almost every tissue and fluid which the body is made of. An increase in the cellular uptake of albumin makes it a good candidate for use in photodynamic localisation.[3,6,9,12,32]

1.1.10.1.5 Low Density Lipoprotein Conjugates

Lipoproteins are particles composed of hydrophobic lipids, surrounded by an outer shell of polar lipids and apoproteins, who have two main roles: to solubilise highly hydrophobic lipids and regulate the passage of specific lipids into and out of particular target cells and tissue. This passage occurs *via* a process of specific receptor binding in the plasma membrane of non-hepatic cells, internalising through endocytosis to form a

vesicle within the cell. They fuse with lysosomes and hydrolyse the protein component of the LDL (LDL are the major carrier of cholesterol around the body *via* the blood system). The LDL receptor is then returned to the plasma membrane unaltered.[3,12,32] Conjugates of peptides, sugars and nucleotides have also been investigated by a number of groups.[3]

1.1.11 Luminescence

1.1.11.1 Fluorescence

The manner by which fluorescence occurs is based on a three stage process. The first stage sees the absorption of a photon of electromagnetic radiation in the form of light energy. If the energy of this photon is of the right magnitude, an electron is promoted from the ground state of the fluorophore (S_0) into a higher-energy singlet state (S_n). Partial non-radiative decay of the electron in the excited singlet state *via* internal conversion (IC) yields the first excited singlet state (S_1). Depopulation of this state dissipates the energy *via* fluorescence and the excited electron returns to the ground state (S_0, figure 14). It has already been mentioned that there are other ways to depopulate the electronically-excited singlet state, namely through thermal (non-radiative) decay and *via* intersystem crossing (ISC), the latter populating the excited triplet state (T_1) from which radiative phosphorescence originates (figure 14, see section 1.1.6).

It was also noted earlier (see section 1.1.6) that a photosensitiser in its excited triplet state ($^3Psen^*$) can interact with molecular oxygen ($^3O_2$) to generate the cytotoxic species singlet oxygen ($^1O_2$, figure 19, see section 1.1.6) and that high yields of singlet oxygen formation (Φ_Δ) are crucial to the success of eradicating diseased cells and tissue *via* photodynamic therapy. In comparison, one of the definitions of a good fluorophore is one with a high ($\Phi_{fl.}$ >0.5) fluorescence quantum yield (the ratio of the number of photons emitted to the number of photons absorbed, with a value between zero and one). Alternatively, if the excited singlet state (S_1) is depopulated by a transition other than fluorescence emission, a fluorophore is deemed to be poor. If a molecule has enough structural flexibility to allow rapid thermal relaxation from the excited singlet state to the

ground state, then these molecules are neither efficient fluorophores nor photosensitisers. Conversely, the structure of a porphyrin macrocycle presents sufficient structural rigidity to inhibit thermal relaxation and prolong the lifetime (τ) of the singlet excited state (S_1), permitting fluorescence or, *via* ISC, population of the excited triplet state (T_1). It is notable at this point, that the ISC of the electron from the excited singlet state to the excited triplet state also lowers the fluorescence quantum yield ($\Phi_{fl.}$) of the fluorophore (*i.e.* it is impossible for a light activated molecule to posses both a high fluorescence quantum yield and a high triplet quantum yield). Although, it is possible for a chromophore to possess a "medium" fluorescence quantum yield and a "medium" triplet quantum yield.

1.1.11.2 Photobleaching

In theory, a fluorophore has an infinite lifetime and thus can absorb and emit photons in an almost cyclical manner; however, this catalytic ability becomes diminished when a fluorophore is damaged. Fluorophores, like any other molecule, are susceptible to damage which can alter their luminescence characteristics. In particular, fluorophores are susceptible to irreversible damage by photochemical reactions; this undesirable process is known as photobleaching and is often an unwilling sacrifice associated with a high fluorescence quantum yield.

Photobleaching, is a process thought to happen when singlet oxygen or other ROS (which have been produced upon illumination) react with the photosensitiser itself, in a manner which reduces the photosensitiser's efficiency for further photosensitisation processes.[3,5,21]

Fluorophores can also be susceptible to fluorescence quenching - a process which reduces their fluorescence quantum yield. Fluorescence quenching is a bimolecular process which results from momentary excited-state interactions, known as collisional (dynamic) quenching or, from the formation of non-fluorescent species in their ground state. Porphyrins are examples of fluorophores that are known to exhibit self-quenching. Their

flat macrocycle allows an efficient π-π stacking arrangement (figure 31) to be achieved; hence, very close proximities between one another can be accomplished, enabling efficient fluorescence quenching.

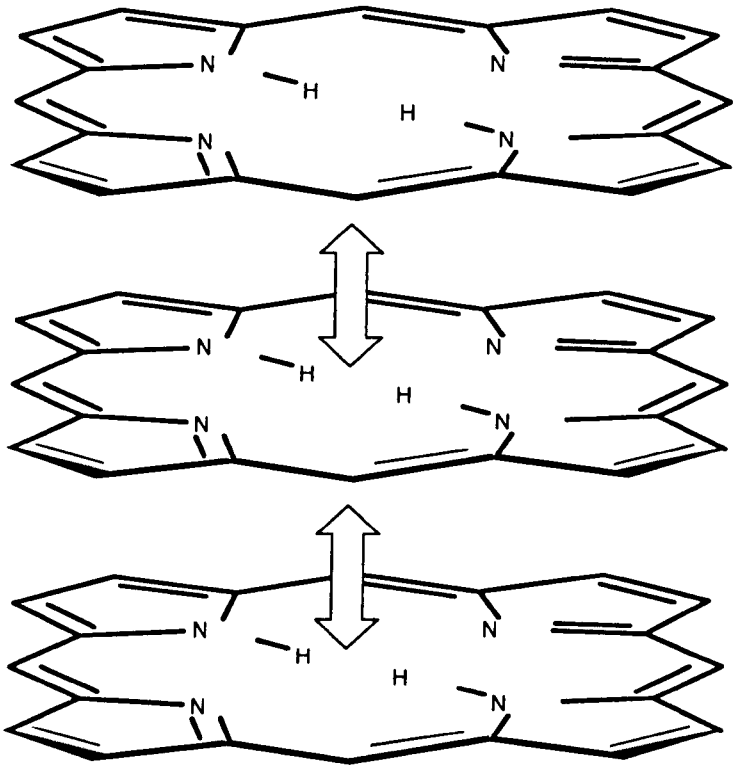

Figure 31 - Porphyrin π-π stacking

1.1.11.3 Förster/Fluorescence Resonance Energy Transfer (FRET)

FRET is a physical phenomenon describing the distance-dependent process of energy transfer (E_T) between two molecules: a donor and an acceptor.

When a fluorescent molecule is illuminated at its excitation wavelength the resulting excited-state fluorophore would normally be expected to decay radiatively *via* fluorescence, generating the fluorophore's characteristic emission spectrum. If however, another molecule (the acceptor) exists in close proximity to this fluorophore (the donor), with its energy state characterised by an absorption spectrum overlapping with the emission spectrum of the donor (figure 32), non-radiative energy transfer may occur

between the two. Resulting in the donor fluorophore returning to the electronic ground state and the acceptor molecule being electronically excited into a higher energy state. This leads to a reduction in the donor's fluorescence intensity and excited-state lifetime and an increase in the acceptor's emission intensity. The acceptor molecule does not have to be a fluorophore for the energy transfer to take place, the only criteria it must fulfil is to be within close proximity to the donor and absorb within the emission spectrum of the donor; under these circumstances the process is termed Förster resonance energy transfer and not fluorescence resonance energy transfer. It is noted that although the term fluorescence is used, energy transfer is not *via* fluorescence but through electronic coupling *via* long range dipole-dipole interactions.

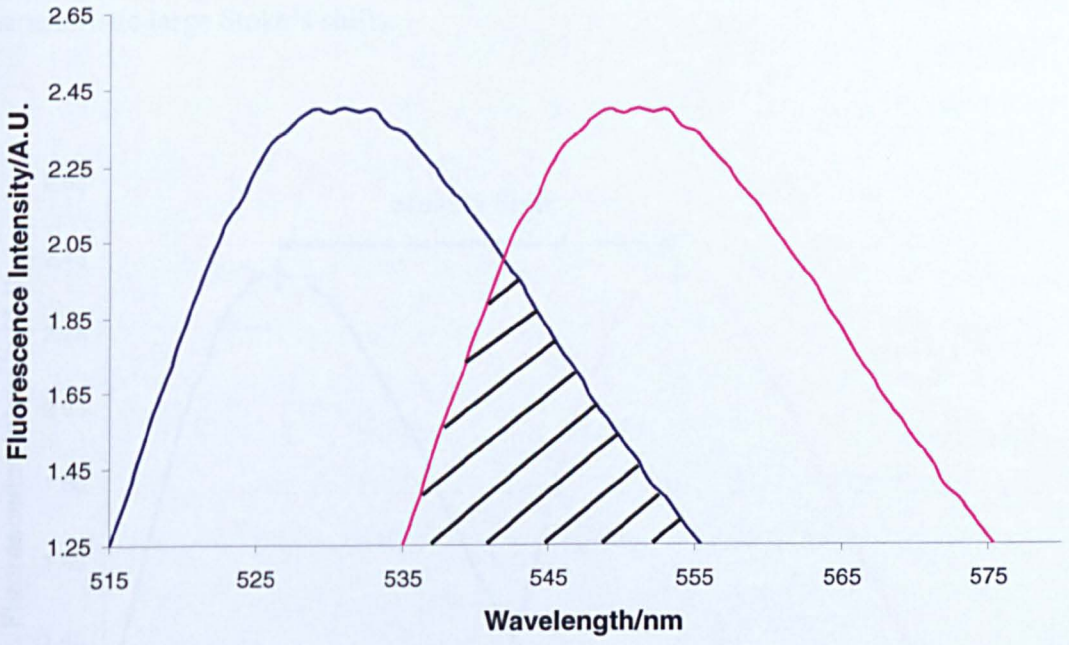

Figure 32 – FRET Effect of Spectral Crossover

Förster/fluorescence resonance energy transfer is a powerful technique which can be utilised to measure distance-dependent interactions on a molecular scale. FRET is particularly suited to measuring distances on the order of 20 – 90 Å; a length below the resolution limit of an optical microscope, thus, highlighting the power of FRET *in vivo* and *in vitro*.

1.1.11.4 Stoke's Shift

When an electron relaxes from an excited singlet state back to the ground state, there is a loss of (vibrational) energy. This energy difference is relayed through the observation of a longer wavelength fluorophore emission spectrum relative to the fluorophore's excitation spectrum. The difference between the two spectra (excitation and emission $\lambda_{max.}$ values) is known as the Stoke's shift (figure 33) and is fundamental to the sensitivity of fluorescence techniques by allowing emission photons to be detected against a low background isolated from the excited photons. A molecule's Stoke's shift is directly related to the time it takes for the excited state molecule to relax from the S_1' vibrational sub-level to its lowest excited state S_1. Porphyrins are known to relax through many discrete electronic sub-levels, prolonging the S_1' to S_1 transition time giving rise to their characteristic large Stoke's shifts.

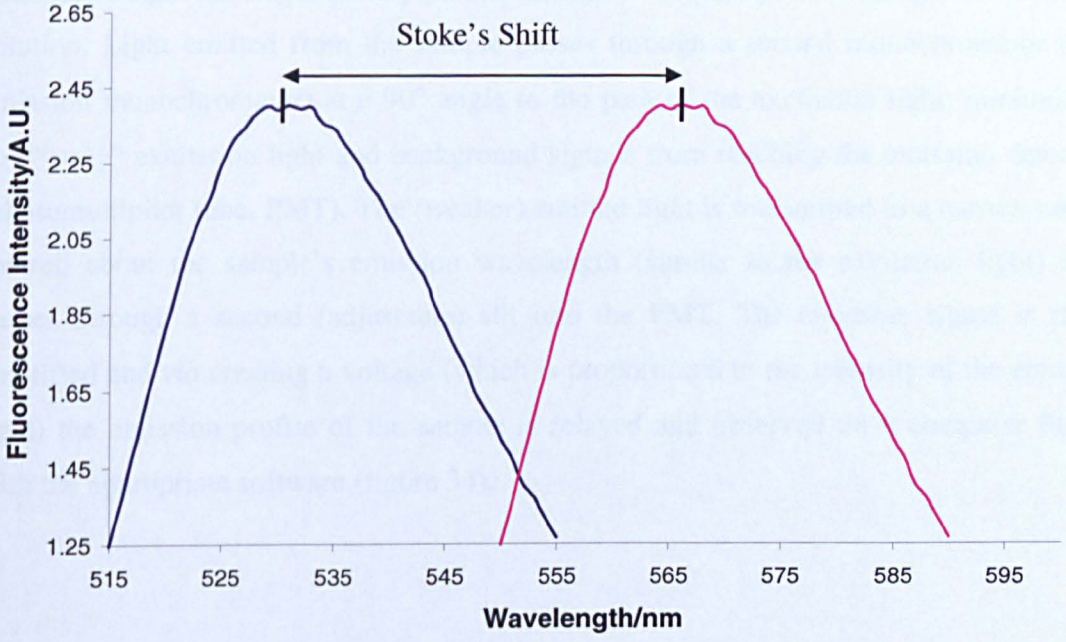

Figure 33 – Stoke's Shift

1.1.11.5 Fluorescence Instrumentation

1.1.11.5.1 Spectrofluorimeter

A spectrofluorimeter typically measures the luminescence properties of chromophores in solutions, as opposed to fluorescence and confocal laser scanning microscopes which observe the two- and three-dimensional spatial distributions of chromophores localised within specimens.

In general, when a spectrofluorimeter light source is ignited photons over a wide energy spectrum (~200-900 nm) strike an excitation monochromator, which in turn selectively transmits a narrow range of light centered about the excitation wavelength of the sample chromophore. The transmitted light then passes through adjustable slits, which through controlling the magnitude and resolution of the light, further reduces the range of transmitted light that subsequently passes through a sample cell containing a luminescent solution. Light emitted from the sample passes through a second monochromator (the emission monochromator) at a 90° angle to the path of the excitation light; minimising any "stray" excitation light and background signals from reaching the emission detector (photomultiplier tube, PMT). The (weaker) emitted light is transmitted in a narrow range centred about the sample's emission wavelength (similar to the excitation light) and passes through a second (adjustable) slit into the PMT. The emission signal is then amplified and *via* creating a voltage (which is proportional to the intensity of the emitted light) the emission profile of the sample is relayed and observed on a computer fitted with the appropriate software (figure 34).

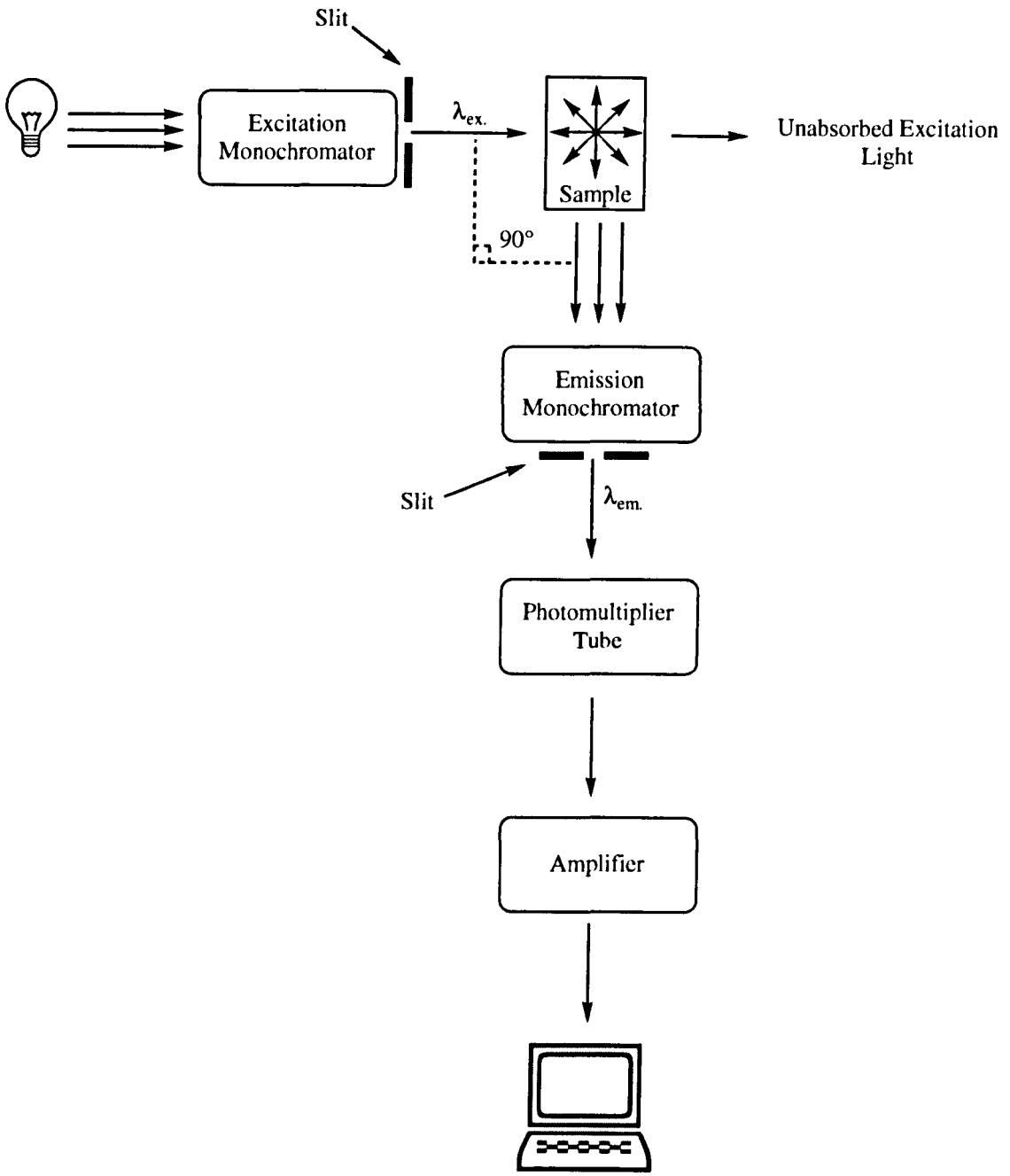

Figure 34 – Simplified Diagram of a Spectrofluorimeter

The light sources generally used in a spectrofluorimeter include: mercury lamps; xenon arc lamps; xenon flash lamps; and lasers. The choice of light source depends on the system used. For example, the mercury lamp is particularly useful when filter sets are employed in the instrumentation; although mercury lamps do suffer from lower intensity

problems compared to xenon arc lamps which are capable of emitting continuous intense and stable light ranging from 300 to 1300 nm.

1.1.11.5.2 Fluorescence Imaging

Fluorophores (soluble in physiological media) allow the study of biological systems with reduced biological toxicity and health hazards in comparison to the traditional methods of employing radioactive isotopes. Nevertheless, fluorescence imaging does have its drawbacks: fluorescence is not as suitable to large scale procedures as magnetic resonance imaging (MRI) and positron emission tomography (PET), although significant progress can be made at the bench by employing fluorescence imaging techniques.

1.1.11.5.2.1 Fluorescence Based Microscopy

Fluorophores in the form of fluorescent dyes can be excited and detected in a number of molecular species and cellular localisations (for example, mitochondria and lysosomes), with fluorescent microscopy being one technique used to image these structures. Excellent temporal resolution of subcellular events can be obtained through fluorescence microscopy with rates lower than 10^{-8} seconds achieved using the appropriate equipment. There are few limitations to the number of cellular structures which can be imaged with fluorescence microscopy. These subcellular structures range from the nucleus to the endoplasmic reticulum.

There are two distinct types of fluorescence microscopy: conventional fluorescence microscopy, known simply as fluorescence microscopy and confocal laser scanning microscopy (CLSM).

A fluorescence microscope is similar to a conventional compound microscope which employs a high intensity lamp or a laser to illuminate the sample field. A system of filters and dichroic mirrors (beam-splitters) is used to direct the light onto the sample. The fluorescence emission from the sample is then received by an objective lens and filtered before being viewed or photographed directly through an ocular lens (figure 35).

However, there is a limitation to conventional fluorescence microscopy. Fluorescence can only be resolved as a function of spatial coordinates in two dimensions *i.e.* the microscope can only focus and resolve fluorescence in a single fixed, focal plane; therefore, the best sample resolution is achieved when the sample depth is as narrow as possible.

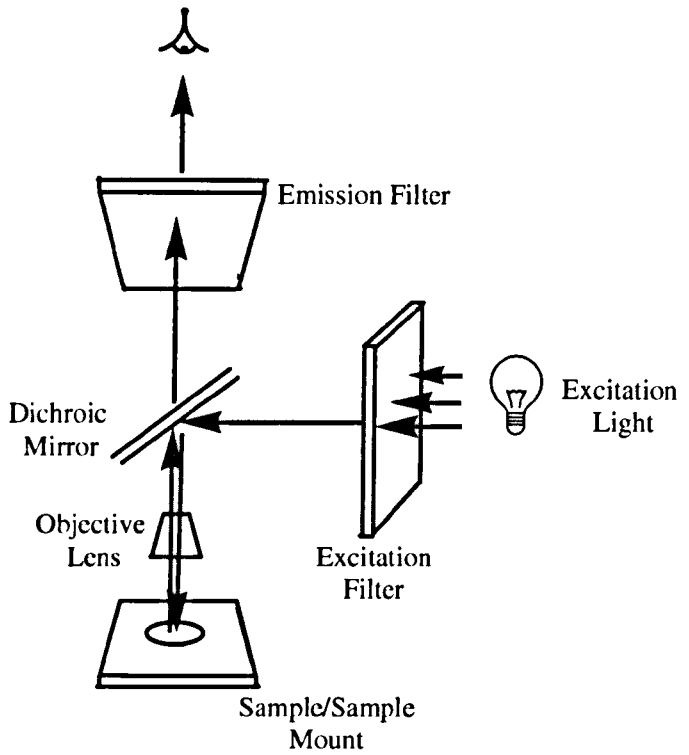

Figure 35 – Simplified Diagram of a Fluorescence Microscope

1.1.11.5.2.2 Confocal Laser Scanning Microscopy

Confocal laser scanning microscopy is an adaptation of conventional fluorescence microscopy (CLSM). A major advantage of CLSM is its ability to image thick objects as a result of its optical sectioning property.

The optical sectioning property of a confocal microscope allows fluorescence to be resolved as a function of spatial coordinates in three dimensions, as opposed to the two dimensions observed with the fluorescence microscope. Confocal microscopy allows the

sample to be scanned "up" or "down"; resolving the fluorescence emitted from each individual focal plane one-by-one. These fluorescence data are then normally merged; resulting in a detailed three dimensional sample image.

A confocal microscope works by focusing the laser light through an objective lens onto the sample. Light is then reflected, or emitted, and focused onto a photodetector *via* a beam-splitter. A confocal aperture or pinhole is placed in front of the photomultiplier tube/detector and an image is built up by scanning the focused spot relative to the object (figure 36). This data is normally stored in the form of digital information within a computer imaging system. By observing the image digitally a vast range of electronic image processing techniques can be applied to the data including: contrast enhancement; subtraction of background fluorescence; and image restoration.

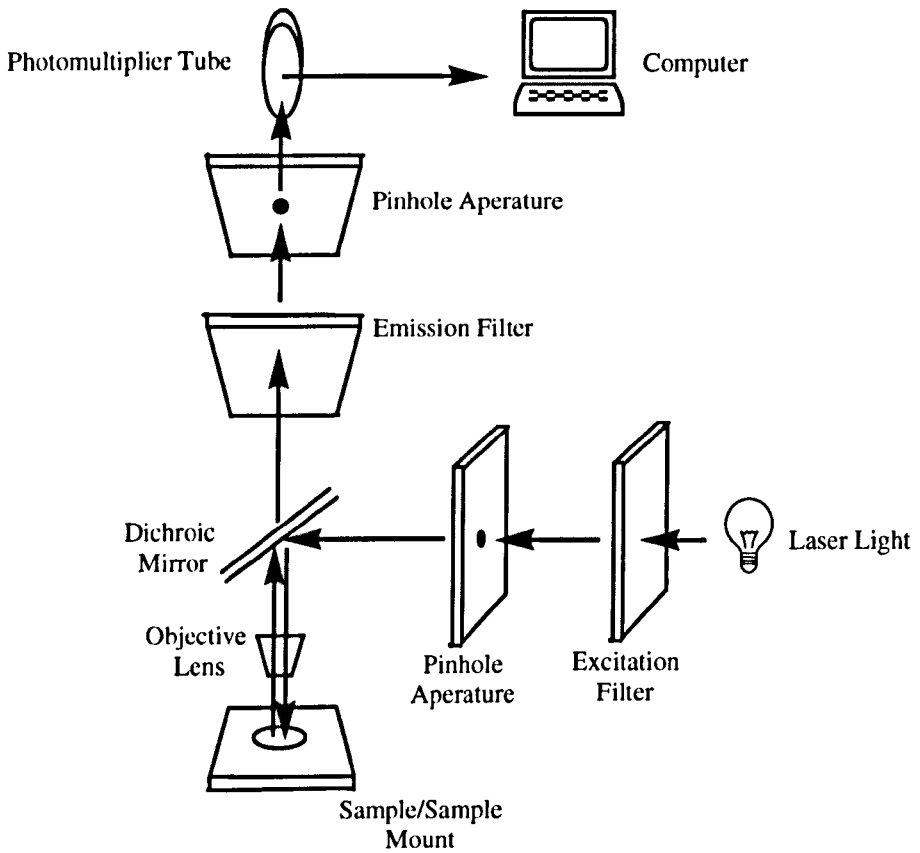

Figure 36 – Simplified Diagram of a Confocal Microscope

There are a number of lasers which can be employed in confocal microscopy, typically covering the ultraviolet-visible range of the electromagnetic spectrum. The choice of laser used is dependent upon the absorption peaks of the fluorophore. The most commonly used laser is the argon-ion laser which has four main fixed excitation lines: 457.9, 476.5, 488.0, 514.5 and 528.7 nm. It is possible to use tunable lasers which offer multiple excitation lines. However, these type of laser sources are generally expensive and difficult to maintain.

The success of both conventional and confocal microscopy is highly dependent on the availability of a range of different fluorescent dye molecules; a range which is constantly improving, along with the skill of the microscopy technician.

1.1.11.6 Fluorophores

The majority of the fluorophores that are employed in biological imaging are composed of an aromatic ring system. This delocalised conjugated system forms the basis of the absorption and emission ability of the fluorophore. In general, as the aromatic ring system increases in size, the absorption wavelength also increases; as too does the fluorescence quantum yield ($\Phi_{fl.}$) of the molecule. The fluorescence quantum yield is also increased by electron donating substituents and ring activators. In contrast, electron withdrawing groups reduce the fluorescence quantum yield of a fluorophore. The presence of heavy atom ring-substituents are observed as having an effect on fluorescence. Heavy atoms attached to aromatic rings are known to enhance the probability of ISC occurring from the excited singlet state to the excited triplet state, decreasing a molecules fluorescence quantum yield. In addition, halogenated aromatic ring systems also subject a fluorophore to fluorescence quenching; iodide substituents are observed to almost entirely eliminating fluorescence (I > Br > Cl).[4]

A large number of fluorophores used are polycyclic aromatic systems. In order to observe fluorescence, the ring systems must be coplanar or in the same dimensional plane; hence, a degree of rigidity should be present. Good examples of fluorophores are the dipyrromethene chromophore and boron-complexed BODIPY analogue (figure 37). The

dipyrromethene is an intense red/orange colour which is non-fluorescent, whereas the BODIPY analogue is completely planar and fluorescent.

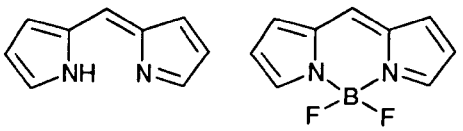

Dipyrromethene BODIPY

Figure 37 – Example Fluorophores

One common feature between fluorescent dyes is their sensitivity to changes in their chemical environment including: the type of media; media pH; buffer components; media polarity; and the presence of dissolved oxygen. These can all affect the fluorescence quantum yield of the dye.

1.1.11.7 Porphyrins and Fluorescence Imaging

In theory, porphyrins should be good examples of fluorescent dyes, with many of the properties to fulfil this criterion discussed earlier (see section 1.1.7). They do generally however, also posses some undesirable luminescent properties, with the most significant their low fluorescence quantum yield ($\Phi_{fl.}$); an inadvertent consequence of their effectiveness as photosensitisers. Good fluorescent dyes typically have fluorescence quantum yields above 0.7. Compare this to the typical fluorescence quantum yields of porphyrins, ranging from 0.1 – 0.2, and it can be seen that very weak fluorescence would be observed from a porphyrin dye.[30,42] The fact that porphyrins are good photosensitisers is another major limitation of their potential to be fluorescent dyes. Photosensitisers by their nature cause irreversible damage or death to cells upon illumination; so as soon as the porphyrin molecules were excited by the appropriate light-energy, serious cell damage or cell death would be incurred. One thought could be to sub-optimally excite the porphyrin; this would have a two-fold affect as: (i) not only would cell damage/death be potentially reduced, so too would the (ii) fluorescence intensity of the dye. It is perhaps

therefore evident why there are no commercial examples of porphyrin-based fluorescent dyes.

However, some use can be drawn from the ability of a porphyrin to fluoresce. For example, this property can be successfully utilised to observe photosensitiser localisation (diagnostic applications) and degree of tumour uptake.

1.1.12 Photophysics

It is important to determine a chromophore's photophysical properties in order to assess its luminescence efficiency; these key features include a chromophore's associated quantum yield (Φ), lifetime (τ) and rate constants (k). These parameters are particularly important for the determination of fluorescence quantum yields ($\Phi_{fl.}$), for example of a new fluorescent dye; or in establishing the potential therapeutic efficacy of a photosensitiser (triplet-state lifetime (τ_T) and yield (Φ_T) and singlet oxygen quantum yield (Φ_Δ)).

A range of techniques and specialised instrumentation exist which allow the determination of such properties ranging from: (i) steady-state luminescence methods, employed in the highly selective and non-invasive fluorescence monitoring of species and widely used in the study of bimolecular reactions; to (ii) time-resolved spectroscopy, applied in the investigation of samples containing multiple luminescent species.[91]

Each of the luminescence techniques are based on a similar principle, mainly differing only in the excitation light source used and the degree of sensitivity which the method can achieve. Steady-state luminescence spectroscopy has sensitivity down to the sub-nM range, with time-resolved spectroscopy demonstrating picomolar sensitivity in the femto second (10^{-15}) range; a consequence of the increased sensitivity time-resolved methods exhibit towards environmental changes, in comparison to steady-state measurements.

The technique which is going to be discussed further is time-resolved emission spectroscopy. This is also known as time-resolved correlation spectroscopy and time-correlated single photon counting (TCSPC).[91-95] The technique works by exploiting the time-dependent nature of luminescence and will be the method of choice for determining the relevant photophysical parameters ($\Phi_{fl.}$, Φ_{Δ} and τ_T/τ_{Δ}) of the photosensitising and analyte-sensitive components of the Project's target system (Chapter 4).

1.1.12.1 Time-Correlated Single Photon Counting Spectroscopy

Time resolved fluorescence spectroscopy (an extension of conventional fluorescence spectroscopy) is a multifunctional method capable of providing kinetic information relating to the concentration and chemical nature of reactive intermediates formed from photochemical reactions. One of the most powerful forms of time resolved spectroscopy is flash photolysis. This technique was developed in the 1950's by Nobel Prize winners (The Nobel Prize in Chemistry, 1967) Norrish and Porter and uses either a laser or discharge lamp to generate a short-duration pulse (flash) capable of initiating the desired photochemical reaction at a user-selectable wavelength. The transient changes in the concentration of the reactants, products, or more commonly the reaction intermediates, are monitored as a function of emission intensity over a defined period of time after the "release" of the excitation pulse. A series of spectra, varying in measurement times, can then be acquired and a time profile of the photochemical species constructed (figure 38). The maximum absorption (vertical line on figure 38) occurs immediately after the laser pulse (flash).

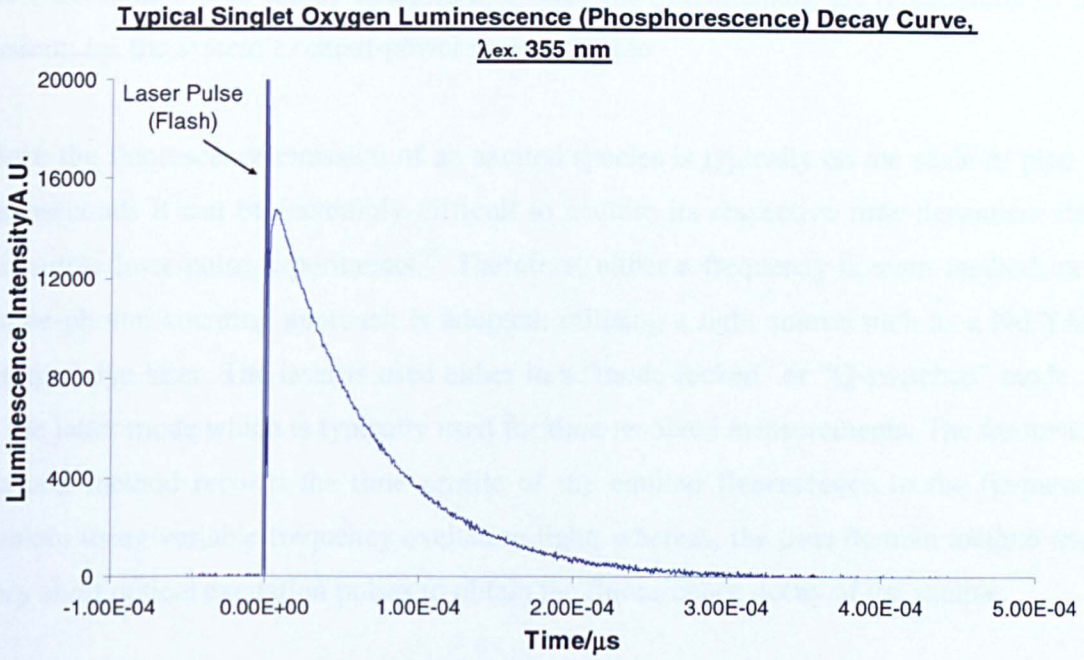

Figure 38 – A Typical Decay Curve

The time dependence of fluorescence emission is far more sensitive to environmental changes than steady state measurements of peak emission intensity or wavelength, since the fluorescence lifetime ($\tau_{fl.}$) of a molecule is very sensitive to its molecular environment. The excited state lifetime of a species can reveal a number of important things about the state of the fluorophore. Time resolution measurements can be performed in a number of manners, depending on the sensitivity and time resolution required, these include;

(i) Fast detection electronics (nanosecond sensitivity and slower)

(ii) Streak-camera (picoseconds or slower)

(iii) Optical gating (femto to nanosecond sensitivity)

The latter method ((iii)) operates *via* a short-pulse (flash) acting as a "gate" for the detection of the emitted (fluorescence) light. Only the emitted light which arrives at the detector simultaneous to the time of gate "pulsing" is detected. By using a gating system

the flash light source can be operated at a fixed rate, maintaining the temperature of the system, *i.e.* the system's output-power remains stable.

Since the fluorescence emission of an excited species is typically on the scale of pico to nanoseconds it can be incredibly difficult to acquire its respective time-dependent data *via* single laser pulse experiments.[96] Therefore, either a frequency domain method, or a single-photon counting approach is adopted, utilising a light source such as a Nd:YAG pumped dye laser. The laser is used either in a "mode-locked" or "Q-switched" mode. It is the latter mode which is typically used for time-resolved measurements. The frequency domain method records the time profile of the emitted fluorescence in the frequency domain using variable frequency excitation light; whereas, the time domain method uses very short optical excitation pulses to obtain the fluorescence decay of the sample.

A "Nd:YAG laser" is a solid-state laser which uses a neodymium-doped yttrium aluminium garnet crystal as a lasing medium. The laser is optically pumped either *via* a flash or continuous gas discharge lamp, or through a laser diode system, emitting in the infra-red region of the electromagnetic spectrum ($\lambda_{em.}$ 1064 nm). Pulsed Nd:YAG lasers are typically operated in the "Q-switched mode"; an optical switch ("cavity dumper") is inserted into the laser cavity and "opens" only when a maximum population inversion of the neodymium ions exists. The laser beam then traverses through the cavity and depopulates the excited lasing medium. The parameters, which can be typically accomplished in this mode, are flash (pulse) durations of less than 10 nanoseconds and a power output of up to 20 megawatts.

For many applications the emission wavelength of the laser light may be too long to appropriately excite the sample species. In such cases the infra-red light from the Nd:YAG laser can be "frequency doubled" or "tripled". This is achieved by passing the light through special crystals to obtain visible (532 nm, second harmonic) or ultra-violet (355 nm, third harmonic) light; such non-linear optical materials include lithium triborate and ammonium dihydrogen phosphate crystals. The mixed laser beam is then able to pass through a filter (such as a cobalt sulphate solution) to remove any remaining unwanted light (for example green light (532 nm)) from the Nd:YAG output. The majority of the

"desired" light (for example ultra-violet light) from the beam is subsequently reflected from a beam-splitter into the sample cell/cuvette.

1.1.12.2 Quantum Yields

The idea of photochemical quantum yields (Φ) were introduced to the reader in section 1.1.6 and are one of the key measurements made in the photochemical techniques described above. According to the Stark-Einstein Law;

"every photon absorbed by a species excites only **one** molecule of the species", this was later refined to "one **particle** is excited for each quanta of radiation absorbed" (Second Law of Photochemistry).

The quantum yield can therefore be described as the number of molecules undergoing the process of interest (formation of product or consumption of reactants) for each quantum of radiation energy absorbed (equation 1). For example, to determine the quantum yield of singlet oxygen (Φ_Δ) produced by a photosensitiser, the number of molecules of singlet oxygen ($^1O_2$) produced as a function of the number of photons of radiation absorbed must be determined.[94,97]

$$\Phi = \frac{\text{number of species undergoing process of interest}}{\text{number of photons absorbed}}$$

Equation 1 – Quantum Yields

Quantum yields may also be expressed in terms of the rate of the reaction;

$$\Phi = \frac{\text{rate of chemical process/event}}{\text{intensity of absorbed light}} = \frac{d[x]/dt}{I_{abs}}$$

Hence, the quantum yield(s) for a species cannot be greater than unity ($\Phi \leq 1$), unless a secondary reaction or a series of chain reactions are taking place within the sample, in which case the quantum yields are respectively $\Phi \leq 2$ and $\Phi \geq 2$.

The quantum yield value (and the variation of this value under different reaction conditions) can yield important information and clues to the photochemical mechanism(s) taking place during a reaction. However, the quantum yield of a species should not vary with temperature, concentration or wavelength; for such photochemical investigations the primary concern is not with the experimental conditions the sample is subject to, but with the requirement that the species have a strong absorption at their λ_{max}.[94] It is important to remember that luminescence lifetimes are highly solvent dependent; electronic relaxation (for example, of singlet oxygen) is highly forbidden.[29,98]

1.1.12.3 Singlet Oxygen Quantum Yields

The quantum yield of formation of singlet oxygen (Φ_Δ) is determined *via* the following equation:

$$\Phi_\Delta = \Phi_T \frac{k_{\Delta O_2}[O_2]}{(k_{\Delta O_2} + k_{\Sigma O_2})[O_2] + k_{nr} + k_r}$$

where, Φ_T = the quantum yield of triplet state formation

$k_{\Delta O_2}$ = the rate constant for quenching by ground state oxygen ($^3\Sigma_2$), in the generation of singlet oxygen ($^1\Delta_g$)

$k_{\Sigma O_2}$ = the rate constant for quenching by ground state oxygen to give the higher-energy singlet oxygen ($^1\Sigma_g$) species

k_{nr} = the rate constant for non-radiative (nr) deactivation of the triplet state (T_1)

k_r = the rate constant for radiative (r) deactivation of the triplet state (T_1)

In general, quenching of the excited triplet state (T_1) by molecular oxygen occurs much faster than the other deactivation processes. Therefore, radiative (r) and non-radiative (nr) decay constants are considered to be negligible, allowing the above equation to be further simplified:

$$\Phi_{\Delta} = \Phi_T \left(\frac{k_{\Delta O_2}}{k_{\Delta O_2} + k_{\Sigma O_2}} \right)$$

The collection of the rate terms effectively affords the fraction of the excited triplet state molecules quenched by molecular oxygen to produce singlet oxygen ($^1\Delta_g$) and hence, can be represented as S_{Δ}, simplifying the equation even further:[9]

$$\Phi_{\Delta} = \Phi_T S_{\Delta}$$

The excited electronic state of singlet oxygen can be deactivated in a number of ways; namely (i) non-radiative decay; decay through transfer of vibrational energy to surrounding solvent molecules or chemical/physical quenching by secondary species and (ii) *via* radiative decay (luminescence).[99] It has been suggested that the major relaxation mechanism of singlet oxygen ($^1\Delta_g$) is *via* the non-radiative decay route, hence the latter mechanism (phosphorescence) which gives rise to the characteristic singlet oxygen emission peak around 1270 nm is **weak** (figure 39). However, both the non-radiative and radiative decay routes/constants are solvent dependent; the non-radiative relaxation mechanism is controlled by solvent molecules acting as an energy sink through absorption of the vibrational energy of the excited state molecules. Singlet oxygen may also be detected through the use of chemical traps and quenchers, such as cholesterol (see section 3.7) and diphenylisobenzofuran; although, the latter methods are of limited use since side reactions and solubility problems exist.[29,39,100]

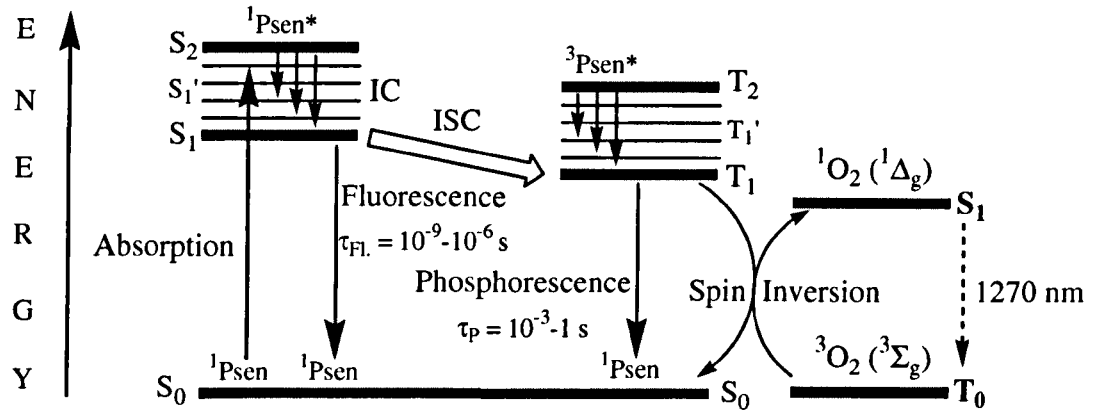

Figure 39 – Simplified Jablonski Diagram

To measure the quantum yield of a species in absolute terms is a complex process, it is therefore more common practice to perform comparative actinometry: the measurement of the number of photons absorbed by a species, with a standard photosensitiser of known quantum yield under comparative conditions. Particularly important, for experiments undertaken with broad band excitation sources, is the identification of a standard sample with an absorption spectrum similar to the species under investigation. In addition, the same solvent should be used for the luminescent samples under investigation as used with the standard reference, since singlet oxygen is known to have a solvent-dependent lifetime; solvent perturbations are known to enhance the probability of spin-forbidden transitions occurring.[29,30,94]

1.1.12.4 Luminescence Lifetimes

The lifetime (τ) of an excited species is the average time the species remains in an excited state before emitting a photon of energy. The fluorescence lifetime ($\tau_{fl.}$) of a species is the average time the species remain in the excited singlet state (S_1). In comparison, the excited triplet state (T_1) or phosphorescence lifetime (τ_T) of a species is the time a species remains in the excited triplet state before relaxing back to the ground state *via* phosphorescence (figure 39). It is from this excited triplet state that the singlet oxygen lifetime (τ_Δ) can be determined, *i.e.* the probability that an excited photosensitiser (S_1,

$^1Psen^*$) converts to the excited triplet state (T_1) and is quenched by molecular oxygen ($^3O_2$). Each individual excited molecule emits energy (photon) in a random manner after excitation. Therefore, a number of the excited species will fluoresce/phosphoresce **before** the average emission lifetime, as well as a number of the excited species relaxing back down to the ground state **after** the average lifetime. The fluorescence and phosphorescence lifetimes of species typically varies in magnitude from 1-10 nanoseconds (fluorescence) and 0.01-1 second (phosphorescence) and can yield important data about the kinetics of the relaxation/decay processes an electronically excited species undergoes.

1.1.12.5 Singlet Oxygen Measurements

The excited triplet state of a photosensitiser can be quenched by molecular oxygen ($^3\Sigma_g$) to generate highly reactive singlet oxygen ($^1\Delta_g$ and $^1\Sigma_g$, see section 1.1.6). The singlet oxygen has a lifetime in gaseous media of up to several minutes; a result of the spin-forbidden nature of the decay transition ($^1\Delta_g \rightarrow {}^3\Sigma_g$). Both the fraction of triplet-state photosensitiser that is quenched by ground state molecular oxygen (which leads to the production of the reactive toxic species) and the quantum yield of formation of singlet oxygen (Φ_Δ), can be determined as a function of time by luminescence spectroscopy techniques (weak singlet oxygen phosphorescence at 1270 nm, figure 39); the total number of singlet oxygen luminescence photons observed after each pulse is proportional to the concentration of singlet oxygen produced by that pulse.

The key parameter for singlet oxygen reactions is the quantum yield of formation of singlet oxygen; these findings will reveal how efficient molecular oxygen ($^3O_2$) is at quenching the triplet state of a photosensitiser ($^3Psen^*$, T_1), and if the ROS is a desired product (for example, in eliciting cellular damage and death), this parameter is important in determining the efficiency of ROS generation and the potential efficacy of the photoinduced effect. Ideally, the quantum yield of singlet oxygen formation should be greater than 0.5 (Φ_Δ = 0.62 tetraphenylporphyrin (organic solvent) and 0.74 tetra-(*N*-methylpyridiniumyl) porphyrin (water) accomplished to date).[29,30]

The lifetime of the ROS is also important, since singlet oxygen is known to have a short radius of action; hence, its lethal effects can only be executed within close proximity to its site of generation (see section 1.1.6); however, the main criterion is a high quantum yield of formation. If the photosensitiser is a poor singlet oxygen generator, then a high dose of photosensitiser would be required to effect the same response as a more efficient photosensitiser, regardless of its subcellular localisation.

1.1.12.6 Instrumentation

The instrumentation employed in time resolved spectroscopy is similar to that used in steady-state experiments; with the exception that the time resolved technique uses a pulsed excitation light source rather than a continuous source, along with a gated emission detection method. An excitation beam with a narrow wavelength range is directed at the sample. Solution or solid phase samples, temperature controlled solutions (325-377 K) and even human skin have been investigated and the luminescence emission of the sample is measured at a 90° angle to the excitation light (see section 1.1.11).[91] The detected emission then enters a detector which registers and relays the emission data to a personal computer (PC) ready for analysis (figure 40).

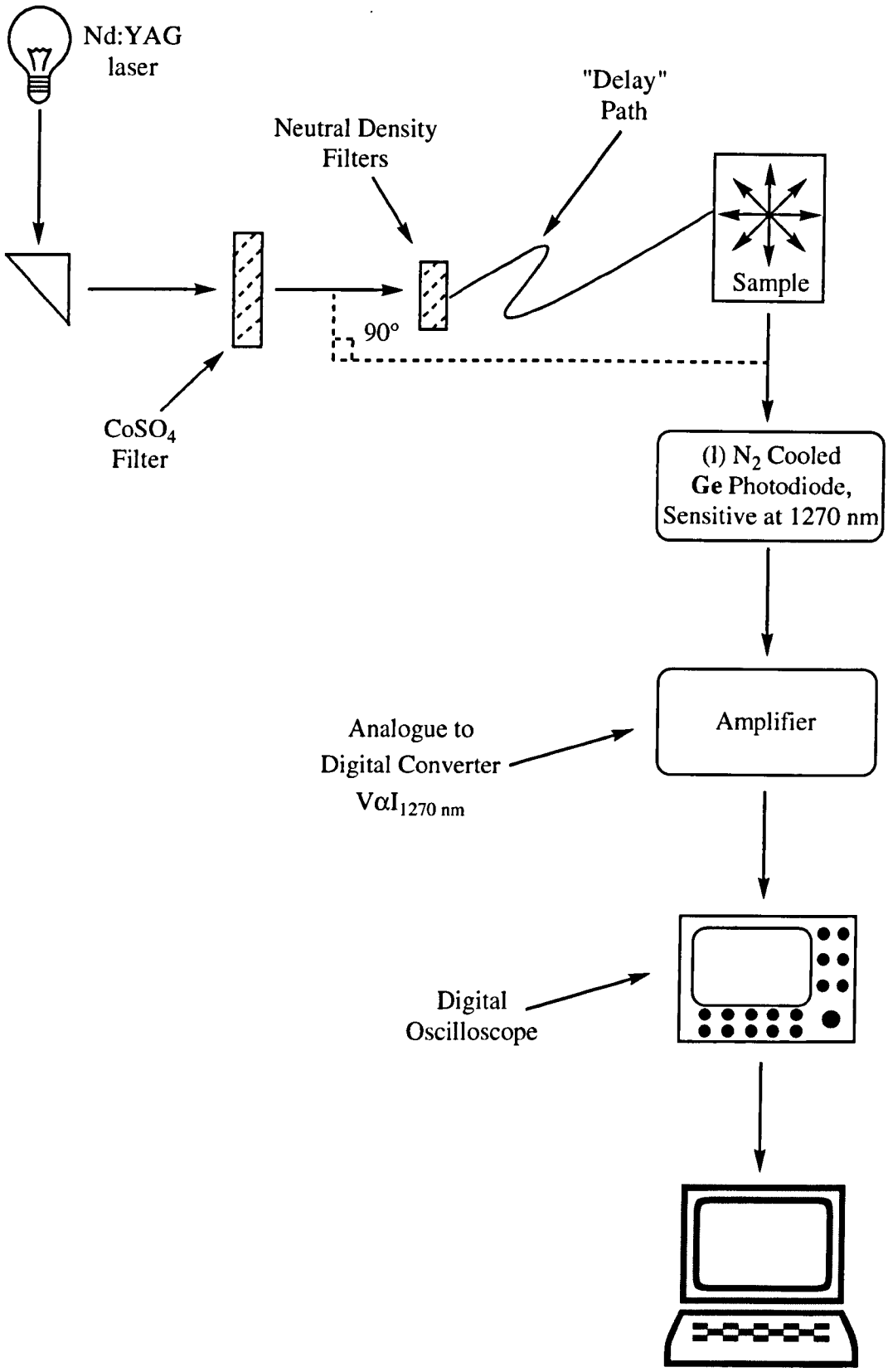

Figure 40 – Simplified Diagram of Time-Resolved Spectroscopy Instrumentation

The two main types of pulsed light sources employed in time resolved spectroscopy are flash lamps and lasers - the latter more powerful laser is the preferred source. Lasers are: (i) highly monochromatic, allowing selective excitation; (ii) permit very short (duration) light pulses to be used, useful for high resolutions; from which (iii) high powers can be achieved (beneficial in experiments which require high intensity light sources), for example, for "forbidden" transitions; and (iv) have a high peak beam intensity, also useful for experiments concerned with "forbidden" transitions.[95] A number of considerations need to be taken into account when using laser sources. If a laser is termed "free-running" then the phenomenon known as "jitter" (the variation in the time between pulses) will be relatively low and a "pre-trigger" can be employed to trigger the timing generator.[92] If the time between this pre-trigger and the output of the laser is sufficiently long enough, it is possible to adjust the timing generator to catch each laser pulse. However, if the time between pre-trigger and laser output is insufficient then the delay can be appropriately adjusted to catch the subsequent pulse. If on-the-other-hand, the jitter experienced by the system is significant, the acquisition of data can be "triggered off/from" the laser pulse itself; circumventing the need for a pre-trigger. "Triggering off" from the laser flash can be achieved by diverting a small percentage of the laser beam to a high-speed photodiode, such as a germanium diode. It is important that the laser pulse is then "delayed" long enough to permit the photodiode trigger to reach the: (i) timing generator; (ii) for the timing generator to synchronise with the incoming trigger; and (iii) for the gated pulse to reach the detector. The laser flash can be delayed by increasing the (i) optical path the laser beam travels in air or (ii) by launching the laser pulse into a fibre optic cable of the required length.

There are three key features in a time resolved spectroscopy detector which are desirable: (i) sensitivity; (ii) repetition rate; and (iii) response time.[91] It is preferable for a detector to have a significantly high detection rate since the decay signal emitted from the excited species is relatively weak, typically only a few fluorescence photons per pulse. Repetition rate is important since most pulsed-laser sources operate in the kilo hertz (kHZ) range. If the detector cannot gate at least as fast as the laser then some of the laser pulses will be missed. This problem can be particularly prevalent when ultra-violet light sources are used. Image intensifiers in the instrumentation are sensitive to radiation in

this region of the electromagnetic spectrum, therefore even when the intensifier is not turned on, light is still able to reach the detector, creating a misleading and unwanted signal. Time resolution is an important parameter; with a long laser pulse width, or intensifier gate width, a detector with a short time resolution is able to differentiate between the excitation pulse and the emission energy ("deconvolution").

1.1.12.7 Data Analysis

The luminescent data output from the emission detector is amplified and AC coupled to a digital oscilloscope. The oscilloscope digitises and averages the emission/decay transients and displays the luminescent intensity of the species against time at a set wavelength. The voltage at the oscilloscope has a linear correlation with the intensity of light detected by the photodiode/PMT; the signal from the photodiode/PMT (or if used, amplifier) and the vertical amplitude of the pulse are proportional to the light intensity; *i.e.* the time difference between the two separate light pulses is known and the emission spectrum of the sample, at a given period of time post-excitation, is built-up. Evaluation of the data at gradually increasing time intervals reveals the pattern of luminescence decay the excited species undergo; the decay curve formed is represented by the pulse amplitude. This data is then relayed to a PC where it is analysed; for example, the reiterative least-squares algorithm can be fitted to the series of (time-resolved) decay curves, from which the average lifetime of the species can be determined. For singlet oxygen measurements, the total number of singlet oxygen luminescence photons after each pulse is proportional to the concentration of singlet oxygen generated by that pulse.[101] A number of alternative mathematical techniques exist which may be applied to the analysis of single photon counting data in addition to the aforementioned process. These include, "straight line fitting", "phase plane plot" and "Fourier transforms", for which the reader is referred to the "Data Analysis" Chapter (6) of the O'Conner and Philips text on Time Correlated Single Photon Counting for further explanations.[102]

1.1.12.8 Decay Curves

Each component of the initial excitation distribution decays at a different rate, therefore the population distribution of excited states changes with time and the luminescent data collected takes the form of a decay curve. It is this change in distribution that gives the decay curve its particular shape and causes the deviation from first-order kinetics (figure 38).[103] Subsequent mathematical analysis allows the calculation of the species' lifetime, as well as rate constants for luminescent decay, in the presence and absence of quenchers.

1.1.12.9 Least-Squares Analysis

Although the significance of results generated from least-squares curve fitting has been highlighted by a number of researchers, the algorithm is probably the most widely used deconvolution technique for single photon counting data. It has been successfully applied in the generation of "good" results, particularly in comparison to other techniques and "better accounts" for instrumentation noise than some of the other analysis methods.[102,104] The nature of the technique is based on a statistical procedure, therefore it is important that the decay parameters produced from the method are checked for consistency and compared with independent experimental results (reference standards).

The basic principle of the method is to minimise a given quantity which expresses the difference between the acquired data and a fitted function. This quantity is known as the χ^2 value and can be expressed as;

$$\chi^2 = \sum_{i=n_1}^{n_2} \frac{[I_0(t_i) - Y(t_i)]^2}{I(t_i)}$$

where,

n_1 = the first data channel

n_2 = the last data channel

$Y(t_i)$ = the fitting function

$I_0(t_i)$ = the correction variance

$I(t_i)$ = the uncorrected count

There appears to be no "official" upper limit set for χ^2 values, but it is generally accepted that a "good" χ^2 value ranges from 0.8-1.2; although, ideally the closer the value to unity, the better the "fit". However, in some cases higher values have been accepted. Although, values as high as 1.5 should be carefully scrutinised and are usually symptomatic of a significant deviation from the theoretical model or from artefacts in the sample/system.[102,104] Values much lower than unity (≤0.75) are usually the result of data for which an insufficient number of counts have been made/collected.

The fitting algorithm also generates a residual functional (calculated values – observed values), which when successful fits have been achieved, the "normalised" residual (plotted against the channel number) should be randomly distributed about zero. Thus, a residual fit about zero and a χ^2 value close to unity are a clear indication of a good fit to the experimental data, from which the luminescence lifetime of the species can be calculated.[102,104]

1.1.13 Porphyrin Synthesis II

Porphyrins may be synthesised *via* a number of different synthetic routes, with their synthetic utility increased by substitution at the *meso* and/or *β*-positions on the porphine macrocycle (figure 1, see section 1.1.4).

1.1.13.1 *Meso*-Substituted Tetraphenylporphyrins

Porphyrins substituted at their *meso*-positions seem to be the more studied examples of substituted porphyrins, with tetraphenyl (TPP) derivatives being the most common. One of the simplest routes to monofunctionalised porphyrins is the result of an acid-catalysed condensation between pyrrole and stoichiometric quantities of benzaldehyde(s) (scheme 3). This route is well known and was first reported in the mid to late 1930's by Rothemund. The low yielding synthetic strategy was later enhanced by Adler and co-workers in the 1960's.[14-17]

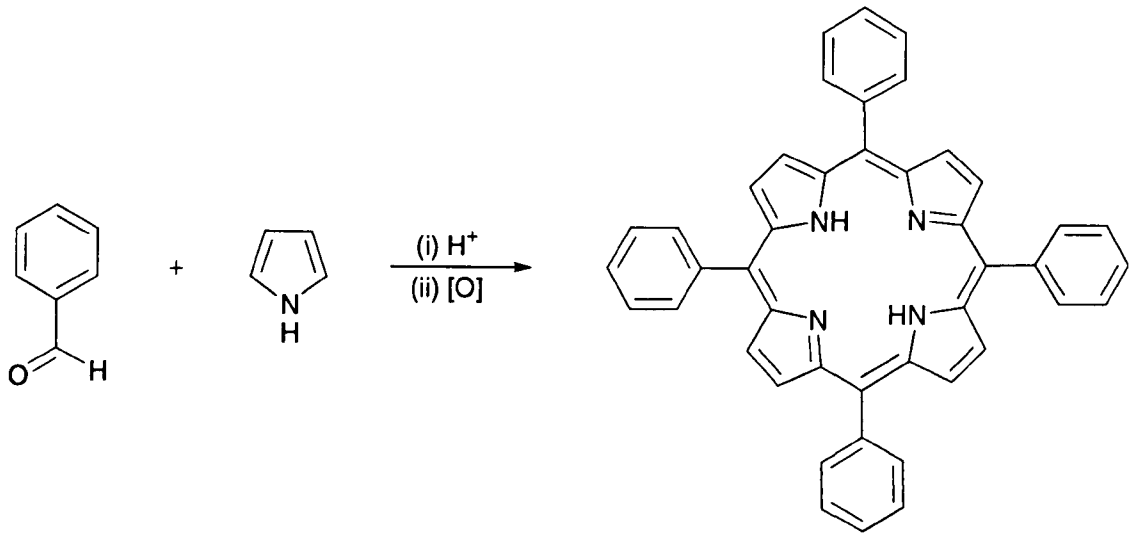

Scheme 3 – Tetraphenylporphyrin Synthesis

Instead of reacting pyrrole and a benzaldehyde in sealed tubes for twenty four hours (85-90°C, formaldehyde in methanol) or forty eight hours (220°C, pyridine), Adler allowed the starting materials to reflux in propionic acid for thirty minutes, open to the air: a much more facile procedure.[105,106] Although Adler's method gave the desired tetraphenylporphyrin in higher yields (up to 20%) there was a drawback. Condensation of pyrroles or benzaldehydes bearing acid-sensitive functional groups was not permitted. More recently, this set back was overcome by Lindsey and co-workers who developed a much milder set of conditions, using only acid catalysis and mild heating to afford the desired tetraphenylporphyrin (scheme 4); facilitating the condensation of less stable benzaldehydes and minimising their potential decomposition during the reaction.[17] Lindsey's method affords higher yields (30-40%) than the Adler method, since an equilibrium porphyrinogen (**A**) concentration is allowed to establish under inert conditions before the addition of the oxidants.

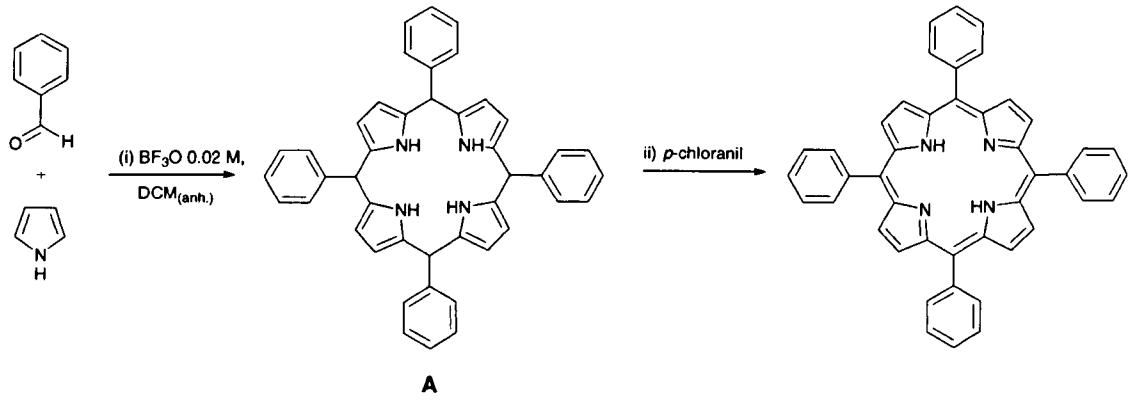

A

Scheme 4 – Lindsey Tetraphenylporphyrin Synthesis

The Rothemund, Adler and Lindsey methods all have one common drawback - the need for careful chromatographic separation of the products. If two differently substituted starting benzaldehydes are used (scheme 5), a total of five different porphyrins will be produced, including the desired monofunctionalised A_3B porphyrin, along with the by-products comprising of two symmetric porphyrins A_4 and B_4, the AB_3 and the *cis* and *trans* isomers of the A_2B_2 porphyrin. The formation and subsequent removal of these by-products reduces the overall yield of the desired porphyrin. However, the formation of these by-products can be minimised by optimising the relative concentrations of the two benzaldehydes utilised in the mixture. Yields for the symmetrically substituted porphyrin afforded from this type of methodology are typically in the order 20%, whereas the yields for the desired monofunctionalised porphyrin are somewhat lower at around 5%: the consequence of the significant quantity of linear polypyrrolic derivatives produced. However, the equilibrium between the concentrations of polypyrrole and benzaldehyde derivatives is strongly shifted away from the formation of the polypyrrolic derivatives and towards the formation of stable tetrapyrrolic products, *i.e.* the formation of the porphyrin macrocycle is driven by the aromaticity of the resulting molecule.

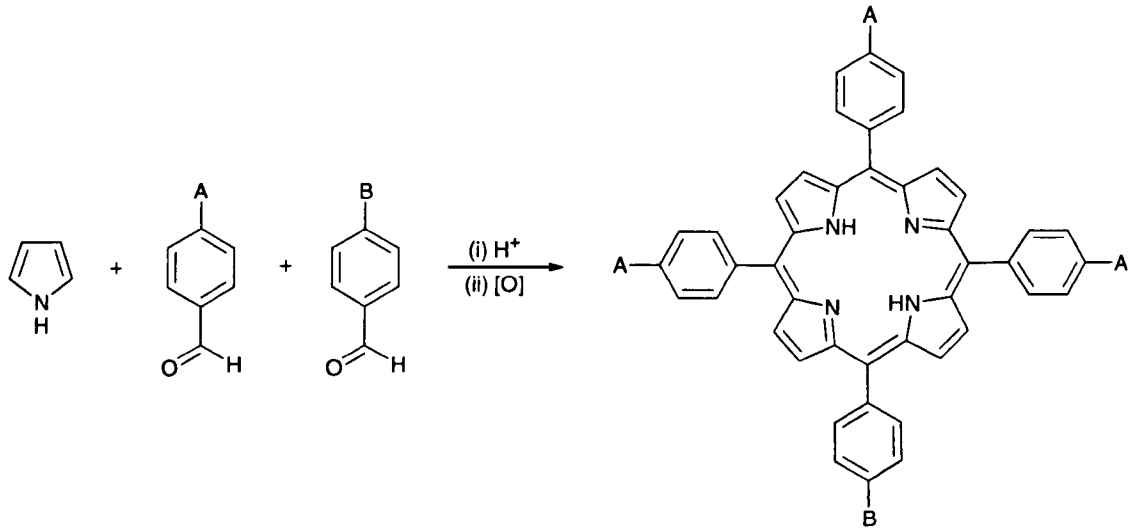

Scheme 5 - Synthesis of Monofunctionalised Tetraphenylporphyrin

1.1.13.2 β-Substituted Porphyrins

β -substituted porphyrins, such as octaethylporphyrin, are generally synthesised *via* the cyclotetramerisation of four substituted pyrrole units (scheme 6).[15,17] The pyrrolic diethyl ester (often used as a starting material) is reduced *in situ*, followed by acid catalysed cyclisation and oxidation to yield the octaethylporphyrin in good yields (≤66%).[3,107] The formed octaethylporphyrin shows enhanced solubility in organic solvents and exhibits a greater degree of stability compared to the unsubstituted porphine.

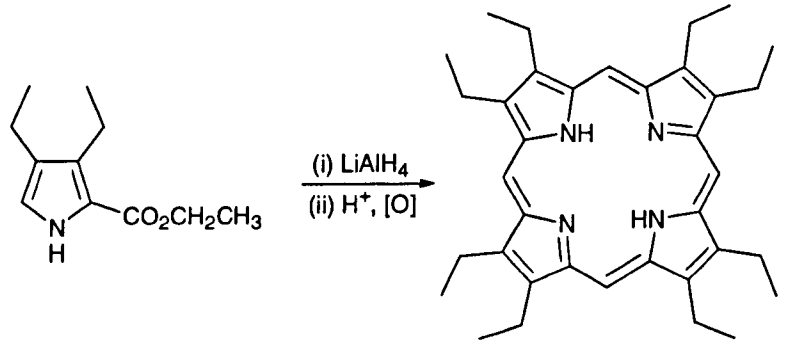

Scheme 6 – Octaethylporphyrin Synthesis

Unfortunately, there are drawbacks to *meso* and β-substitutions. In addition, to the need for chromatographic separation, *meso*-substituted porphyrins have increased steric hindrance inferred, for example, by the presence of phenyl rings (TPP), limiting further modification. The drawback associated with β-substituted porphyrins is the steric hindrance conferred onto the β-positions, making them less accessible to future key optical and electronic modifications; for example, the synthesis of chlorins and bacteriochlorins (figure 23).

1.1.13.3 Diphenylporphyrins

The synthesis of diphenylporphyrins facilitates either *meso* or β-modifications to take place. 5,15-Diphenylporphyrins (scheme 7) have two vacant *meso*-positions and minimum steric hindrance around the β-positions in comparison to octaethylporphyrins (scheme 6), making these positions more readily accessible towards incoming reagents. The relative ease of diphenylporphyrin synthesis and the overall yield is dictated by the starting reagents utilised in their synthesis.

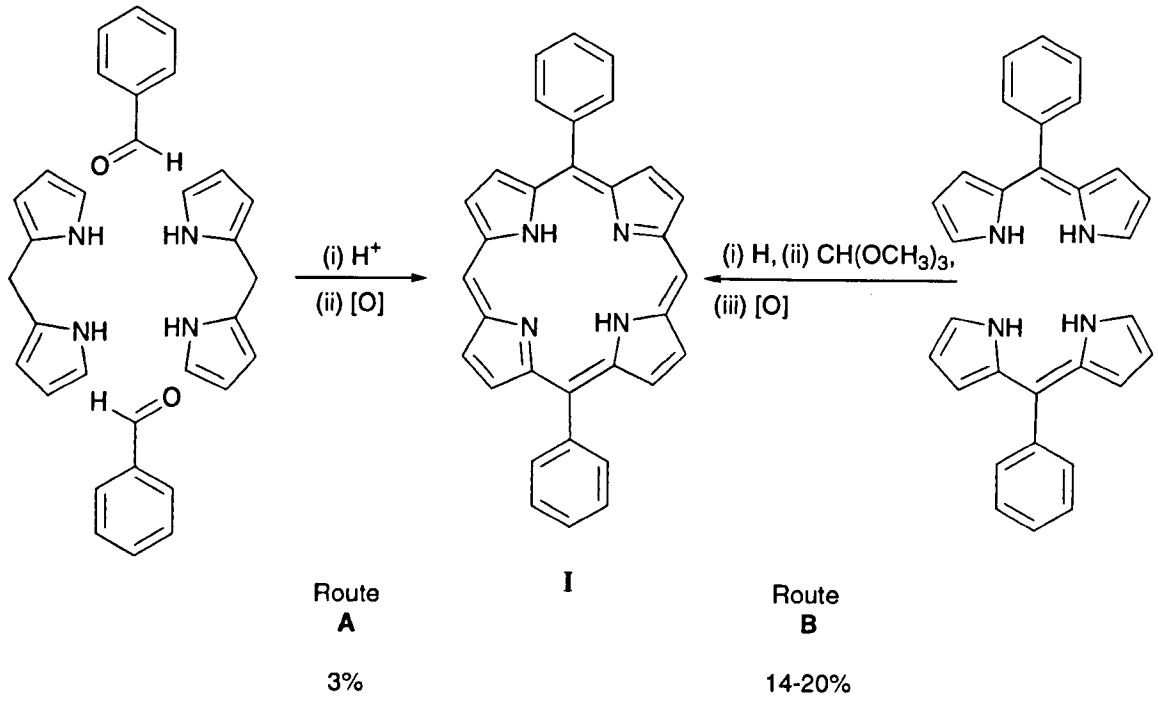

Scheme 7 – 5,15-Diphenylporphyrin Synthesis

A number of synthetic routes to symmetric and asymmetric diphenylporphyrins using dipyrromethanes exist.[15,108-110] Symmetric diphenylporphyrins ("I", scheme 7) can be synthesised *via* the condensation of benzaldehyde and dipyrromethane (route **A**), with the benzaldehyde acting as the source of the two bridging *meso*-carbons in the porphyrin. Diphenylporphyrin synthesis following this method was first reported in 1968 by Treibs and co-workers. However, the overall reaction yield was very poor at only 3%, reportedly a result of the instability associated with dipyrromethanes. Boyle and co-workers later reported an improved synthesis of the same symmetric porphyrin ("I") using 5-*meso*-phenyldipyrromethane (route **B**); a route now most commonly used to afford symmetric diphenylporphyrins.[109] A further route was described by Baldwin and co-workers demonstrating the condensation of 5-*meso*-phenyl-3,4,7,8-tetramethyl-dipyrromethane with trimethylorthoformate, in dichloromethane at room temperature followed by air oxidation of the intermediate porphyrinogen, to afford the 5,15-diphenyl-2,3,7,8,12,13,17,18-octaalkylporphyrin (30% yield, scheme 8).[111]

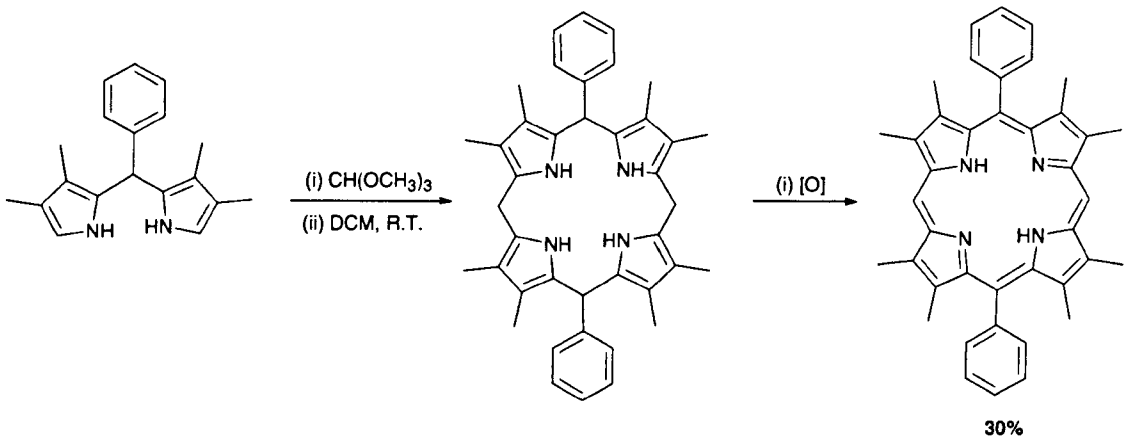

Scheme 8 – Baldwin Diphenylporphyrin Synthesis

Asymmetrically substituted diphenylporphyrins (scheme 9), synthesised *via* the above described routes, can only be isolated by chromatographic separation from the isomers (produced through the mixed condensation reaction). The desired diphenylporphyrins are therefore afforded in low yields.

In order to minimise the outcome of mixed condensation reactions and afford only the desired asymmetric diphenylporphyrin (A′B′), the ability of each reagent (A′ or B′ dipyrromethane) to react with itself should be minimised. This can be achieved by synthesising the individual dipyrromethanes (A′ or B′) with both *meso*-carbons in place, before forming the porphyrin macrocycle. With no external source of *meso*-bridging carbon atoms (-CHO), there is only one possible product - the desired asymmetric porphyrin (A′B′, scheme 9).

MacDonald and co-workers first reported this type of methodology in the early 1960's, with good yields for uroporphyrin II (65%) and uroporphyrin III (55%).[112] Macdonald's methodology (scheme 9), commonly referred to as a "2+2" reaction, has since become a common means to synthesising asymmetric diphenylporphyrins.

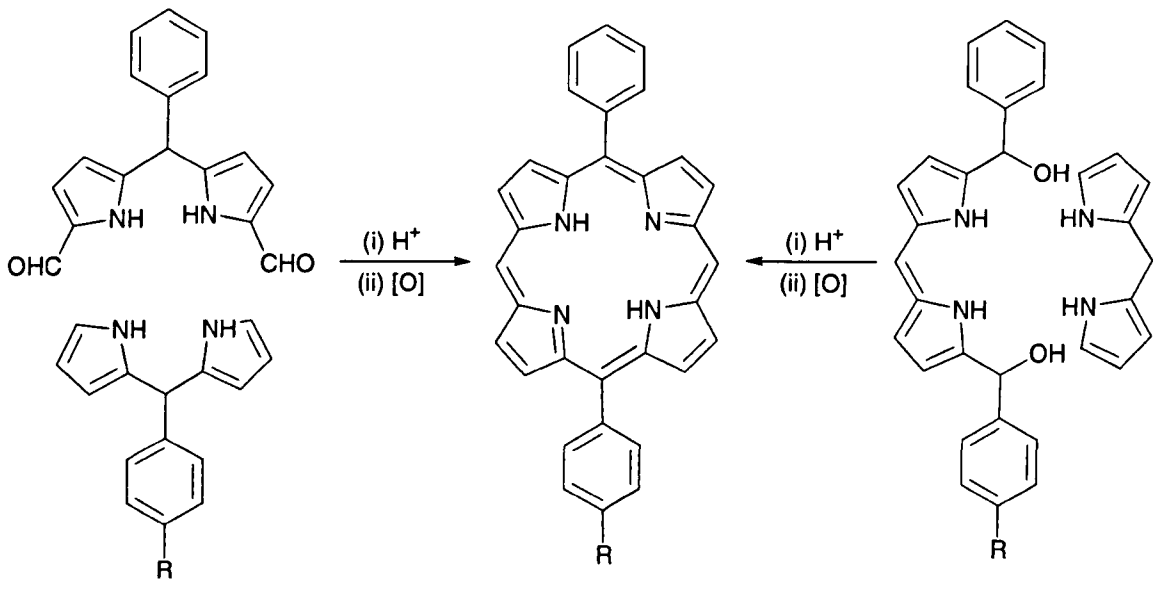

Scheme 9 – MacDonald "2+2" Diphenylporphyrin Synthesis

The methodology employed to synthesise monofunctionalised diphenylporphyrins *via* dipyrromethanes has a significant advantage over the acid catalysed condensation of pyrrole and benzaldehyde; if two differently substituted dipyrromethanes are used, only three possible porphyrin products, A'_2, $A'B'$ and B'_2, at a ratio of 1:2:1 can be generated; theoretically, simplifying chromatographic separation. In addition, milder conditions are used in the reaction, allowing the use of relatively sensitive aldehydes in "2+2" type syntheses.

1.1.13.4 Isothiocyanato Functionalised Porphyrins

Porphyrins may also be selectively functionalised to facilitate the creation of bifunctional systems, for applications such as directed delivery in photodynamic therapy and cellular imaging tools. However, the conjugation of these species is often complicated by solvent incompatibilities and/or the forcing conditions commonly required to react the substituents on the porphyrin periphery; in addition to the cross-linking problems encountered during the conjugation procedure and the significant amounts of porphyrin which non-covalently bind with their conjugate counterpart. Nevertheless, recent advances have now been made by Boyle and co-workers in the development of a water

soluble porphyrin bearing a single isothiocyanate group (figure 41) through which the facile attachment of a primary amine bearing species can be made.[113,114]

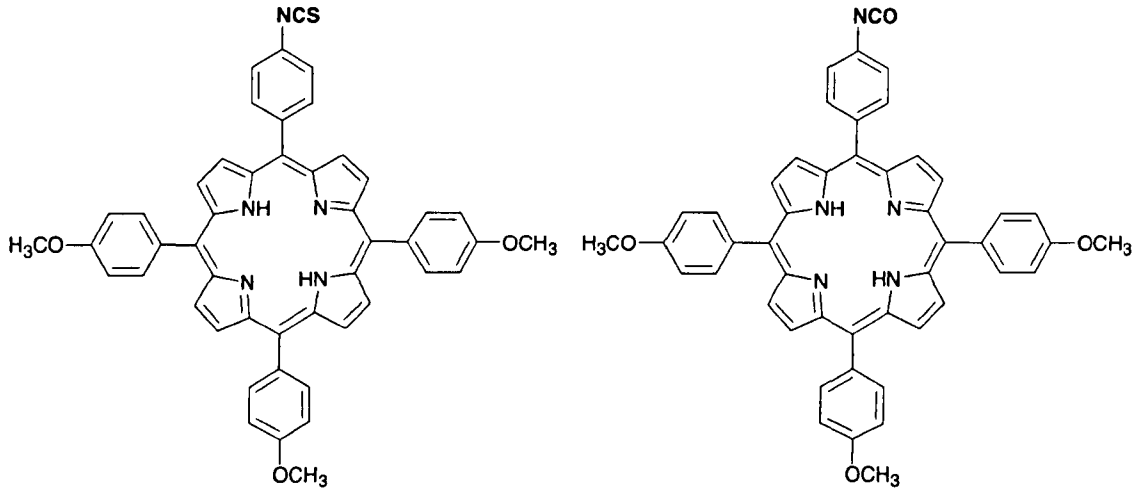

Figure 41 – Isothiocyanatoporhyrin and Isocyanatoporphyrin

Isothiocyanate bearing molecules are common intermediates used for the attachment of fluorescent probes to sensitive biological substrates under very mild conditions with the absence of by-products.[113,114] Isothiocyanates are preferred over isocyanates (figure 41), since rapid hydrolysis of the NCO group of isocyanates occurs upon exposure to moisture. Isothiocyanates are slightly less reactive but are considerably more stable, with their hydrolysis somewhat slower under aqueous conditions. Experiments have suggested that the isothiocyanate functionality reacts cleanly and in good to excellent yields (≥60%) with most amines.[114] Primary aliphatic amines were found to react the fastest (~ thirty minutes), while aromatic and secondary amines reacted more slowly. The combination of these structural features in the same molecule resulted in no detectable product being formed, even after ten days.[114]

The most common method to synthesise the isothiocyanate functionality is *via* the treatment of primary amines with thiophosgene.[114] Paradoxically, thiophosgene is a highly toxic, volatile liquid which makes its use somewhat undesirable. Ideally, a cheap, commercially available reagent is sought. One such reagent is 1,1'thiocarbonyldi-2,2'-

pyridone (TDP). Treatment of a primary amine-bearing porphyrin with two equivalents of TDP in dichloromethane at room temperature, affords the corresponding isothiocyanato porphyrin in excellent (~98%) yields (scheme 10).[113] Excess TDP and the 2-hydroxypyridine by-product can be easily removed by column chromatography to yield a pure isothiocyanato porphyrin derivative.

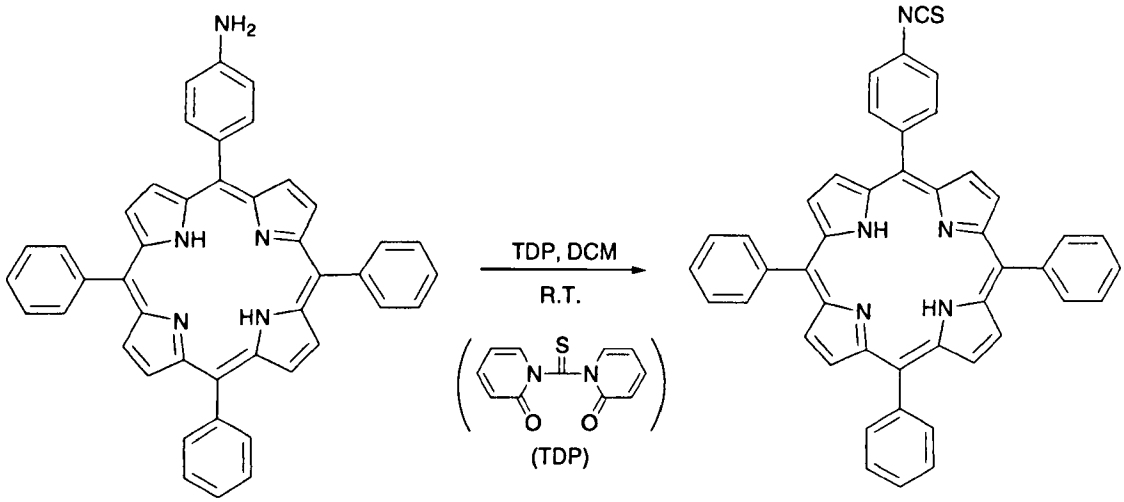

Scheme 10 – Synthesis of Isothiocyanate Functionality

1.1.13.5 Water Soluble Porphyrins

In order optimise the efficiency of attaching an isothiocyanate-bearing porphyrin to a free amino-bearing nanospecies and be able to deliver the subsequent coupling product in biological media, the porphyrin must be soluble in aqueous media.

As previously mentioned, the hydrophilicity of a porphyrin can be increased by incorporating charged groups onto the porphyrin molecule (see section 1.1.8). These can include: functionalising the molecule with anionic carboxyl or sulphonate groups; or alternatively, cationic groups, such as quaternised nitrogen centres. By increasing the number of these groups substituted onto the porphyrin molecule, the hydrophilicity of the molecule can be (simultaneously) increased further, *i.e.* multiply charged moieties are more hydrophilic than their singly charged counterparts. However, there have been

suggestions that in aqueous basic solution (pH 9), dimerisation can take place between the above mentioned anionic porphyrins.[115,116] The cationic porphyrin is believed to remain in a monomeric state; a consequence of the charged moiety "pulling" π–electron density away from the macrocycle core and thereby minimising the possibility of dimer formation. In addition, a further advantage of moieties bearing cationic charges is the proposal that they are able to pass more readily through cell membranes and into the mitochondria than their hydrophobic counterparts.[32,56]

1.2 CELL DEATH

1.2.1 Apoptosis

There comes a time when every mammalian cell must die and there are two main pathways with which this process can occur; cells are either killed by injurious agents (necrosis) or are induced to commit suicide (apoptosis).

The word apoptosis is derived from the Greek words "*apo*" (from) and "*ptosi*" (fall) and describes the orchestrated collapse of a cell. The collapse is characterised by key morphological and biochemical changes that are followed by rapid engulfment of cellular remains by neighbouring cells (phagocytosis). These key changes include: maintenance of adenosine triphosphate (ATP) levels; caspase activation; membrane blebbing; cell shrinkage; chromatin condensation; DNA fragmentation; and the formation of small intact fragments known as apoptotic bodies.[32,117,118] Apoptosis is distinguished from necrotic cell death by the distinct absence of an associated inflammatory response.

Apoptosis is commonly referred to as programmed cell death. However, programmed cell death is not always indicative of apoptosis, since programmed cell death may be applied to other forms of cellular death, which do not fulfil some or all of the morphological criteria inferred by apoptosis.

In response to intracellular damage and certain physiological cues, and in order to eradicate cells under diverse physiological and pathological settings, cells enter the self-destruct program of apoptosis. Apoptosis is carried out in a highly ordered manner, with controlled demolition of the cell orchestrated by a family of at least fourteen different cysteine proteins, known as caspases. The apoptotic process is implicated in key biological processes, ranging from embryogenesis to ageing and from normal tissue homeostasis to many human diseases. For example, the differentiation of human digits in foetal development requires the interdigital web cells to initiate apoptosis. In adulthood, about 10 billion cells die every day in order to maintain a balance with the new cells produced by the body's stem cell population; a homeostatic process regulated through apoptosis.[119-122] With ageing, apoptotic responses to DNA damage may be less tightly

controlled and exaggerated, contributing to degenerative diseases. Increased apoptosis is characteristic of Acquired Immune Deficiency Syndrome (AIDS) and neurodegenerative diseases such as Parkinson's and Alzheimer's disease. Alternatively, decreased apoptotic sensitivity or inhibited apoptosis is thought to be a feature of many malignancies, autoimmune disorders and some viral infections.[119,123]

1.2.1.1 Biochemical Changes

Integral to many forms of apoptosis are the caspase family. Caspases are typically activated in the early stages of apoptosis by the release of cytochrome C from mitochondria. They act by breaking down or cleaving key cellular substrates that are required for normal cellular function including, structural proteins in the cytoskeleton and nuclear proteins such as DNAases (which act by cleaving nuclear DNA). The result of these biochemical changes is the appearance of distinct morphological features within the cell.[124-130]

1.2.1.2 Morphological Changes

Typically, the cytoplasm begins to shrink following the cleavage of lamins (nuclear proteins) and actin (protein) filaments. Nuclear condensation is then observed following the breakdown of chromatin and nuclear structural proteins, and in many cases, the nucleus can be observed to take on a "horse-shoe" appearance. Cells continue to shrink, packaging themselves into a form which allows easy clearance by phagocytes, thus, removing the apoptotic cells from tissue in a clean and tidy fashion. Membrane changes can often be observed morphologically through the appearance of membrane blebs or blisters, which often appear towards the end of the apoptotic process. The cell is finally broken down into multiple apoptotic bodies, which are phagocytised by neighbouring cells and because cellular contents are not released, this occurs with little or no inflammation.[124-130]

1.2.1.3 What Makes a Cell Decide to Commit Suicide?

The balance between the withdrawal of positive signals (those required for the continued survival of the cell) and the receipt of negative signals (those which initiate cell death) must be strictly maintained in order to sustain regulated tissue homeostasis and healthy cells.[126,128,130]

1.2.1.4 Withdrawal of Positive Signals

Most cells require continuous stimulation (from other cells) in order to survive and in many cases, continued adhesion to the surface on which they are growing. Examples of positive signals include neuron growth factors and interleukin-2; a known vital factor in the mitosis of lymphocytes.[126,128,130]

1.2.1.5 Receipt of Negative Signals

Examples of negative signals include: (i) increased oxidant levels within the cell; (ii) resultant DNA damage from these oxidants or alternatively, (iii) damage from ultra-violet light; (iv) x-rays; (v) chemotherapeutic agents; (vi) accumulation of proteins which have failed to fold properly into their tertiary structure; and (vii) molecules which bind to specific receptors on the cell surface and signal the cell to begin the apoptosis process. These death activators include:- [126,128,130]

- TNF-α (tumour necrosis factor) which binds to the TNF receptor
- Lymphotoxin (TNF-β) which also binds to the TNF receptor, and
- Fas-Ligand (FasL); a molecule which binds to a receptor on the cell's surface known as Fas (CD95).

1.2.2 Induction of Apoptosis

There are a number of suggested mechanisms by which apoptosis can be induced in cells. In the simplest form, apoptosis may be considered in terms of initiation, genetic regulation and effector mechanisms.[119,121] The sensitivity of cells to any of these stimuli can vary depending on a number of factors including, the expression of pro- and anti-apoptotic proteins, the severity of the stimulus and the stage of the cell's life-cycle.[124-126] Initiators of apoptosis have already been mentioned in terms of deprivation of survival factors, and through a variety of pathways, these stimuli can in turn generate a characteristic pattern of gene expression. The cytoplasmic Bcl-2 family of genes is the most studied and includes both pro-apoptotic (death) and anti-apoptotic (survival) proteins, which govern the permeability of the mitochondrial membrane (MMP). The tumour suppressor gene p53 is also a well characterised apoptotic agent, which can sense DNA damage and halt the progression of the cell cycle by inducing apoptosis, whilst the principal effectors of apoptosis are caspases. Some of the major stimuli that are thought to induce apoptosis are outlined below.

1.2.2.1 Apoptotic Mechanisms

The three different mechanisms proposed by which a cell can undergo apoptotic death are:- [124-126]

(i) *Initiation and Genetic Regulation*

Internal signals – the intrinsic (mitochondrial) pathway: the outer membrane of healthy cell organelles such as the mitochondria, either express the protein Bcl-2 or see the protein congregate on their outer surface (OMM). Internal damage to the cell, for example, from ROS, causes the Bcl-2 protein to activate the related pro-apoptotic Bax protein. The Bax protein penetrates the mitochondrial membrane resulting in leakage of cytochrome C and other pro-apoptotic factors from the mitochondria, such as the apoptosis inducing factor (AIF) and endonuclease G. The released cytochrome C and a "free" cytosolic apoptotic protease activating

factor-1 (apaf-1) molecule come together and bind with molecules of ATP and molecules of pro-caspse-9, forming a complex known as an apoptosome, which accordingly aggregates in the cytosol. The apoptosome activates the pro-caspase-9 molecules, which in turn activates caspase-3.[41,53,122,131,132]

Upon activation, initiator caspases activate the effector caspases by proteolysis; generating an explosive cascade of caspases, which in turn dismantle key cellular structures, generating the apoptosis phenotype.[133]

(ii) *Effector Mechanisms*

External signals – the extrinsic (death receptor) pathway: Fas and the TNF receptor are integral membrane proteins with their receptor domains exposed at the cell surface. Binding the complementary death activators (FasL and TNF respectively) transmits a signal to the cytoplasm which leads to activation of caspase-8; initiating a torrent of caspase activation that leads to phagocytosis of the cell. For example, when cytotoxic T cells recognize their target, the concentration of FasL at their surface increases, allowing complimentary binding with the target cell's surface-Fas, evoking apoptotic cell death.[122,131]

(iii) *Apoptosis inducing factor* (AIF) – neurons and other cells, such as cardiomyocytes and colorectal carcinomas, have a different way to self-destruct. This pathway is not caspase dependent but instead involves the mitochondrial intermembrane protein AIF.[134,135] When the cell receives a signal to die, AIF is:-

(a) Released from the mitochondria

(b) Migrates into the cell nucleus

(c) Binds to DNA, which

(d) Triggers the destruction of DNA, culminating in cell death.[122]

The exact mechanism by which AIF induces caspase-independent apoptosis is currently unclear and remains the subject of intense biological scrutiny.[123]

However, it has been proposed that the early stages of apoptosis are reversible; in some cases, final destruction of the cell is only guaranteed with engulfment of the cell by a phagocyte.

1.2.2.2 Mitochondria

Before we proceed, it is perhaps worth mentioning the vital role of mitochondria in healthy cells. Mitochondria are the principal energy sources, in terms of ATP, of the cell. They contain the oxidative enzymes utilised by the cell to metabolise ingested foodstuffs into sources of cellular energy. Therefore, a cell with a damaged mitochondrion will have an impaired, if not impossible, ability to move, divide and produce secretory products.

1.2.2.3 Cytochrome C

Cytochrome C is ordinarily a life-promoting protein which is an essential component of the electron transfer chain in the cell's energy production pathways.

Cytochrome C release during apoptosis appears to be the result of the interacting pro- and anti-apoptotic Bcl-2 proteins. The pro-apoptotic family members (Bax and Bak, which ordinarily reside in the cytoplasm) translocate to the outer mitochondrial membrane, where they are subject to a conformational change. They then oligomerise and insert into the mitochondrial membrane, facilitating the release of cytochrome C. Conversely, anti-apoptotic Bcl-2 family members such as Bcl-xL, Bcl-w and Bcl-2 itself, appear to act, at least in part, by selectively binding Bax in the active conformation, thereby preventing insertion of the Bax molecule into the outer mitochondrial membrane.[117,122,123] Although these polypeptides are loosely associated with the mitochondrial membrane in some cell types, in others they are cytoplasmic. Thus, it is possible that a conformational change or some other post-translational modification is necessary before these molecules reach the surface of the mitochondria.[117,123,136,137]

1.2.2.4 Caspases

Caspases are **c**ysteine **asp**artate specific prote**ases** that cleave proteins exclusively after aspartate residues and are synthesised as inactive precursors called procaspases or zymogens.[117,122-130,133,137] Cleavage and activation of these procaspases can occur as a result of exposure to a variety of stimuli, including DNA damage and activation of cellular death receptors.

Caspases involved in apoptosis can be broadly grouped into initiator (upstream) or effector (downstream) caspases depending on the role they play during apoptosis.[133,138] Initiator caspases, such as caspase-9, are the first to be activated in response to pro-apoptotic stimuli and are responsible for cleaving and activating effector caspases. This sequential activation of one caspase by another sees the creation of a deluge of proteolytic activity. The effector caspases, primarily caspases -3, -6 and -7, are thought to be responsible for the majority of substrate proteolysis observed during apoptosis. The effector caspases cleave downstream targets, including DNA repair enzymes, cytoskeletal proteins and any proteins involved in the progression of the cell cycle. These targets are responsible for implementing the downstream pathways which culminate in the morphological changes associated with apoptosis, the loss of cell viability and phagocytosis of the devastated cell.[117,122,133,138]

1.2.2.5 Mitochondria and the Bcl-2 Family

It has been previously mentioned that mitochondria have a pivotal role in the regulation of cell death, particularly with respect to apoptosis and cytochrome C release. The anti-apoptotic Bcl-2 family members (Bcl-2 and Bcl-xL) are known to be located in the outer mitochondrial membrane and act as cellular guardians by blocking the release of mitochondrial cytochrome C; thereby, promoting cell survival. Their cytosolic relatives (Bad and Bax) also mediate their pro-apoptotic effects through the mitochondria, either *via* interactions with the Bcl-2 or Bcl-xL proteins, or by directly interacting with the mitochondrial membrane.[117,124]

Exactly how these pro- and anti-apoptotic proteins evoke and inhibit these apoptotic pathways has been the subject of intense research over recent years and will be discussed later. However, it must be noted that these death mechanisms are far from fully understood and investigations are underway to further elucidate their function/involvement in apoptosis.[117,124]

1.2.2.6 The Bcl-2 Family

The Bcl-2 family of proteins all share a characteristic domain of conserved homology termed the "Bcl-2 homology (BH) sequence motif" (BH1 - BH4). The BH domains are crucial in effecting the family's desired pro- and anti-apoptotic functions. These motifs are formed by α-helices and enable the different family members to form either homo- or heterodimers, thereby regulating one another. The anti-apoptotic proteins, including Bcl-2 and Bcl-xL, harbour at least three of these BH domains (always inclusive of the BH4 domain, figure 42), along with their structurally similar relatives, Bak and Bax, which contain domains BH1, BH2 and BH3, that act not to promote cell survival but instead to induce apoptosis. The third sub-family of Bcl-2 proteins share only the BH3 domain: essential for both their interaction with their relatives and their death-promoting activity. These proteins are otherwise unrelated to the Bcl-2 family.[117,122,123,133,136,137]

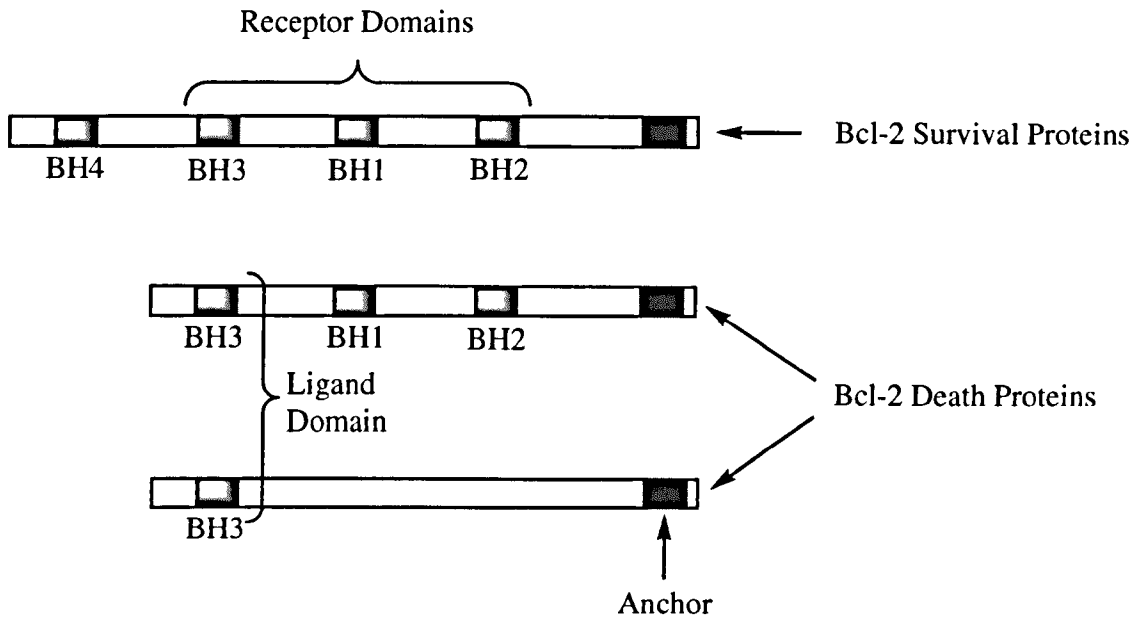

Figure 42 – The Domains of the Bcl-2 Family

Family members of opposing factions readily dimerise *via* their BH domains forming either homo- or heterodimers.[122,137] The amphipathic BH3 α-helix of the apoptogenic proteins can bind to the hydrophobic groove on the pro-survival proteins, created by α-helices present in the BH3, BH1 and BH2 regions of the protein.[136] For the pro-survival proteins this ability to bind a BH3 domain only partially accounts for their pro-survival action.[136] Thus, a BH3-only protein, it would appear, can serve as a ligand that locks the anti-apoptotic protein into an inactive conformation. Although, the second sub-family of pro-apoptotic proteins, such as Bax, can also assume a conformation that facilitates heterodimerisation through the BH3 domain (allowing them to bind to and regulate the activity of membrane-bound Bcl-2 relatives), they can also induce apoptosis *via* at least one alternative mechanism.[136] The conformational change(s) this second sub-family undergoes allows Bak and Bax to homodimerise on the mitochondrial membrane and associate with their Bcl-2 relatives; thus, preventing heterodimerisation occurring with the pro-survival proteins (figure 43).[122,136,137] The established apoptotic inhibitors Bcl-2 and Bcl-xL can form heterodimers with pro-apoptotic agonists in their active conformation, such as Bax. This dimerisation effectively renders the Bax protein inactive and unable to insert into the outer mitochondrial membrane.[133] However, the pro-survival

effects of Bcl-2 and Bcl-xL can be counteracted by the "BH3" only death promoting relatives Bad, Bid and Bik (as already discussed). Heterodimerisation between the BH3-only death proteins and survival proteins allows the multiple-BH domain death proteins, such as Bax, to insert into the mitochondrial membrane and deliver their desired effects, *i.e.* only the BH3-only proteins can inactivate the Bcl-2 family of survival proteins (figure 43).

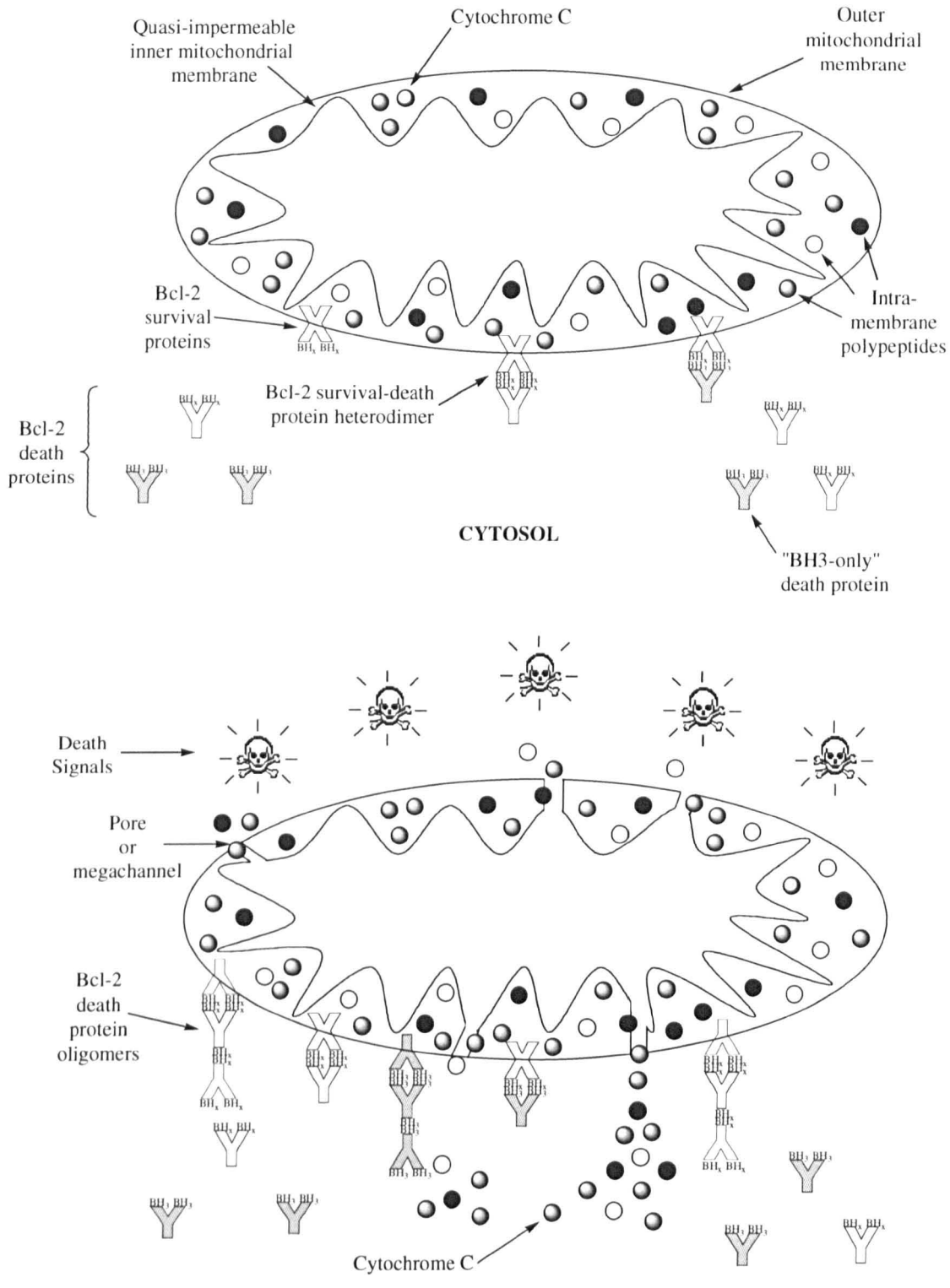

Figure 43 – Simplified Diagram of a Mitochondrion and the Bcl-2 Family promoting (i) Cell Survival and (ii) Cell Death

Translocation of the death proteins is triggered by specific post-translational modifications unique to each protein. Following a death signal several changes affect these proteins leading to their activation. Firstly, they translocate to the mitochondria from the cytosol: then undergo a conformational change (accompanied by oligomerisation); and finally, insertion into the outer mitochondrial membrane. This sequence of events is rapidly followed by the efflux of mitochondrial cytochrome C into the cytosol (figure 43); an action implicated in the cytotoxic action of the death proteins.[122,136,137]

1.2.2.7 The Balance between Life and Death

The sensitivity of cells to apoptotic stimuli is thought to be dependent on the balance between pro- and anti-apoptotic Bcl-2 family members. When the balance lies over to the pro-apoptotic Bcl-2 proteins, cells show an increased sensitivity towards apoptosis; whereas, a balance in favour of anti-apoptotic Bcl-2 proteins, shows a decreased sensitivity of the cell towards apoptosis.[122,124]

In summary, pro-apoptotic Bcl-2 proteins, such as Bad and Bax, normally reside within the cytosol, where their primary role is thought to be as sensors of cellular damage and stress. Upon receipt of the appropriate signals, Bad and Bax relocate to the primary residence of the anti-apoptotic Bcl-2 and Bcl-xL proteins (the outer mitochondrial membrane). The subsequent interaction between the anti- and BH_3-only pro-apoptotic Bcl-2 proteins disrupts the normal functioning of the anti-apoptotic proteins, and along with the homodimerisation and membrane insertion of the BH_1-BH_4 pro-apoptotic proteins, leads to the release of intra-mitochondrial polypeptides - inclusive of cytochrome C. Why and how pro-apoptotic Bcl-2 proteins translocate to the mitochondrial membrane and what they do when they reach the membrane remains a mystery.[139] Two prevailing theories currently exist postulating the mechanism behind the efflux of these polypeptides into the cytosol. The first of these hypotheses suggests the non-specific rupture of the outer mitochondrial membrane, while the second considers the formation of pores or conducting channels through which the polypeptides can pass.[117,122,123,136,137]

1.2.2.7.1 Outer Mitochondrial Membrane Rupture

It is thought that the water and solutes which enter the mitochondrial matrix during apoptosis cause the organelle to swell. However, with respect to the inner mitochondrial membrane having a much larger surface area (in comparison to its outer membrane), the expansion conferred on the inner mitochondrial membrane can lead to rupture of the outer mitochondrial membrane. This rupture triggers the release of the mitochondrial intermembrane contents (including cytochrome C) with subsequent dilution of the cytosol.[137] But since the inner membrane undergoes only expansion and not rupture, the contents of the mitochondria remain embraced within the matrix.

Two models have been hypothesised for this theory. The first implicates the hyperpolarisation of the inner mitochondrial membrane before the release of cytochrome C into the cytosol. It has been postulated that this initial hyperpolarisation may be a result of the inability of a mitochondrion to exchange its ATP for cytosolic adenosine diphosphate (ADP) during apoptosis; a process normally mediated *via* the voltage dependent anion channel (VDAC) or mitochondrial porin (present in the outer mitochondrial membrane) and the inner membrane adenylate translocator (ANT). Impairment of the ATP-ADP exchange process by the closure of the porin, should contribute to the hyperpolarisation of the inner membrane. It is thought the resulting increase in mitochondrial transmembrane potential will promote an osmotic swelling of the matrix.[117,122,136,137] However, this hypothesis is in disagreement with a second theory, relating to apoptosis induced through the release of intra-mitochondrial components through mitochondrial pores/channels; this will be outlined in the ensuing paragraphs (also, see section 1.3).

1.2.2.7.2 Mitochondrial Pores

The loss of the mitochondrial transmembrane potential ($\Delta\Psi_m$) is often observed during apoptosis and has been associated with the opening of mitochondrial permeability transition pores, or mega-channels, through which small molecules and ions can pass (see section 1.3.6). It was thought that cytochrome C may leave the mitochondria *via* these

pores; rather than the Bcl-2 family members forming new mitochondrial pores, they may instead stabilise or perturb these pre-existing channels. These channels are believed to form across sites of contact between the inner and outer membranes; with the likelihood, the inner and outer membrane pores will be gated. It is thought that the pro-apoptotic proteins, Bak and Bax, keep these pores and channels open allowing, the passage of cytochrome C from the mitochondria into the cytosol.[117,122,132,133,136,140] However, it has been proposed that mitochondrial pore-opening is a secondary process, preceded by the initial release of cytochrome C: a proposal based on the ability of the mitochondria to maintain their membrane potential during the initial stages of cytochrome C release, suggesting that the release of cytochrome C is not through mitochondrial pores, but instead proffers a specific permeabilisation associated with the outer mitochondrial membrane. It is with this in mind, that a growing body of evidence is now pointing towards the involvement of certain members of the Bcl-2 family, specifically the "BH3-only" relatives, having a pivotal role in the promotion of cytochrome C release.[133,136]

1.2.3 Necrotic Cell Death

The term necrosis is derived from Greek word for death "*nekrosi*" and is a form of uncontrolled death, with a somewhat less ordered process of events than those which are observed with its deathly counterpart, apoptosis.

Necrosis generally takes place under pathological settings such as infections, physical injury, ischemia (deficiency of oxygenated blood supply) or excessive accumulation of ROS, resulting in cellular swelling and membrane rupture. Cellular debris is released directly into the surrounding tissue, often prompting a local inflammatory response.[137,141,142]

If a cell is subject to such a severe insult or injury, for example from toxins, as to compromise either its ATP-generating mechanisms or the integrity of its permeability barriers, it is likely to lyse. This lysis causes the organelles within the cytoplasm to become disorganised and witnesses distinct mitochondrial changes including accumulation of lipid-rich particles and dilation, with the inner mitochondrial membrane

shrinking away from the outer mitochondrial membrane. The cyto-architecture of the cell is subsequently lost at later stages (with the general release of proteases, nucleases and lysosomal contents) with the chromatin becoming flocculent and disperse. Rupture of the cell membrane leads to the release of the cellular contents and pro-inflammatory cytokines into the surrounding tissue, leading to the recruitment of monocytes and macrophages to the site of cell death.[143,144]

The main differences between apoptotic and necrotic cell death are outlined in table 1.

PATHOLOGICAL FEATURES AND MECHANISMS		
	APOPTOSIS	**NECROSIS**
Pattern of death	• Single cells affected	• Multiple, neighbouring cells affected
Cell size	• Shrinkage	• Early swelling
Fragmentation	• Yes, apoptotic bodies	• No, cell lysis
Plasma Membrane	• Persists until late stages • Blebs	• Smooth • Compromised, early lysis
Mitochondria	• Increased membrane permeability • Efflux of mitochondrial contents into cytosol • Structure remains relatively preserved	• Swells • Disordered structure
Organelle Shape	• Contracted • Apoptotic bodies	• Swells • Disrupts
Nuclei	• Chromatin clumps and fragments	• Membrane Disruption

DNA Degradation	• Fragments • Internucleosomal cleavage • DNA present in cytosol	• Diffuse • Random
Cell Degradation	• Phagocytosis • No inflammation	• Inflammation • Macrophage invasion
Stimuli	• Developmental programs • Endogenous signals • Intracellular signals • Disease processes • Death activators • Toxins • DNA damage • Mild ischemia	• Disease processes • Toxins • Severe ischemia
Cellular Processes	• Cell suicide • ATP maintenance • Cytochrome C release • Caspase activation • Torrent of caspases • Cellular disruption and shrinkage • Formation of apoptotic bodies • Phagocytosis	• Uncontrolled death • ATP depletion • Cell swelling • Membrane lysis • Release of cellular contents • Inflammatory response

Table 1 – Cell Death: Apoptosis *versus* Necrosis

1.2.4 Apoptosis and Photodynamic Therapy

Photodynamic therapy can induce cell death *via* necrosis and apoptosis, both *in vitro* and *in vivo*. However, the factors which determine the overall contribution of either of these mechanisms (individually or combined) to the process of cell death are not fully understood and groups, such as those of Fabris and Kessel, are currently undertaking a number of investigations to try and further understand the prevailing mechanisms that lead to cell death.[12,145]

Most photosensitisers induce cell/tissue photodamage through the production of ROS (mainly singlet oxygen) which have a short lifetime ($^1O_2$ ≤40 ns) in biological systems and hence, a minuscule radius of action (≤20 nm). This implies that the sites of initial cell damage are very close to the sites of ROS/singlet oxygen formation and are thereby, highly governed by the cellular distribution of the photosensitiser. The cellular distribution is determined by both the physicochemical characteristics of the photosensitiser and the cell/photosensitiser incubation protocol adopted prior to light exposure. Consequently, loss of cell viability may occur with a very different efficiency when using photosensitisers that produce cytotoxic species with comparable quantum yields (Φ), but localise in fairly vulnerable and different cellular sites.[6,146] Fabris and co-workers have investigated parameters including, cell/photosensitiser incubation times and photosensitiser dose (particularly in relation to photosensitiser localisation) in the hope of drawing upon possible correlations between the mechanism(s) of cell death and sites of primary photodamage.[146]

Data from Fabris and co-workers suggested that the cell/photosensitiser incubation times are related to the mechanism(s) behind cell death (when a zinc phthalocyanine photosensitiser is employed). Results led them to conclude that necrotic cell death represents the mode of death when cells are dark-incubated with zinc phthalocyanine for 2 hours and irradiated with a light dose; culminating in ≥99.9% loss of cell viability.[145] Conversely, they believed that cells irradiated post 24 hours of incubation, with the same photosensitiser, displayed characteristic morphological changes typical of apoptotic cells,

3 hours after photodynamic therapy. The mechanism of cell death was further confirmed as apoptotic by the increased activity of the pro-apoptotic protein, caspase-3. In cells irradiated after short incubation periods, apoptosis is observed only with light doses causing partial reduction of survival. In cells irradiated after a long incubation period, apoptosis is observed with light doses causing complete cell mortality. Apoptosis is probably also favoured by the low doses of light required for inducing cell death when zinc phthalocyanine is localised in the mitochondria and by the fact that these organelles, not the plasma membrane, are the primary targets of photosensitisation.[146]

Fabris and co-workers found that only after a prolonged (zinc phthalocyanine/cell) incubation period (24 hours) could mitochondrial localisation be clearly observed with a fluorescence microscope; whereas, a shorter incubation period (3 hours) demonstrated mainly localisation in the Golgi apparatus.[146] They concluded that the disruption of mitochondrial membrane functions, induced by the zinc phthalocyanine photosensitiser, was potentially responsible for the observed apoptotic cell death.

Investigations led by Kessel and co-workers focused on specific targets, namely the mitochondria, lysosomes and the plasma membrane to try and further their understanding of photodynamic therapy-induced cell death, particularly with respect to apoptosis. As a result of their findings, they postulated that apoptosis is induced prior to a reduction in the mitochondrial membrane potential. This suggested that mitochondrial modification is a secondary process to the initiation of apoptosis and, that the loss of the mitochondrial membrane permeabilisation is a result of photodynamic action rather than a consequence of apoptotic mechanisms.[32,145]

It could therefore be hypothesised that factors which determine the mode of cell death are dependent, in part, on the site of photosensitiser localisation, the photosensitiser/cell incubation time and time of cell irradiation, and that mitochondria do have a role in the photodynamic therapy-induced late stages of apoptotic cell death.

1.2.5 Concluding Remarks

In summary, the pathways behind the phenomenon of cell death remain mysterious, but what is known, is that apoptosis is a process of deliberate life relinquishment by the removal of superfluous, infected, transformed or damaged cells, through the activation of an intrinsic program of suicide, of which the mechanisms remain biochemically cryptic and subject to intense experimental investigations.

1.3 CALCIUM

1.3.1 What is calcium?

Calcium is one of the most important minerals in our diets and is the most abundant metallic element in the body. It is a structural component of bones, teeth and soft tissues and is vital in a number of our body's metabolic processes. 99% of the calcium present in our bodies is deposited in our bones and teeth, with the remaining 1% present in cells and body fluids (accounting for 1-2% of the body's total weight).[147-150]

Calcium is essential in maintaining total body health and at low levels plays a key role in cell biochemistry (signaling), muscle contraction (and relaxation), nerve impulse transmissions, cell metabolism and blood clotting. It is also implicated in cell injury at elevated levels and a deficiency in calcium leads to diseases such as Rickets, colon cancer, hypertension and osteopenia (the precursor to osteoporosis - brittle bones).[147,149, 151,152]

The body's calcium needs change throughout life, with greater amounts required during periods of growth, including the baby and teenage years, pregnancy and for women during the post-menopausal years.[148,149]

The life-sustaining role of calcium in the body necessitates its concentration to be carefully regulated within various compartments of the body. There are three key regulators which maintain the levels of calcium in the body: namely, the parathyroid hormone (PTH), vitamin D and calcitonin.

The parathyroid hormone is produced and secreted by the parathyroid gland and prevents levels of calcium becoming too low in the blood by: (i) increasing the dietary absorption of calcium in the gastrointestinal tract; (ii) inducing the bones to release some of their calcium; and (iii) by triggering an increase in the level of phosphorous excreted from the kidneys, (indirectly) boosting the levels of calcium in the blood. Vitamin D works alongside the parathyroid hormone in respect to the bones and kidneys and is important in

the efficient intestinal absorption of calcium. Vitamin D is drawn from two main sources either from the diet or from the sun (exposure of the skin to the sun's rays). Calcitonin is also a hormone produced by the thyroid gland and works by lowering the blood's calcium concentration by promoting the deposition of calcium into the bones. The majority of calcium taken into our bodies *via* our diets is absorbed in the small intestine and transported into the bloodstream bound to a protein known as albumin.[148]

When the level of calcium in our blood drops too low, the vital divalent mineral is "borrowed" from our bones and is replaced only by the calcium from our diets.[148,149] A long-term dietary deficiency of calcium can eventually manifest itself in our bodies through the weakening of the bones, increasing the likelihood of skeletal deformities (Rickets) and fractures (osteoporosis). Strictly speaking, Rickets is a result of a vitamin D deficiency but since the aforementioned is needed for efficient absorption of calcium, calcium levels are directly affected. A low level of blood calcium is not strictly the result of a poor dietary intake of calcium, since low levels of the parathyroid hormone or vitamin D can also have a significant impact on the concentration of calcium in the blood. Low calcium-blood levels are also implicated in nerve and muscle impairment leading to skeletal muscle spasms and abnormal beating of the heart, to the extent of complete heart failure being observed.[148,152]

It is worthy to note that it is not just a deficiency in calcium which can have a detrimental effect in the healthy functioning of the body as excess levels of calcium can affect the body in a negative way too. Calcium is also a key component in a plethora of physiological diseases and cell death. Perturbations in the normal intracellular calcium levels and homeostasis underlie many pathological conditions. These range from cardiac hypertrophy to ischemic death of neurons and, when cells become surplus to requirements, calcium signaling pathways are believed to induce the cell death *via* apoptosis (see section 1.3.6).[148,150-155]

Long-term ingestion of excess levels of calcium, or indeed the combination of calcium with increased levels of vitamin D, can lead to the increased absorption of calcium in the gastrointestinal tract. Toxicity from these raised levels expresses itself as: abnormal

deposition of calcium in tissues (calcification, observed in atherosclerosis); by rapidly dividing cells (microcalcification); and by elevated levels of calcium in the blood (referred to as hypercalcemia) which can infer a decrease in the density of bones, abdominal discomfort and the formation of kidney stones, with severely raised levels of calcium carrying a significantly elevated possibility of seizures and a coma.[148,156] So not only is calcium vital in ensuring that cells perform their appropriate duties, it is also a major contributor to cell dysfunction and death, both functions vital in sustaining a healthy life; a notion perhaps ordinarily conceived, on the surface, as contradictory. It is therefore of utmost importance, for total body well-being, that a healthy calcium level is maintained.[131,151,152,157,158]

1.3.2 Calcium as an Intracellular Messenger

Calcium is an example of a universal second messenger and plays a major part in controlling the function of all body cells by acting as a carrier of intracellular messages. Second messengers are molecules which relay and amplify signals received by receptors on the cell's surface. The body relays its instructions to cells through various hormones and neurotransmitters (first messengers) which bind to the cell's surface. These chemical messengers serve to initiate or terminate a particular cellular event. Many of these messages are disseminated by the release of calcium ions either from internal stores (such as the mitochondria or endoplasmic reticulum) into the cytoplasm; or through an influx of extracellular calcium into the cytoplasm through the opening of membrane channels like the voltage-operated calcium channels (VOCC's), which open in response to a change in membrane potential; and the transient receptor channels (TRP's) which open when they bind to a neurotransmitter (figure 44).

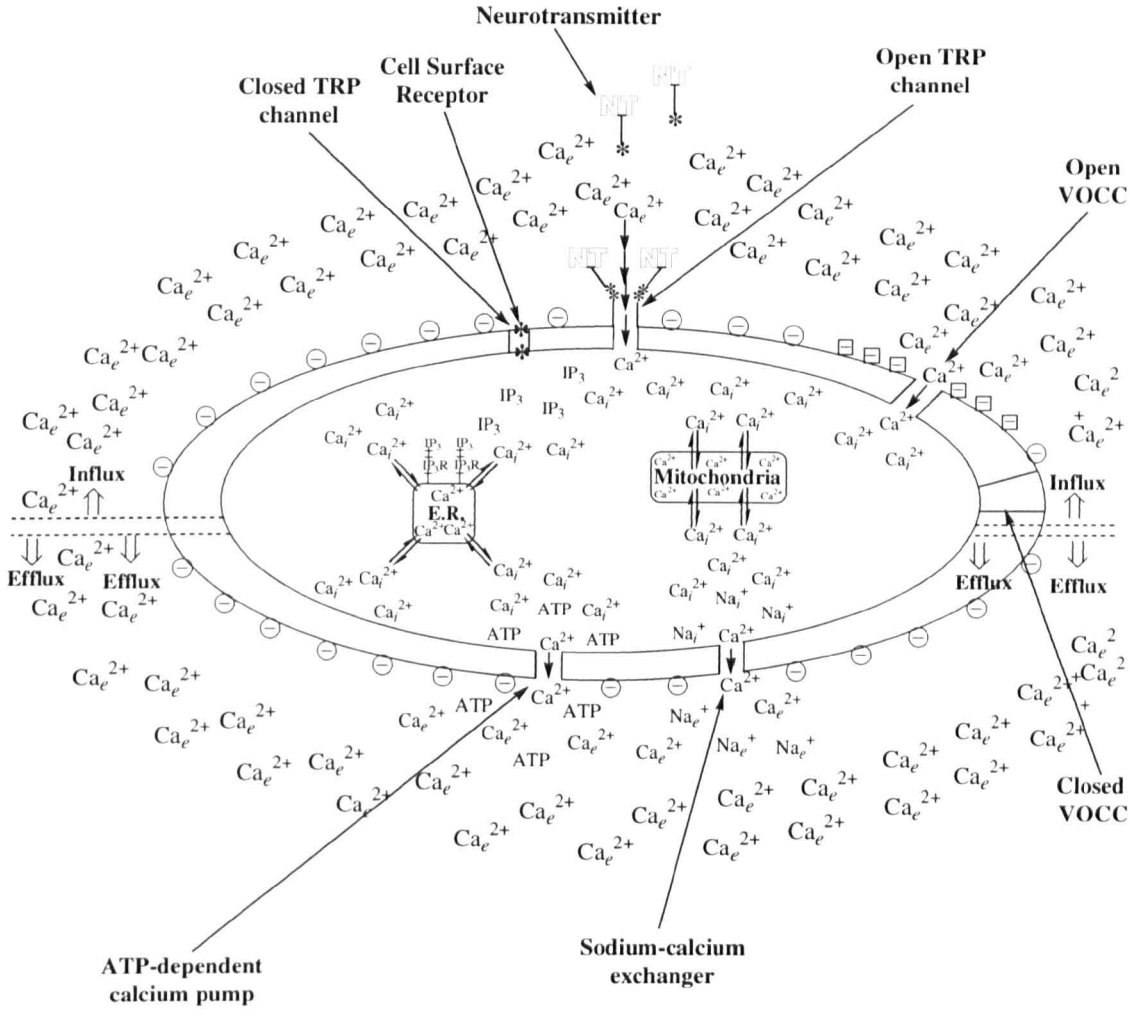

Figure 44 – Simplified Diagram of a Cell and Calcium Movement

These two routes generate distinct signals with extracellular calcium entering the cell *via* membrane channels leading to local cellular effects, and calcium released from internal stores producing global cellular effects; localised signals are involved in events such as secretion and global signals observed during smooth muscle contraction. The localised signal is the result of two effects. Firstly, the calcium ions are unable to diffuse far from their point of entry (into the cell) since the membrane channels open only briefly. Secondly, there is a high concentration of calcium chelating proteins present in the cytoplasm (such as calsequestrin and calreticulin) exerting a tight control over the movement of calcium ions in the cytoplasm.[152] The release and uptake of calcium from the internal stores generates an oscillatory change in the intracellular calcium level, which sweeps across the cell in the form of calcium transients and/or pulses, regulating an array of physiological responses.[121,126,140,150-168] By relaying and amplifying the strength of the signals transmitted from the binding of a ligand to a single receptor, calcium ions can go on to evoke great changes in the biochemical activities of the cell.

The ability of calcium ions to simultaneously control a variety of cellular processes is a direct result of the manner in which intracellular calcium levels can be varied and is a contributing factor in why calcium ions are universally used by all cell-types in signal transduction.[151-153] In order for calcium ions to act as a cell signaling commodity, the cell must first create a calcium gradient across its membrane. An approximately 10,000-fold difference in the calcium concentration across the plasma membrane (1.5 mM outside of the cell and 0.1 μM inside the cell) exists and is achieved by actively driving calcium ions across the membrane and into the cell through the calcium-permeable influx channels (VOCC's and TRP's), in addition to the electrical potential present at the plasma membrane (figure 44).[121,126,151,152,156,160-166,168-172] These resultant gradients are used in a range of signaling systems mediated by gated-ion channels. There are also significant (but variable) concentration gradients across the membranes of key organelles, including the mitochondria and the endoplasmic reticulum, with the same type of calcium pumps present in the cell membranes also present in these organelle membranes; this allows the passage of calcium ions into the organelle matrix. In addition to the presence of these concentration gradients, the relatively small size of calcium ions (ionic radius 1.07 Å)

means they are able to diffuse with relative speed; a crucial characteristic for messenger molecules.[151,153,157,158,160,162,166,173]

The calcium pumps are enzymes known as ATPases. They transport the calcium ions across the plasma or organelle membranes and are powered by the energy from the hydrolysis of the "energy molecule" ATP.[151] Mammalian calcium pumps are primarily located within the plasma membrane or the inner membranes of the endoplasmic/sarcoplasmic reticulum and mitochondria, and fall into one of three categories: the plasma membrane ATPases (PMCA), these extrude calcium from the cell; endoplasmic/sarcoplasmic reticulum ATPases (SERCA), which sequester calcium within intracellular organelles; or the secretory pathway ATPases (SPCA), whose role/function is so far only crudely understood.[132,151,153,157,158,161,173]

1.3.3 Internal Calcium Stores

The release of calcium from internal stores is more complex in nature than the passage of extracellular calcium ions through membrane channels and involves further messenger molecules. The activation of calcium channels present in the membranes of the internal store organelles (endoplasmic and sarcoplasmic reticulums) are primed to open, at least in part, by the inositol 1,4,5-triphosphate (IP_3) and cyclic ADP ribose (cADPR) messenger molecules, whose main function is to mobilise calcium ions present in these storage organelles (figure 44).[121,126,132,140,152,153,162,174-176]

Both IP_3 and cADPR are water-soluble messengers released in response to the binding of hormones and neurotransmitters to the cell's surface receptors. IP_3 and cADPR can diffuse across the cell priming the release of calcium channels over a wide area (figure 44). Hence, when calcium is released from one area of the internal calcium stores it can result in the activation of adjacent calcium channels eliciting a chain reaction, which subsequently initiates a wave of calcium ions to sweep across the cell and generate a global calcium signal.[121,126,140,152,153,162]

1.3.4 Calcium Removal

For any repetitive physiological event, dependent upon an intramitochondrial calcium level, a homeostasis must be maintained so that the influx of calcium ions during a signaling pulse is matched by the efflux of calcium ions during the period between two pulses; thereby avoiding calcium accumulation or depletion. There are two separate modes of mitochondrial efflux known as; the ATP-dependent (sodium-independent) and the sodium-dependent mechanisms.[126,140,152,168,173]

Calcium ions are removed from the cells cytoplasm and returned to the extracellular fluid *via* two mechanisms of active transport. The first of these mechanisms involves a plasma membrane ATP-dependent calcium pump, which actively removes calcium from the cell, with the second mechanism utilising a sodium-calcium exchanger (NCE, figure 44). The exact mechanism by which this exchanger works remains elusive. However, the NCE is an electrogenic ion exchange protein and maintains a steady concentration of cellular calcium by removing an amount of calcium from the cell equal to that which enters it. It is known that calcium and sodium ions are able to flow in either direction across excitable membranes (including the brain and muscle cell membranes (sarcolemma)) and that the energy harnessed from three sodium ions (flowing down their concentration gradient) pumps one calcium ion across the calcium concentration gradient, creating an electrogenic potential. The direction which these ions flow (either inbound or outbound) depends on the membrane potential and the chemical composition of the cell gradient.[126,140,152,168,171,173,177]

An increase in the intracellular concentration of sodium sees the sodium ions compete with calcium ions *via* this exchange mechanism, leading to an increase in the intracellular concentration of calcium ions. An example of this mechanism in action is observed when the activity of the sodium-potassium ATPase pump is reduced. The transport of sodium ions out of the cell and potassium ions into the cell normally takes place *via* an ATP-dependent pump. When the activity of this pump is reduced, for example, through cellular hypoxia, an increase in the intracellular levels of sodium is witnessed. The NCE exchanges the increased number of sodium ions for calcium ions by transporting the

sodium ions out of the cell, leading to an increase in the intracellular calcium ion concentration. But care must be taken, for as previously mentioned, too much calcium in the cell can lead to calcium overload and cause damage to the mitochondria and other subcellular processes.[126,160,162,173]

To recapitulate: the role of calcium in cellular signaling processes is regulated by the concentration of free calcium in the cytosol. In response to the appropriate signals calcium enters the cytosol either from internal stores or through membrane channels; allowing intracellular and extracellular calcium into the cytosol. To maintain the intracellular homeostasis, calcium is then returned back to its source either *via* ATP-mediated molecular pumps or the NCE mechanism. By these means a relatively "simple" ion (calcium) is able to relay a number of calcium-specific signals; thereby, governing a wide range of vital body functions and thus, promote a healthy life.

1.3.5 Calcium and the Mitochondria

It appears evident that mitochondria play an important role, and quite possibly an active one, in the process of calcium signaling, both in the healthy functioning of vital bodily processes (such as nerve impulse transmission and muscle contraction) and cell death.[140,151,153,154,156,162,173]

We have already discussed (see sections 1.1.8 and particularly, 1.2) the important role that mitochondria play in apoptosis through the release of apoptosis-inducing factors, such as cytochrome C, *via* the mitochondrial permeability transition pores. These are in part controlled by calcium ions present in the mitochondria. Thus, through **mitochondrial calcium** the cell can potentially be induced to enter the process of death.

Mitochondria can exhibit a calcium-induced calcium release process making the mitochondria an essential element in the relay of calcium wave propagation. It must be emphasised that the modulation of cell calcium signals by the mitochondria depends on their energetic status; thus, making mitochondria an essential link between energy metabolism and calcium signaling processes within the cell.[41,153,154,162,168,178]

1.3.5.1 Calcium, Mitochondria and Cell Death

As the cell's principal energy power-plant mitochondria are of paramount importance in the life and death of a cell. They provide the vital energy needed for cellular respiration and under normal physiological conditions are involved in cellular calcium homeostasis and cell signaling. It has been widely accepted that a disruption to these processes is involved in a range of pathological conditions (including the already mentioned neurodegenerative and heart diseases), particularly when combined with oxidative stress.[118,131,132,154-156,162,165,167-171,175,179-182]

There is consistent observation of mitochondrial dysfunction prior to the nuclear changes associated with apoptotic cell death. This implies that mitochondrial dysfunction may be a critical regulator of metabolic events involved in the controlled release of cytochrome C, reduction in ATP production, and loss of membrane potential: all key events in the induction of the apoptotic cascade.[117,118,120,122,162,171,179,181]

In some circumstances, it would seem that with an enhanced production of ROS, mitochondrial calcium uptake can switch from a useful regulatory mechanism to a potentially harmful process, which can initiate the progression of the cell towards death. These processes have mostly been attributed to situations arising from where mitochondrial calcium accumulation is accompanied by some form of oxidative injury.[154,162,171,181]

The ensuing discussion will focus on the role of elevated intracellular calcium levels and the involvement of mitochondria in key processes leading to the liberation of cytochrome C and/or the activation of the permeability transition pore, *i.e.* the initiation of cell death *via* mitochondrial calcium dyshomeostasis.[171,179,181,182]

1.3.6 Calcium and Oxidative Cell Injury

It has been proposed that oxidative stress causes a reduction in the activity of calcium-translocating enzyme systems, resulting in an uncontrolled rise in intracellular calcium levels. There are a number of ways oxidative stress/damage may result in an increase in intracellular calcium levels and three of these pathways are outlined below:-

(i) *Intracellular calcium release* – the calcium hypothesis proposes that oxidative injury associated with the oxidation of sulfhydryl groups (present on calcium ATPases) inhibits ATPase activity, decreasing the ability of organelles (like the endoplasmic reticulum) to sequester calcium, and of the plasma membrane pumps to extrude calcium from the cell; hence, any initial toxic lesions formed may result in an increase in intracellular calcium levels and in turn activate calcium-dependent degradative pathways leading to cell death.[156,170,171,178,183]

(ii) *Influx of extracellular calcium* – a result of toxin-induced plasma membrane damage (which causes an increase in cellular cytosolic calcium levels) is essentially a secondary process/event preceded by a toxic lesion. Calcium may enter the cell through sodium channels or through pores formed by a damaged cell membrane. If the cell is unable to pump calcium out through ATP-dependent mechanisms, intracellular calcium levels will increase; possibly activating degradative processes causing a toxic lesion.[170,183]

(iii) *Pathological influx of extracellular calcium* – occurs in association with loss of cell viability, whereby the cell membrane has become physically damaged, allowing the passage of extracellular calcium into the cytosol.[183]

Data from a number of groups, who have undertaken investigations exposing a variety of cells to a range of toxic agents, supports the second postulation, (ii). Conversely, these

groups found that incubation of cells with a low-calcium buffer prevented a rise in the intracellular levels of calcium.[183]

1.3.6.1 Intracellular Calcium and Mitochondrial Dysfunction

There are two common hypotheses which can be considered in order to try and explain lethal cell injury in terms of the relationship between intracellular calcium levels and mitochondrial dysfunction. These are:-

(i) *Calcium cycling in mitochondria* – it has been suggested excessive cycling of calcium across the inner mitochondrial membrane is responsible for reduced mitochondrial function during oxidative stress. Calcium continuously cycles across the inner mitochondrial membrane and is taken up by a highly calcium-selective ion channel (the mitochondrial calcium uniporter (MCU)) and released *via* an antiport (exchanger) system in exchange for proton/sodium ions. It has been proposed that if mitochondria were to take up excessive volumes of calcium, collapse of the mitochondrial membrane potential would be observed. The reasons and mechanisms by which this depolarisation occurs remain elusive and the subject of concerted research.[118,131,132,139,154,156,162,168,178,181,183]

(ii) *ATP depletion* – it is known that oxidative stress causes a permeability transition of the inner mitochondrial membrane which involves: (i) increased permeability to ions; (ii) mitochondrial swelling; (iii) uncoupling of oxidative phosphorylation; and (iv) collapse of the mitochondrial membrane potential ($\Delta\Psi_m$). Evidence suggests that this transition is caused by changes in the deacylation-reacylation cycle of the inner mitochondrial phospholipids. Oxidative stress inhibits reacylation of lysophosphatides and deacylation is stimulated by an enhanced phospholipase A_2 (calcium-dependent enzyme involved in lipid hydrolysis) activity in response to increased mitochondrial calcium

levels. The subsequent accumulation of lysophospholipids and free fatty acids results in a permeability change of the inner mitochondrial membrane. This transition can be stimulated by exogenous lysophospholipids, ameliorated by phospholipase A_2 inhibitors and cyclosporin A. Therefore, it may be possible that calcium plays a role in activating phospholipase A_2 in the inner mitochondrial membrane, potentially leading to increased permeability of the inner mitochondrial membrane and loss of the mitochondrial membrane potential.[12,41,120,163,171,178,180,181,183,184]

Calcium cycling is an unlikely process during oxidative stress as the energy needed for cycling is modest and very large fluxes would be required in order to depolarise the membrane. One would therefore expect a major increase in intracellular calcium concentration prior to mitochondrial depolarisation.[132,181,183]

It is known continuous charging of mitochondria with calcium will sustain the activation state of the mitochondrial dehydrogenases and may also be important in sustaining the mitochondrial membrane potential; hence, mitochondrial energy production. It has been suggested failure of this mechanism has implications in the depression of mitochondrial ATP generation, further supporting the ATP depletion hypothesis, (ii), which ultimately leads to cellular pathophysiology.[154,171]

1.3.6.2 Mitochondrial Membrane Permeability Transition Pore

Intramitochondrial calcium controls vital oxidative phosphorylation (the formation of ATP from ADP) and may contribute to the potentially life-threatening induction of the mitochondrial permeability transition within a cell. Cellular calcium accumulation can provoke the cessation of ATP production and prompt ATP synthase to begin hydrolysing rather than producing ATP. This produces an energy deficit in the cell at a time when energy is vitally needed in order to maintain the activity of ion pumps, such as the sodium/calcium exchanger; "healthy" ion pumps are important in the removal of excess calcium present in the cell.[154,155,161,166,170,175,178,180,185-188]

Under normal conditions, the inner mitochondrial membrane is quasi-impermeable to small molecules, allowing the creation of an electrochemical gradient (known as the mitochondrial membrane potential ($\Delta\Psi_m$)) between the mitochondria and the cytosol: developed and maintained by mitochondrial respiration and a necessity for the healthy functioning of the mitochondria. The collapse of the membrane potential as a response to pathological states, for example a traumatic brain injury, during anoxia (absence of oxygen) or in response to disordered mitochondria, can limit calcium uptake and contribute to cellular pathophysiology.[118,166,168,171,180,184]

The mitochondrial membrane permeability transition can be induced by a variety of second messengers which are elicited by cellular stress and include calcium and oxygen radicals. These act on the mitochondrial membrane proteins, bringing them together to form a pore - the permeability transition pore. The opening of permeability transition pores (mega-channels) results in a sudden permeability increase (permeability transition) of the inner mitochondrial membrane permitting the free distribution of ions, small solutes and select proteins with a molecular mass of less than 1,500 Da; thereby, disrupting the mitochondrial membrane potential and associated mitochondrial functions (figure 45). The activation of the pore can result in osmotic swelling of the mitochondria (edema), with rupture of the outer mitochondrial membrane effectuating cytochrome C release. Hence, there is a massive permeability transition across the mitochondrial membrane which can terminate in cell death.[12,120,131,132,154,166,168,171,172,177,178,180,181,184-186,188,189]

The principal proteins involved in the formation of this non-specific pore include the adenine nucleotide translocator (ANT, inner membrane) and the voltage-dependant anion channel (VDAC, outer membrane), with a mitochondrial inner membrane protein transporter (Tim) and an outer mitochondrial membrane protein transporter (Tom) also thought to play a part. These proteins are converted into the pore either alone or in collaboration with Bax-like proteins, with ANT and VDAC the main adenosine nucleotide exchange mediators (figure 45).[120,132,155,172,184,189]

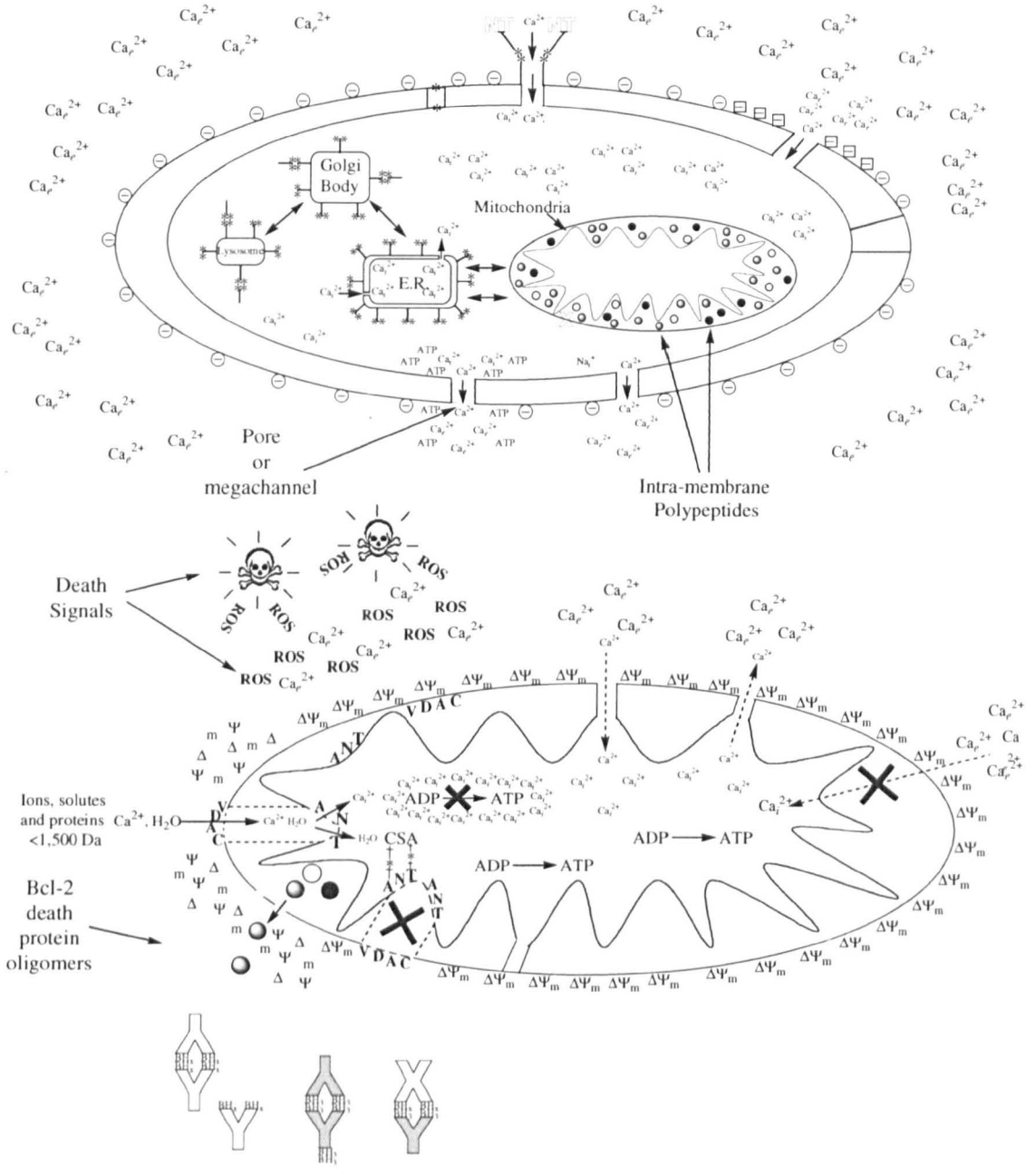

Figure 45 – Simplified Diagram of a Cell Showing Calcium, the Mitochondrial Permeability Transition and the Mitochondrial Permeability Pore

ANT is the most abundant protein in the inner mitochondrial membrane, forming a transmembrane channel, which catalyses the export of ATP in exchange for ADP (antiport) between the mitochondria and cytosol (figure 45). A number of studies have demonstrated that ADP/ATP translocase is involved in the mitochondrial membrane permeability transition; although, the exact mechanism by which this occurs remains unknown. Mitochondria from different cell types (for example, the heart and liver) are known to vary in their ANT content and it is proposed that the levels are proportional to their ability to accumulate calcium. A reduction in this translocase content shows a correlation with the reduction in the calcium-loading capacity of the mitochondria. This potential perturbation in mitochondrial calcium homeostasis may well be a crucial factor in cell death.[120,132,155,184,189] It would therefore appear ANT, VDAC and Bcl-2-like proteins may serve as sensors of external pro-apoptotic signals passing through the cell.[132]

The collapse of the mitochondrial membrane potential and uncoupling of the electron transport chain from ATP production have been shown to promote a mitochondrial membrane permeability transition. Additionally, sequential to the disruption or collapse of the mitochondrial membrane potential and the induction of the mitochondrial membrane permeability transition, is the loss of matrix calcium and further depolarisation of the inner membrane (figure 45); thereby, increasing the gating potential for the mitochondrial permeability pore. As the consequences of the membrane permeability transition are also involved in the induction of the transition, the mitochondrial permeability transition may function as a self-amplifying "switch", which, once it has been activated, irreversibly commits the cell to death.[120,161,171,181,183]

1.3.6.2.1 Function of the Mitochondrial Membrane Pore

The existence of an organelle permeability transition pore which causes cell death, with no apparent consensus for its physiological role, has led to speculation about its possible evolutionary cause. Some have speculated that this mitochondrial pore may minimise cell injury by causing gravely injured cells to die quickly and by preventing cells from oxidising substances that may be found elsewhere. Others have suggested that: (i) the

pore presents a way of clearing the mitochondrial matrix of damaged/unwanted molecules; (ii) provides an important pathway for inducing apoptosis; or (iii) may simply act to offer a way of removing damaged mitochondria.[168]

1.3.6.3 Inhibition of Membrane Permeabilisation

The mitochondrial membrane permeability transition can be inhibited by several pharmacological modulators which are thought to act on the permeability transition pore. These inhibitors include cyclosporin A which competitively binds to an enzyme located in the inner mitochondrial membrane (a proposed component of the mitochondrial permeability transition pore) and maintains the proteinaceous pore in a closed state. Inhibitors of the permeability transition pore are thought to prevent the induction of the permeability transition by the pore-forming pro-apoptotic agents such as ANT and VDAC.[120,154]

Since disruption of the mitochondrial membrane potential has been shown to induce and, be a consequence of the mitochondrial membrane permeability transition, reduction of the potential and the subsequent induction of the membrane permeability transition, may be decisive events in the apoptotic pathway following treatment with mitochondrial respiration inhibitors and uncouplers.[120] Therefore, the existence of agents capable of inhibiting the mitochondrial permeability transition may offer a way of treating undesirable damage and death occurring in the cell. Although, extreme caution should be practiced since it is known that some of the agents which act to block internal calcium pumps are known apoptotic stimuli themselves, including thapsigargin and xestospongin.[152]

1.3.6.4 Calcium, the Mitochondria and Cell Pathology

The subcellular events that lead to cell death are fundamental to understanding and developing treatments for an array of human disorders.

Factors, including the idea of a mitochondrial permeability transition and the formation of a mitochondrial membrane pore, combined with the increased understanding of the apoptotic role of cytochrome C, mean mitochondria have become the focus of intense research in toxic, hypoxic and ischemic cell injury.[118,131,132,154-156,162,166,171,175,181,185]

Diseases implicated in elevated levels of intracellular calcium include: the neurodegenerative diseases Alzheimer's, Parkinson's and Huntington's; some cancers; cardiovascular disease; cerebrovascular accidents (strokes); epileptic seizures; severe hypoglycemia; and Timothy syndrome (an arrhythmia disorder associated with dysfunction in multiple organ systems, including congenital heart disease, syndactyly, immune deficiency and autism).[118,151,154,156,162-164,166,167,169-171,180,181,184,185,190]

Proteins encoded by infectious pathogens, such as the *Helicobacter pylori* bacteria and *Neisseria gonorrhoeae*, are also thought to directly induce a transition of the mitochondrial membrane permeability by acting on the VDAC or ANT proteins respectively. In addition, inhibitors of the respiratory chain are thought to elicit their pro-apoptotic effects *via* direct mitochondrial effects; although, these mechanisms remain cryptic.[132]

1.3.6.5 Calcium, Other Organelles and Cell Death

There is evidence to suggest that other organelles, like the endoplasmic reticulum, lysosomes or Golgi apparatus, are further significant points of pro-apoptotic signaling or damage sensing. Each organelle is thought to express sensors capable of detecting specific alterations and locally activate signal transduction pathways; subsequently, emitting signals capable of establishing inter-organelle cross-talk.[132,162]

The role of these organelles in calcium-associated cell death has been discussed by a number of authors. For the scope of the following paragraphs, particular attention will only be paid to the endoplasmic reticulum. It is known the endoplasmic reticulum interacts particularly closely with the mitochondria during cell death.[131,132,156,174,190]

During conditions associated with perturbed endoplasmic reticulum functions, it is thought that the close physical and functional relationship between the endoplasmic reticulum and mitochondria may contribute to the spread of pathological signals from the endoplasmic reticulum to the mitochondria; resulting in a disturbed mitochondrial calcium homeostasis, *i.e.* mitochondrial dysfunction may occur downstream of endoplasmic reticulum dysfunction.[156,174]

The endoplasmic reticulum senses local cellular stress through a number of mediators (chaperones, calcium-binding proteins and calcium release channels) and initiates the apoptotic mechanisms *via* at least two different pathways; the already mentioned calcium signaling pathway and/or the *unfolded* protein response (UPR) pathway.[131,132,172,191]

Calcium is present in the endoplasmic reticulum in both its free-form and bound to matrix proteins. It is taken up into the endoplasmic reticulum from the cytosol *via* the sarcoplasmic/endoplasmic calcium-ATPases (SERCA) and released through the IP_3 receptor channels, with endoplasmic reticulum calcium oscillations key in the normal functioning of the cell. It has been suggested that calcium released from the endoplasmic reticulum is highly controlled by cytosolic calcium activity and perturbations in the endoplasmic reticulum calcium levels can therefore potentially trigger a transition in the mitochondrial membrane permeability; hence, giving rise to cell death.[131,132,162,175,176,187]

It may be of interest to mention that in contrast to the cytoplasm and mitochondria, the endoplasmic reticulum requires a high calcium activity for its healthy functioning. Therefore, it is a decrease and not an increase in calcium activity (as in the cytoplasm and mitochondria) which proves lethal for cells.[132,156,163]

1.3.6.6 Free Radicals

Free radicals can also cause tissue calcification by damaging the integrity of cell membranes; therefore, prompting leaks to appear in cell walls, in addition to damaging enzymatic cell wall transport pumps. If a calcium pump becomes weakened, or if the integrity of a cell wall is compromised, the calcium pump is no longer able to remove

calcium ions leaked inside of the cell. As a result, intracellular calcium levels rise, disturbing cellular calcium homeostasis and cause cellular malfunctions and eventually cell death.

Although, it is often possible to remedy a damaged calcium pump by using calcium channel blockers, these cellular paramedics can also poison the cell. Therefore, it would be more appropriate to try and repair the cell membrane, as opposed to blocking channels which would prevent the passage of vital cellular ions.

1.3.7 Summary – Calcium, the Mitochondria and Cell Death

Nuclear DNA damage and ligation of plasma membrane death receptors have long been recognised as initial triggers of apoptosis which induce mitochondrial membrane permeabilisation and subsequent caspase activation.[132]

Increasing the mitochondrial membrane permeability causes the organelle to become depolarised meaning that the membrane potential, *i.e.* the difference in voltage between the inside and outside of the membrane is lost. The induction and opening of a permeability transition pore leads to the collapse of the proton-motive force, disruption of ionic homeostasis, mitochondrial swelling and massive ATP hydrolysis. It is this sequence of events which has drawn considerable attention to the permeability transition (observed at the inner mitochondrial membrane) as a potential player in the pathways leading to cell death.[120,132,155,163,171,178,184,189]

The preceding discussion has highlighted the theory that a major determinant of cell death (induced by oxidative stress) is the reduction and/or depletion of ATP formation. This reduction in mitochondrial energy metabolism has been linked to a reduction in mitochondrial membrane potential, mitochondrial membrane pore formation and the release of pro-apoptotic stimulants (namely cytochrome C). The pore formation is linked to high intramitochondrial calcium levels and oxidative stress; thereby, implicating the role of mitochondrial dysfunction as a central element of oxidative stress and cell

death.[118,120,131,180,181,183,187,189] Therefore, it would seem fair to proffer that maintenance of the membrane potential, exhibited by mitochondria, is necessary for cell survival.[120]

It is noteworthy to mention that the disruption of cellular calcium homeostasis and loss of mitochondrial membrane potential has been proposed to be critical events in both apoptosis and necrosis. Although the focus of the preceding discussion has been particularly concerned with the intrinsic pathways (perturbations of intracellular homeostasis) of apoptosis, both forms of cell death can result from a reduced mitochondrial membrane potential.

Briefly, these two modes of cell death can be described as: (i) the unanticipated colossal destruction of organelles (including the mitochondria) leading to disordered cell death (necrosis); (ii) through mild perturbations of organelles, the trigger of a coordinated sequence of events which culminate in apoptotic cell death. The latter process involving a torrent of caspase activation, either alone or in conjunction with mitochondrial membrane permeabilisation); thus, suggesting an intimate link between caspase activation and mitochondrial membrane permeabilisation (since mitochondrial membrane permeabilisation stimulates caspase activation through mitochondrial release of caspase-activating proteins, in particular cytochrome C).[117,118,132,154,162]

It is further noted, that in a state of reduced ATP generation or severe oxidative stress, apoptosis may proceed until ATP stores are depleted; at which time the mechanisms of cell death move towards the necrotic pathways. However, the mechanisms which determine whether the cell dies apoptotically or necrotically remain enigmatic.[117,120,154] It must be remembered that alternative pathways towards apoptosis, other than *via* transitions in the mitochondrial permeability, exist (see section 1.2).

Increases in cytoplasmic free calcium levels have been shown to precede cell death in cells undergoing apoptosis. However, the specific role of mitochondrial calcium uptake in cell death processes is still unclear and remains to be established. It also remains to be seen if **mitochondrial dysfunction** is the **cause** or **effect** of disease and continues to be the subject of in-depth investigations.[118,132,162,166]

Finally, the relationship between calcium and cell death is complex. It remains unclear whether calcium deregulation acts solely by directly killing the cell or whether it is a secondary effect consequential to this perturbation. What does seem clear is that a change in intracellular calcium homeostasis, with particular respect to the mitochondria, somehow plays a central role in the cell death processes involved/present in many pathophysiological states.[162,163,166,192]

An increasing number of authors have now been able to conclude that specific types of cell death are a primary consequence of toxin-induced disturbances to the homeostasis of intracellular calcium, with mitochondrial calcium uptake an early event in apoptosis and necrosis leading to the collapse of the inner mitochondrial membrane potential.[118,120,122,154-156,166,167,171,179,181] However, in order to fully understand the exact mechanisms behind calcium-mediated cell death further investigations are needed.

1.4 NANOTECHNOLOGY

1.4.1 What is Nanotechnology?

Nanotechnology is a rapidly expanding, new and powerful discipline capable of measuring, manipulating and manufacturing materials at the atomic, molecular and supramolecular levels. This new field is bringing together scientists, engineers and physicians in an interdisciplinary manner to develop new platforms for novel imaging and diagnostic tools; thereby, propelling crucial work at the cellular and molecular levels, as well as mediating the creation of more effective therapeutic delivery platforms. Together these developments hold the potential to facilitate dramatic advances in biomedical sciences; the market alone for molecular imaging has been estimated to be worth $45 billion (USA dollars) by the year 2010.[193-200]

The focus of the following discussion will concentrate on one particular area of nanotechnology: biologically-focused nanoparticles. Nanoparticles can be described as ultra-fine particles with sub-micron dimensions; lying somewhere in the region between molecular and microscopic-type systems. They hold the potential to provide the much needed insight into the biological realms that are currently implicitly difficult or otherwise near-impossible to study.[201] Nanoparticles can be more precisely described as a particular type of colloidal system: a system where one substance (a solid) is finely dispersed in another (a liquid), whose components have nanometre dimensions and can be sub-divided to include: nanocapsules; nanospheres; liposomes; particular types of emulsions; and polymeric micelles.

The term nanoparticle is quite often used interchangeably to describe one or all of the above species causing great confusion. Therefore, for the purpose of this discussion and from this point forwards the phrase "nanospecies" will be used when referring to general systems with nanometre dimensions.

Nanospecies of many different compositions and for a variety of applications have been described in the literature.[196-201,203-234] These species are generally, but not exclusively,

synthesised from polymers and due to their minute size are comparable to biological molecules.[74,214,234-236] Through the ability to fine-tune both their physical and chemical properties (physicochemical), a range of versatile nanospecies can be synthesised with varying sizes, compositions and surface chemistries.[155,193,199,201,203,209,211,213,214,216,223,231, 235,237-243]

1.4.2 Nanosystem Applications

The ability to create species with nanometre dimensions brings with it the potential to bring about life-changing advances in both science and medicine. The design and synthesis of novel nanospecies can have a dramatic effect in the fields of: biological sensing/detection/imaging; drug delivery/disease therapy; targeted diagnostics/delivery; forensic science; and in the field of engineering.[64,74,193,196-198,199,203-205,207,211-214,216-218,220,222-224,228-232,234,237-239,243-260]

The development of nanosized biosensors, brings the scientific dream of understanding cellular events, one step closer by probing the inner space of individual living cells and monitoring their intracellular processes. Therefore, it may be possible to increase our present knowledge of the fundamental events occurring at the cellular level. The potential to increase the knowledge base around intricate and complex cellular mechanisms offers huge promise, particularly in the field of disease states. By gaining direct information on intracellular trafficking and molecular functions, it may be possible to gain a better understanding of disease mechanisms and therefore, tailor disease management to treat the cause, rather than the symptoms, of a disease.

An example of the application of nanospecies in disease therapy is the concept of nano-sized carriers. This type of system offers the ability to more efficiently deliver therapeutic agents to the disease site: thereby, minimising the required administration dose; systemic side effects; and the toxicity commonly associated with drugs in their free state. Nanospecies of this type have been increasingly sought in the management of cancers (especially in conjunction with photodynamic therapy) and for the delivery of gene-therapy agents. [194,203,207,209,213,217,228,232,257] A great deal of work has also been put into the

concept of directing species towards a specific "disease" target (such as for tumours) for the directed delivery of therapeutic agents or imaging systems; these targeted species can therefore (potentially) improve intracellular internalisation of the nanospecies.[74,196,199,210,213,214,216,218,219,231,232,237,239,242,249,251,252,255,261,262] Typically, such strategies have included the use of antibody "loaded" carriers, receptor/ligand-mediated or tyrosine aminotransferase (TAT) peptide-loaded systems.[195,205,216,218,239,242,243,262,263] Magnetic nanospecies have also been developed and have shown potential in facilitating the detection and treatment of some diseases. They have been linked to: the *in vivo* detection of cancer; drug delivery; for use in the PDT treatment of cancer; and in the delivery of insulin.[199,214,220,250] Magnetic nanospecies can further act as imaging contrast (MRI) agents to: enhance the detection of diseased tissue; in targeting strategies; and in the near infra-red management of tumours. Reports suggest a nearly fifty percent increase in the magnetic susceptibility of these systems compared to the gadolinium chelates approved for magnetic resonance imaging.[199,200,215,216,220,222,231,233,239,240,245,250,251,255] Nanospecies have also more recently shown some promise in the field of forensic science.[258,259]

1.4.3 Synthetic Materials and Techniques

The different types of nanospecies described can be synthesised from a range of materials and techniques; particularly important when considering the end application and, if applicable, the route of species administration. The most popular materials and techniques used in the synthesis of these nanospecies will be briefly described in the ensuing paragraphs, with special attention paid to emulsion polymerisation techniques.

In general, the most common synthetic materials for synthesising colloidal nanosystems involve various polymers, bio-based and inorganic materials.[74,195,196,199,203,204,208,211-219,222-224,228,229,231,232,234,237,239,243-245,249-252,254,257] Examples of these materials include, poly(esters), poly(acrylamides), poly(lactic) acid (polymers), lipids, peptides, liposomes and sporopollenin (the outer layer of pollen, bio-based), and various silica based materials (inorganics).[74,195,203,204,207,208,211-214,217-219,223,224,228,229,231,232,234,235,237,240,244,249-252,254,257]

Metals such as gold, silver, palladium and platinum have also been employed, in addition to the use of metal oxides (inorganic) in the fabrication of magnetic nanospecies.[195,196, 200,220,231,240,250,251,252]

The colloidal properties and classification of the nanospecies product (*i.e.* nanoparticles, nanospheres or nanocapsules) are dictated by the reagents used, the general synthetic procedure followed and the composition of the final nanoproduct. A typical colloidal particle can be suspended as a quasi-stable sol in an aqueous solution, offering long-term stability to nanospecies dispersion.[200,222] The stability of the system depends on the physical properties of the particles; they need to be small enough to minimise precipitation by gravitational forces. The steric and coulombic repulsions present between dispersed particles can also affect the stability of the nanospecies.[202,251] These two forces (steric and coulombic) arise from a particle's charge and surface chemistry: (i) anionic surfactants can form an electric double layer (generating electrostatic repulsions between the particles) with (ii) hydrophilic groups (from non-ionic surfactants) present at the micelle/particle surface able to "attract" water molecules (forming a "protective (water) barrier" between the particle), minimising coagulation (thickening/clotting). Hence, these forces both act to stabilise the particles/system by minimising particle coagulation.[264]

The method of nanospecies preparation typically involves an emulsion technique, such as: (i) emulsion polymerisation; (ii) solvent evaporation emulsification; (iii) emulsion diffusion; (iv) phase inversion; (v) interfacial polycondensation; (vi) interfacial polymerisation; and (vii) interfacial nanodeposition of a preformed polymer; all of which involve the formation of an intermediate micellar system.[203,207,214,217-219,232,250,251,252] The methods of preparation also dictate/are dictated by the starting reagents; for example, whether the preparation starts from monomers or preformed polymers, inorganic materials, such as silicas, or whether natural molecules such as proteins, polysaccharides and more recently, sporopollenin are involved.[234,252]

Silica nanospecies can be further divided into two categories; ultra-fine silica nanoparticles or organically modified silica nanoparticles (ORMOSIL's).[194,210,214,245] The

latter species have the potential to overcome the limitations which may otherwise be associated with "unmodified" silica based nano-counterparts.

Nanospecies, with the intention of being used for magnetic based applications, commonly encapsulate superparamagnetic iron oxide (magnetite). They may also be surrounded by stable noble metals (such as gold particles) which act to prevent the degradation of the metallic species.[196,197,199,214,215,220,231,232,240,250,251,257]

However, for the purpose of this discussion, particular attention will be paid to polymeric materials since they are particularly well suited for bio-nanotechnology applications. Due to their unique characteristics they can be highly water soluble; show low toxicity; exhibit prolonged circulation in the blood system; are biodegradable (days to months); can be readily modified to incorporate surface functionality; encapsulate various guest molecules; their size can be varied with relative ease; and they have been safely used in the human body for over 30 years.[74]

1.4.4 Polymers - What are they?

Polymers are macromolecules generated through the sequential reaction of a number of small elementary units, known as monomers. The monomer sub-units add together *via* a series of chain reactions (known as propagation steps) to form a core repeating segment, known as the polymer. This repeating block can take on the form of a number of compositions and can be classified as linear, branched, chain or networked. Polymers can also be classified as homo- or heteropolymers; homopolymers have a repeating unit, for example, of $-[AA]_n-$, and random (hetero-) co-polymers are made up from more than one monomer unit and are represented, for example, as $-[ABAABBBBABAAA]_n-$. Alternating co-polymers are also made up of more than one monomer unit and can be represented as $-[AB]_n-$, while block co-polymers are generally represented as $-[AAABBB]_n-$. The square brackets "enclose" the structure of the repeating polymer unit and the subscript "n" identifies the number of these units from which the polymer is made. The ends of the polymer structure are left unspecified since they are an insignificant proportion of the total polymer molecule. Multiple polymer chains can also

be linked together joining adjacent polymer chains *via* cross-linker monomer units. In addition, a number of structural orientations, including *cis*- and *trans*-geometries, head-to-head or head-to-tail arrangements exist (figure 46).

Head-to-head Polymer

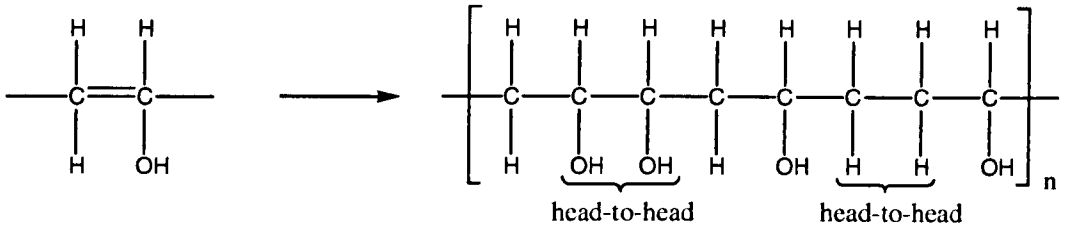

Monomer - vinyl alcohol

Polymer - poly(vinyl alcohol)

Head-to-tail Polymer

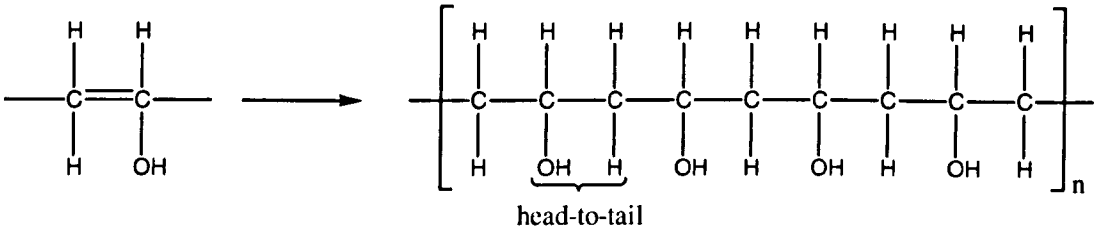

Monomer - vinyl alcohol

Polymer - poly(vinyl alcohol)

Figure 46 – Examples of Head-to-Head and Head-to-Tail Polymers

Polymers are typically described as thermoset: plastic which can be "cured" by application of heat or by chemical means to form a cross-linked structure that cannot be softened at high temperatures, or thermoplastic: plastic capable of being repeatedly softened (heating) and/or hardened (cooling). These plastics have an extensive range of applications including electrical insulators and melamine (thermoset plastics) and polystyrene and nylon (thermoplastic).

1.4.4.1 Monomers

In contrast to polymers, monomer molecules are implicitly smaller and simpler in nature, reacting together *via* their multiple bonds to form the basic structural unit of the polymer. These multiple bonds are usually double in nature and can be thought of as the molecule's "active centre" (bold lines, figure 47), they are cleaved by an initiator molecule to yield a highly reactive monomeric radical intermediate. Examples of monomers include: styrene; methylmethacrylate; vinyl acetate; and butadiene. Their respective polymers are known as poly(styrene); poly(methylmethacrylate); poly(vinyl acetate); and poly(butadiene) (figure 47).

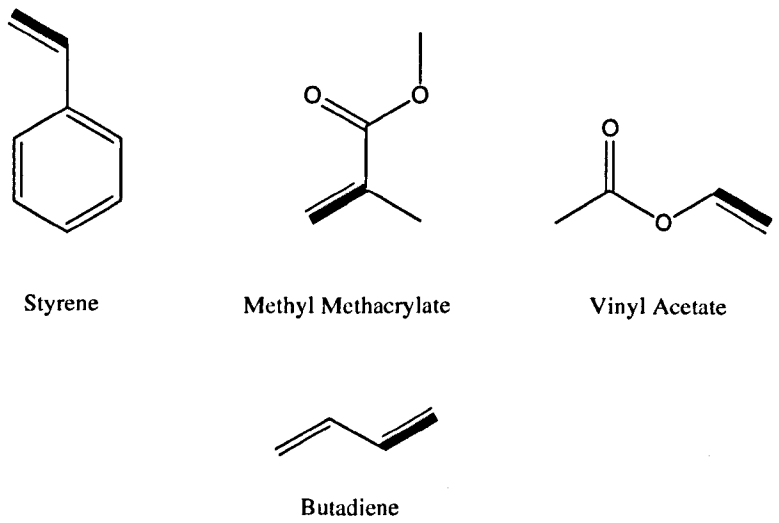

Figure 47 - Examples of Monomer Molecules

Additional monomers may also be used in the polymerisation process (co-polymerisation), with the exact arrangement of multiple "monomer units" varying almost infinitely; however, a certain degree of control over the structural arrangement can be exerted through the relative reactivities and concentrations of the multiple monomer species (see Chapter 3).

It is to be noted that not all polymerisation reactions are driven by the formation of free radicals. Polymers may also be formed by a number of other routes including, cationic and anionic polymerisations and condensation reactions (condensation polymerisation).

1.4.4.2 Initiators

Initiators typically take the form of a relatively unstable molecule which readily decomposes into two free radical species. The formation of the free radicals can be induced by: photochemical processes (ultraviolet radiation); radiative processes (photolysis and radiolysis); or through the use of a second "initiator" molecule. Typically, these can act through the non-radical attack of a reactive nucleophile (such as an amine compound) on the O-O σ-bond present in a peroxide-type initiator species (figure 48).[265]

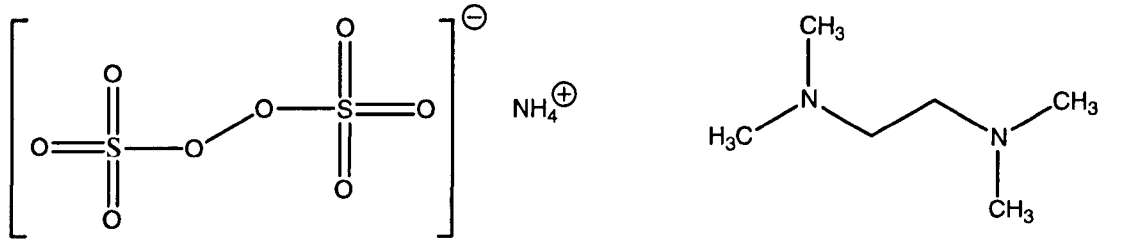

Ammonium Persulphate

N,N,N',N'-Tetramethyl-ethane-1,2-diamine

Figure 48 – Example Redox Initiator System

1.4.5 Emulsion Polymerisation

By far, the most widely used techniques for the preparation of nanospecies, falls into the category of emulsion polymerisation. Emulsion polymerisation generally involves two immiscible phases; typically an aqueous and an oily (organic) phase. The fine particles in one phase are trapped within assemblies of surfactant molecules (dispersed in the continuous domain) known as micelles (figure 49). These surfactant-stabilised micro-cavities provide a confinement effect towards the polymer, limiting particle nucleation, growth and agglomeration.[253] When the size of the particles is in the sub-micrometer

range, the system is referred to as a microemulsion and it is proffered, when the particles are in the nanometre range, the system becomes a nanoemulsion.

The preparation of an emulsion leads to either oil-in-water (o/w) systems (nanocapsules with an oily core suspended in a continuous aqueous phase) or water-in-oil (w/o) emulsions yielding an aqueous core suspended in a continuous oily phase (figure 49). It is also possible to prepare multiple emulsion systems, such as water-in-oil-in-water (w/o/w) and water-in-oil-in-oil (w/o/o) emulsions.[203,214,250,251,253,256,266]

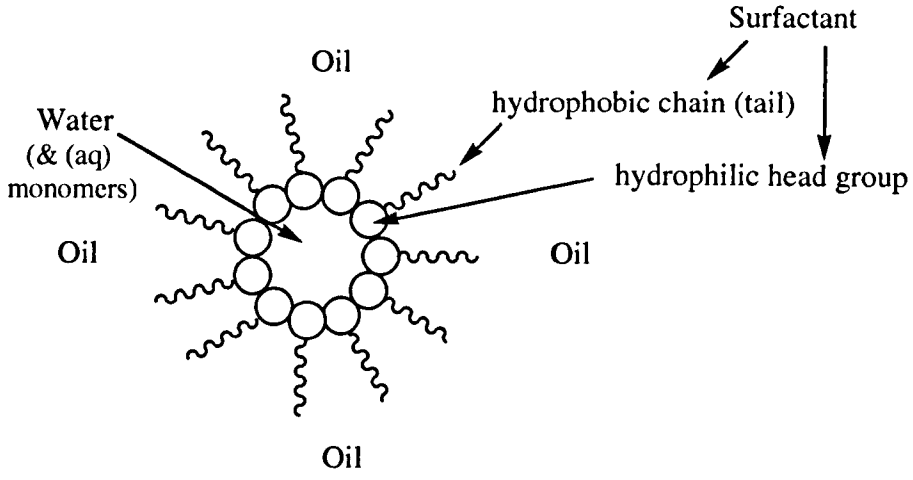

Figure 49 – Reverse Micelle (water-in-oil micelle)

1.4.5.1 Emulsion Techniques

Emulsion polymerisation can be considered as a general "heading" for a group of methods which incorporates: solvent evaporation; emulsion diffusion; phase inversion; and interfacial polymerisation techniques. The choice of synthetic method is primarily dictated by the desired application of the nanospecies.

Solvent evaporation is a process where by the hydrophobic polymer solvent is removed by evaporation. The polymer is dissolved in a water-immiscible solvent with the resultant mixture emulsified in a continuous aqueous phase, forming discrete droplets. The process relies on the organic solvent diffusing into the aqueous phase and evaporating at the

interface between the aqueous phase and air. As evaporation proceeds and the solvent is removed from the system the tiny spheres formed become hard. This procedure has been used in the preparation of poly(lactic) acid and poly(lactic-co-glycolic) acid spheres loaded with a number of different therapeutic agents for use in the delivery of anti-cancer drugs and fertility treatments.[203,214,218,219,266]

Interfacial polycondensation/polymerisation is a chemical method characterised by the formation of a "capsule wall". The "wall" is the result of rapid polymerisation (of the monomers) at the surface of droplets/particles formed from the dispersed core material. A multifunctional monomer is usually dissolved in a solution of core material which is dispersed in the aqueous phase. A reactant is then added to the aqueous phase with polymerisation quickly following at the surface of the core droplet, forming the walls of the capsule.[203,214,267] Interfacial polymerisation sees the polymer formed *in situ* and can be used to prepare both oil-in-water and water-in-oil emulsions.

To prepare oil-in-water systems *via* these methods, solvents need to be capable of dispersing the tiny droplets of oil in the surfactant-containing aqueous phase. It is important that the organic solvent is completely water-miscible in order to allow, as the solvents diffuse towards the aqueous phase and the aqueous domain towards the organic phase, the spontaneous formation of the tiny oil droplets (see section 1.4.7). The rate of polymerisation must be rapid to facilitate the efficient formation of the polymer envelope around the droplet of oil. The oil and monomer are dissolved in the water-miscible organic solvent; the organic phase is then added to the aqueous phase containing the hydrophilic surfactant. Once the nanospecies have formed, the redundant residual aqueous/organic layer (*i.e.* the dispersant) can be removed *in vacuo* to yield the nanospecies. The polymerisation in both the oil-in-water and water-in-oil cases is initiated by nucleophilic species; either from reagents present in the polymerisation medium or from the dissociation of water molecules (scheme 11).[214]

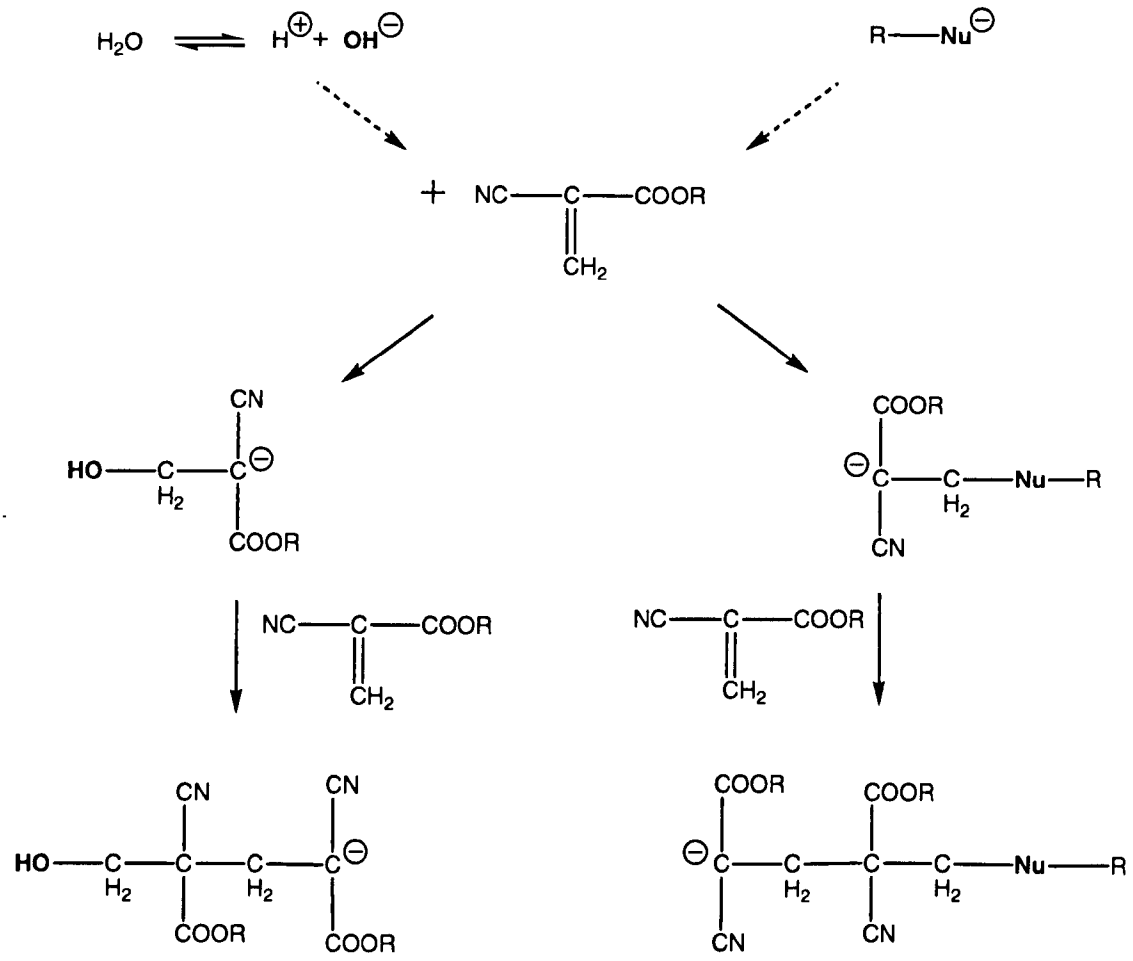

Scheme 11 – "Nucleophilic" Polymerisation

1.4.6 Inorganic Non-Polymer Synthesis

Nanospecies can also be synthesised from inorganic materials such as silica. Briefly, silica based nanosystems may be formed *via* the sol-gel method, whereby a silica shell is formed within a micelle cavity, or by the Stöber method (also based on micelle formation, similar to emulsion polymerisation) *via* the hydrolysis and condensation of silane precursors.[196,215,235] Typically, alkyl- and silane-based precursors (such as triethylvinylsilane and phenyltrimethoxysilane) are combined with water, an alcohol and a catalyst. The silane precursor undergoes hydrolysis generating silanol groups (SiOH), which *via* condensation with the alkyl or silanol species, go on to form either alkoxy (SiOR) or siloxane type intermediates; eventually culminating in the desired polymeric

species (scheme 12). The properties of the nanospecies can be controlled/tailored by controlling the reaction parameters and conditions, including: (i) the type and amount of alkyl species present (these act as network modifiers by terminating the silica intermediates); (ii) varying the hydrolysis time; and (iii) the water to surfactant ratio (increasing the ratio is reported to decrease the final nanospecies size); and (iv) by adding a hydrophilic polymer, such as polyethylene glycol, to the reaction mixture. Polyethylene glycol (PEG) is a steric stabiliser, which prevents nanospecies aggregation, having the ultimate effect of "reducing" the particle size. Finally, (v) by using different alkyl reagents which increase the hydrophobicity and porosity of the nanospecies matrix.[196,215]

$$Si(OR)_4 + xH_2O \longrightarrow Si(OR)_{4-x}(OH)_x + xROH$$

$$\begin{cases} Si(OR)_{4-x}(OH)_x + Si(OR)_{4-x}(OH)_x \longrightarrow (RO)_{4-x}Si\text{-}O\text{-}Si(OR)_{4-x} + xH_2O \\ Si(OR)_4 + Si(OR)_{4-x}(OH)_x \longrightarrow (RO)_{4-x}Si\text{-}O\text{-}Si(OR)_{4-x} + xROH \end{cases}$$

Scheme 12 – Silica Hydrolysis and Condensation

Magnetic nanosystems may also be synthesised from solution techniques; from aerosol/vapour phases; phase inversion; or by creating a micellar system as described above (when using an emulsion polymerisation method).[195,199,240,250,251]

1.4.7 Microemulsions – what are they?

Microemulsions are a relatively new area of emulsion science. They were first reported in a scientific paper in 1943 (Schulman) – with the term microemulsion first used/noted in 1959. This was in despite of their use to clean woollen garments in the early 1900's in Australia, and the discovery of commercial liquid waxes in 1928 (Rodawald).[268-270] Today, microemulsions are employed in a number of lucrative commercial fields including: enhanced oil recovery; for fuels and lubricants; as coatings; and in the cosmetics industry.

Many descriptions and definitions of microemulsions have been noted over the years, varying slightly with each report. Some reports prefer to use the term "swollen micelles", others, "micellar emulsions". However, all of the microemulsion descriptions point to a common theme: an optically transparent or translucent liquid system of low viscosity, composed of an "oil" and an aqueous phase, stabilised by amphiphilic compounds (surfactants) present at the oil/water interface.[250,253,268,270-279] These micro-systems, to a certain degree, are akin to macroemulsions ("traditional" emulsions). However, in contrast to these "traditional" emulsions and under the right conditions (the critical micelle concentration, c.m.c.), microemulsions form spontaneously in a system composed of (i) surfactant molecules and (ii) aqueous and oily domains. They are thermodynamically stable and as a result of a surfactant-stabilised oil-aqueous interface, they are able to take on a wide variety of structures, including globular, lamellar, rod, bicontinuous or cubic; thus, minimal direct contact between the oil and aqueous phases exists.[253,268,271-274,278]

1.4.7.1 Micelles

Micelles are the simplest of the microemulsion structures. They are formed/stabilised by an interfacial layer of surfactant molecules, which separate the oil and aqueous phases through the creation of oil droplets dispersed in a continuous aqueous phase (o/w, micelle); or droplets of the aqueous phase dispersed in a continuous oily domain (w/o, reverse micelle), both of which are stabilised by surfactant molecules (figure 49).[251,253,255,270,275] The possibility of these tiny droplet cores acting as loci for polymerisation reactions (a concept first published in the 1970's) has since been widely documented.[272] The size of the tiny species formed during the microemulsion process mean the reaction system appears optically transparent; whereas, in a conventional emulsion a typically milky appearance is observed: a result of the larger dispersed droplets (>0.1 μm) acting as efficient scatterers of light. The nanometre size of the final microemulsion particles results from the collision and fusion of the original micelles.[253,268,270,273] Micelles can be formed from single dual-chain (sodium bis-(2-ethylhexyl) sulfosuccinate, AOT) and non-ionic surfactants (polyoxyethyl alcohol, POE) but it is common to use a second surfactant molecule, known as a co-surfactant,

particularly if the "primary" surfactant is ionic and contains only a single hydrocarbon chain (such as sodium dodecylsulphate, SDS, figure 50): the co-surfactants act by increasing the solubilisation capability of the system and are usually medium-sized aliphatic alcohols.[268,273,277]

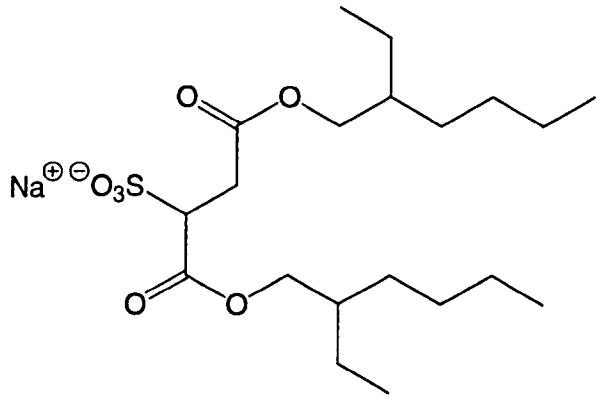

AOT

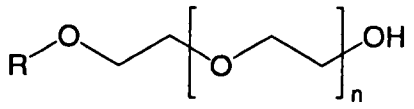

POE

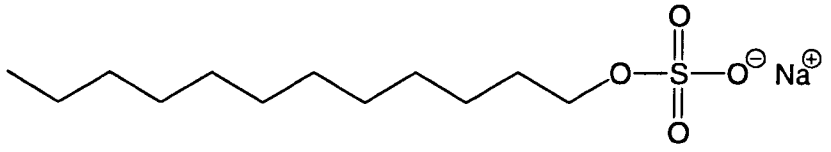

SDS

Figure 50 – Sodium Bis-(2-ethylhexyl) Sulfosuccinate, Polyoxyethyl Alcohol and Sodium Dodecylsulphate Surfactants

1.4.7.2 System Stability

A fundamental property of microemulsions is the ultra-low interfacial tension ($\gamma_{o/w}$) between the two different domains. The main role of surfactant molecules is to minimise the energy required to increase the surface area of the micelles (enabling the spontaneous dispersion of aqueous or oil droplets in the continuous phase); thereby, forming a thermodynamically stable system. Without the ultra-low tension the micelles simply would not form.[268]

The differences in the stability between the two different emulsion systems (conventional and micro-) is a result of the differing micelle growth mechanisms between the two systems. In classical emulsions, the average micelle size grows continuously with time and as a consequence phase separation occurs under gravitational force, *i.e.* conventional emulsions are relatively thermodynamically unstable but "kinetically stable".[268,269]

An additional difference between macroemulsions and microemulsions arises from the quantity of surfactant needed to stabilise the system. Microemulsions routinely require much larger quantities of surfactant molecules; commonly amounting to 10% of the total mass of the polymerisation system, approximately 6% more than for traditional emulsions.[272] Such a high percentage can have a consequential drawback for nanospecies prepared *via* the microemulsion method with regard to their end application/use. In particular their use in bio-based fields may be somewhat limited: surfactants are thought to be able to interact with the fat from which cells are composed (after all they are "soap" molecules). They are also thought to affect the skin by interfering with the structure and function of keratinocytes: major epidermis cells that synthesise the key protein keratin, also found in hair and nail cells. Through restricting cellular development this can lead to an impaired barrier function of the skin; in addition to an increase in the amount of water lost through the skin.[279]

One of the greatest features differentiating macroemulsion and microemulsion systems comes from the polymerisation mechanism of the initial dispersions. As already mentioned, in the microemulsion process particle nucleation is continuous throughout the reaction: in contrast to emulsion polymerisation where nucleation stages only occur in the preliminary stages of the process, characterised by a high ratio between the micelle to radical concentrations.[253,272,280] This difference culminates in a greatly reduced number of polymer chains present in the tiny microemulsion particles formed, in comparison to the several thousand polymer chains co-existing in particles formed through traditional emulsion polymerisation.[272]

1.4.7.3 Predicting Microemulsion Type

Microemulsions can be classified according to the type of surfactant(s) present in the system, with particular importance resting on the molecular arrangement of the surfactants at the interface between the immiscible phases. The nature of the classification is based on four different types of phase equilibria, described as Winsor type's I-IV (figure 51).[268,276,279]

Winsor type I microemulsions arise when surfactant molecules are preferentially soluble in the aqueous phase of the system, resulting in oil-in-water microemulsions. The "surfactant-rich" water phase co-exists with the oil phase where surfactant molecules are present only at low concentrations.

Winsor type II systems are the result of the greater affinity displayed by surfactant molecules for the oil phase, yielding water-in-oil microemulsions; the "surfactant-rich" oil phase and "surfactant-poor" aqueous phase co-exist together.

Winsor type III systems are generated from a three phase system whereby a "surfactant-rich" middle phase co-exists with an "excess" of the aqueous and oil phases (both "surfactant poor"), generating bicontinuous structures (randomly partitioned oil and aqueous domains, forming a "sponge-like" structure), (Winsor III or middle-phase microemulsion).

Winsor type IV microemulsions result from a single phase (isotropic) micellar solution, formed upon addition of sufficient amounts of surfactant and co-surfactant.[268,276,279]

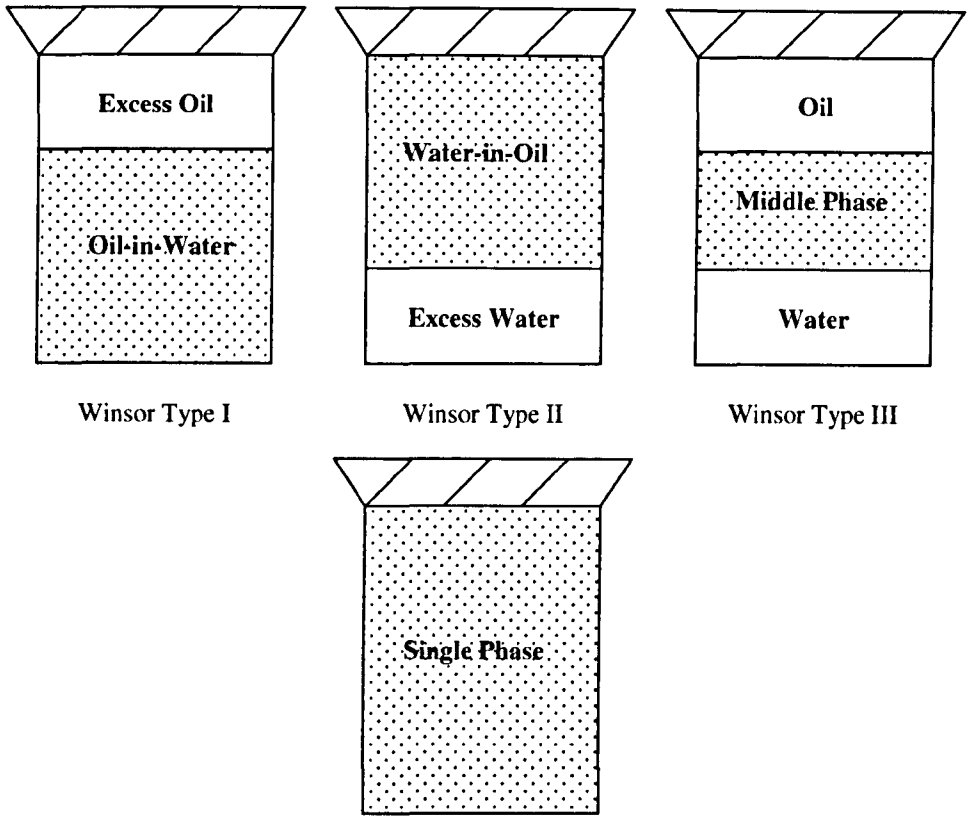

Figure 51 – Simplified Diagram of "Phase Composition" and Winsor Classification/Type

1.4.7.4 Theory of Microemulsion Formation

In order to contemplate how a microemulsion is spontaneously formed, one must first consider the energetics of the system and visualise the dispersant as tiny droplets present in the dispersed phase; from this the energy change associated with creating the "new interface" of the surfactant-stabilised structures can be determined. The associated free energy ($\Delta G_{form.}$) for creating the stabilised structures can be expressed through the configurational entropy (ΔS) and the energy for creating the "new interface" ($\Delta A\gamma_{12}$, where ΔA is the change in the interfacial area and γ_{12} is the interfacial tension between the two phases) and T is the temperature of the system (equation 2).

$$\Delta G_{form} = \Delta A \gamma_{12} - T\Delta S$$

Equation 2 – Gibbs Free Energy Formula

On dispersion, the number of dispersed droplets increases and the configurational entropy becomes positive. If the surfactant molecules can sufficiently reduce the surface tension of the system, the energy term (ΔA) will therefore be minimised and become positive - a favourable (negative) change in free energy and spontaneous formation of the microemulsion structures.[268]

1.4.7.4.1 Interfacial Tension (γ)

Three distinct regions are recognisable in a microemulsion system: (i) the oil (organic) region; (ii) the aqueous layer; and (iii) that of the surfactant. The interfacial region created between the oil and water phases by the surfactant will not necessarily be composed solely of the surfactant molecules. It is likely small amounts of the two immiscible phases (organic and aqueous) will be present as well (figure 52). Cohesive interaction energetics, such as water-water, oil-oil, hydrophilic-hydrophilic and hydrophobic-hydrophobic interactions, will therefore be present in this region, determining the interfacial stability of the surfactant film.[268]

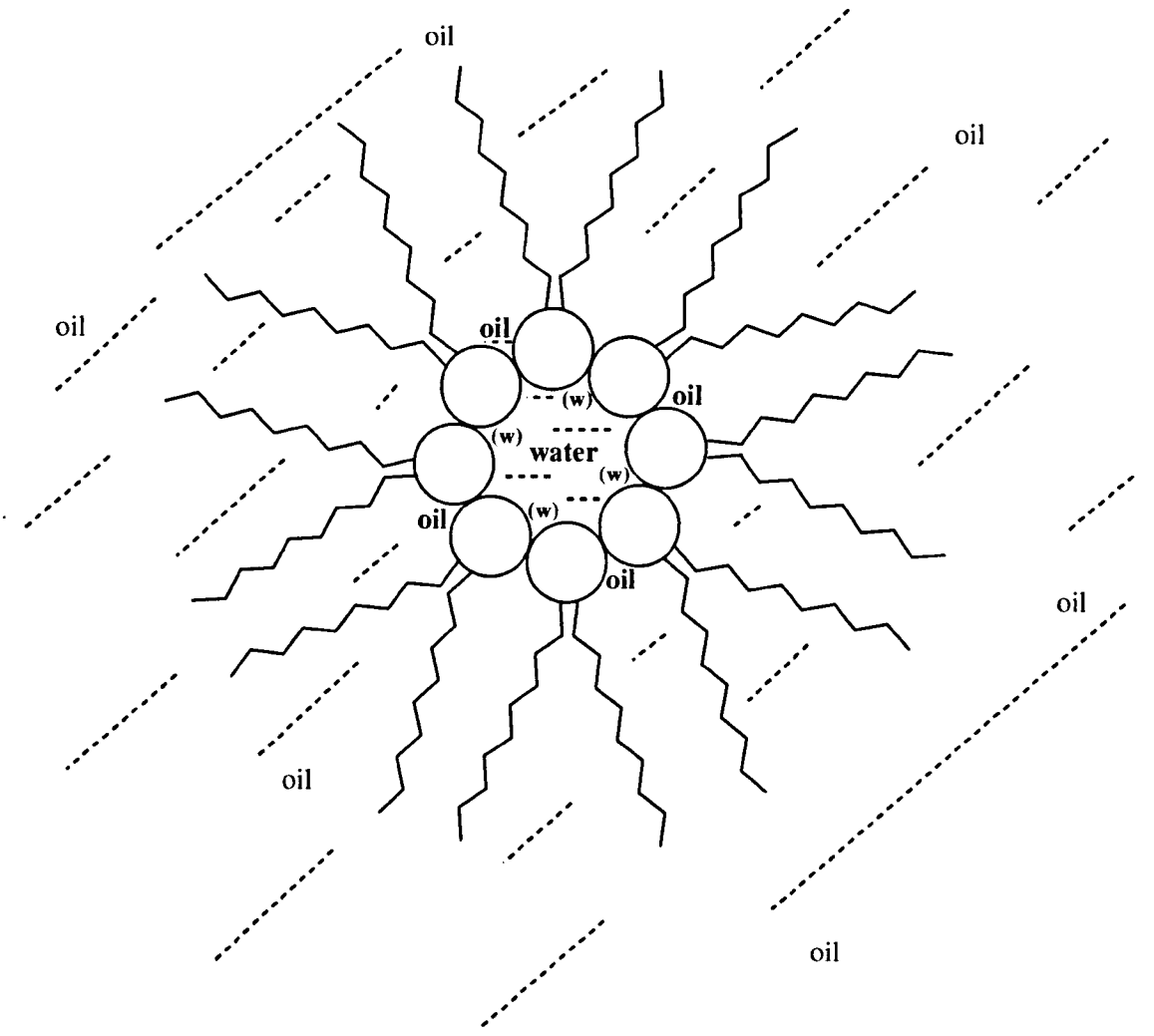

Figure 52 – Multi-Phase Interfacial Region

1.4.7.4.2 Interfacial Curvature

The direction and extent of interfacial curvature in the system may be considered in terms of the interactions present at the adsorbed interfacial domain and can be described by Bancroft's rule. Bancroft's Rule takes into account the consideration that a surfactant layer/adsorbed layer has a dual nature, *i.e.* an "inner" and an "outer-side" of interfacial tension, that are independent of one another. The presence of such a system will cause the adsorbed layer to curve, with greater interfacial tension present on the "inner" curvature surface rather than the "outer" one. Bancroft's rule states that;

"the external (continuous) phase will be the one in which the emulsifier (surfactant) is most soluble", *i.e.* surfactants promote dispersion of the phase in which they are least soluble; hence, oil soluble emulsifiers (surfactants) will form water-in-oil emulsions and *vice versa*.[268]

The influence surfactant molecules and solvents have on the interfacial curvature in the system can be considered in terms of the R-ratio (as proposed by Winsor). The R-ratio is based on the relationship between the interaction energetics present between the oil and aqueous phases and the surfactant layer. It allows the dispersion affinity of the surfactant molecules in the oil phase to be compared with their affinity to disperse in the aqueous phase. If a greater affinity for one phase exists, the surfactant layer (*i.e.* the interfacial region) will present a desire to take on a definite curvature.[268,272]

1.4.7.4.3 Interfacial Stability

To ensure the interfacial layer remains stable interactions between the oil and aqueous phases need to be relatively small. If the interactions become too great, the surfactant will have a greater affinity for one phase over the other and the stability of the system will be significantly reduced/lost and a "phase separation" will occur. If the R ratio is greater than one ($R > 1$) the interface tends to increase its area of contact with the oily phase, and therefore decrease its contact area with the aqueous phase. Thus, the oil phase tends to become the continuous phase and the system can be referred to as a Winsor type II.[268]

The preferred curvature present in the microemulsion system, and hence the microemulsion type, is influenced by the relative areas of the surfactant head- (a_o) and tail-groups (v/l_c). If [268,279]

$a_o > v/l_c$, an o/w microemulsion forms

$a_o < v/l_c$, a w/o microemulsion is formed

$a_o \approx v/l_c$, a middle-phase microemulsion is generated.

Alternatively, if equal amounts of the aqueous and oil (organic) phases are present in the microemulsion system, then the surfactant layer is free to take on the configuration of the

lowest energy and spontaneous curvature of the interfacial surfactant layer will take place.[268]

1.4.7.4.4 Phase Behaviour

Phase diagrams are complex in nature and with respect to this discussion will only be briefly mentioned and simply described. For further details the reader is referred to the published texts on the subject matter.[235,268,275,277]

The solubility and interfacial properties of a microemulsion are related to the nature and relative concentrations of the components present in the system, in addition to the pressure and temperature the system is exposed to. It is therefore important to take into consideration phase diagrams and be aware of how they are drawn from a number of system variables.

Phase diagrams allow the existence and stability of the different microemulsion phases to be described, along with the "location" of the structures present in the microemulsion system.[235,268,275,277] Stable dispersions can be formulated over a range of oil and aqueous phase volumes. The microemulsion can be composed of oil-in-water or water-in-oil droplets in the region of the phase diagram where low concentrations of either the oil or aqueous phase are encountered (figure 53). A transition between the two types of system (oil-in-water or water-in-oil) can be brought about by varying the volumes of the two different phases.[275]

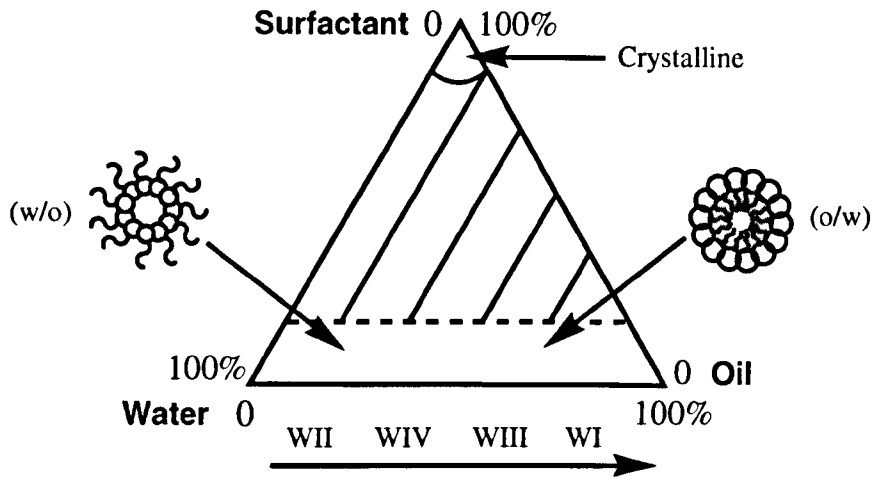

Figure 53 - Simplified Phase Diagram

A note - the aqueous phase is actually much more complex in nature than that described above. It is composed not only of "water" but also of the polymerisation monomer(s); consequently, the number of degrees of freedom and complexity of the system are increased. Therefore, for simplicity and the purpose of this discussion, the aqueous phase will be considered only as a single component of the phase diagram.[277]

A phase diagram is governed by the phase rule (equation 3). The rule allows the identification of the number of variables present in the system to be determined depending upon the composition and conditions the system is subject to, such as temperature and pressure.[235,268]

$$F = C - P + 2$$

Where,

F = the number of possible independent state changes

C = the number of independent chemical constituents

P = the number of phases in the system.

Equation 3 – The Phase Rule

A system composed from three different components with two phases can therefore be described as univariant; since F = 1 at a fixed temperature and pressure, and can be graphically depicted as a ternary phase diagram. A system is described as divariant, trivariant and so forth when F = 2, 3 and so on.[268] For example, a univariant system (o/w or w/o) can be identified as a Winsor type I or II (figures 51 and 53).

1.4.7.5 Surfactants

Surfactants are a group of organic surface activating molecules, also known as emulsifying agents and soaps/detergents, which can be isolated from natural and synthetic sources, including cell membrane lipids (natural) and cleaning detergents (synthetic). They act by minimising the interaction between the different phases present in the system by "activating" the interface between the two (immiscible) phases. They have a particular type of molecular structure composed of two components with differing solvent affinities; a hydrophilic head group and a hydrophobic tail group, which work to stabilise the system (figure 54).[268,274,276,281-283] When surfactant molecules are present in a multi-component system at a low concentration, they can orientate themselves and adsorb at the interface (boundary) between the two immiscible phases, so that their hydrophilic head group can maintain favourable contact with the aqueous phase and therefore reduce any interaction with the oil phase; hence, minimising the interfacial tension between the two domains.[268]

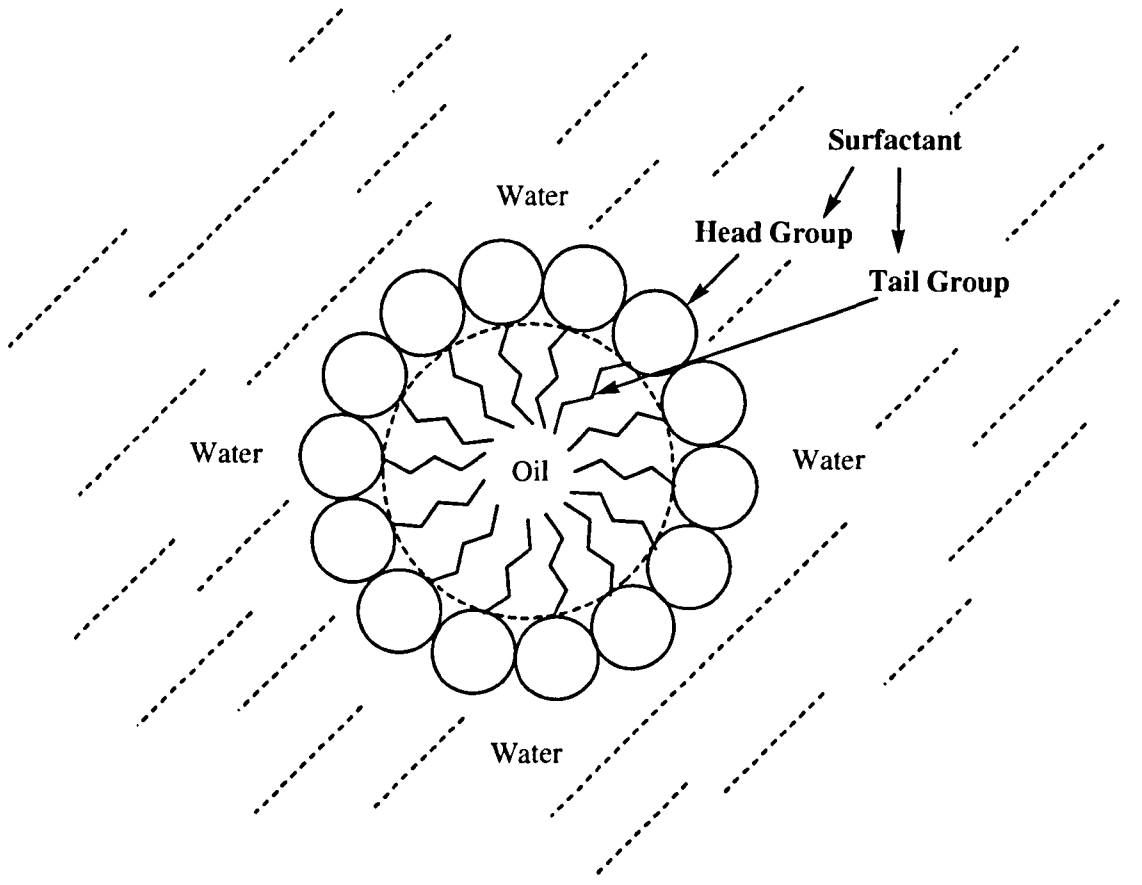

Figure 54 – Simplified Diagram of a Surfactant-Stabilised System
(Oil-in-Water Microemulsion)

It has already been mentioned that by forming micelles the surfactant molecules reduce the rigidity of microemulsion systems, *i.e.* they increase the molecular disorder of the system.[268,273] These aggregates (micelles) are spontaneously formed when a specific concentration, known as the critical micelle concentration (c.m.c., the transition from "free" surfactant molecules to surfactant "aggregates") is reached.[281,282,284] Below the c.m.c. surfactants are loosely integrated in the aqueous phase. It is only when the c.m.c. is approached that the surfactant molecules begin to orientate and form micelles. The adsorption of surfactant molecules at the system interface is favourable in terms of system energetics (with respect to surfactant molecules). The energy of the surfactant molecules, solubilised in either the oil or aqueous phase, is greater than the energy needed for the surfactant molecules to come together and form oriented molecular

structures (namely monolayers or self-assembly structures (micelles and vesicles)) at the interface between the two systems. This energy difference results in the spontaneous formation of surfactant monolayers or aggregates and the subsequent decrease in interfacial (surface) tension present in the system.[268]

1.4.7.5.1 Surfactant Properties

The surface activating properties of the surfactant molecule are dictated by the number and arrangement of their hydrocarbon tail groups, along with the nature and position of their polar head groups.[268]

The surfactant tail is usually an alkyl chain (typically 8-18 carbon atoms long) and the charge present on the polar head group (anionic, cationic, non-ionic or zwitterionic, figure 55) dictates the primary classification (after dissociation in aqueous solution) of the surfactant molecule.[268,282,283] Anionic head groups normally take the form of carboxylates ($-CO_2^-$), sulphates ($-OSO_3^-$) sulphonates ($-SO_3^-$) or phosphates ($-OPO_3^-$), with cationic surfactants arising from an amine derivative ($-NH_x^+$), and non-ionic surfactants from a highly polar (non-charged) moiety, such as polyol groups ($-OCH_2CH_2O-$). In each of the above cases, the more polar surfactant head group shows a greater affinity towards water molecules than its hydrocarbon tail. As a result, when surfactants are added to aqueous and oil phases, the surfactant molecules rest at the oil-water interface and arrange themselves in a manner which sees the hydrophilic head group aligned in the aqueous phase (with the hydrophobic tail residing in the oil phase). This orientation witnesses the formation of "normal" micelles (o/w) or "reverse" micelles (w/o) and is a result of the hydrophobic effect, *i.e.* stronger intermolecular interactions exist between the polar surfactant head group and the aqueous phase; in comparison to the non-polar tail and aqueous phase.[268,274,281-284]

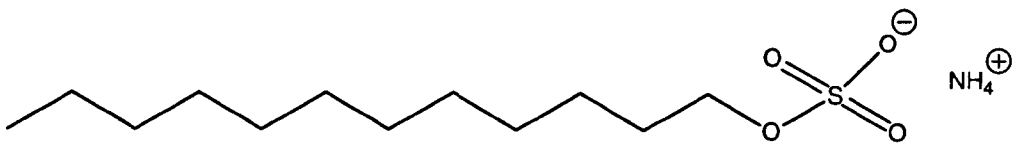

Ammonium Lauryl Sulphate (Anionic)

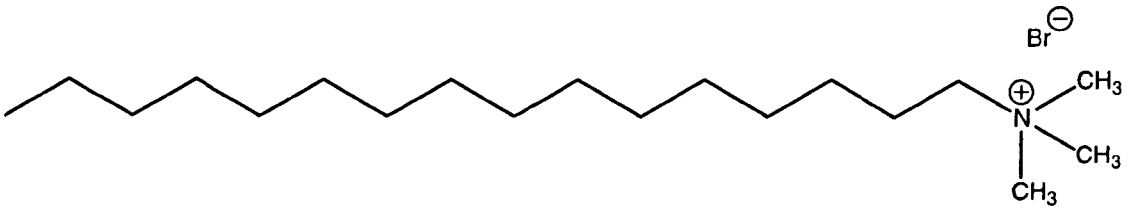

Hexadecyltrimethylammonium Bromide (Cationic)

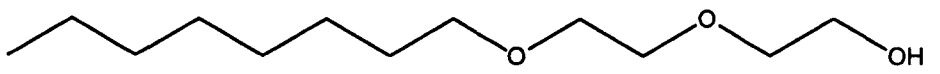

Diethylene Glycol Monooctyl Ether (Non-ioinc)

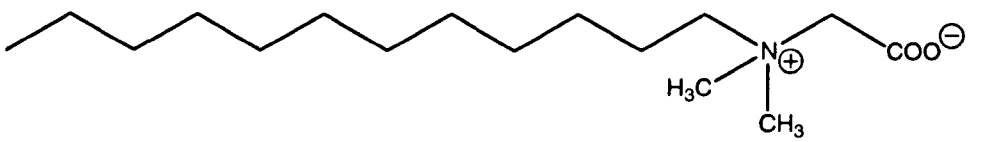

N,N'-dodecyl-*N,N'*-dimethyl Betaine (Zwitterionic)

Figure 55 - Examples of Different Surfactant Molecules

The range of different chemical structures surfactant molecules can possess allows them to be used in a variety of applications including: industrial process (cationic surfactants); household detergents and fabric softeners (anionic surfactants); and personal health care products (anionic and zwitterionic surfactants).[268]

1.4.7.6 Water-in-Oil Microemulsion Polymerisation – Free Radical Polymerisation

Microemulsion systems can be home to polymerisation reactions. Water-in-oil microemulsions are generally prepared *via* a free radical polymerisation process involving a (i) monomer; (ii) surfactant; (iii) an aqueous; and (iv) an oil phase.[272] The monomer-containing aqueous phase is dispersed in the "surfactant-rich" oil phase under strong magnetic stirring and a continuous inert atmosphere (figure 56). The success of the reaction depends on the rapid polymerisation of the monomer in the surfactant-stabilised aqueous cores. However, care should be taken not to stir the system too vigorously: excessive stirring will generally result in the generation of too much foam from the surfactant molecules.

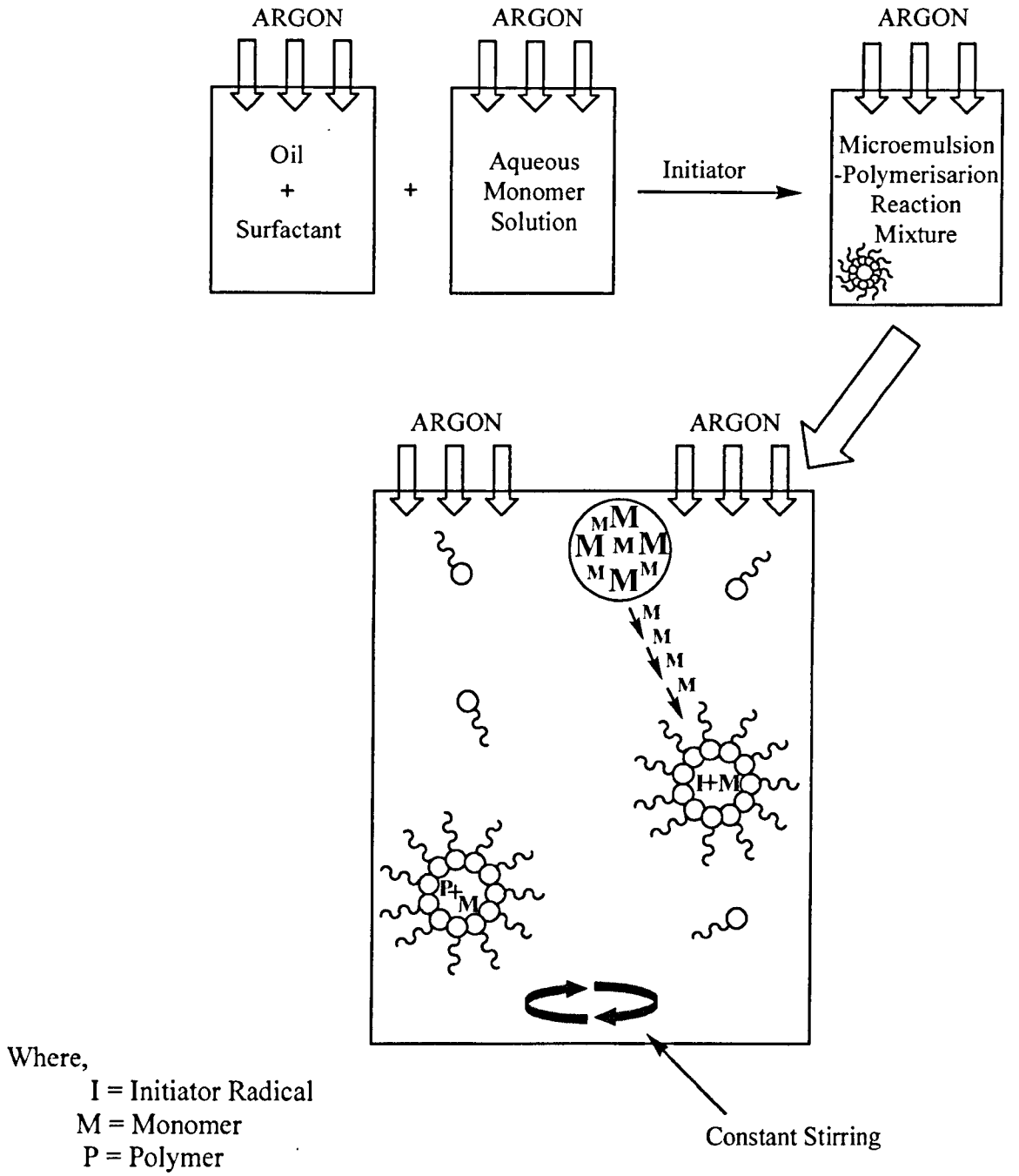

Figure 56 – Simplified Schematic of Microemulsion Polymerisation Reaction (Oil-in-Water)

The aqueous phase of the system consists of the "primary" monomer to be polymerised, along with any cross-linking monomer and/or functionalised monomer (necessary for the desired particle properties), dissolved in water (or buffer). The aqueous monomer

solution (deaerated) is added to the surfactant-containing organic (oil) phase (deaerated) and is purged with an inert purified gas, such as nitrogen or argon; a **vital** step to ensure the system is free from any residual oxygen (figure 56). The polymerisation of the monomers is then initiated by a water-soluble initiator or a redox initiator system (such as an ammonium persulphate/*N,N,N',N'*-tetramethylethane-1,2-diamine (APS/TEMED) mixture) allowing lower temperatures to be sought. The initiation system generates the initial free radical species which attack the double bond present in the monomer(s), inducing co-polymerisation of the "primary" monomer (polymer backbone) with any cross-linking and functionalised monomers. Once polymerisation has been initiated the clear and fluid microemulsion mixture becomes turbid and highly viscous. The end of the polymerisation process is characterised by a return back to clarity and fluidity; typically in less than thirty minutes.[253,272,285] The organic phase can then be removed under vacuum and the viscous colloidal dispersion of water-swollen particles purified; ensuring maximum removal of the residual organic phase and surfactants. The purification and recovery of the nanospecies typically involves centrifugation in a solvent in which the nanospecies are insoluble, allowing the precipitation and collection of the nanoproduct.

1.4.7.6.1 Polymerisation Mechanism

When the three microemulsion components (the monomeric aqueous phase (i), and the surfactant (ii)-containing oily (iii) phase) have been added together, for example, in a water-in-oil system, large monomer droplets become "loosely" stabilised by a proportion of the surfactant molecules: these droplets act solely as a monomer reservoir during the polymerisation process (figure 57). The remaining surfactant molecules form the smaller aqueous micellar structures (at the c.m.c): the loci of the polymerisation process. Upon initiation the free-radical species attack the monomer molecules that have migrated into the aqueous micellar core, propagating the formation of polymer chains. As the monomer concentration in the micelles is decreased, more molecules from the large monomer droplets diffuse across the oily domain and into the micelle. The polymerisation process continues and the polymer chains continue to grow until the residual monomer levels are depleted or chain termination occurs. Once the polymerisation process has begun the micelles become known as particles. In addition to the initial driving force for the

diffusion of the monomer molecules into the micellar core (a result of the minimal solubility the monomer displays for the continuous oily domain: also the reason for the formation of the large monomer droplets), the relatively small total-surface area of the monomer droplet renders the large droplets ineffective in competing with the micelles for the "incoming" radical species.

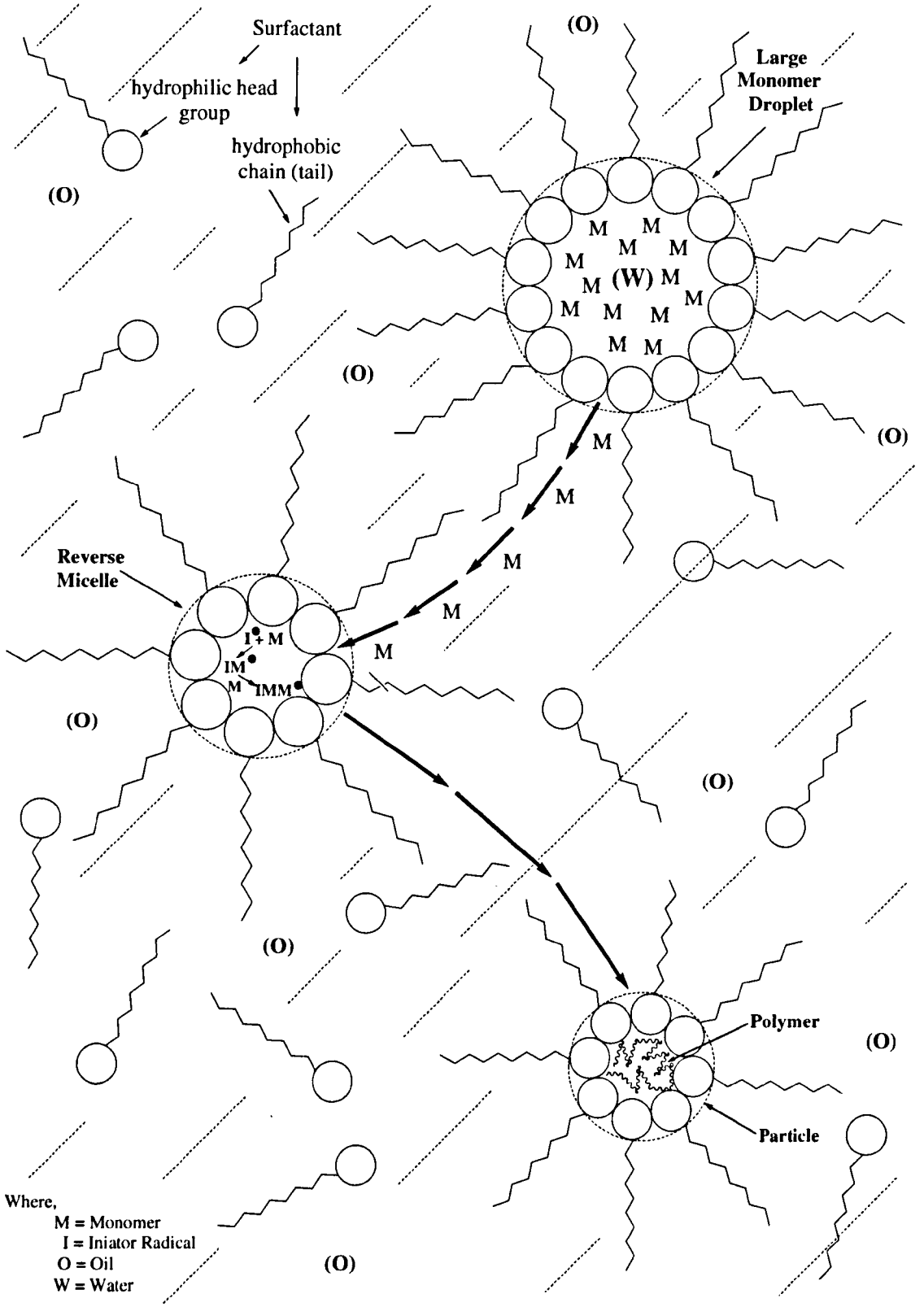

Figure 57 – Microemulsion Polymerisation

1.4.7.6.2 Free Radical Polymerisation Mechanism

Free radical polymerisation proceeds *via* three distinct phases: initiation; propagation; and termination and involves the addition of one monomeric molecule to another in order to generate the addition polymer.

1.4.7.6.2.1 Initiation

Initiation can be viewed as the "birth" of the polymerisation process. An initiator molecule such as benzoyl peroxide, potassium persulphate (water soluble) or azoisobutylnitride (AIBN, oil-soluble, figure 58), homolytically dissociates into two free radical species. One of these highly reactive species then reacts with an electron-rich π-system in the monomer molecule forming a σ-bond with one of the monomer "π-atoms". The remaining monomer "π–electron" becomes the newly formed molecule's (the polymer's) active centre: like the free-radical which attacked the "mother" monomer, this radical species can now go on to attack a second monomer molecule, generating a new reactive intermediate. It is also possible, although highly unlikely if the initiator concentration is low enough, for the "new" initiator radical species to attack a second initiator free radical species ("self-destruction") in a series of chain-propagating steps.

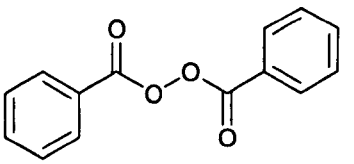

Benzoyl Peroxide

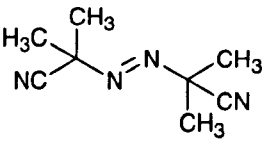

AIBN

Figure 58 – Examples of Free Radical Initiators

1.4.7.6.2.2 Propagation

Propagation is viewed as the process of polymer growth. Once the polymerisation process has been initiated the propagation phase becomes dominant, occurring thousands of times until either all of the radical species are destroyed (through a termination reaction) or the monomer levels become depleted.

The propagation phase witnesses the transfer of the "new" free radical (active centre) to a new "carbon" atom as the active centre moves down to the "free end" of the growing polymer chain. The growth of the polymer chain occurs over a rapid period of time (fraction of a second) and is limited only by the presence and concentration of the monomer molecules and a radical species.[286,288]

1.4.7.6.2.3 Termination

The termination phase of the polymerisation process witnesses the "cessation" of polymer growth. Termination steps begin when the monomer levels are depleted, technically known as living polymerisation, or by combining the two active centres of two reactive intermediates. The new species can be formed by bringing together two polymer radicals (dimerisation, figure 59) and generating a species with no active sites ("dead polymer", known as "combination") or *via* disproportionation (when two radical species collide and one of them donates a proton to the other, but retains one of the electrons to use with its own free radical to form a π-bond, figure 59). Disproportionation can also be achieved through the use of a chain transfer agent, such as sodium formate, or *via* a reaction between an active centre and any impurities present within the reaction mixture, or indeed molecular oxygen. Hence, the demand for (i) high purity reagents, (ii) purging the system with inert gas, and (iii) clean reaction equipment.[286-288]

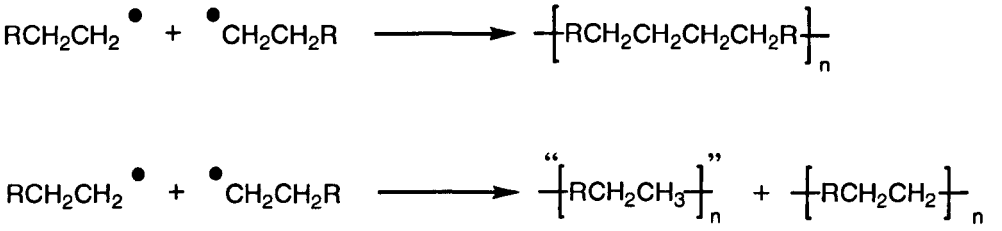

Figure 59 – Dimerisation (upper structure) and Disproportionation (lower structure)

1.4.7.6.2.4 Reaction Kinetics

The kinetics of the (free radical polymerisation) reaction can be described (figure 60), whereby:

Start – *initial free radical formation*

$$I \xrightarrow{k_I} 2R^{\bullet}$$

Initiation

$$R^{\bullet} + M \xrightarrow{kp'} RM^{\bullet}$$

Propagation

$$RM^{\bullet} + M \xrightarrow{kp''} RMM^{\bullet}$$

$$\textit{i.e. } R^{\bullet} + (M)_n \xrightarrow{k_P} R(M)^{\bullet}_{n+1}$$

Termination

$$R(M)^{\bullet}_{n+1} + R(M)^{\bullet}_{m} \xrightarrow{k_T} R(M)_{m+(n+1)}$$

i.e. 2 reactive monomer chain intermediates → final polymer

(non-radical products)

where,

I = Initiator molecule

$R^{\bullet}$ = Initiator radical species

M = Monomer

$RM^{\bullet}$ = Monomer radical species

k_I = Initiation rate constant

k_P = Propagation rate constant

k_T = Termination rate constant

$$-\frac{d[I]}{dt} = k_I[I] \Rightarrow \text{rate}_I = k_I[I]$$

$$-\frac{d[M]}{dt} = k_{p'}[M][R^\bullet] = -\frac{d[R^\bullet]}{dt}$$

$$-\frac{d[RM^\bullet]}{dt} = k_{p''}[RM^\bullet][M]$$

$$-\frac{d[RM^\bullet_{n+1}]}{dt} = k_T[RM^\bullet_{n+1}][RM^\bullet_m] \Rightarrow \text{rate} = k_T[RM^\bullet]^2$$

Figure 60 – Free Radical Reaction Kinetics

Initially, the decomposition of the initiator molecule dominates; therefore, it can be assumed that initiator decomposition is rate limiting.[289]

The rate of the propagation reactions are all equivalent to each other and the overall rate is controlled by one step; the rate determining step (RDS). If just one of the reactions has a rate constant which is too small, chain propagation will cease. Conversely, for chain propagation to be efficient (good yield) the rate constant for each reaction in the chain must be sufficiently high (figure 60). Note, other termination reactions are neglected.[265, 289]

1.4.7.7 Nanospecies Modifications

1.4.7.7.1 Surface Functionalisation

The size, composition, network porosity and surface chemistry of a nanospecies are all important properties and dictate the field/area in which the species will be applied. These parameters can be selectively controlled during the synthesis of the nanospecies by varying the ratio of the synthetic reagents and the microemulsion environment, allowing specific tailoring of species towards the properties of choice. For example, it is often desirable, particularly in imaging and therapeutic studies, to control and limit the cellular

uptake/intracellular localisation of the nanospecies used. One way of achieving this is to selectively direct nanospecies to the specific area/site of interest. This can be achieved by chemically modifying the surface of the nanospecies in a number of ways; namely, through the incorporation of a range of functional groups.[74,194-196,199,203,209,210,213,215-218,220,222,232,239-242,255] For example, by conjugating the nanospecies to a target-specific molecule (such as an antibody), the system can be selectively directed towards sites of interest or "delivery sites" and facilitate the delivery of imaging and drug-loaded nanospecies. Such systems can offer reduced side effects from drug delivery and surgical procedures, making them suitable for a range of different biomedical situations.

The ability to control surface chemistry can also play a part in increasing the retention/circulation time of the nanospecies in the body. Foreign particles in the body/cell are known to be captured and removed by the reticuloendothelial uptake system (RES): the major defense system of the body; in particular, by macrophages (immune system scavenger cells which engulf and destroy "invading" organisms) before they have had time to reach their destination and/or the opportunity to "image their environment"/"deliver" their therapeutic-load.[74,199,209,218,219,237,255] To minimise species removal *via* this route, selective control over nanospecies size and surface chemistry can play a crucial role: species with sizes below 100 nm are thought to evade capture by the RES, along with nanospecies bearing hydrophilic surfaces. Therefore, by selectively modifying the nanospecies surface to be more hydrophilic, for example *via* PEGylation, the interactions between the nanospecies and plasma proteins can be minimised, and through the control of the nanospecies size, their retention time in the body can be increased.[74,202,203,240,241,252,254,255] Another idea that has been put forward to try and minimise RES clearance considers creating species that are "invisible" to the RES.[214,216,252] These "stealth" species show reduced phagocytotic uptake and clearance by creating a "shield" around the nanospecies, such as the PEG coating mentioned.[74,202,203,218,241,252,254,255] PEG is a hydrophilic polymer which can increase the hydrophilicity of the species. Biomimetic systems could also be developed which seek to imitate cells or pathogens, therefore minimising phagocytotic uptake and inhibition of complement activation.[253,290]

The types of functional groups that can be incorporated into the nanospecies surface are numerous and include hydroxyl (OH), sulphonate (SO_3^-), carboxylic acid (COOH) and amino (NH_2) groups (figure 61), as well as bio-reactive groups such as folate and antibodies.[281] Antibodies and folate ligands work by selectively targeting complimentary biomarkers expressed on the surface of cells (antibodies are selective for antigens and folate ligands for folate-binding proteins). Tumour cells are known to over-express certain biomarkers on their surface (such as certain antigens) for which antibodies can be raised against and subsequently conjugated to the nanospecies; facilitating the directed targeting of the nanospecies towards specific bioreceptors with high degree of affinity and specificity, making them ideal targeting candidates.

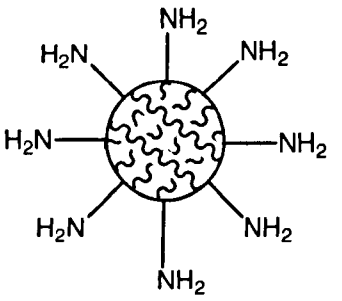

Figure 61 – Surface-Functionalised Nanospecies

The addition of peripheral functional groups can be imparted into the nanospecies surface either during particle synthesis or post-synthesis, *i.e.* polymeric nanoparticles can be directly surface functionalised by incorporating functionalised monomers into the microemulsion reaction mixture or through grafting groups directly onto the species surface.[216,242,245,281] The most versatile approach to accomplish surface functionality is probably through the use of functionalised monomers.

1.4.7.7.2 Variation of Particle Properties

The average diameters of human cells range from 10-20 μm, with cell organelles varying from a few nanometres (ribosomes ~ 20 nm) to a few microns (nucleus ≤10 μm) in size.[74,255] Therefore, it is important that nanoparticles designed for biomedical purposes

can be synthesised in a variety of sizes to allow their efficient penetration and passage through biological barriers (such as blood vessels and tissues) and experience minimum uptake and clearance by the body's defense system.

1.4.7.7.2.1 Particle Diameter

Particle size has been widely reported to be a function between the total monomer concentration and the ratio of surfactant molecules present during the initial synthetic step. Larger particles are believed to result from a higher proportion of total monomer molecules in comparison to the total number of surfactant molecules present in the microemulsion system: at a relatively low surfactant concentration, the average micelle/particles size increases with increasing total monomer concentration, *i.e.* as the number of monomer/polymer molecules in the micelle core increases; the core volume and therefore the average diameter of the micelles/particles increases (figure 62).[195,202,206,209,216-218,250,252,272,276,284,291-298] The length of the surfactant tail is also believed to affect the average particle size, with shorter surfactant spacer groups yielding a greater number of smaller micelles and nanospecies. Larger surfactant spacer groups have enhanced tail "flexibility"; implying that the volume inside a micelle (oil-in-water) is greater than that of micelles formed from smaller-tailed surfactants (at the same relative surfactant concentrations).[194,195,199,211,216,217,222,276,277,284,285] Smaller nanoparticles can also be generated by reducing the interfacial tension and viscosity of the oil-phase present in the system; interfacial tension appears to be a dominant factor over the viscosity of the oil.[252]

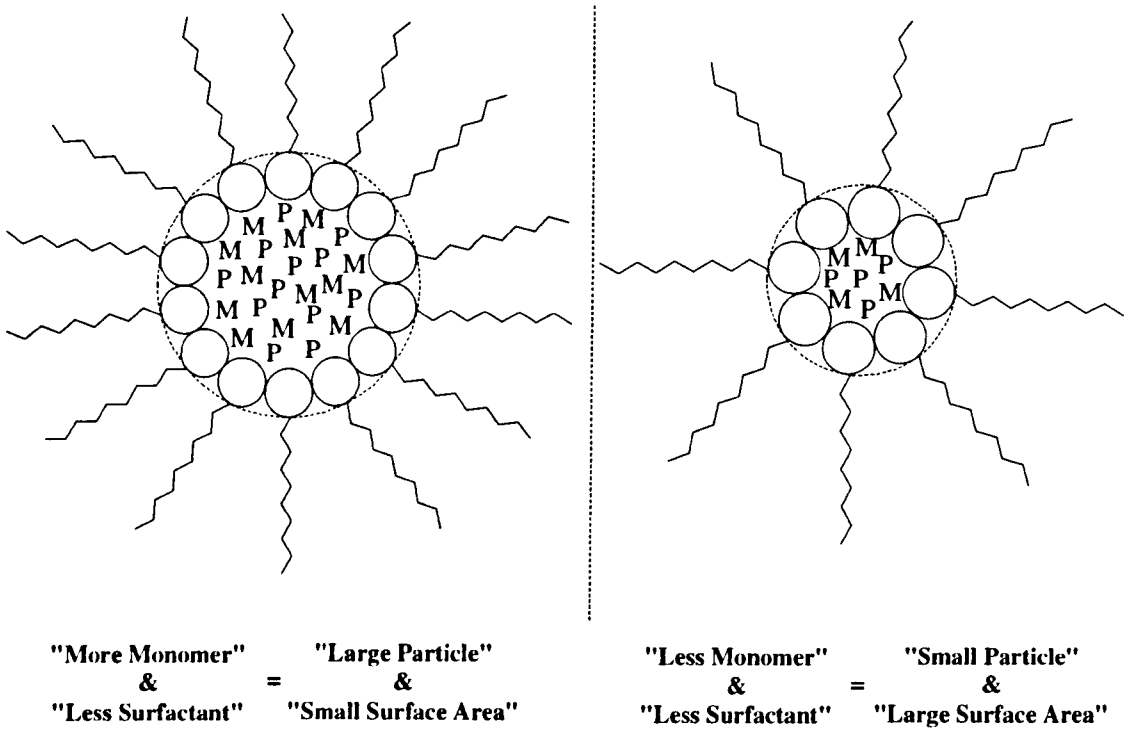

Figure 62 – Diagram Showing the Relationship between Particle Size and Total Monomer Concentration, M = monomer and P = polymer

However, it must be noted that the relationship between the total monomer and surfactant concentration is **not** as simple as described above. The total monomer concentration is not directly proportional to the particle size; it becomes much more complicated at a wider range of molar ratios. This is an observation which has been the subject of intense research over the years and one which so far has remained elusive, even from the authors of reports as recent as February 2007 who are (still) unable to fully explain the mechanisms.[272,277,291,297]

1.4.7.7.2.2 Pore Size

Porous nanospecies generally work on the basis that small molecules and ions are able to flow freely through the nanospecies matrix. It is therefore important that the pore size and the number of pores present in the matrix can be controlled to accommodate molecules

and ions of different sizes and allow their efficient diffusion towards the entrapped analyte-sensitive fluorophore.

Variations between the proportions of total monomer and cross-linking agent present in the initial monomeric solution have been reported to influence the porosity and stability of the nanospecies. Greater amounts of the total cross-linking monomer, in comparison to the "primary" monomer, have been suggested to yield species with smaller diameter pores.[196,242,244,285]

Cross-linking agents are monomers capable of joining together two polymer chains, so when a monomeric solution containing such an agent is added to a microemulsion system, gelation between random growing polymer chains can take place forming a covalent network of pores, *i.e.* a mesh-like matrix is created (figure 63). The cross-linking process essentially takes place at random intervals along the polymer "backbone" chains, dictated of course by the presence of a free radical species and monomeric π-bonds. When the proportion of the cross-linking agent is increased (relative to the primary monomer concentration) the incidence of cross-linking polymer chains increases; thereby, reducing the average diameter of the pores. Pore sizes are reported to be at a minimum when the concentration of the cross-linker is ~5% of the total monomer concentration. Above this concentration, polymer chains become "cross-linked" into increasingly large bundles, with large spaces between them effectively increasing the pore size.[244,285]

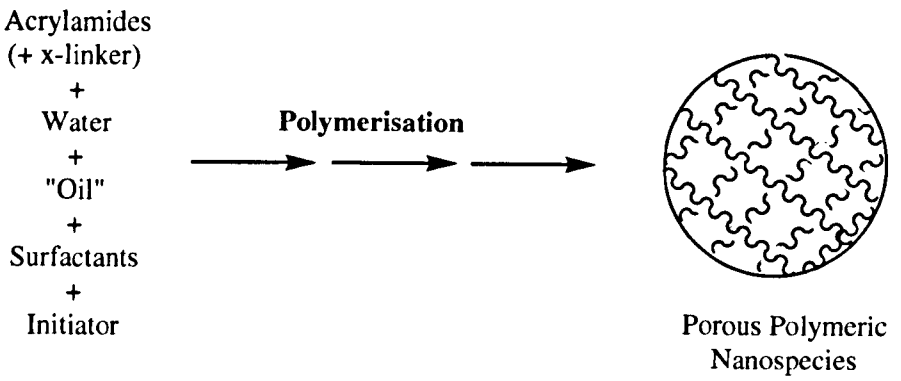

Figure 63 – Formation of Mesh-Like Nanospecies

It is also believed that these covalent "cross-linkers" (similar to those observed in natural self-assembly structures) increase the stability of the nanospecies structure.[241,242,250,285]

1.4.7.8 Nanospecies Characterisation

Electron microscopy, particularly scanning and transmission microscopy, can prove useful for characterising the morphology and size of a nanospecies. A typical electron microscope used for this technique is capable of producing high resolution images of a material's surface. Due to the manner in which the image is generated, electron micrographs have a characteristic three-dimensional appearance.[265]

An electron microscope uses a highly energetic electron beam to image objects, as opposed to traditional microscopes which use light. They can be used to determine: (i) surface features, textures and properties (topography) of a sample material; (ii) the size and shape (morphology); (iii) crystallographic information (how the atoms are arranged, conductivity and electrical properties) on the sample; and (iv) reach magnifications greater than 10,000 A.U.. The electrons in an electron microscope are accelerated through a thin monochromatic beam which is focused onto the sample *via* magnetic lenses. Interactions between the high energy electrons and the "inside" of the sample alter the electron beam. These "interactions" are then detected and relayed to a PC and subsequently visualised through a micrograph image.

1.4.7.8.1 Transmission Electron Microscopy

Transmission electron microscopy (TEM) was the first type of electron microscope to be developed (1931, by Knoll and Ruska) and works by focusing the beam of electrons onto a sample allowing the operative to "see through" the sample material.

In practice, a small amount of the material to be studied is deposited onto an electron-transparent surface (such as a plastic or carbon film) which is supported by a fine copper mesh grid. The technique involves the scattering of electrons from the sample's surface out of the field-of-view. The final image of the sample can then be viewed on a fluorescent screen and photographed. The degree of electron scattering from the sample depends on the thickness and the atomic number of the atoms forming the sample material: therefore, organic molecules are deemed to be relatively electron-transparent and show little contrast against the background on which they are deposited. In contrast, materials containing heavy metal atoms typically make ideal TEM sample materials.[194]

A typical sample preparation for TEM involves dispersing the particles in a solvent such as deionised water and spreading a drop of the dispersion onto carbon-coated copper grid.[203,204,209,245,253]

1.4.7.8.2 Scanning Electron Microscopy

Scanning electron microscopy (SEM) was developed a few years after TEM (1942) and is based around the electron beam "scanning" across the sample. A fine beam of medium-energy electrons scans across the sample material in a series of parallel tracks. The electrons interact with the sample material to generate various signals, each of which can be detected and then displayed on a fluorescent screen and photographed. SEM allows a particle's size and height to be studied, along with the presence of pores and the aggregation behaviour of the particles.

A typical material is prepared for SEM by coating a support such as a glass plate or a gold-coated wafer with a drop (typically 200 μL) of the sample material dispersed in an

aqueous medium (figure 64). The sample-coated plate is then allowed to dry under ambient conditions (for up to one day) and coated with a thin layer of gold prior to imaging.[203,222,230] The gold coating works by making the sample's particle surface conductive to electrons, *i.e.* minimises charging at the surface. The "sputter coating" of polymer surfaces is normally conducted over shorter periods of time (~ 30 seconds) and repeated several times (rather than applying "one short coat" (~ two minutes)), in order to avoid melting the polymer.[230]

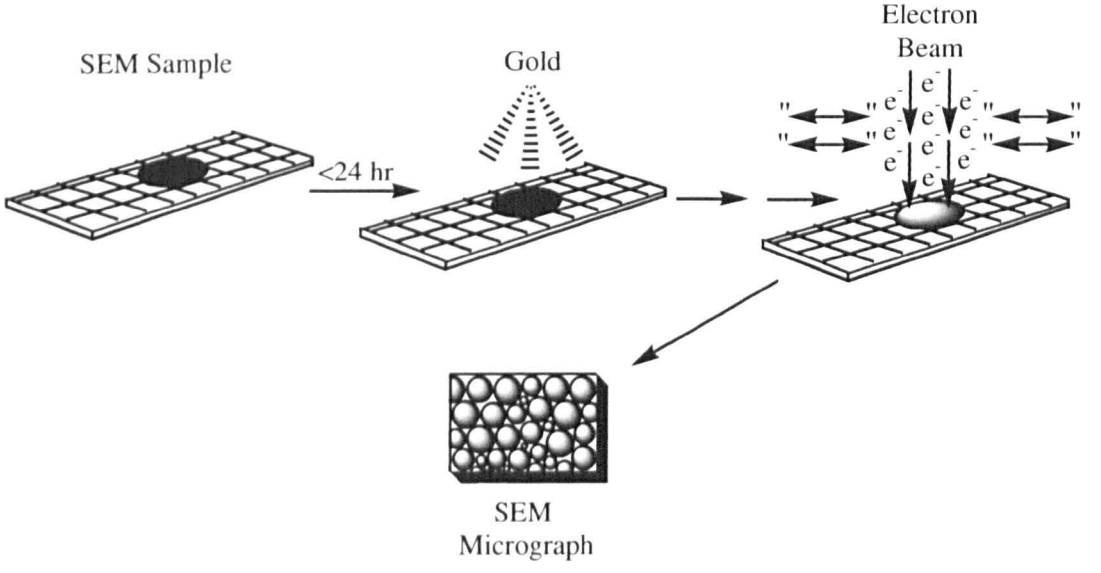

Figure 64 – Typical SEM Sample Preparation

SEM and TEM both carry advantages and disadvantages; the magnification achieved from a SEM is in general less than that of a TEM; SEM can achieve a greater depth of focus in comparison to the TEM technique.[220,230,285,299]

1.4.7.8.3 Atomic Force Microscopy

The atomic force microscope (AFM) was developed in the late 1980's and is a high resolution imaging technique, which facilitates the "imaging" of single atoms or molecules with dimensions in the small nanometre range.

The AFM is an out-breed of scanning probe microscopy and works by probing a sample's surface with a sharp silicon-tip attached to a cantilever arm. The cantilever arm moves in response to the force present between the sample's surface and the probe tip. The deflection the tip is subject to is recorded and the topography of the sample's surface is imaged (figure 65). An AFM is therefore able to generate quantitative and qualitative information, such as a particle's size (length, width and height), morphology and surface texture.

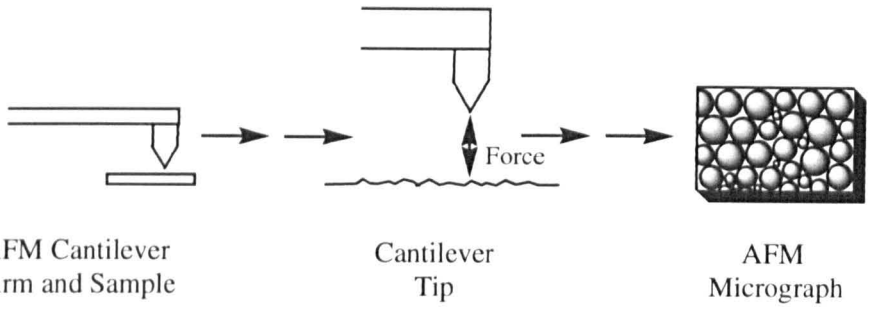

Figure 65 – Simplified Diagram of Atomic Force Microscopy

AFM holds a major advantage over other microscopy techniques, such as electron and optical microscopy: AFM offers the opportunity to achieve a greater degree of sample resolution. Traditional electron and optical microscopes generate a two-dimensional horizontal view of a sample's surface; whereas AFM is able to provide vertical images of the sample in addition to horizontal ones. A second advantage of AFM is the ability to scan the sample in ambient, inert or liquid environments, as opposed to under the vacuum conditions used with TEM and SEM (providing that the sample dispersant is not corrosive towards the probe tip). In addition, there is a potential to recover the sample since the tip is deflected away from the sample surface, *i.e.* it never comes into direct contact with the sample; thus, minimising sample contamination.

One important factor in the success of the AFM technique is the affinity the sample material has towards the flat surface it is mounted on: if the sample under study shows a

greater affinity for the probe tip than its flat-surface mount, then the image resolution will be reduced/lost and any images achieved will appear streaky and inconclusive.

1.4.7.8.4 Photocorrelation Spectroscopy

Photocorrelation spectroscopy (PCS; also called quasi-elastic light scattering (QELS) and dynamic light scattering (DLS)) is a technique used to measure the colloidal size of particles by observing their Brownian (random) motion. When a beam of laser light is passed through a colloidal dispersion the tiny particles diffract some of the light. The intensity of this scattered light varies rapidly as a function of the movement of the particles in the liquid medium. These fluctuations are dependent on the size of the particle: the pace of particle movement is inversely proportional to the size of the particles, *i.e.* smaller particles diffuse faster. The pace is detected by analysing the time dependency of the light intensity fluctuations scattered from the particles. A calculated correlation function then generates a diffusion coefficient for a given temperature, viscosity and scattering angle, which can be converted to yield particle size (hydrodynamic radius, R_h) distribution data.[222]

A typical sample is prepared for PCS by suspending the material in a liquid medium in an optical cuvette. It is vitally important to ensure that the sample is **free** from dust and any contaminants.

1.4.7.8.5 Sorption Experiments

The specific surface area, pore size and pore volume of a nanospecies can be determined using sorption techniques. The nitrogen adsorption method involves physical adsorption of nitrogen atoms onto the solid nanospecies surface, forming a molecular layer of nitrogen atoms around the species. The amount of adsorbed nitrogen can be measured either volumetrically or gravimetrically. The volumetric method is typically used to measure surface areas greater than 30 m^2/g and the gravimetric method employed for surface areas in the range 1 - 30 m^2/g. A BET isotherm (figure 66) can then be

constructed from which the total surface area of the sample can be determined.[195,222,223,245,300,301]

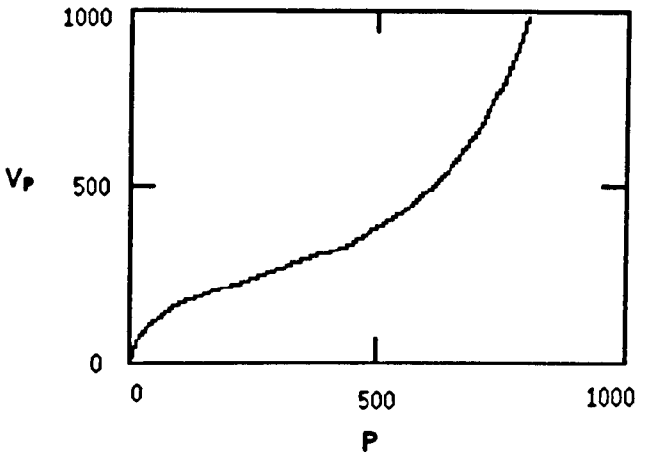

Figure 66 – A typical BET Isotherm[302(modified)]

The adsorption of a species onto a substrate is described through an isotherm. A BET isotherm is a derivation of the Langmuir isotherm, which takes into account the possibility that the nitrogen molecules may not form a monolayer around the nanospecies but instead, form a multilayer (figure 67), *i.e.* some of the nitrogen molecules may adsorb onto nitrogen molecules that have already adsorbed onto the nanospecies surface.[300,303]

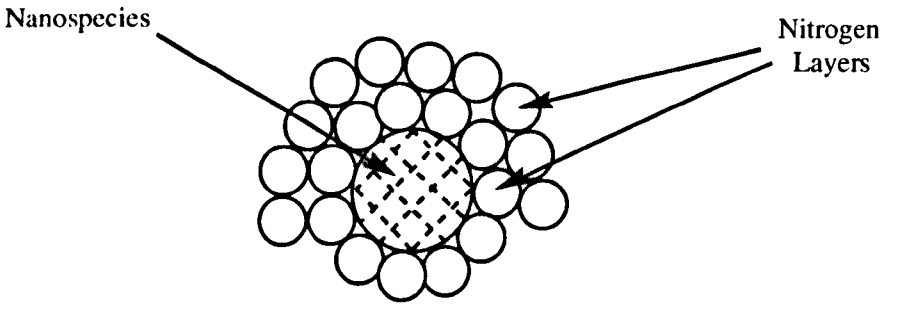

Figure 67 – Adsorbed Nitrogen Layers

In addition to the nitrogen sorption technique, the pore size distribution in the nanospecies can also be determined using a mercury penetration method. For pore size distribution, nitrogen desorption is used where the nanospecies pores are completely

filled with liquid nitrogen. The pressure exerted on the system is then gradually lowered and results in the desorption of the nitrogen molecules from the nanospecies, in measurable quantities, from which pore volume and pore size distribution can be determined. Nitrogen desorption is typically sought when species have pore radius' ranging from 50Å to 55μm. The mercury penetration method used for determining the pore sizes of nanospecies is a consequence of the high surface tension demonstrated by mercury, along with the strong non-wetting properties it exhibits towards most surfaces. The nanospecies pore volume and size are determined from the amount of mercury which is forced into the pores as a function of pressure.[300]

An "envelope density" method can also be used to determine the pore volume and porosity of a nanospecies. This technique involves dividing the mass of the nanospecies by its total volume.[300]

1.4.7.9 Nanospecies Delivery

A number of techniques may be used to deliver nanospecies to cells including, endocytosis; natural ingestion (phagocytosis); lipofection (liposomal ingestion); gene gun delivery and picoinjection.[194-196,206,209,213,215-218,235,248,252,255,262,304]

The ideal mode for delivering nanospecies into cells would be: (i) one which allowed a high degree of internalisation to be achieved; (ii) one which worked for a range of species and cell-lines; and most importantly, (iii) one which caused minimal perturbation to the cell membrane and the cell's health; allowing the cell to "function" as normally as possible.

Each of the techniques listed are quite different, with the exception of endocytosis and phagocytosis, and bring with them their own unique advantages and disadvantages. Each technique will be briefly described.

Endocytosis, can simply be translated as meaning within (endo) the cell (cytosis) and is a process by which extracellular materials enter a cell without directly passing through the cell membrane. Instead, the plasma membrane creates an inward fold, known as an invagination, which surrounds the extracellular material to be taken up. This membrane-loaded vesicle is then "pinched" away from the cell surface and becomes free to diffuse through the cytoplasm; fusing with the cell's endosomes and lysosomes.

Endocytosis can be more intimately described as pinocytosis and receptor-mediated endocytosis. Pinocytosis describes the specific engulfment of an aqueous extracellular material as opposed to large particulate material such as bacteria or cell debris. On the other hand, receptor-mediated endocytosis involves receptors on the surface of the extracellular material binding specifically with ligands present on the cell's surface. This technique is a natural cellular process and can be considered as a relatively "gentle process" towards the cell. However, the technique may only be applicable for delivering nanospecies in the lower nanometre size range.

Pico-injection involves inserting a fine needle (tip diameter in the pico-range, 10^{-9}) into the cell membrane and injecting pico-litre volumes of a nanospecies-containing solution into the cell. This method is particularly invasive and may cause the cell to leak or quickly lose its viability; a second major disadvantage is that only one cell can be prepared at any one time, making it a time consuming and specialised technique.

Gene gun delivery, originally used for delivering genetic material to cells, utilises (high) pressure to deliver the species. The experimental setup involves loading a carrier membrane with the chosen system. This membrane sits below a "rupture" membrane positioned in front of the gun's pressure outlet. The pressure of the gun is then built up (usually from a helium source) and when the desired firing pressure is reached the gun is fired; destroying the "rupture" membrane and "shooting" the sample species from the carrier membrane across the cell membrane and into the cell (figure 68). A few to thousands of species can be delivered simultaneously per cell over a relatively short period of time with this technique. The location of the species (cytoplasm or nucleus) is

generally determined by the momentum of the sample species as they are released from the carrier membrane.

Gene gun delivery can be useful if a large number of species need to be delivered simultaneously to the cell; however, it is a relatively harsh technique that was developed for use with thick, robust plant leaves and not delicate mammalian cells. It is therefore a process which constantly carries with it a worry that the cells may not always remain viable.

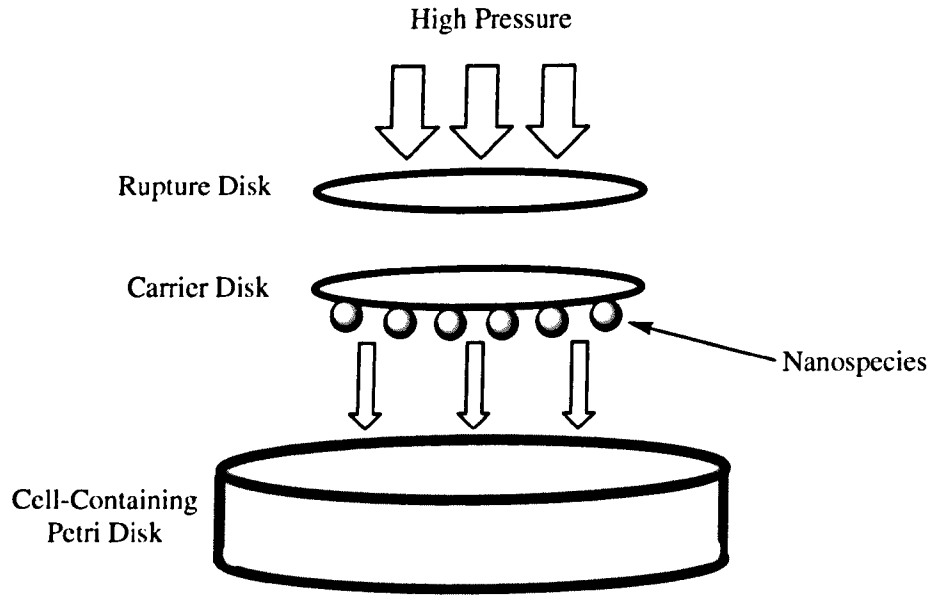

Figure 68 – Simplified Diagram of Gene Gun Delivery

Lipofection or liposomal delivery, a relatively "cell-friendly" method, takes advantage of natural carriers (liposomes) which are able to fuse with the cell membrane and release their contents into the cell (figure 69). A typical liposome-nanospecies solution is prepared and added to a cell culture solution. The number of nanospecies delivered to the cells depends on a number of variables including: (i) the initial concentration of the nanospecies solution; (ii) the concentration of the liposomes added to this solution; (iii) the affinity of the liposomes for the nanospecies; (iv) the concentration of the liposome-nanospecies solution added to the cells; and (v) the time the cells are incubated with the

liposome-nanospecies solution. Using this method a number of cells can be simultaneously loaded with a range of nanospecies concentrations. Liposomes are commercially available and include examples such as those based on the dimethyldioctadecylammonium bromide (DDAB) lipids and the commercial transfection reagents, such as Lipofectamine™.

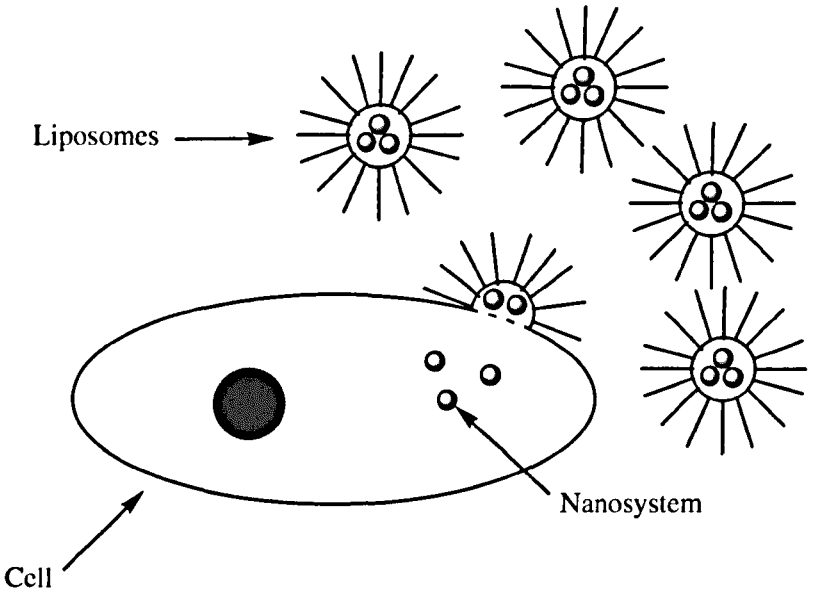

Figure 69 – Lipofection Delivery

The above techniques generally relate to delivery methods concerned with *in vitro* studies, but it is important to consider the delivery of nanospecies *in vivo* (important for imaging nanospecies and drug delivery vehicles) since their composition and physical characteristics will play an important role in their administration route and application. There are a number of different *in vivo* routes by which the nanospecies can be delivered and these are typically divided into direct and non-direct delivery vectors: generally including, oral administration; topical and parenteral delivery; as well as the active targeting methods already mentioned.

1.4.7.9.1 *In Vivo* Delivery

Oral administration is a non-invasive and particularly attractive method for the direct targeting of intestinal mucosal sites with therapeutic agents loaded into the nanospecies. However, problems are encountered as a result of the corrosive environment presented by the stomach, causing degradation of the nanosystem. Consequently, the sustained delivery/release of therapeutic agents *via* this route somewhat challenging.

Nanospecies can also be applied topically, for example, on the skin or hair follicle. This is particularly important in the delivery of nanospecies carrying agents relating to genetic immunisation and for the management of alopecia.[74]

Ocular delivery *via* intravitreal administration is important in the treatment of eye disease and allows sustained release of the drug: thereby, eliminating the need for painful repeat injections into the eye.[74,252,305]

Parenteral delivery of nanospecies (*i.e.* generally through the blood system, including intravenous, intramuscular and subcutaneous delivery, but usually not through the gastrointestinal tract) is good for superficial disease areas: although, this method may not be as effective/efficient for deeper disease targets. Problems may be encountered with this technique if there are circulation problems associated with the nanospecies, such as removal by the RES or accumulation in the liver and/or spleen; hence, the initial administration concentration of the species needs to be adjusted accordingly. One way to overcome this problem would be to use the "stealth" nanospecies described earlier (see section 1.4.7.7). Nanospecies can also be delivered to the target site through the active targeting mechanisms described earlier (see section 1.1.7).

1.4.7.10 Intracellular Localisation

Nanospecies can potentially localise in a variety of subcellular compartments typically dependent on their physical characteristics, such as charge and size. Some nanospecies have been reported to selectively localise within specific compartments/areas, while others have appeared to show no specificity for one intracellular area over another.

The cellular internalisation of nanospecies is important since it is likely to play a role in determining the biological activity of the species. It has already been mentioned (see section 1.4.7.7) that the molecular mechanisms mediating the internalisation of the species are dependent on particle size. Particles as large as 500 nm may be internalised by non-phagocytotic cells *via* energy-dependent processes and *via* caveole membrane invagination; while smaller particles, with diameters less than 200 nm, may be internalised *via* clatherin-coated pits.[255]

In addition to creating "invisible" nanospecies, nanospecies internalisation can be enhanced by targeting the species against internalising receptors, such as a CD19 surface antigen which is expressed on a β-cell lymphoma cell-line and a folate receptor (folate-binding protein); this is more commonly known as receptor/ligand-mediated endocytosis. This is currently an active area of research, which can potentially accelerate the internalisation of the nanospecies and avoid uptake/clearance by the RES defense mechanism.[74,218,219,232]

It is possible to identify the area of nanospecies localisation through the use of fluorescent dyes. For example, Lysotracker® and Mitotracker® are commercial fluorophores which selectively localise in the lysosomes and mitochondria. Localisation in a specific intracellular region/subcellular compartment can be particularly important with nanosensors fabricated for studying intracellular signaling mechanisms or imaging. Localisation can also be important in drug delivery systems. It is known that tumours express a greater degree of certain ligands at their surface and nanosystems which are selectively targeted to these ligands have been shown to accumulate at higher concentrations at the periphery of solid tumours (known as the "binding site barrier")

rather than at deeper depths; therefore, minimising diffusion of the nanospecies to the deeper tumour regions. This effect can have a significant impact on the management of tumours and on the initial administration concentration of the drug-loaded vehicle. It is also important to bear in mind the heterogeneous nature of the tumours; certain regions of the tumour will have a greater number of ligand receptors, whilst other areas may not express these receptors at all.[74]

1.4.8 Nanosensors

One of the current challenges which exists across the medical spectrum is the understanding and effective management of disease with minimal drug toxicity, side effects and trauma. It has already been mentioned that treatment efficiency can be increased by using drug-targeting strategies and drug-loaded vehicles: modalities which both show great promise. But the real breakthrough in disease management would come from the observation of intricate signaling processes which occur inside living cells **pre-/during** disease-states. One way of achieving this revolutionary vision would be to create a technique or device that was capable of detecting minute changes in the levels of specific intracellular analytes and relaying the information back to the "investigator" in real-time. Ideally, the sensing system would cause minimal perturbation to the cell; thereby, allowing observations to be made in as natural cellular environment as possible.

A system such as this could be realised by bringing together the applications of colloidal nanotechnology and optical spectroscopy. The combination of these two scientific fields, in the generation of a bifunctional intracellular nanosensor, could be further enhanced by stimulating an *in situ* "diseased-state"; a state which could be created through photosensitiser chemistry

1.4.8.1 Analyte Sensitive Dyes

Analyte sensitive fluorophores/molecular dyes have been used for a number of years in the fields of cell imaging and sensing. They work through the luminescent visualisation of "target molecules or ions" in living cells: they induce characteristic fluorescent

changes in the presence of a target species, either in observed fluorescence intensity or fluorophore emission wavelength. However, there are a number of drawbacks associated with the majority of these dyes, severely restricting cellular studies and somewhat hampering the enhancement of our knowledge of fundamental cellular events. The drawbacks commonly encountered include: (i) the toxicity the free dye presents towards the cell; (ii) interference from cellular constituents towards the dye's sensing capability; (iii) non-specific distribution of the dye molecules; and particularly common, (iv) the observation of a fluorescence signal as a function of the dye concentration and not the desired analyte concentration.

One way to overcome these problems would be to employ a porous carrier system, similar to those used and described for nanocapsule drug delivery methods (see section 1.1.10), which could encapsulate the fluorescence dye. These carriers would have a dual-purpose of (i) protecting the dye from cellular interferants and (ii) the cell from dye-associated toxicity, as well as the potential to limit the above points (iii) and (iv). The porous nature of the matrix would allow the species of interest (an analyte or ion) to flow freely into the matrix and bind with the fluorophore of choice (figure 70). A porous polymer system which is capable of physically incorporating the fluorescent dyes, rather than covalently attaching them to the polymer structure during synthesis, circumvents the need to chemically modify the dyes.

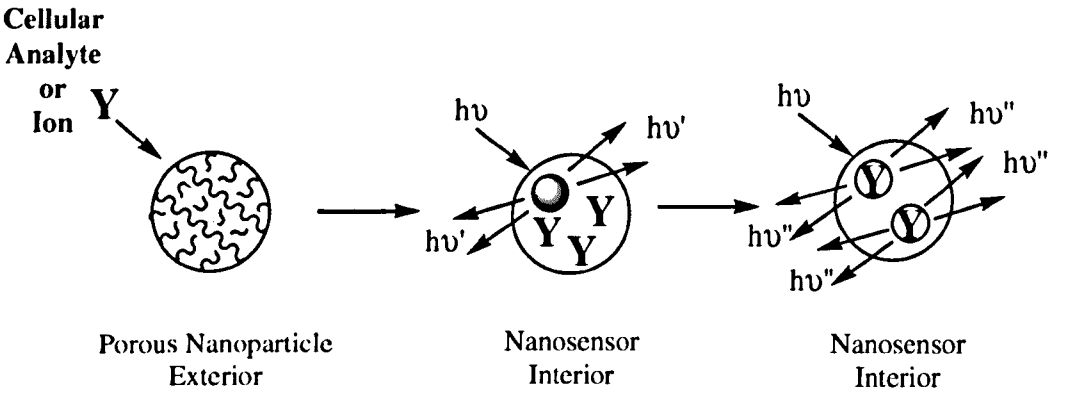

Figure 70 – Luminescent Porous Nanosensor

1.4.8.2 Advantages and Criteria for a Nanosensing System

An advantage of a system like the one described is the greatly increased sensitivity it offers: a result of the large number of dye molecules concentrated in one region, capable of offering a highly amplified and reproducible fluorescence signal in comparison to the "free" dye counterparts.

For a system like this to work the nanospecies would need to be: (i) dispersible and relatively inert in physiological media; (ii) stable during fabrication, storage and use; and (iii) be able to readily incorporate the dye(s) of choice in a simple preparation; with (iv) minimal affect on the sensing capabilities of the dye; and ideally, (v) be a system which can be easily modified to facilitate the incorporation of different dyes and surface functionalities.

1.4.8.3 Polymeric Nanosystems

Whilst a number of systems, such as the one previously described, exist interest will now be paid to those based on polymeric matrices, particularly polyacrylamide nanospecies.

Porous polyacrylamide nanospecies can be fabricated from: monomers of varying nature; cross-linking agents; and can be readily surface-functionalised. Polyacrylamide is also known to have low absorption in the visible region of the electromagnetic spectrum, making it an ideal matrix candidate for an optical sensing system.[223] The generation of a system of this nature should allow small analytes to diffuse freely from the intracellular environment (through the porous matrix) and bind to the fluorescent dye(s) incorporated within the matrix. A sensing system of this type works by observing a change in the dye's fluorescence intensity (or emission wavelength) in response to a change in the level of the target analyte. Such a system has previously been described by Kopelman and his group. In particular, Kopelman has developed his work towards nanospecies sensitive to intracellular pH and variations in glucose and select cellular ion concentrations, including the key signaling ion calcium.[306-310]

Kopelman has used three key matrices to generate these nanosensors, including a polyacrylamide matrix that he has used to encapsulate a number of different analyte-sensitive dyes.[306,309,310] More specifically, Kopelman has trapped fluorophores sensitive to magnesium, calcium, sodium, chloride, zinc and hydroxide ions, including the fluorophore Coumarin 343.[310] Coumarin 343 is sensitive to magnesium ions and "reports" variations in magnesium levels *via* a change in the observed fluorescence intensity; an increase in the magnesium ion concentration results in an increase in the fluorescence intensity of Coumarin 343. These same nanosensors were also shown to be reversible with respect to the fluorophore (Coumarin 343) binding magnesium ions. When a magnesium chelator, such as EDTA, was added to a sample solution (containing magnesium ions and the nanosensor) the observed fluorescence intensity of the Coumarin 343 dye was minimised to base levels; when the concentration of magnesium ions (magnesium chloride) in the sample solution was increased, the fluorescence intensity of the Coumarin 343 dye also increased.[310]

It is also possible to incorporate a second dye into the nanospecies allowing ratiometric measurements to be made (figure 71). This minimises/removes any background fluorescence present in the investigations and thus, enables quantitative measurements to be drawn from the fluorescence data.

Ratiometry is a technique in which a second dye molecule is embedded into the nanospecies. The second dye acts as an internal standard by reporting the concentration of the target species independently of the sensor concentration. Therefore, by analysing the ratio of the fluorescence emitted from the two luminescent species, a "true" luminescent signal can be reported. This technique also allows the fluorescence from artefacts, such as variations in excitation light intensity and equipment fluctuations, to be eliminated.

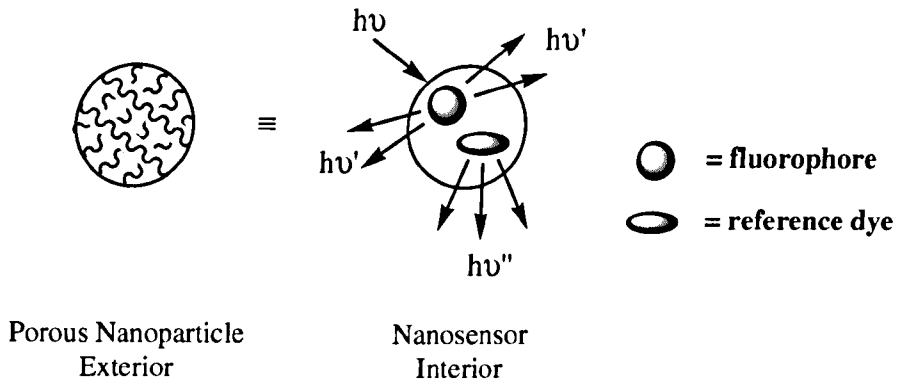

Figure 71– Ratiometric Sensors

1.4.8.4 Analyte-Sensitive Fluorophores

The range and specificity of commercial analyte sensitive dyes is vast, amongst them fluorophores sensitive to calcium and potassium. There are several key analyte-sensitive dye molecules which have been finely tuned to allow different sensing capabilities to be achieved. For example, fluorescein is a common fluorophore whose structure has been further functionalised to allow the development of calcium sensitive dyes, such as calcium green (figure 72). The core structure varies only slightly but a completely different reporter molecule is achieved (figure 73). Each of the available dyes has their own unique advantages and disadvantages: some are much more sensitive, whilst others are more robust. The choice of dye is therefore based upon the type of system to be imaged and the levels of sensitivity one wishes to achieve.

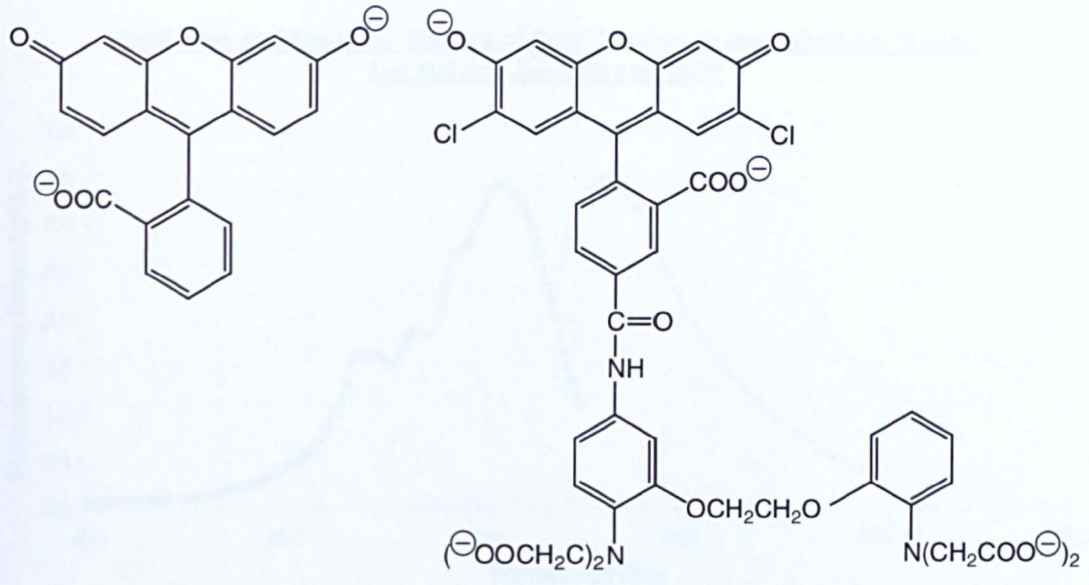

$\lambda_{ex.}$ = 492 nm
$\lambda_{em.}$ = 514 nm

$\lambda_{ex.}$ = 505 nm
$\lambda_{em.}$ = 532 nm

Figure 72 – Structures of Fluorescein (left) and Calcium Green (right)

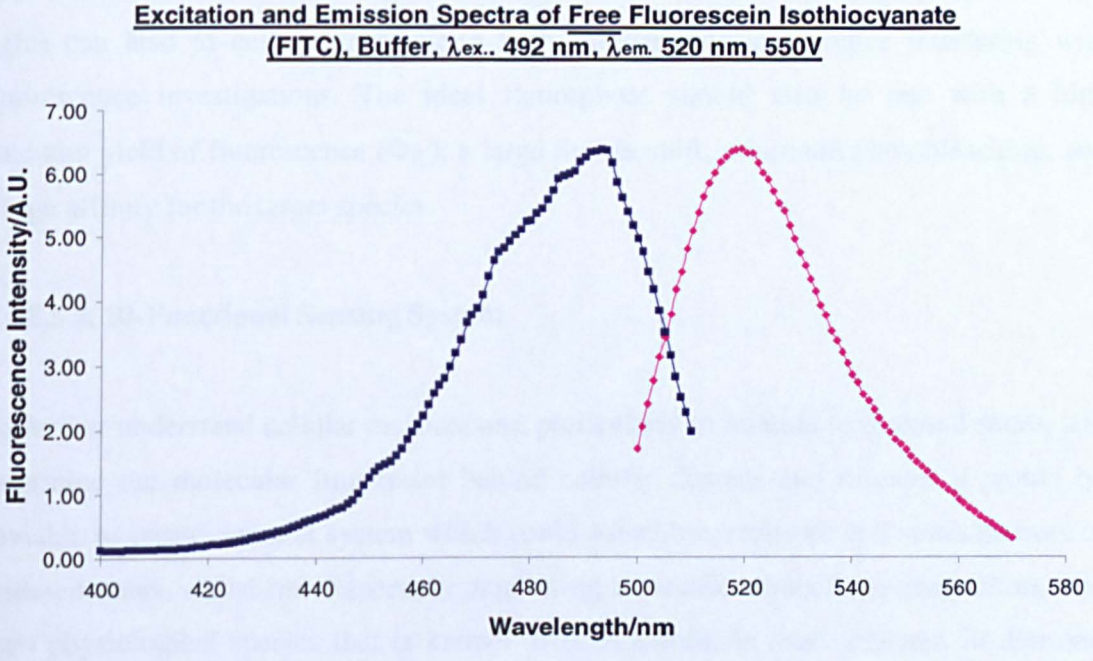

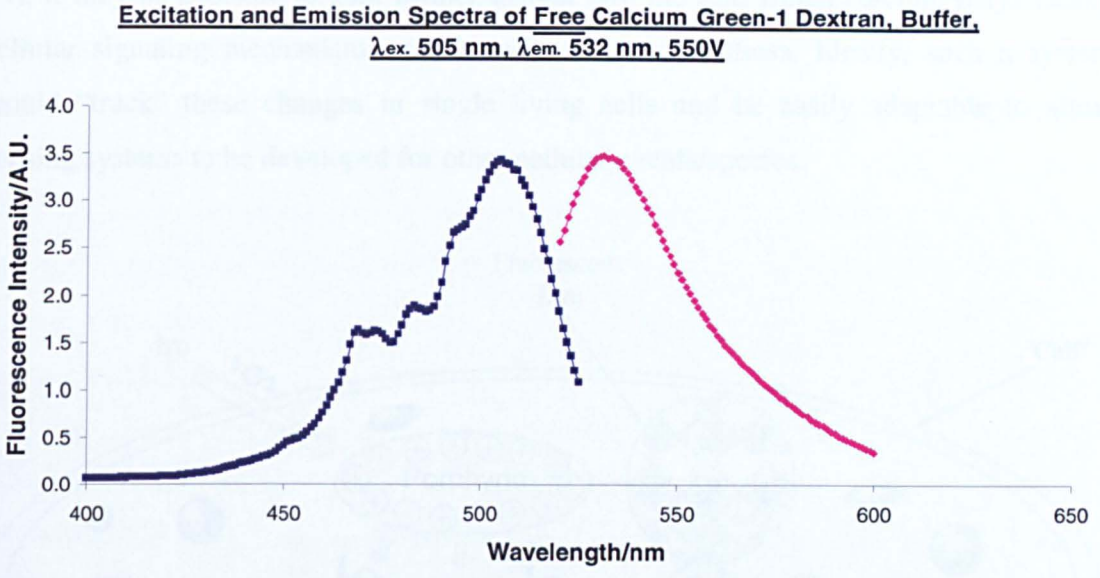

Figure 73 – Excitation and Emission Spectra of Fluorescein Isothiocyanate and Calcium Green (2.5 mmol dm^{-3} and 1.84 μmol dm^{-3} Solutions Respectively)

Fluorescent dyes which are excited by visible light are advantageous in cellular studies over those with shorter excitation wavelengths, since lower wavelength light (ultra-violet light) can lead to cell damage, along with cellular autofluorescence interfering with fluorescence investigations. The ideal fluorophore should also be one with a high quantum yield of fluorescence ($\Phi_{fl.}$); a large Stokes shift; minimum photobleaching; and a high affinity for the target species.

1.4.8.5 A Bi-Functional Sensing System

To further understand cellular mechanisms, particularly in relation to diseased states, and determine the molecular fingerprint behind cellular distress and disease, it would be enviable to create a model system which could somehow, replicate cell stress/distress or diseased states, whilst simultaneously monitoring a specific intracellular analyte/ion. One such physiological species that is known to be involved, in some manner, in diseased states and cell death, is the vital signaling ion calcium (see Chapter 1.3).[311] By creating a bifunctional device capable of generating ROS (particularly the cytotoxic species singlet oxygen) whilst simultaneously detecting changes in intracellular calcium levels (figure

74), it may be possible to gain further insight into the role which calcium plays during cellular signaling mechanisms, particularly during cell stress. Ideally, such a system would "track" these changes in single living cells and be easily adaptable to allow sensing systems to be developed for other cellular events/species.

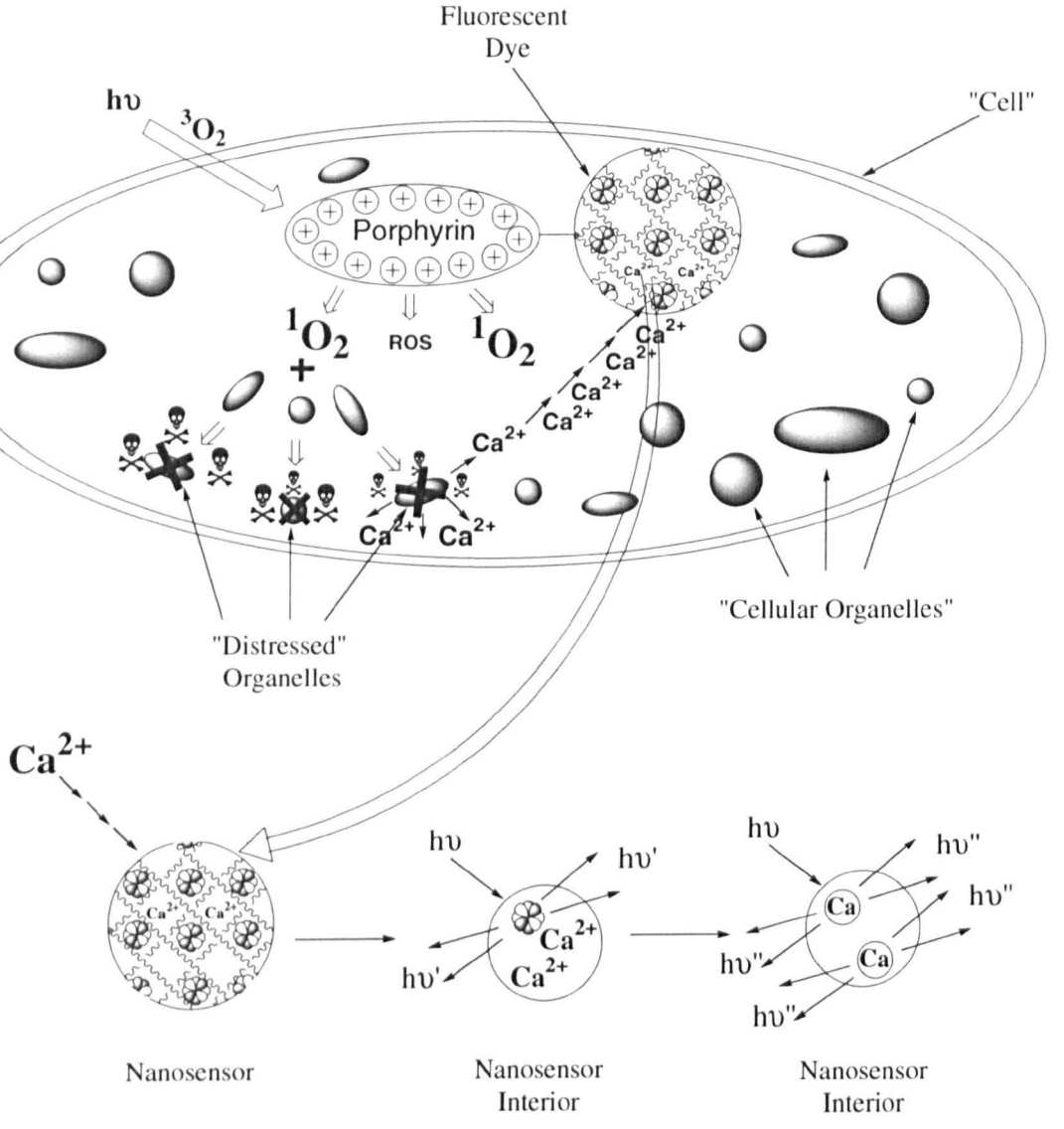

Figure 74 – Bifunctional Analyte-Specific Porphyrin Nanosensor

This idea can be brought to life by attaching a photosensitising molecule, such as a porphyrin, to a nanospecies containing a calcium-sensitive fluorophore. Subsequent irradiation of the system with light of an appropriate wavelength would then allow the

excited porphyrin ($^3Psen^*$, T_1) to interact with molecular oxygen ($^3O_2$) and *via* intersystem crossing, generate singlet oxygen ($^1O_2$): implicated in cell stress and death (see section 1.1.6 and 1.2). Analytes/ions present in the intracellular space/cell should then be able to diffuse freely into the porous nanosensor matrix and selectively chelate with the analyte-specific fluorescent dye. Variations in the luminescent properties of the dye can then be observed/monitored and interpreted, potentially helping elucidate the role of these target species during cell stress, disease and death.

The key to a system like this is to generate only enough of the cytotoxic oxygen to disturb the chemical homeostasis of the cell (*i.e.* to only **induce** cell **stress**); thereby, minimising/delaying cell **death**. By varying the amount of cytotoxic species formed, different degrees of (oxidative) cell stress can potentially be observed, ranging from "minimal" cellular disturbances through to the induction of apoptosis; highlighting the versatility of such a system. It is also important to try and ensure that the emission wavelengths of the two fluorophores, *i.e.* the photosensitiser and the analyte sensitive dye have a large enough difference in their emission maxima so that there is minimal spectral overlap between their individual spectra. In addition, it is vital to try and minimise any leaching of the dye molecules out of the nanospecies matrix and into the cellular environment. One possibility of minimising such leaching would be to use the dextran-conjugated form of the dye. Dextran is an inert polysaccharide, available in different molecular weights, ranging from 10,000 and 70,000 Mw. It essentially acts as a physical anchor preventing the dye molecules from diffusing out of the nanosensor matrix. The dextran does not affect the sensing capability or sensitivity of the dye molecules.

The sensing component of the type system described above is an out-breed of those reported by a number of groups and can be realised through silica nanoparticles, such as the ORMOSIL type (see sections 1.4.3 and 1.4.8.3), and through polydecylmethacrylate, as well as a polyacrylamide-based matrix (see sections 1.4.3 and 1.4.8.3 and Chapter 3). Such sensors have been reported to be selectively sensitive towards a number of species including mercury; calcium; zinc; sodium; copper; glucose (oxygen determination); chloride ions; nitric oxide; and pH.[203,205,212,221-226,312,313] For use in drug, toxin and

environmental applications, including the detection of the potentially fatal bacteria *Escherichia coli* (*E. coli*) and the colloidal delivery of anti-leishmania drugs.[216,252,314,315]

There are numerous advantageous this type of system can offer, particularly in relation to previous single-cell sensing techniques: for example, sensing dyes in their free-state, pulled-fibre optodes and quantum dots. The system described may also be designed to facilitate selective delivery/targeting of nanospecies by tailoring the properties of the porphyrin and nanospecies components. Studies have suggested that cells remain viable through minimally invasive delivery of these systems.[316] The ability to achieve minute sampling volumes affording minimal disruption to the functioning of the cell is an additional advantage these systems can offer.

1.4.8.6 Previous Single Cell Analysis Techniques

Previous imaging methods have typically focused on the use of sensing-dyes in their free-state (see sections 1.1.11.5, particularly, 1.4.8.1) and pulled fibre optodes: both techniques which carry major disadvantages and limit their use. The major concern over these techniques is whether the "true" intracellular process is observed and **not** the consequence of the sensing technique itself.

Briefly, pulled-fibre optodes involve piercing the cell membrane, an action which may itself have a significant affect on the stimulus under study and the response of the cell, including loss of cell viability. These optodes have significant penetration volumes, up to 4% of the cell's total volume, again inflicting significant disruption to the cell. It has been suggested that the polyacrylamide-type nanosensors described above occupy only one part per million (1 ppm) of the cell's total volume, in terms of a direct comparison, 22,000 polyacrylamide nanosensors are thought to have the same penetration volume as one single pulled-fibre optode, with suggestions of acrylamide nanospecies (~20-40 nm species diameter) having a physical perturbation volume of less than 1ppb.[317]

Chapter synopsis: it can be readily observed that there is a clear unequivocal deficit in the understanding of intracellular mechanisms and a need to develop a means by which these delicate and powerful events can be further visualised and understood. An enhanced comprehension of these mechanisms, in both healthy functioning cells and stressed and diseased states, could allow scientists and medics to develop enhanced, eloquent and sensitive investigative techniques and strategies: empowering them with the potential to detect, control and eliminate cellular damage and disease. Such a physiological breakthrough would court major benefits, not only and most importantly, in the health of the patient, but also in the financial arenas associated with the patient and the State. One way in which a vision like this could be realised, is through the creation of a multifunctional analyte-sensitive system developed, through an interdisciplinary approach by bringing together: (i) colloidal and (ii) porphyrinic chemistry; (iii) optical spectroscopy; and (iv) cell biology. Such a system potentially offers the ability to answer many of the mysteries surrounding the biological labyrinth of cellular functioning and life. Attempts at the generation of the target sensing system will now be described in the following Chapter.

CHAPTER 2 PORPHYRIN RESULTS AND DISCUSSION

2.1 Aim

The aim of the Project: to generate a bifunctional nanosystem capable of eliciting and observing an intracellular response to cytotoxic reactive oxygen species (ROS), relies on the ability to bring together an "activator" and "detector" of cellular distress. These requirements can be accomplished through the combination of two distinct and independent species: (i) a photosensitiser (capable of generating ROS); and (ii) a luminescence-based nanosensor for monitoring the changes in a specific intracellular analyte.

2.2 Target System Requirements

The success of such a system is dependent on two main criteria: primarily, the ability of the nanosensor to detect the cytotoxic species generated by the photosensitiser. ROS are known to have a limited radius of action (≤20 nm) and short lifetime (≤40 ns, see section 1.1.6), *i.e.* they elicit their effects close to their site of generation. Therefore, in order to create an efficient observation/monitoring system (where as much information as possible can be gathered with the regard to the effect(s) these species have on intracellular processes, particularly the homeostasis of calcium) the nanosensor should be in a close proximity (≤20 nm) to the site of ROS formation, *i.e.* to the porphyrin component of the target system. This can be achieved by directly attaching the nanosensor to the photosensitiser moiety. The photosensitiser and nanosensor must therefore be selectively designed to incorporate functional groups capable of meditating this crucial criterion.

The second important criterion of the nanosystem target is its solubility in aqueous media. The target system has been designed to image cellular analytes; therefore, a pre-requisite for the porphyrin-nanosensor conjugate is its solubility in physiological media. Given that the nanospecies are essentially insoluble in aqueous media (they disperse), it is crucial to the successful delivery of the target system (into cells) that the porphyrin-

nanosensor conjugate is encouraged to remain in physiological media and not precipitate out. This can potentially be achieved by enhancing the water solubility of the porphyrin component of the target system; thus, the need for an alternative delivery method/vehicle is potentially removed. The attachment of porphyrin molecules to the nanosensors and the solubility of the target system in aqueous media are therefore both key features crucial in contributing to the success of the sensing system.

It is also important to consider the porphyrin's triplet quantum yield (Φ_T); for the target porphyrin to be an efficacious photosensitiser, *i.e.* to be efficient at undergoing ISC and interact with molecular oxygen (see sections 1.1.5, 1.1.6 and 1.1.7) it is desirable that it has a relatively high quantum triplet yield. The criteria for the target system **14** can be accomplished through: (i) the creation of synthetically useful functional groups, capable of facilitating the attachment of the porphyrin molecule to the nanosensors; (ii) by the addition of "water-solubilising" groups onto the periphery of the porphyrin macrocycle; and (iii) a desirable quantum triplet yield (Φ_T); achieved by choosing a porphyrin precursor with a significant triplet yield. The functionalisation of the nanosensor is discussed in Chapter 3, with the synthetic requirements of the porphyrin component addressed in the following discussion.

2.3 Porphyrin Target Molecule/Target Photosensitiser

The two key features required of the porphyrin component of the nano-target **14**: (i) a functional group suitable for conjugation and (ii) enhanced water-solubility need to be combined in a manner which will allow both of the desired elements to remain active, *i.e.* they should not have a deleterious effect on one another's properties. These valuable functional features can be synthetically incorporated into the core porphyrin structure through selective functional group interconversions and methylation of the pyridyl group nitrogen atoms; thus, a multifunctional porphyrin should be afforded with enhanced water solubility and the ability to react with amino-bearing compounds.

2.3.1 Porphyrin Functionalisation

The single point attachment of porphyrin molecules to other species requires the formation of mono-functionalised porphyrin derivatives. The most widely used structural frameworks for these derivatives are those of the *meso*-aryl porphyrins (figure 75). The success of conjugating a porphyrin to a second species is dependent upon the (i) reactivity and (ii) compatibility of the functional groups present on the two coupling components. The two functional groups need to react efficiently and selectively with each other under mild conditions amenable to both species. Ideally, there should be minimum formation of side products and therefore minimal purification steps post-conjugation. Lengthy coupling and purification procedures can be laborious, uneconomical and impractical; potentially risking degradation of the coupling product. The afforded target species should be stable to the conditions/environment it will be subjected to and stable for storage: synthesis of unsymmetrically substituted porphyrins alone is time consuming, often involving multiple chromatographic purification steps and poor yields, particularly of the initial porphyrin macrocycle (see sections 1.1.4 and 1.1.13).

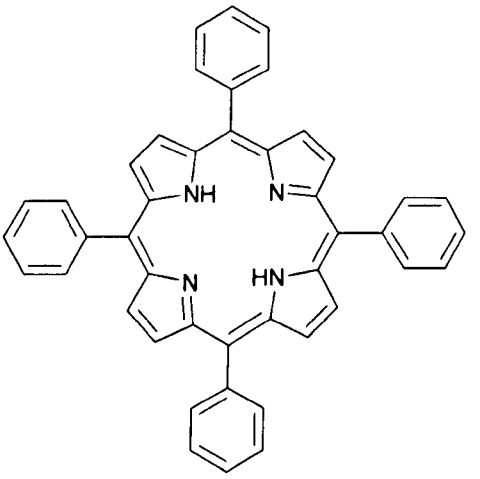

Figure 75 – 5,10,15,20-Tetraphenyl Porphyrin

2.3.1.1 Amine-Reactive Porphyrins

Conjugations between reactive functional groups and amino-bearing molecules, including a wide range of proteins and peptides bearing N-terminal and ε-lysine amines, are commonly performed (bioconjugations). Hence, a number of optimised/facile coupling protocols involving primary amino-species should be present in the literature, from which one could potentially adopt and (given its amenability to modification towards the nanospecies) utilise for the porphyrin-nanosensor coupling reaction.

A number of reactive functional groups, including N-hydroxysuccinimide (NHS) ester derivatives (scheme 13) and carbodiimides (N=C=N), have also been successfully used in conjugation reactions. However, there tends to be a number of recurrent issues between these different species. For example, the outcome of coupling reactions have: (i) shown pH dependence (N-hydroxysuccinimide esters have demonstrated a half-life approaching four hours at physiological pH, whereas at a pH of 8.5-10 the half-life is greatly reduced (10 minutes)); and (ii) have generated by-products, necessitating purification.

Purification of bioconjugates often requires the use of dialysis, a potentially time consuming process (typically three to four days); whilst purification of polymeric nanospecies is usually *via* extensive centrifugation or filtration/washings, both of these purification steps can cause degradation of the sensitive coupling links.[318]

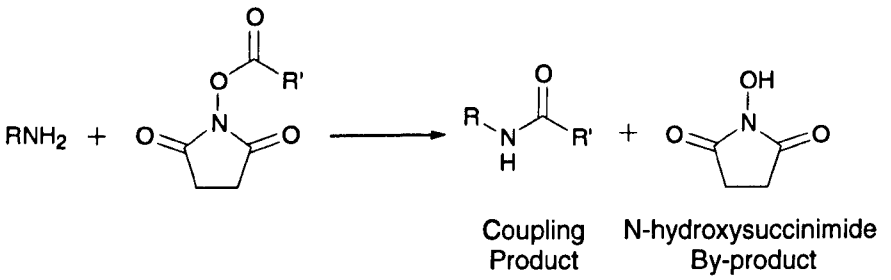

Scheme 13 – N-hydroxysuccinimide Ester Conjugation

One functional group which does not form any coupling by-products is the isocyanate (NCO) group. Isocyanates have been shown to react readily with amino-groups to form a covalent urea bond (scheme 14) between the two conjugation components, minimising the purification step. Simple purification of the coupling product is still required even in the absence of any by-products, since excess reagents must be removed. If one component is of significantly higher mass is present, this can be easily achieved by gel permeation chromatography.[114]

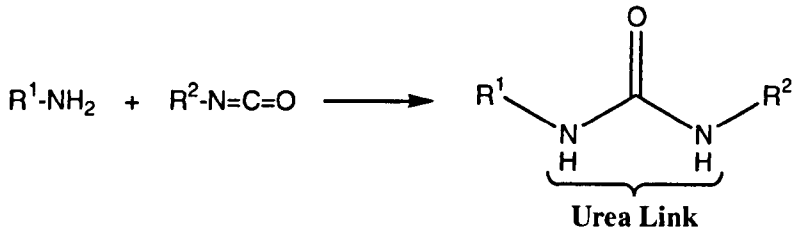

Scheme 14 – Isocyanate Coupling Reaction to a Primary Amine

However, isocyanate chemistry is not without its problems: isocyanates are very unstable to moisture, demonstrated by rapid hydrolysis of the functional group (scheme 15).

Scheme 15 – Isocyanate Hydrolysis

One functionality that has been developed with the above *meso*-substituted porphyrins in mind is that of the reactive isothiocyanate (NCS) group.[113,114] These sulphur isocyanate analogues have demonstrated increased stability towards moisture, with a number of the isothiocyanate compounds extensively used in conjugation reactions. This success is highlighted by the range of commercial isothiocyanate-containing compounds available, such as the fluorescein isothiocyanate and Oregon green isothiocyanate fluorophores (figure 76). These dyes have been successfully coupled to primary amine-bearing species including monoclonal antibodies.[319] The isothiocyanate functionality therefore appeared

to be a promising option in the formation of a mono-functionalised molecule capable of coupling to the amino-nanosensing component of the target system.

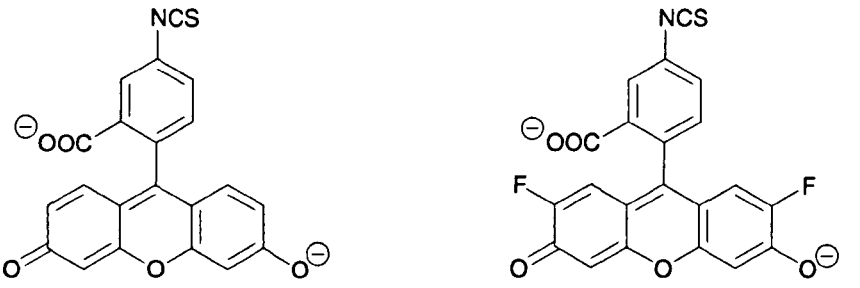

Figure 76 – Fluorescein Isothiocyanate and Oregon Green

2.3.1.2 Isothiocyanatophenyl Porphyrin

Isothiocyanato-bearing compounds can be attached to primary amines *via* a relatively straightforward protocol, whereby the isothiocyanate group spontaneously reacts with the amino-species in aqueous media (~ pH 9) to afford a thiourea-linked coupling product (scheme 16).

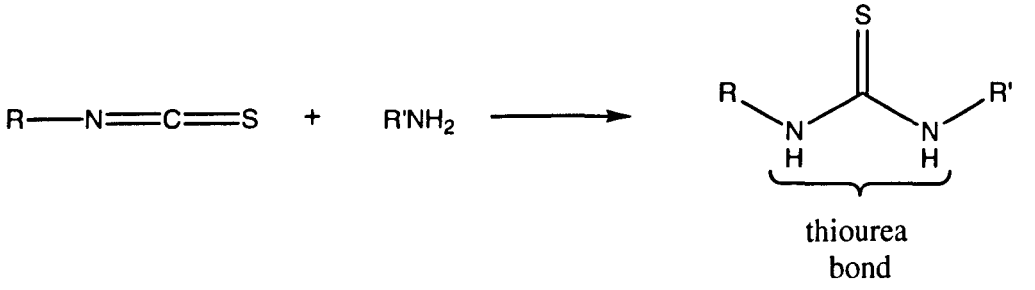

Scheme 16 – Isothiocyanate-Amine Coupling Reaction

It should be borne in mind that non-covalent binding between porphyrins (with multiple reactive functionalities) and amino species may take place during the coupling reaction. However, Boyle and co-workers addressed this concern and suggest that when one of the coupling reagents is highly hydrophilic, then only minimal/negligible non-covalent

binding takes place between an isothiocyanato porphyrin and an amino-bearing substrate during the reaction.[113]

2.3.1.3 Water-Soluble Porphyrins

The hydrophilicity of the target porphyrin molecule is important not only in the delivery of the final sensing system, but also with regard to the coupling together of the porphyrin and nanosensor: the optimal attachment of primary amines to isothiocyanato species is reported to be in aqueous media (sodium bicarbonate buffer, ~ pH 9.4).[114]

It is important to note that a coupling component, which is soluble in the polar solvents dimethylsulphoxide (DMSO) and dimethylformamide (DMF), may still be used in the conjugation procedure with aqueous buffers. However, it is preferred that the system/porphyrin is fully soluble in aqueous media, since it is possible that traces of the polar solvent may inadvertently damage the analyte-sensitive fluorophore or traces of the polar solvent remain in the porous nanosystem, affecting cellular investigations (see Chapter 5).

2.3.1.3.1. Water-Soluble Monofunctionalised Porphyrins

Introducing a functionality, which would facilitate increased solubility of the target porphyrin molecule in aqueous media, whilst retaining the requirements of a single reactive functional group, is not a simple or straightforward task. Pasternack and co-workers investigated water-soluble porphyrins in the late 1970's, concentrating on the carboxy, sulphonate and cationic pyridiniumyl tetraarylporphyrin derivates (figure 77).[115,320]

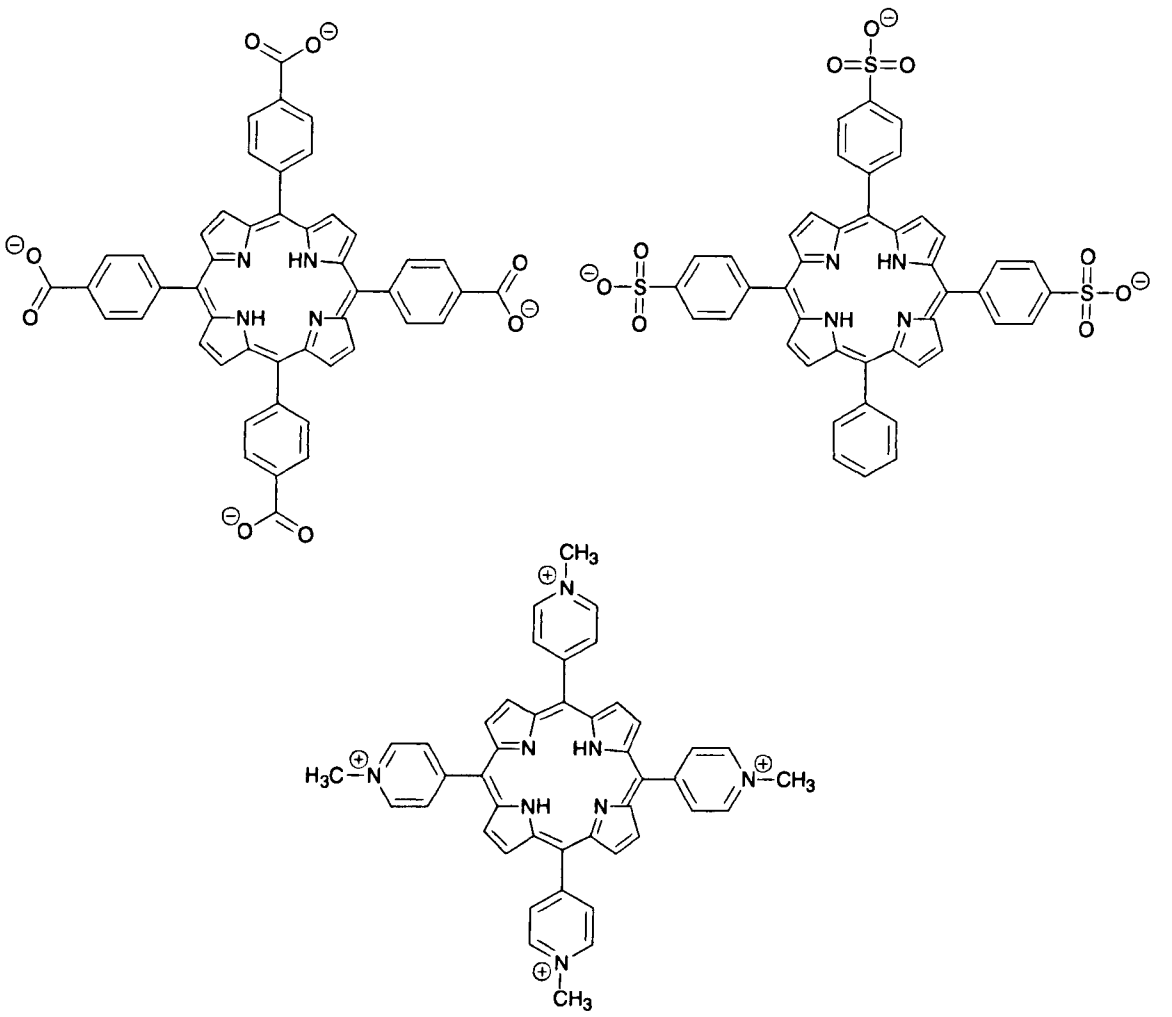

Figure 77 – Water Soluble Porphyrins

These three compounds have since become some of the more commonly studied examples of water-soluble tetraarylporphyrins. Further investigations by Pasternack demonstrated the behaviour of these porphyrin derivatives in aqueous media. It was suggested that at a pH of 7.5 the three porphyrins all exhibited similar behaviour: all existed in their monomeric form, while at pH 9 (aqueous solution) both the carboxy and sulphonate analogues dimerised. It was hypothesised that the charge present on the pyridiniumyl porphyrin minimised the formation of aggregates (see section 1.1.13); hence, a greater affinity for solvation was displayed by the cationic porphyrin. Recent work by Boyle and co-workers followed on from Pasternack's work and centred around the development of an isothiocyanato tri-cationic water-soluble porphyrin. This porphyrin

was later successfully coupled to a primary amino-bearing substrate.[113,114] It is also noteworthy, that although Boyle's group developed the isothiocyanato/water-soluble porphyrin desired for the Project, work was also carried out alongside that of Pasternack's by a number of other groups during the 1990's, including those of Meunier, Meng and Batinic-Haberle.[321-323] These groups successfully synthesised pyridiniumyl porphyrins for a number of applications including, photosensitisation.

2.3.2 Synthetic Strategy of Target Molecule

The synthetic strategy chosen to afford the target porphyrin molecule was the one developed by the Boyle group. It was decided that the cationic *N*-methyl-pyridiniumyl porphyrin demonstrated the key structural requirements of the target porphyrin molecule: (i) a functional group capable of facilitating the attachment of the porphyrin to the amino nanosensor and (ii) the preference for a porphyrin with increased water-solubility. This route would allow a more facile generation and purification of the isothiocyanato functionalised porphyrin and subsequent *N*-methylation of the pyridine rings. *Meso*-substituted tetrapyridyl porphyrins have been reported to have very high quantum yields of triplet formation nearing 0.9 (Φ_T = 0.89), it was therefore anticipated that the target porphyrin **5** should have the required high quantum yield of triplet formation.[29] The synthesis of the aforementioned porphyrin was attempted and is discussed accordingly in the remainder of this Chapter.

2.3.2.1 Synthesis of Target Porphyrin Molecule

The macrocyclic core of the desired porphyrin component was generated *via* the classic Adler method. Subsequent functionalisation of the porphyrin molecule was accomplished through: (i) acid-catalysed hydrolysis of the *meso*-substituted phenyl acetamido group; (ii) conversion of the resulting amine into the isothiocyanate functionality *via* the thiocarbonyl transfer reagent, 1,1'-thiocarbonyldi-2,2'-pyridone (TDP); and (iii) methylation of the pyridiniumyl nitrogen atoms using excess iodomethane. Increased water-solubility of the charged porphyrin was subsequently achieved *via* an anion exchange reaction utilising the resin Amberlite® IRA 400 Cl; where, the counter iodide

ions of porphyrin **4** were replaced by the chloride ions from the resin (scheme 17). Purification and isolation of the appropriate porphyrin intermediates (**1-3**) were achieved through column chromatography and high performance liquid chromatography (**4** and **5**), to repeatedly afford the target water-soluble porphyrin **5**.

It is noted that, although the synthesis of the target porphyrin is described in the respective/relevant literature, its synthesis had not been optimised. Increased yields of the intermediate and final porphyrin molecules, along with an increased purity of the target porphyrin were achieved during this Project.

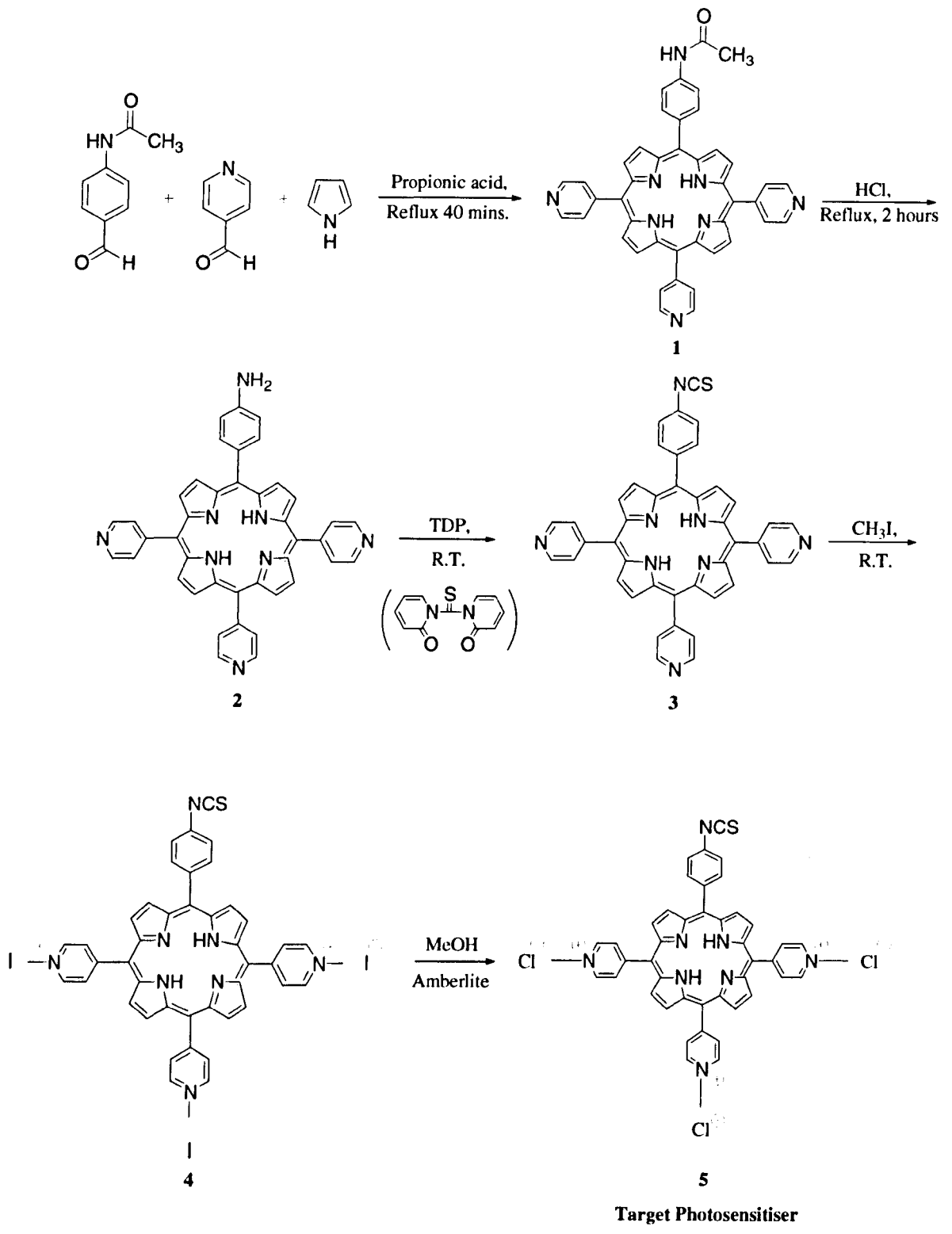

Scheme 17 – Synthetic Scheme Affording 5-(4-Isothiocyanatophenyl)-10,15,20-(4-*N*-methylpyridinumyl)porphyrin trichloride **5**

2.3.2.1.1 Synthesis of 5-(4-Acetamidophenyl)-10,15,20-tri-(4-pyridyl)porphyrin 1

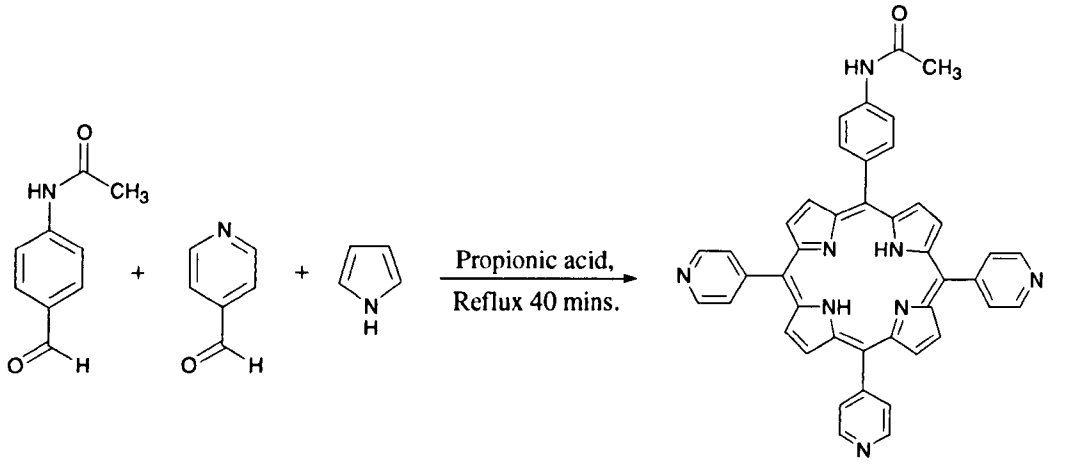

1

The acetamido-functionalised organic precursor was synthesised *via* the Adler mixed condensation route (see sections 1.1.4 and 1.1.13). Briefly, appropriately functionalised aldehydes were brought together in the presence of pyrrole and propionic acid in a ratio of 1:3:4 (4-acetamidobenzaldehyde:4-pyridinecarboxaldehyde:pyrrole). The reaction was allowed to proceed under reflux conditions for forty minutes open to the atmosphere. The desired product **1** was isolated from the crude porphyrin mixture *via* column chromatography. It was analysed by ^{1}H NMR, mass spectrometry and uv-vis. spectroscopy (presented in Chapter 6, section 6.2). Porphyrin **1** was repeatedly afforded as a purple solid, albeit in consistently poor yields (≤4%). The spectral results obtained were consistent with the formation of the desired acetamido porphyrin **1**.

From ^{1}H NMR analysis: the presence of the diagnostic low-field inner proton signals (δ -2.89 ppm), along with the high-field β and pyridyl protons (δ 8.85 and 9.05-9.05 ppm, respectively) supported the formation of the porphyrin macrocycle (see section 1.1.1). The singlet peak present at δ 2.38 ppm was consistent with the methyl group protons of the acetamido functionality; further evidence in support of the successful formation of porphyrin **1**.

The presence of the molecular ion at 675.67 on the mass spectrum of the isolated porphyrin product corresponded with the mass of the desired porphyrin **1**, supporting the conclusions drawn from the ^{1}H NMR spectrum. Analysis of the uv-vis. absorption spectrum of porphyrin **1**, further verified the presence of a free-base porphyrin macrocycle. The presence of the characteristic Soret band and four Q bands observed at 419, 515, 550, 583 and 646 nm was in good agreement with published values for the porphyrin. The combined findings of the three spectral analyses suggest that the compound afforded was in fact the 5-(4-acetamidophenyl)-10,15,20-tri-(4-pyridyl) porphyrin **1**.

The consistently low yields of porphyrin **1** were not considered to be a significant problem with respect to the accomplishment of the target molecule and were therefore, within the scope of this Project, not addressed further. Even at only a 4% yield it was anticipated that there should be sufficient quantities of porphyrin **1** to be carried forward through the synthetic strategy to afford the desired water-soluble isothiocyanato porphyrin **5**. As discussed in Chapter 1 (see sections 1.1.4 and 1.1.13), reactions affording the core porphyrin macrocycle *via* total synthesis methods are notoriously low yielding with regard to the desired product. These yields, particularly with regards to the Adler route, are the consequence of the formation of side-products and the difficult isolation of the desired porphyrin from its isomeric analogues. One way to minimise these unwanted products is through the use of stoichiometric quantities of the reagents (see sections 1.1.4 and 1.1.13).

The Adler route was chosen over the higher yielding Lindsey route, since the former method is more amenable to scale-up: the higher yields achievable *via* the Lindsey protocol are dependent upon high dilution conditions; hence, the scale-up of the latter technique typically involves handling (impractically) large volumes of solvent.

Acid Hydrolysis of 5-(4-Acetamidophenyl)-10,15,20-tri-(4-pyridyl)porphyrin 1

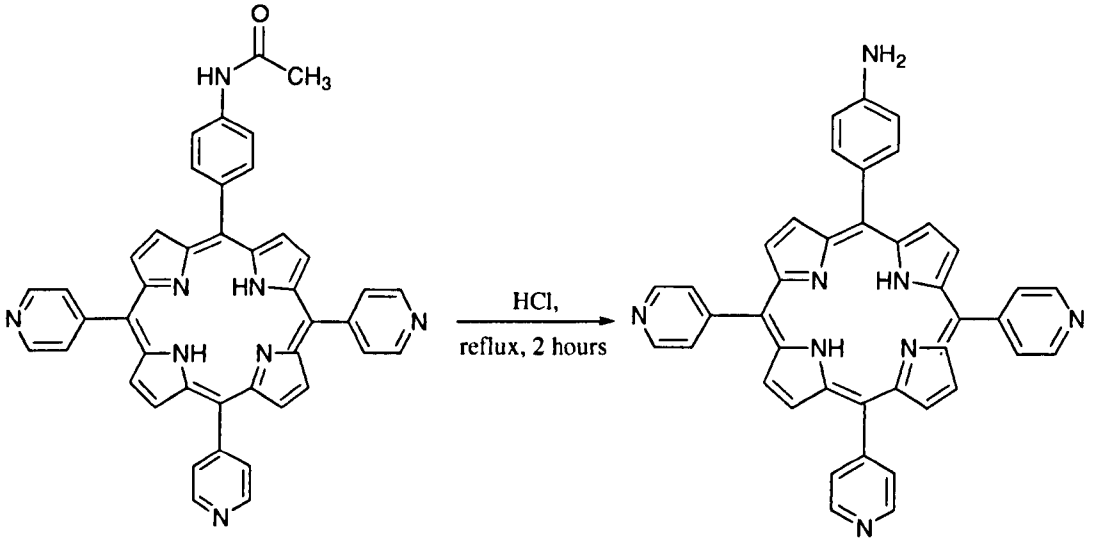

1 **2**

Acid hydrolysis of porphyrin **1** resulted in the formation of the amino porphyrin **2**. The acetamido porphyrin **1** was allowed to reflux in dilute (6M) hydrochloric acid for two hours. The crude reaction mixture was then purified by column chromatography to yield the desired amino functionalised porphyrin **2** as a purple solid; achieving yields of up to 67%. The successful isolation of the amino porphyrin from the crude reaction mixture was confirmed by ^{1}H NMR, mass spectrometry and uv-vis. analysis (outlined in section 6.2). The presence of the amino group could be clearly observed on the ^{1}H NMR spectrum. A broad singlet at δ 4.30 ppm was attributed to the amino protons, while the absence of a singlet at δ ~2.38 ppm (acetamido methyl group) suggested/confirmed the purity of the product.

Amino Conversion to 5-(4-Isothiocyanatophenyl) Porphyrin 3

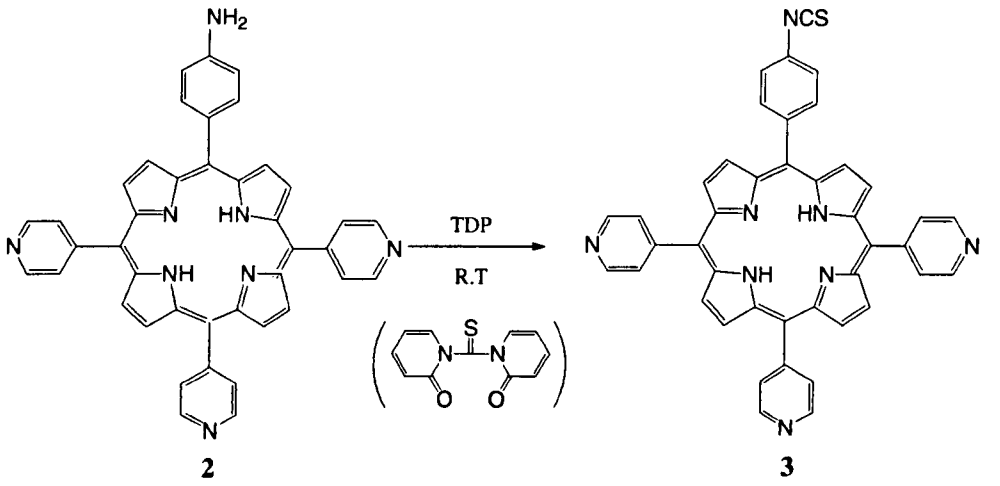

The desired coupling functionality was imparted onto the porphyrin molecule through reaction of porphyrin **2** with the commercial thiocarbonyl transfer reagent TDP. The reaction was allowed to proceed to completion (six hours) in freshly distilled dichloromethane, under an atmosphere of argon to yield a crude isothiocyanato porphyrin mixture. The 2-hydroxypyridine by-product and excess TDP were removed from the reaction mixture *via* column chromatography to afford the desired functionalised purple porphyrin **3** in yields of 93%. ^{1}H NMR and mass spectral analyses of the isolated porphyrin were consistent in confirming the presence of the isothiocyanato porphyrin **3** (see section 6.2): *i.e.* absence of amino protons and the presence of the desired mass ion.

5-(4-Isothiocyanatophenyl)-10,15,20-(4-*N*-methylpyridinumyl)porphyrin triiodide 4

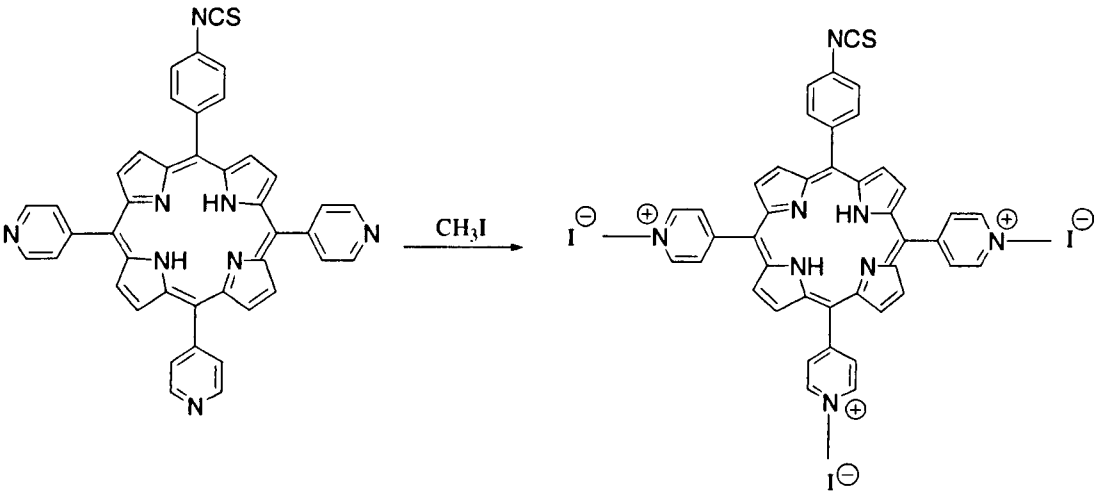

3 4

In order to bestow the cationic charge onto the porphyrin molecule, porphyrin **3** was treated with an excess of iodomethane under a blanket of argon at room temperature. Methylation of porphyrin **3**'s pyridyl groups was monitored by thin-layer chromatography (TLC). The mono-methylated porphyrin was identified as the higher R_f value compound, with the desired tri-methylated analogue represented by the lowest R_f species. The reaction was allowed to proceed until only a single compound (of the lowest R_f value) was observed (≤4 hours): an indication that all of the isothiocyanato porphyrin **3** had been converted into the corresponding tri-cationic porphyrin **4**. Yields of up to 91% were achieved. ^{1}H NMR analysis showed a downfield singlet peak present at δ 4.61 ppm, corresponding to the protons of the *N*-pyridyl methyl groups. Mass spectral analysis was also consistent with the mass of the desired compound (see section 6.2).

Synthesis of Water Soluble 5-(4-Isothiocyanatophenyl)-10,15,20-(4-*N*-methylpyridinumyl)porphyrin trichloride 5

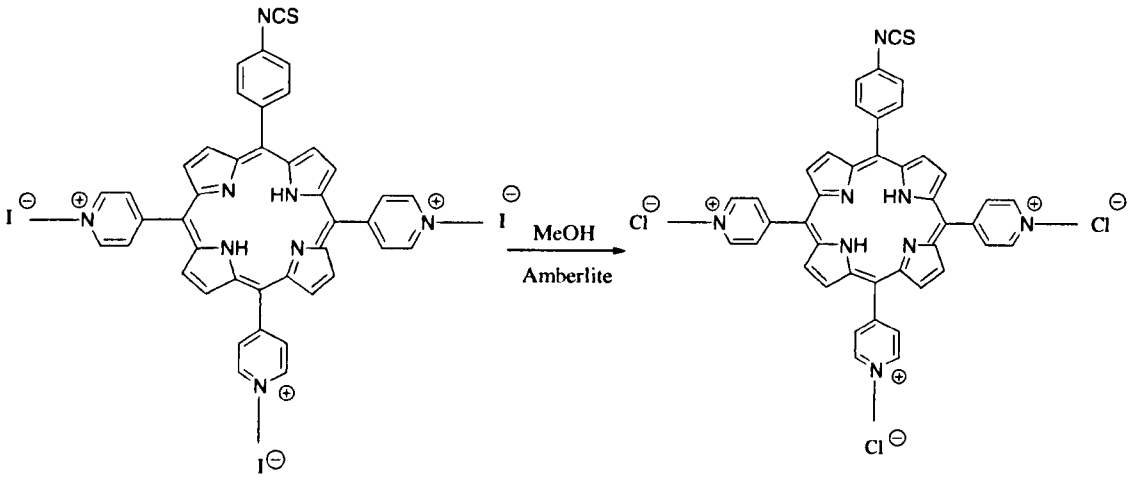

4 5

Increased water solubility was conferred on to porphyrin **4** *via* reaction with the chloride Amberlite® anion exchange resin. The reaction was allowed to proceed for one hour at room temperature under an inert atmosphere of argon. The Amberlite® resin was removed by vacuum filtration and the porphyrin filtrate recovered and concentrated *in vacuo* to afford the highly water soluble porphyrin **5** in yields of 91%. HPLC analysis of the formed porphyrins **4** and **5**, verified the presence of single compounds of different compositions (R_f), *i.e.* the anion exchange reaction had "gone to completion" and the target tri-cationic water-soluble porphyrin **5** had been synthesised as a pure compound. Compound/porphyrin **4** and **5** were further readily distinguishable from one another on account of the spontaneous solubilisation of porphyrin **5** when added to aqueous media.

2.3.2.1.1.1 Luminescence Characterisation

It was important to determine the luminescence properties of the target porphyrin **5** for a number of reasons. Primarily, determining the absorption profile of the final porphyrin compound and comparing it to the relevant published values would allow further confirmation that the target porphyrin molecule had been afforded. In addition, the absorption profile would assist in highlighting the excitation and emission profiles of the

porphyrin molecule, particularly important with regard to the analyte-sensitive fluorophore. It was essential to identify the porphyrin luminescence spectra to ensure that there was minimal spectral overlap between the porphyrin and the luminescence profile/peak of the analyte-sensitive dye, *i.e.* a significant difference/gap between the calcium green emission peak and the emission peak of the target porphyrin should exist, facilitating the easy identification of their respective emission profiles in the target system **14** (the porphyrin-nanosensor system). This is particularly important given that the target sensing system **14** is based on a luminescence response to increasing levels of the analyte of interest (calcium). Although, the calcium green emission peak intensity increases with rising (free) calcium ion concentration, deconvolution of the calcium green emission peak from that of the porphyrin at low calcium concentrations, in the absence of a significant maxima emission difference, may not be as easy as for a combined spectrum where a desirable emission difference is displayed.

Luminescence analysis of porphyrin **5** revealed that when excited at its maximal absorption wavelength (426 nm, Soret band, figure 78) the porphyrin has a broad emission profile (~640-740 nm) with a maximal emission at ~696 nm (figure 78). This encouraging result suggests that there should be a emission difference of ~180 nm present between the maximal emission of the calcium green fluorophore ($\lambda_{em.}$ 532 nm, figure 78) and porphyrin **5**. It was anticipated that this band gap would be sufficient to allow the emission peaks of the two chromophores to be identified in the target system **14**, *i.e.* the two independent emission peaks from the porphyrin-nanosensor target system should be separated.

It is noted here that the porphyrin emission band (figure 78) is unusually broad and poorly defined. This observation could be the result of multiple luminescent species being present in the sample solution; possibly, the result of porphyrin molecules aggregating together or the result of their decomposition in the sample solution. This observation was not an anomaly since it was repeatedly observed and could therefore be a result of the nature of the porphyrin species.

U.V.-Visible Absorption Spectrum of Target Porphyrin 5,

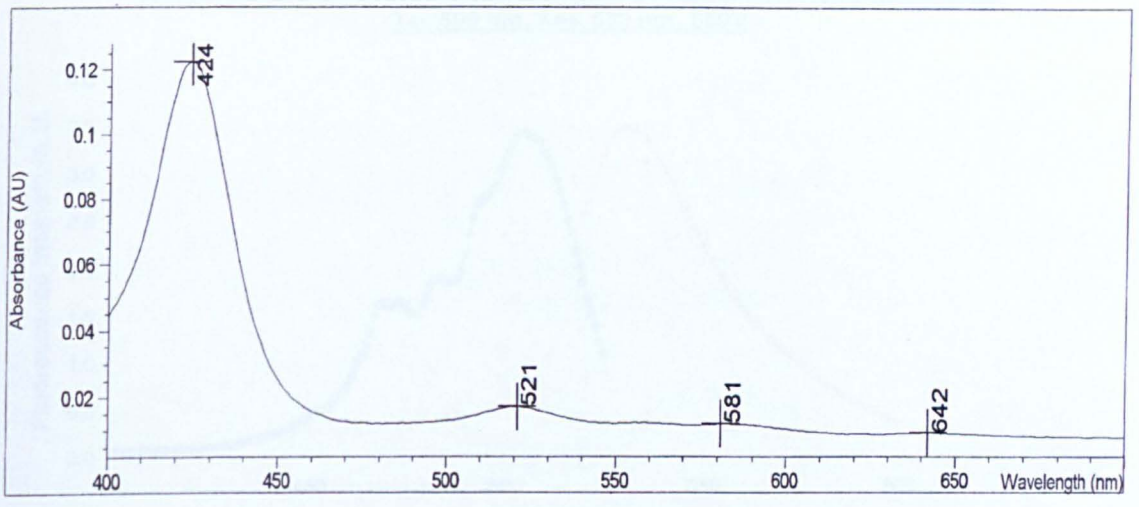

Excitation and Emission Spectra of Target Porphyrin 5, Buffer, $\lambda_{ex.}$ 426 nm, $\lambda_{em.}$ 696 nm, 550V

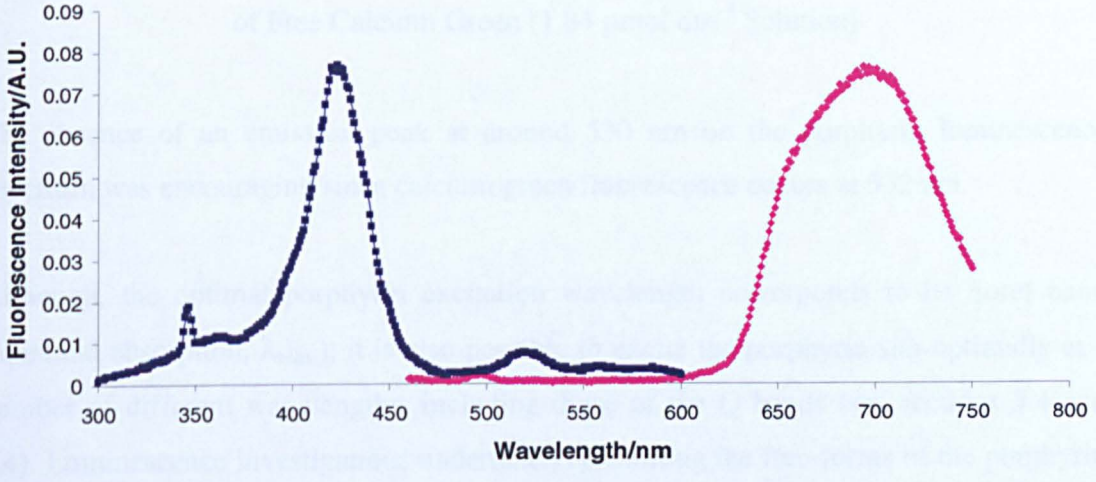

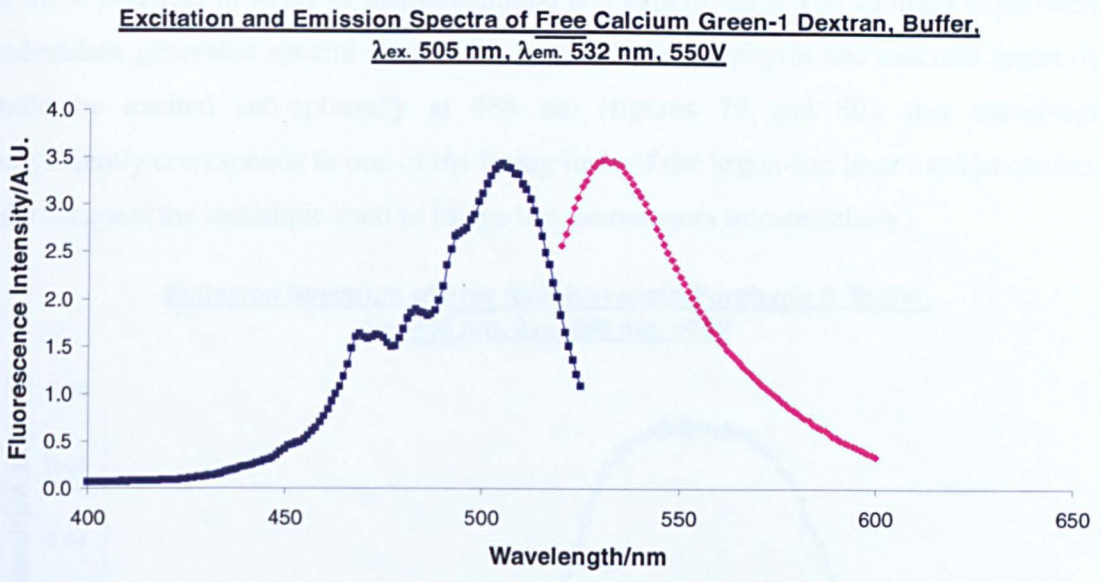

Figure 78 – Absorption, Excitation and Emission Spectra of Target Porphyrin **5** (1.94 μmol dm^{-3} Solution) and Excitation and Emission Spectra of Free Calcium Green (1.84 μmol dm^{-3} Solution)

The absence of an emission peak at around 530 nm on the porphyrin luminescence spectrum was encouraging since calcium green fluorescence occurs at 532 nm.

Although, the optimal porphyrin excitation wavelength corresponds to its Soret band (maximal absorption, $\lambda_{max.}$), it is also possible to excite the porphyrin sub-optimally at a number of different wavelengths, including those of the Q bands (see sections 3.4 and 6.4). Luminescence investigations undertaken concerning the free-forms of the porphyrin and calcium green dye (see sections 3.4 and 6.4) revealed the ability to excite the porphyrin at a range of wavelengths including 327, 426, 488, 493 and 505 nm. Particularly encouraging was the ability to excite the porphyrin and calcium green fluorophore at a mutual wavelength of 488 nm (figure 79). The porphyrin and calcium green both have different maximal absorptions ($\lambda_{max.}$ 426 and 505 nm, respectively), so to be able to excite the fluorophores at a single wavelength would have a number of benefits such as: (i) the simultaneous identification of both species could be made (particularly important in identifying the location of the species and confirming the presence of both fluorophores in/on the target system); and (ii) a single excitation wavelength would also

be more practical in terms of instrumentation and experiments. The solution experiments undertaken generated spectra suggesting that both the porphyrin and calcium green dye could be excited sub-optimally at 488 nm (figures 79 and 80); this wavelength conveniently corresponds to one of the lasing lines of the argon-ion laser used in confocal microscopes (the technique used to image the nanosensors intracellularly).

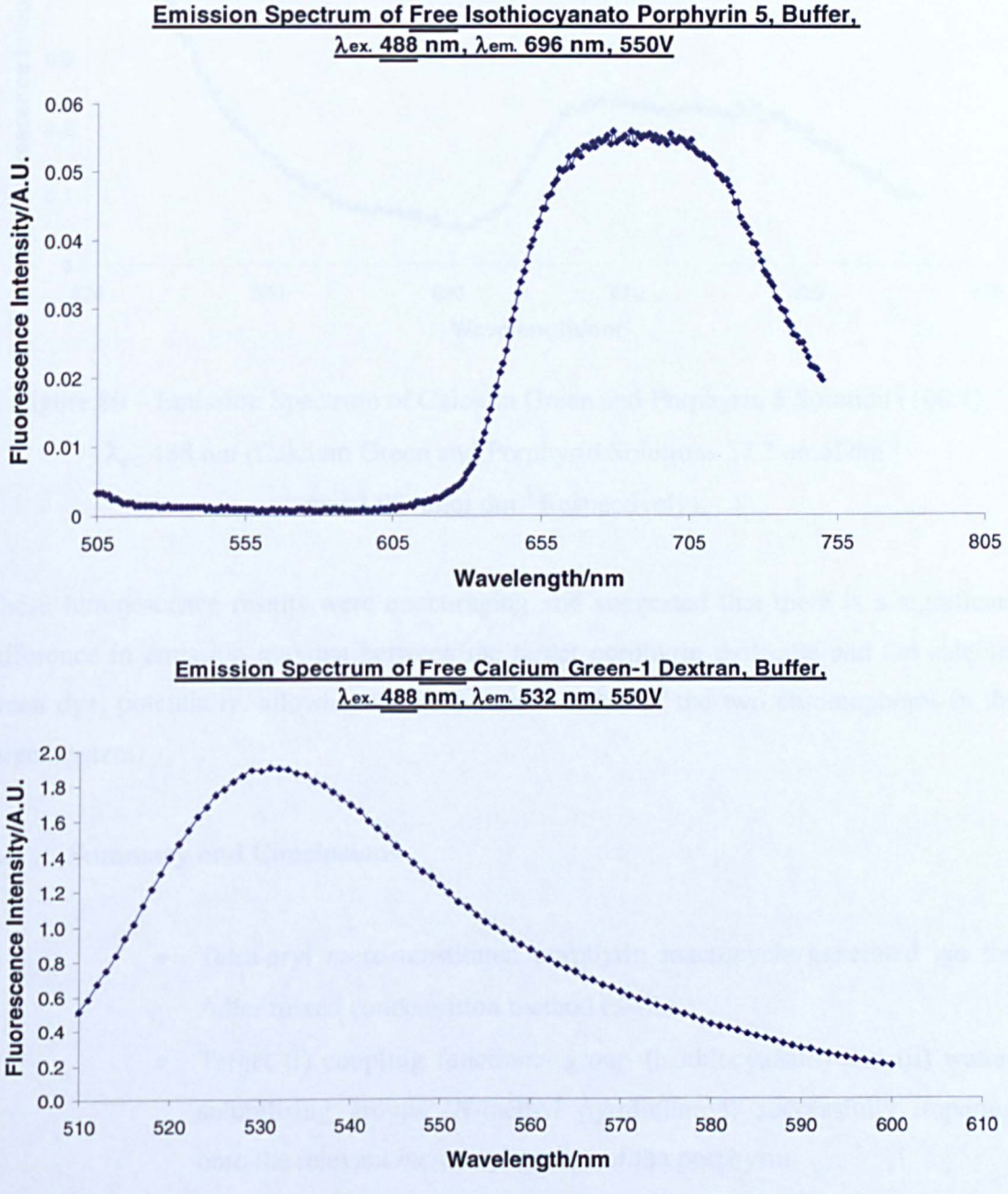

Figure 79 – Emission Spectra of the 2 Target-System's Component Chromophores, $\lambda_{ex.}$ 488 nm (Porphyrin and Calcium Green Solutions 1.94 and 1.84 μmol dm^{-3} Respectively)

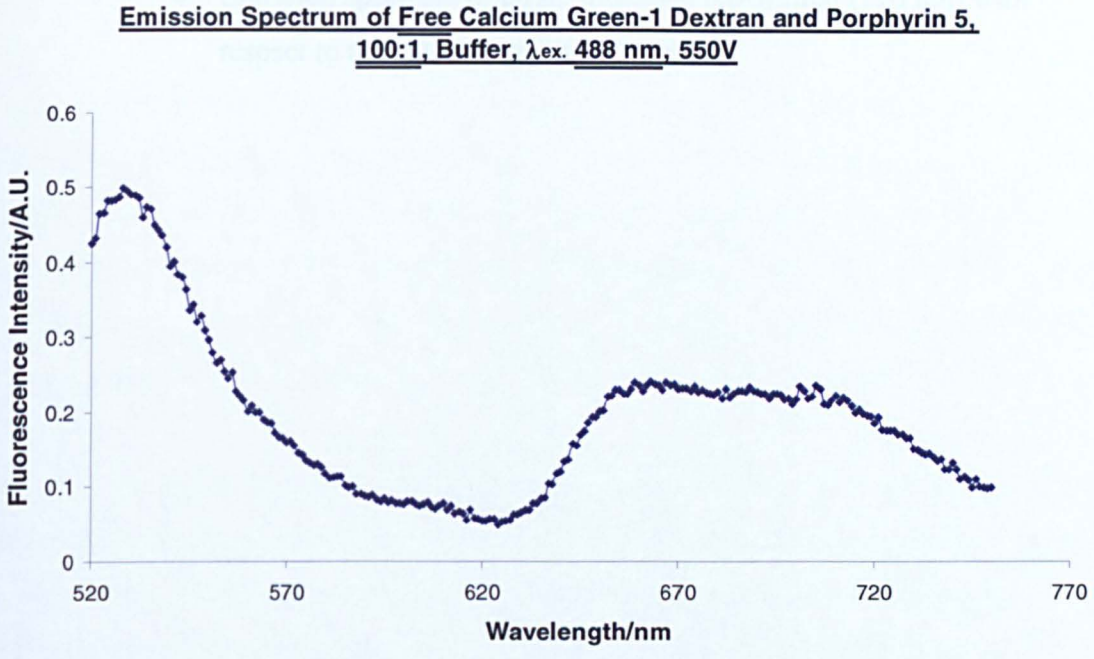

Figure 80 – Emission Spectrum of Calcium Green and Porphyrin **5** Solution (100:1), $\lambda_{ex.}$ 488 nm (Calcium Green and Porphyrin Solutions 37.2 nmol dm^{-3} and 3.98 nmol dm^{-3} Respectively)

These luminescence results were encouraging and suggested that there is a significant difference in emission maxima between the target porphyrin molecule and the calcium green dye; potentially, allowing the easy identification of the two chromophores in the target system.

2.4 Summary and Conclusions

- Tetra-aryl *meso*-substituted porphyrin macrocycle generated *via* the Adler mixed condensation method (≤4%).
- Target (i) coupling functional group (isothiocyanato) and (ii) water-solubilising groups (*N*-methyl pyridiniumyl) successfully imparted onto the relevant *meso*-aryl groups of the porphyrin.
- Target molecule **5** synthesised in yields of ≤91%.

- Emission spectrum of target molecule red-shifted (110 nm) with respect to the calcium green fluorophore.

CHAPTER 3 NANOSPECIES RESULTS AND DISCUSSION

The central aim of the Project: to simultaneously induce and indirectly monitor cellular stress in response to *in situ* generated (intracellular) ROS has been introduced in Chapter 1. This Chapter will focus on the chemical requirements of the analyte-sensitive nanospecies component of the target system **14** and initial attempts at its synthesis.

3.1 Nanospecies Synthesis

The four necessary elements of the desired analyte-sensitive nanospecies are: facile suspension in aqueous media; a porous matrix; the encapsulation of an analyte-specific fluorophore; and surface functionalisation. These four elements, should all work together in a mutually exclusive manner to allow the creation of a selective and efficient analyte-sensitive bifunctional nanosensor. The desired physical features of the nanosensor (functionalisation and a porous matrix) can be synthetically attempted and optimised to: (i) allow the generation of the chosen "surface-handle", able to facilitate the coupling reaction to the target porphyrin **5**; and (ii) include pores of an appropriate size, enabling the diffusion/passage of the analyte species (calcium, ionic radius 1.07Å) into the sensor matrix (whilst simultaneously minimising leaching of the entrapped fluorophore into the sensing environment).

Although, there are a number of routes through which the required nanospecies may be generated (see sections 1.4.3 particularly, 1.4.5), the method of choice for this Project was the well documented and relatively simple technique of microemulsion polymerisation (see section 1.4.7).[253] Here, co-monomers, acrylamide and *N,N'*-methylenebisacrylamide are brought together, in the presence of a surfactant-containing oily phase and an initiator system, to generate porous three-dimensional polyacrylamide gels in the nanometre range. The reaction typically proceeds for two hours at room temperature, with constant stirring under a **vital** atmosphere of inert gas (argon). Purification of the polymeric nanospecies (*via* ethanolic centrifugation) follows the *in vacuo* removal of the oily phase. The success of the polymerisation reaction was demonstrated by the recovery (microfiltration) of a white solid species. The gels formed

were typically spherical in nature (with an aqueous inner core): a consequence of the microemulsion chemistry.

It is worthy to note at this point the reason why the synthesis of the nanospecies was allowed to proceed for two hours. Although visible gelation of the reaction mixture usually occurs within thirty minutes of reaction initiation (see section 1.4.7), polymerisation actually occurs for much longer periods of time; mixtures which have been initiated with an ammonium persulphate/*N,N,N',N'*-tetramethylethylenediamine (APS/TEMED) system, and contain the cross-linking monomer *N,N'*-methylenebisacrylamide, can continue to react for up to two hours. The reaction mixture should therefore be left undisturbed well past signs of visible gelation to ensure maximum morphological reproducibility of the species; particularly with respect to the size of the pores.[324] The handling protocol for APS is also important. APS is hygroscopic and begins to decompose almost immediately when dissolved in water; therefore it was important to keep it **cooled** on ice and only added to an aliquot of the aqueous media **seconds** before addition to the reaction mixture.

Although, Kopelman and his group have published a number of scientific papers relating to the polyacrylamide nanospecies originally developed by Daubresse's group, difficulties were repeatedly encountered during the Project in reproducing Kopelman's work.[253,306-309,317] In particular, significant problems were encountered when trying to successfully synthesise the nanospecies when following the synthetic procedure as reported by Kopelman.[317]

Kopelman states, that the polyacrylamide nanospecies can be generated following a modified microemulsion procedure (described by Daubresse).[317] More specifically, Kopelman describes the polyacrylamide preparation as: "a polymer solution composed of acrylamide (27%), *N,N'*-methylenebisacrylamide (3%) and, if appropriate, a fluorescent dye." When a fluorescent dye is include in the preparation, Kopelman uses a buffer instead of purified water. He goes on to say, that the polymer solution (1 ml) should then be added to a hexane solution (20 ml hexane) which contains the surfactants Brij 30 (4.24 mM) and dioctyl sulfosuccinate sodium salt (1.8 nM). Kopelman follows on that, the

microemulsion reaction mixture should be placed in an ice bath and stirred under nitrogen for twenty minutes. The initiators (10% APS solution (24 μl) and TEMED (12 μl)) should then be added and the reaction allowed to proceed at room temperature for two hours.[317]

When nanospecies were generated *via* the above protocol, they were done so in very poor yields and demonstrated minimal dispersion in aqueous media, even with mechanical agitation (sonication). The resulting synthetic results were therefore sporadic and inconclusive when following Kopelman's synthetic protocol. Subsequently, it was decided a number of key experimental/system variables should be investigated (see section 3.1.3 for full discussion). These investigations lead to the development of an optimised and reproducible experimental procedure (see section 3.1.4 for further discussion and other procedural changes), whereby small (≤44 nm), dispersible nanospecies could be easily generated. The key differences between Kopelman's protocol and the one developed during this Project are highlighted in section 3.1.4. Particular attention is brought to the **rigorous degassing** of the individual reaction components and reaction mixture in the optimised polyacrylamide nanospecies synthesis; this **crucial** step is absent from Kopelman's procedure.

3.1.1 Reaction Mechanism

The polymerisation reaction which affords nanospecies **6** proceeds *via* a free radical water-in-oil polymerisation mechanism (see section 1.4.7.6). Briefly, the aqueous cores of the surfactant-stabilised micelles act as the loci for the polymerisation reaction, and it is proposed that the initial free radicals, formed from the APS/TEMED initiation system, attack the π-bond of one of the monomer units: with a higher probability of this bond belonging to the primary monomer (acrylamide). The primary monomer is present in higher concentrations than the cross-linking monomer (*N,N'*-methylenebisacrylamide) and when applicable, the functionalised monomer (*N*-(3-aminopropryl)methacrylamide hydrochloride, see section 3.2). The polymerisation reaction then progresses through a number of propagation steps, with the size of polymer chain limited by the size of the

micelles/particles formed. The propagation stage continues until the monomer reserves become depleted or the free radical species combine with one another; severely reducing the concentration of free radicals available to attack any remaining monomeric π-bonds.

3.1.2 Nanospecies Dispersion

Although the polyacrylamide nanospecies **6** had been successfully synthesised, repeated problems were encountered with the dispersion of the nanospecies in aqueous media and consistently poor polymerisation yields. Thus, further investigations were necessary if species which were readily dispersible (in aqueous systems), *i.e.* with minimum physical or mechanical effort, were to be generated consistently (and) in good to high yields. These set-backs were of particular concern since the final aim of the Project was to use the nanosystem in physiological media without the use of an additional delivery vehicle. Without their dispersion, it was feared that the nanospecies would precipitate out of the physiological media and severely impede/prevent intracellular studies. Repeatedly poor yields could also seriously hamper the Project since it is very difficult to work with such small quantities (≤21 mg, ≤3%): primary and repeated analyses of the species and coupling reactions become increasingly difficult with reduced quantities, and of course there would be a constant need to repeat the nanospecies synthesis.

It is commonly believed that nanospecies with a hydrodynamic radius (R_h) below 1 μm exhibit enhanced dispersion properties. However, it is actually the presence of minimum: (i) Oswald's ripening: a process by which larger particles grow at the expense of their smaller counterparts (due to the higher solubility of the smaller particles and molecular diffusion through the continuous phase); (ii) flocculation: the separation of solid particles from a liquid to form loose aggregates (flocs); and (iii) creaming: the migration of a substance in an emulsion (under the influence of buoyancy) to the top of the sample whereby, particles do not flocculate but remain separated, which give rise to enhanced dispersion properties. These phenomena can be controlled/minimised through altering a species physical properties, including its wettability; surface energy; and hydrophilicity/hydrophobicity. If a suspended/dispersed sample of nanospecies undergo

Brownian motion and can overcome the gravitational forces they are subject to in the system, they should remain free from flocculation and not settle-out of the medium. Since a particle's size and shape affects its colloidal properties, it was decided to perform a number of basic investigations involving parameters known to affect the size (R_h) of the species (see section 1.4.7). Given that microemulsion techniques typically form particles in the sub-micron range, it seemed reasonable to expect that the desired polymeric nanospecies could still be afforded from this technique.

3.1.3 Nanospecies Size, Dispersibility and Yield

The final size of polymeric species, fabricated *via* the microemulsion process, can be dictated through varying the relative molar ratios between the monomeric and surfactant components of the system. This technique (briefly discussed in section 1.4.7) is brought about by limiting the size of the micelles formed within the reaction mixture: controlling the size of the micelles governs the length of the polymer chains formed during the polymerisation reaction and consequently the size of the resulting particles (and final nanospecies). Therefore, it was anticipated that by increasing the ratio of surfactant molecules present in the reaction mixture, a greater number of smaller micelles would be formed; hence, smaller particles and nanospecies could be produced. Having identified a protocol by which the poor dispersion properties of the initial nanospecies could potentially be corrected, a second attempt was made at the synthesis of polyacrylamide nanospecies. In this attempt, various molar ratios of the non-ionic surfactant, Brij 30, ranging from 8.5 (x 1), 12.75 (x 1½), 17.0 (x 2) to 25.5 mmol (x 3) were used in the microemulsion reaction mixture.

The nanospecies afforded from the experiments were analysed by photocorrelation spectroscopy (PCS) and found to have a diameters ($z_{ave.}$) ranging from 52.4 to 219.4 nm (table 2); supporting the hypothesis, that species below 1 μm disperse more readily than their larger counterparts.

SURFACTANT RATIO	SIZE ($z_{ave.}$)/nm	DISPERSE	YIELD/%
1	219.4	✓	≤3
1½	156.7	✓	≤6
2	84.7	✓	≤9
3	52.4	✓	≤8

Table 2 – Effect of Surfactant Concentration on (i) Nanospecies Size ($z_{ave.}$) and (ii) Dispersibility in Aqueous Media

The results from the experiments varied; although, dispersible polymeric species could be generated with all three of the surfactant ratios (the majority of the time), there still seemed to be a persistent absence of any consistency in the yields produced. This relentless problem required immediate investigation (see section 3.1.4).

Parallel experiments were also run varying the ratio of the polymerisation effectors APS and TEMED. It appeared from the investigative results that when increasing concentrations of the APS initiator (0.4382 (10%), 0.8764 (20%), 1.3146 (30%), 1.7528 (40%) and 2.1911 (50%) mol dm^{-3}) only minimal success in generating the dispersible species (table 3 and figure 81) was achieved.

APS RATIO/%	DISPERSE	SIZE ($z_{ave.}$)/nm	YIELD/%
10	×	–	≤3
10	×	–	≤21
10 (Argon)	✓	**36**	**≥90**
10 ("Fresh" Chemicals)	✓	**42.7**	≤20
20	×	–	≤3
20 (Argon)	✓	36.1	≤40
30	✓	34.0	≤5
30	×	–	≤28
30 (Argon)	✓	26.4	≤74
40	×	–	≤90
40 (Argon)	✓	33.1	≤90
50	×	–	≤16

50 (Argon)	✓	21.2	≤90
50 ("Fresh" Chemicals)	✓	**25.3**	**≤82**

Table 3 – Effect of APS Concentration on Species Dispersibility in Aqueous Media and Species Yield

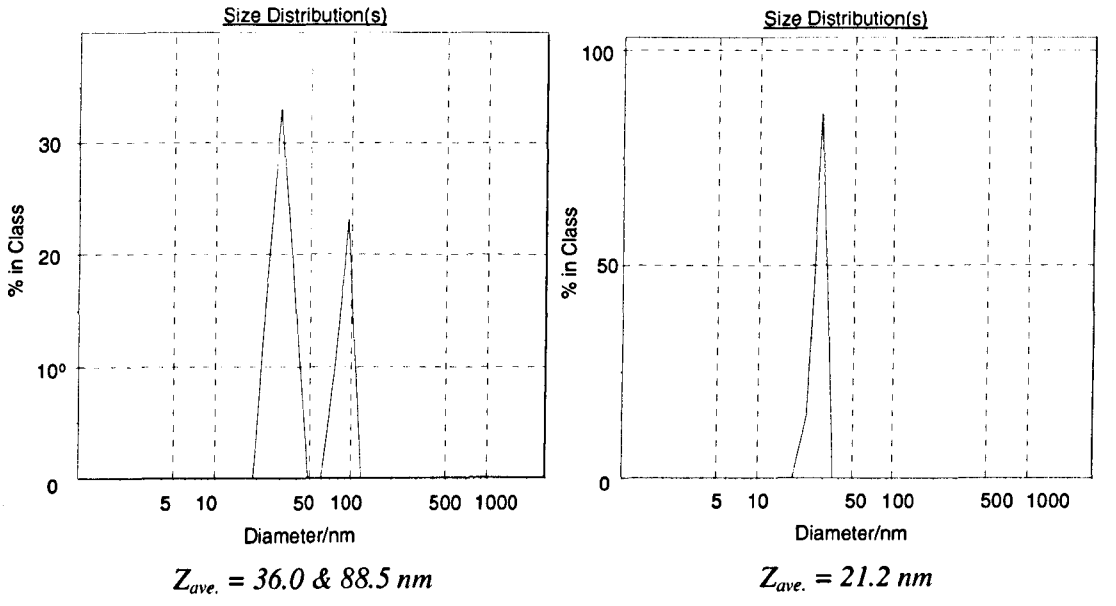

$Z_{ave.}$ = *36.0 & 88.5 nm* $Z_{ave.}$ = *21.2 nm*

Figure 81 - PCS Spectra for Nanospecies Generated with 10% APS (argon) and 50% APS (argon)

However, it became apparent from these investigations that a significant increase in the yield (from 3 - 90%) of the species was generated when the inert gas argon was employed (rather than nitrogen). The observation did not appear to be atypical since it was repeated in 80% of the experiments undertaken using argon. So, it seemed that although increasing the concentration of the APS initiator appeared to successfully increase the yield of the

nanospecies, it did not alone necessarily affect the dispersibility of the nanospecies in a positively consistent manner. It was also observed, that nanospecies with a greater affinity to disperse (in aqueous media), were being generated when a "fresh" batch of polymerisation reagents were being used in the reaction, even when the standard APS concentration of 10% (0.4382 mol dm^{-3}) was employed (in conjunction with a nitrogen atmosphere); although, the species yield was still not desirable at just under 20%.

The parallel experiments run with the second initiator component (TEMED) showed no consistency, and a very limited range of positive results were obtained when varying the molar ratio of TEMED relative to APS. These experiments investigated molar ratios of ½ (0.1 μmol, 15 μl) and 2 (0.4 μmol, 60 μl), and included experiments excluding the TEMED initiator altogether, and simultaneously varying the concentration of APS (table 4).

TEMED RATIO	APS CONCENTRATION/%	DISPERSE	YIELD/%
0	10	×	≤48
½ ("fresh" chemicals and argon)	**10**	✓	**≥90**
1	10	×	≤10
1 (argon)	10	✓	≤30
2	10	✓	≤8
2 ("fresh" chemicals)	10	✓	≤59
2	20	✓	≤8

Table 4 – Effect of TEMED Concentration on Species Dispersibility in Aqueous Media and Species Yield

The experimental results (table 4) suggested, that on occasion, polymeric species could be generated in the absence of TEMED (once reaching a yield of 48%); although, none of these species were dispersible in aqueous media. Once again, results appeared somewhat sporadic when the initiator molar ratio was doubled (APS constant at 10%); sometimes generating dispersible yields of up to 59%. However, when the ratio of APS was also doubled, only (dispersible) yields of 8% were achieved (same TEMED concentration (x2)).

Although, it did periodically appear from these experiments, possible to achieve dispersible nanospecies, in good to high yields (~59%), when increasing the concentration of TEMED, it was decided to attempt the polymerisation reaction and observe the outcome when a lower TEMED concentration (x ½, table 4) was employed. Results from these experiments suggested that dispersible nanospecies, in good yields (≥90%), could be afforded.

The inconsistent results from the latter (TEMED) set of experiments had so far proved inconclusive in terms of repeatedly producing dispersible polymeric nanospecies in good to high yields. This was starting to cause great concern since it was important to be able to master a synthesis which could provide the desired nanospecies with the necessary physical features in a reproducible and reliable manner.

However, some encouraging results did seem to be emerging from one set of experiments concerning TEMED. There seemed to be a positive trend in the affinity of the species to disperse in aqueous media when argon and the "fresh" batch of chemicals were employed in the microemulsion polymerisation reaction. The species not only showed enhanced dispersibility, but they were also afforded in greater yields (≥90%) than had been observed in the initial experiments. These observations were in good agreement with the results obtained for the "APS" experiments.

A note to bear in mind: the polymerisation reagents (the monomers and initiators) decompose over time and if the highest quality reagents are not used and/or stored under the correct conditions, significant amounts of contaminants, including polyacrylamides and metals in the monomer stocks, may be present in the reaction mixture and have a deleterious effect on the polymerisation product. These reagents can be purified by recrystallisation and distillation.

So far within the Project, it had appeared to be hit and miss whether dispersible nanospecies in desirable yields could be generated *via* the route of choice (microemulsion polymerisation). This suggested that there was a more fundamental problem with the

synthetic step. Therefore, it became critical that the issues were rapidly and thoroughly addressed.

3.1.4 Free Radical Polymerisation

It was decided that the underlying mechanism(s) behind the polymerisation/microemulsion processes should be looked at in closer detail. The chemical mechanism behind the polymerisation process (a free radical mechanism) has the rudimentary requirement of the appropriate free radicals. Free radicals initiate the polymerisation process by attacking monomeric π-bonds (see sections 1.4.4 and particularly, 1.4.7). The site of attack itself then generates a free radical and becomes known as the active centre, where additional monomer units can add (propagation). Such propagation steps see the polymer chains grow until either: (i) all of the monomer units are consumed through addition to the growing polymer chains or (ii) when two radical species (monomeric/polymeric) combine, preventing further growth of the polymer chains. Therefore, it could be readily anticipated that if either a high enough concentration of the initiator molecules (the initial free radicals) are not present in the reaction mixture or, alternatively, if there are any substrates present which are quenching the free radical species in a negative manner, then the polymerisation mechanism will not proceed efficiently.

It is widely known that ground state molecular oxygen is a diradical molecule (figure 18), *i.e.* a free radical scavenger, and it was evident from the investigations already undertaken (involving varying APS and TEMED concentrations, see section 3.1.3), that greater yields of nanospecies could be generated when the inert gas argon was used in the reaction: an obvious result since argon is generally of a higher purity grade and more likely to be drier than its counterpart nitrogen. Argon is also heavier than nitrogen and will typically exclude greater amounts of oxygen under identical conditions to those used with nitrogen, *i.e.* when combining the microemulsion/polymerisation reagents (aqueous and oil phases) oxygen is less likely to displace the more dense gas (argon). It was therefore decided that, since positive results had already been observed with argon and that the complete absence of any "foreign" radical scavengers was such an integral part of

the polymerisation process, the synthesis of the nanospecies would be repeated again using the argon gas. Extended degassing periods of: (i) the individual reaction components (aqueous and oil phases); as well as the usual gaseous evacuation of (ii) the combined reagents would be practiced; and to be extra vigilant, (iii) the balloon (used to provided the constant inert atmosphere during the reaction) would also be purged with argon several times. Indeed, this new protocol seemed to prove successful by repeatedly affording nanospecies **6** in yields in excess of 80% (table 5).

REACTION COMPONENT	DEGASSING PERIOD/minutes	YIELD/%	DISPERSE
Oil (hexane)	≤30	≤3	×
Individual Components **+** **Oil (hexane)** **+** **Balloon**	**10 – 20** **40** **Several Times**	**≥80**	✓

Table 5 – Relationship between the "Component"/System Degassing Times and the Success of the Microemulsion Polymerisation Reaction

The thorough degassing of the reagents and reaction mixture appeared to not only increase the yield of the desired nanospecies **6**, but also remedy the problem of (repeatedly) achieving dispersible nanospecies. Thus, it could be concluded that the **thorough** evacuation of any radical scavengers from the polymerisation reaction mixture was a **critical** and **vital** step in the generation of dispersible nanospecies in good to high yields.

As a result of these findings, along with those for the "initiator" experiments, it was decided that the concentration of surfactant to be used in all future nanospecies synthesis would remain at the lower molar value (8.5 mmol, x 1). With mixed results from the

"initiator" investigations it was decided that the "standard" APS concentration of 10% (0.4382 mol dm^{-3}) and the TEMED concentration of ½ (0.1 μmol) would be used in all future nanospecies synthesis, along with the heavier argon gas and the "fresh" set of polymerisation reagents. In addition, no further investigations would be undertaken with regard to varying the surfactant or initiator concentrations, especially given that it is desirable to use the least amount of surfactant and initiator in the polymerisation reaction as possible: excess surfactant(s) and persulphate can cause altered function of epidermal cells (see section 1.4.7) and oxidation of proteins and nucleic acids (APS).[324]

3.1.5 Dispersibility and Nanospecies Size ($z_{ave.}$)

The dispersibility of the nanospecies was initially tested in a rather crude (but importantly quick and easy) manner. A few milligrams (≤2 mg) of the nanospecies were added to an aliquot (2 ml) of purified water. This simple test would allow one to easily observe if: (i) the nanospecies dispersed; (ii) the dispersion was optically transparent; and (iii) the species remained dispersed. The amount of polymeric species added to the aqueous media was increased until either saturation levels or ~5 mg/ml were achieved. The value 5 mg/ml was significant as this was the initial concentration of nanospecies which was being sought to carry out the preliminary conjugation reactions involving the nanospecies (see sections 3.3 and 3.6).

It is important to point out that the size ($z_{ave.}$) distribution of polymeric species is polydisperse; consequently, any resulting dispersion formed from this type of nanospecies will not be homogeneous in nature. Therefore, there may well be a small proportion of nanospecies which are clearly visible to the naked eye and may go on to flocculate/"settle-out" of the dispersion medium more quickly than their smaller counterparts.

Indeed, it was observed that the polymerisation reactions did not always afford nanoproducts which were in the same size range, *i.e.* a single population size distribution: a second size population was sometimes present in the size distribution data (figure 82).

However, the occurrence of bi-/multimodal distributions seemed to be significantly diminished when the reaction conditions/process had been optimised (figure 83).

PCS Spectra Showing Multiple Size Population Distribution of Nanospecies

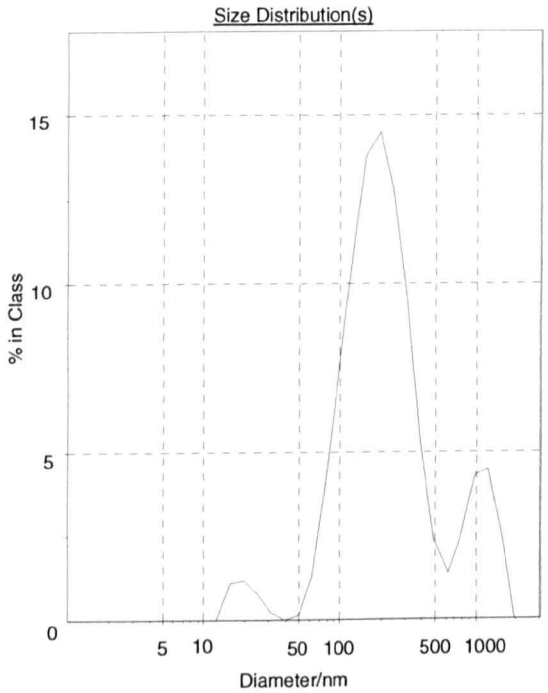

(a) Poorly Dispersible Species

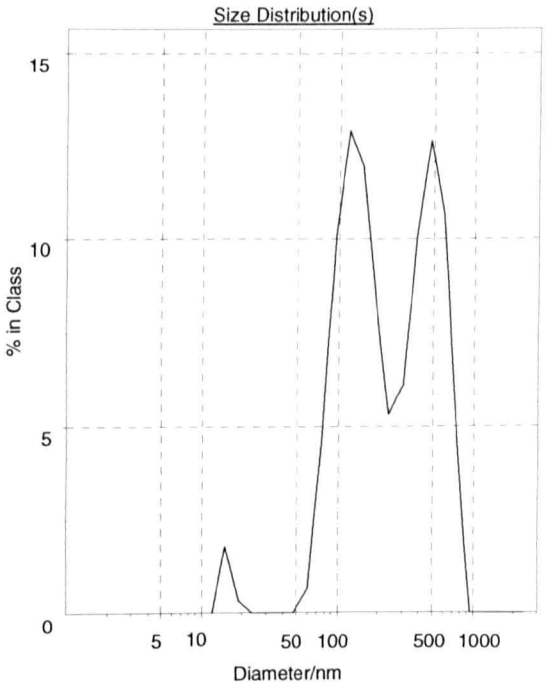

(b) Poorly Dispersible Species

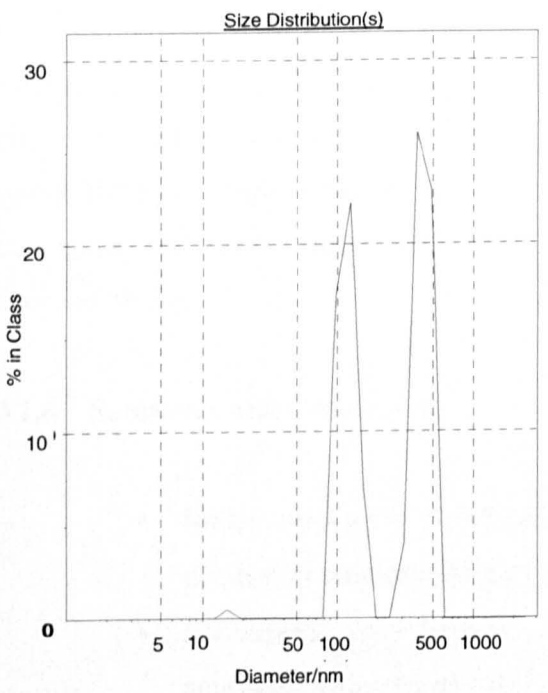

(c) Medium Dispersible Species

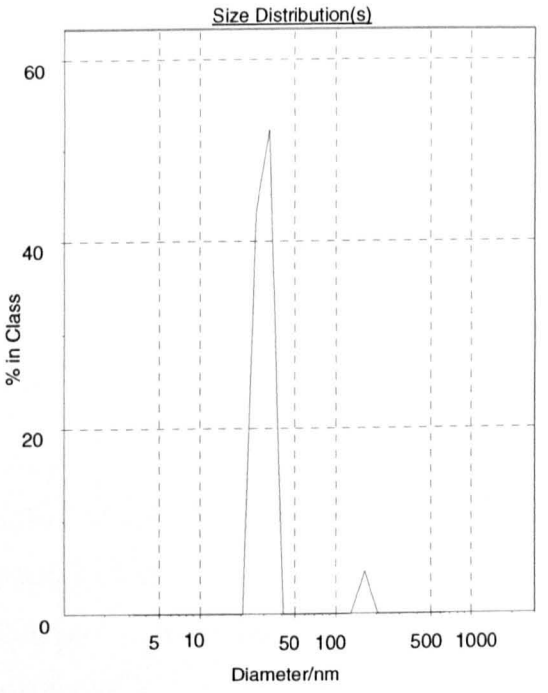

(d) Dispersible Species, Still >1 Population

Figure 82 – Multiple Population PCS Spectra

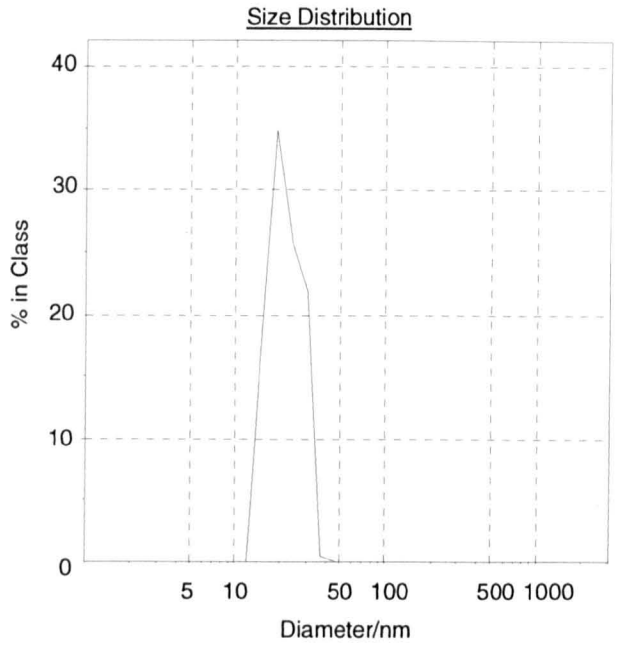

Figure 83 - Single Population PCS Spectrum
(30% APS, argon, $z_{ave.}$ = 26.4 nm)

Extensive efforts were made to confirm the structural features of the nanospecies *via* electron microscopy (TEM and SEM) and atomic force microscopy. Unfortunately, these efforts proved unsuccessful and the characterisation of nanospecies was regrettably, solely through photocorrelation spectroscopy; fluorescence spectroscopy (nanospecies conjugates and nanosensors); and, on whether the nanospecies visually dispersed in aqueous media.

3.1.6 Summary and Conclusions

- Initial nanospecies synthesis afforded polymers with minimal (aqueous) dispersion affinities, in poor yields (≤3%).
- Subsequent investigations concerned with particle/species size ($z_{ave.}$) generated sporadic and unexpected results.

- Dispersible particles/species only recurrently formed/produced in good yields (≥80%) when the reaction components and system were **repeatedly** and **thoroughly** evacuated of free radical scavengers.

3.2 Surface Functionalisation

The creation of the desired bifunctional sensing system requires the coupling of two individual components: the nanosensing species and the photosensitising porphyrin moiety. In order to assemble a conjugated system of this nature, the nanospecies and the porphyrin molecules must possess reactive functional groups capable of promoting the binding reaction. It was anticipated that this coupling criteria could be easily met since the functionalisation of the polyacrylamide gels and the selective functionalisation of porphyrins *via* the appropriate synthetic precursors and reactions has been well documented (see sections 1.1.4, 1.1.13 and 1.4.7). However, the question that needed to be answered was: with which functional groups would the desired coupling of the two components be accomplished?

It was discussed in Chapter 1 (see section 1.1.13) that a primary amino-bearing substrate can react efficiently and in good to excellent yields (≥60%) with an isothiocyanato-bearing porphyrin to produce a relatively stable, covalently linked (thiourea bond), conjugate of the amino-bearing substrate and the porphyrin moiety (figure 84).[113,114] This appeared to be a promising route, since the synthesis of the polyacrylamide nanospecies **6** had been optimised and it was anticipated that their synthesis could be modified further by incorporating the appropriately functionalised acrylamide monomer into the polymerisation mixture; thus, generating primary amino-bearing nanospecies. The synthesis and conjugation of an isothiocyanato porphyrin has also been documented and it was anticipated that the coupling protocol could be easily modified to take into account the use of nanospecies and not the substrates used in the original and subsequent protocols (bovine serum albumin (BSA) and monoclonal antibodies).[49,50,113] Therefore, it was decided that the above conjugation procedure would be adopted and (*via* the

synthesis of the relevant component parts) investigated as an early synthetic objective towards the desired nanospecies product (figure 84).

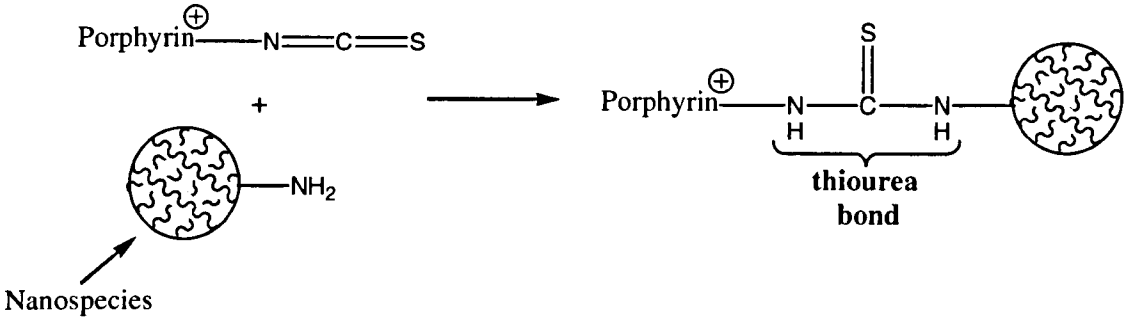

Figure 84 – Porphyrin-Nanospecies Conjugation

3.2.1 Amine Functionalised Nanospecies

It was foreseen that the co-polymerisation of an amino-bearing monomer could be used as a means of introducing the primary amino groups onto the nanospecies surface. These would, in turn, provide one half of the functional handle required for the attachment of the porphyrin moiety **5** (the second half of the "coupling handle") onto the nanospecies. The commercially available amine monomer, *N*-(3-aminopropyl)methacrylamide hydrochloride (figure 85), seemed an appropriate reagent to begin the functionalisation investigations, since it was known to introduce the desired functionality into polyacrylamide gels and would circumvent the need to chemically modify the existing acrylamide monomer.[325]

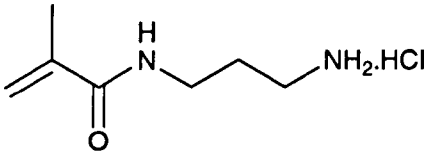

N-(3-aminopropyl)methacrylamide hydrochloride

Figure 85 – Structure of Functional Acrylamide Monomer

The reaction was briefly investigated. The functionalised monomer was co-polymerised with the acrylamide and *N,N'*-methylenebisacrylamide monomers under the same reaction conditions successfully employed in the optimised synthesis of the polyacrylamide nanospecies **6**. The total concentration of the combined monomers remained the same, only the primary monomer (acrylamide) concentration was altered (to take into account the addition of the amino-monomer). The co-polymerisation reaction proceeded smoothly to yield the desired amino-bearing nanospecies **7**, in consistently good dispersible yields (≥88%, figure 86 and table 6): comparable results to those achieved for the standard polyacrylamide nanospecies. Thus, supporting the postulation that the extended degassing of the reagents/reaction mixture with argon, is a more reproducible and reliable procedure (in the synthesis of the species) than the technique followed at the start of the Project.

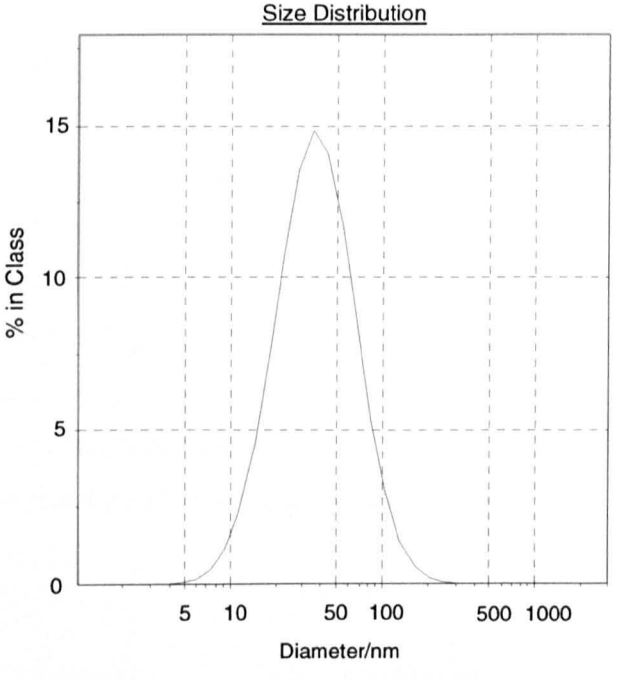

Figure 86 - PCS Spectrum of Amino-Functionalised Nanospecies **7** generated from Optimised Reaction Conditions, $z_{ave.}$ = 38 nm

MATRIX	SIZE ($z_{ave.}$/nm)	DISPERSE	YIELD/%
Polyacrylamide **6**	37	✓	≥90
Amino-Polyacrylamide **7**	38	✓	≥88

Table 6 - Comparative Table of Some of the Polyacrylamide and Functionalised-Nanospecies Features

The presence and reactivity of the primary amino groups was quickly checked through the use of the non-fluorescent reagent, fluorescamine (scheme 18). Fluorescamine allows freely available primary amino groups to be identified through optical spectroscopy and is commonly used in the assay of primary amines down to the picomolar range. Fluorescamine reacts with primary amines almost instantaneously at room temperature in aqueous media to generate highly fluorescent products ($\lambda_{ex.}$ ~365 nm and $\lambda_{em.}$ ~475 nm); unlike, the reagent and its degradation products which are non-fluorescent. Studies have suggested that the fluorescamine-primary amino reaction goes to near completion (~80-95%), even when the non-fluorescent reagent is not present in large excess.[326,327]

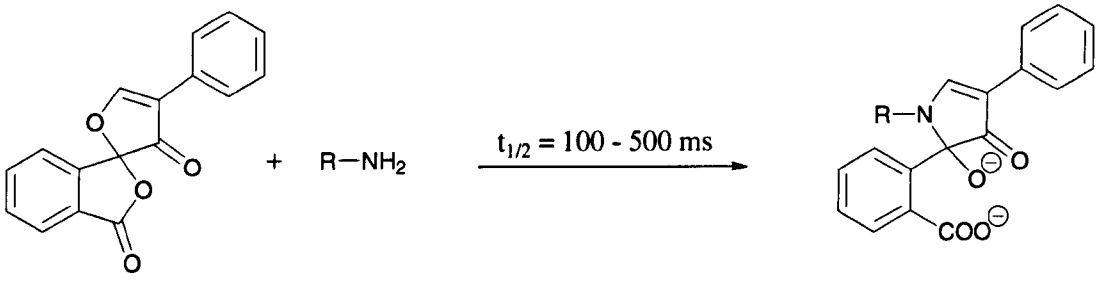

Non-Fluorescent Fluorescent

Scheme 18 – Reaction of Fluorescamine and Primary Amines

The assay requires the amino-bearing nanospecies to be buffered to an appropriate pH (≥7); depending on the nature of the amino species. Peptides have been found to present a greater fluorescence intensity near pH 7, whereas amino acids have a maximum fluorescence intensity around pH 9 (table 7).[326,327]

AMINE SPECIES	pH 7	pH 9
Peptides	Maximum Fluorescence	Minimum Fluorescence
Amino Acids	Minimum Fluorescence	Maximum Fluorescence

Table 7 – Table of Relative Fluorescence Intensities of Two Primary Amine Species at Different pH Values

Once a few milligrams (≤2 mg) of the amino-nanospecies **7** had been buffered (~pH 9), a small aliquot of the fluorescamine reagent was added to the dispersion and the resulting sample exposed to a standard ultra-violet light source ($\lambda_{ex.}$ ~365 nm). The resulting fluorescence intensity of the sample is proportional to the concentration of the primary amines.[326,327]

A range of control solutions/dispersions were prepared to allow the direct identification of the primary amino groups on the amino-nanospecies **7** (table 8). The dispersion containing the amino-nanospecies and fluorescamine was the only sample to fluoresce upon illumination. These results suggested the definite presence of free primary amino groups on the amino-functionalised nanospecies **7**.

SAMPLE	FLUORESCENT
Buffer	x
Fluorescamine	x
Buffer + Fluorescamine	x
Buffer + Fluorescamine + Amino-Nanospecies 7	✓
Buffer + Fluorescamine + Polyacrylamide Nanospecies **6**	x
Buffer + Amino-Nanospecies **7**	x
Buffer + Polyacrylamide Nanospecies **6**	x
Glass Sample Tube	x

Table 8 – Fluorescamine-Primary Amine Tests

Regrettably, this simple assay does not confirm the location of the amino groups. Consequently, it was decided a coupling reaction involving the nanospecies should be attempted to ensure that freely accessible primary amino groups were present on the nanospecies surface. A model conjugation reaction between the amino nanospecies **7** and a commercial isothiocyanate fluorophore (see section 3.3) was performed. The presence of the amino groups was clearly confirmed by optical spectroscopy (figure 87).

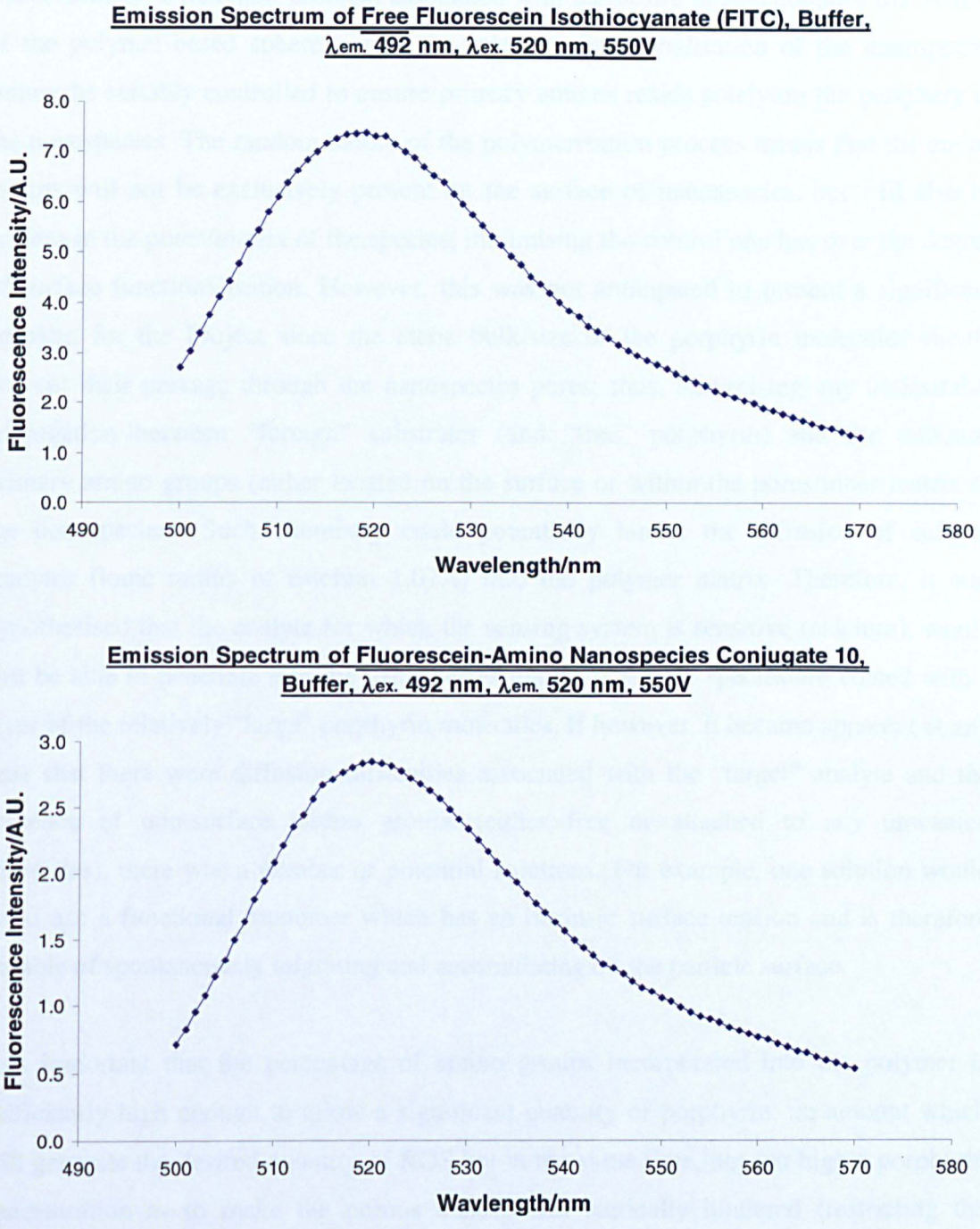

Figure 87 – Emission Spectra of Free FITC (2.5 mmol dm^{-3} Solution) and Fluorescein-Amino-Nanospecies Conjugate **10**

Unfortunately, a potential problem associated with the desire to functionalise the surface of the polymer-based sphere exists: the selective functionalisation of the nanospecies cannot be suitably controlled to ensure primary amines reside solely on the periphery of the nanospecies. The random nature of the polymerisation process means that the amino groups will not be exclusively present on the surface of nanospecies, but will also be present in the pores/matrix of the species; minimising the control one has over the degree of surface functionalisation. However, this was not anticipated to present a significant problem for the Project since the steric bulk/size of the porphyrin molecules should prevent their passage through the nanospecies pores; thus, minimising any undesirable conjugation between "foreign" substrates (and "free" porphyrin) and the unbound primary amino groups (either located on the surface or within the pores/inner matrix of the nanospecies). Such chemistry could potentially hinder the diffusion of cellular analytes (ionic radius of calcium 1.07Å) into the polymer matrix. Therefore, it was hypothesised that the analyte for which the sensing system is sensitive (calcium), would still be able to penetrate into the nanospecies matrix when the species are coated with a layer of the relatively "large" porphyrin molecules. If however, it became apparent at any time that there were diffusion difficulties associated with the "target" analyte and the presence of non-surface amino groups (either free or attached to any unwanted substrates), there was a number of potential solutions. For example, one solution would be to use a functional monomer which has an intrinsic surface tension and is therefore capable of spontaneously migrating and accumulating on the particle surface.

It is important that the percentage of amino groups incorporated into the polymer is sufficiently high enough to allow a significant quantity of porphyrin: an amount which will generate the desired quantity of ROS but at the same time, not too high a porphyrin concentration as to make the porous nanospecies sterically hindered (restricting the diffusion of the free analyte (calcium ions) into the nanospecies matrix), to be bound to the nanospecies. Too few accessible primary amino groups on the other hand, may mean that not enough porphyrin is loaded onto the nanospecies to elicit the desired effect, *i.e.* a fine balance should be sought for the target system **14** whereby, there is enough porphyrin present to initiate a change in the intracellular homeostasis of the cell, but not too much porphyrin that the cell rapidly begins the grave pathway towards cell death.

3.2.1.1 Degree of Functionalisation

The degree of the amino groups incorporated within the nanospecies can be varied by altering the relative concentration of the amino monomer in the polymerisation mixture. This route was briefly investigated and proved seemingly efficient in the generation of dispersible amino nanospecies **7** (in good yields).

The molar ratios of the amino-functionalised monomer initially chosen were $1:^{1}/_{23}$ (~0.3 mmol), $1:^{1}/_{46}$ (~0.15 mmol) and $1:^{1}/_{92}$ (~0.08 mmol). All three of the ratios generated species which were dispersible in aqueous media and in good to excellent yields (59 – 90%, table 9).

RATIO OF AMINO MONOMER	DISPERSE	YIELD/%
$1:^{1}/_{23}$	✓	≤59
$1:^{1}/_{46}$	✓	≤70
$1:^{1}/_{92}$	✓	**≥90 (optimised conditions)**

Table 9 - Varying the Degree of Polymer Functionalisation

Summary and Conclusions

- Preliminary attempts at generating amino-functionalised nanospecies **7** proved successful, supporting hypotheses that: (i) thorough gaseous evacuation of free radical scavengers is **vital** in the success of the reaction; and (ii) that the optimised polymerisation reaction is easily modified to afford primary amino groups in the final polymer matrix.
- Degree of functionalisation readily varied by altering the ratio of functionalised monomer present in the aqueous-monomer phase.
- Identity and presence of the primary amino groups confirmed *via* fluorescamine.

The facile and flexible synthesis of the amino nanospecies was particularly encouraging and represented a critically important landmark towards the formation of the target nanosystem **14**.

3.3 Fluorescein Isothiocyanate Conjugation

Having successfully synthesised the dispersible amino-functionalised nanospecies **7**, it was decided that the "reactivity" of the amine functional groups should be evaluated through model binding studies with a commercially available isothiocyanato functionalised fluorophore. This would allow the presence of primary amine groups and the reactivity of the amino-functionalised nanospecies **7** (towards the isothiocyanato group) to be assessed (along with the suitability of the nanospecies for the required coupling reaction). Initial coupling reactions were attempted with the commercial fluorophore fluorescein isothiocyanate (FITC) and amino nanospecies **7**.

It appeared desirable to investigate and optimise a model coupling reaction given the lengthy and poor yielding (acetamido porphyrin ~4%, see section 6.2) synthesis of the isothiocyanato functionalised porphyrin **5**, relative to the nanospecies. Fluorescein isothiocyanate was chosen since it has a high fluorescence quantum yield ($\Phi_{fl.}$ = 0.93); is

readily soluble in aqueous media above pH 6; and most importantly, has been widely used in the labeling of number of substrates, including proteins.[329] The coupling reaction between FITC and the nanospecies proceeded with relative ease to yield the desired product **10** (figure 88); clearly confirmed by optical spectroscopy (figure 87). To ensure that the FITC molecules were binding to the amino groups and that there was no non-covalent binding (NCB), a control conjugation reaction was performed employing the amino-free nanospecies **6**.

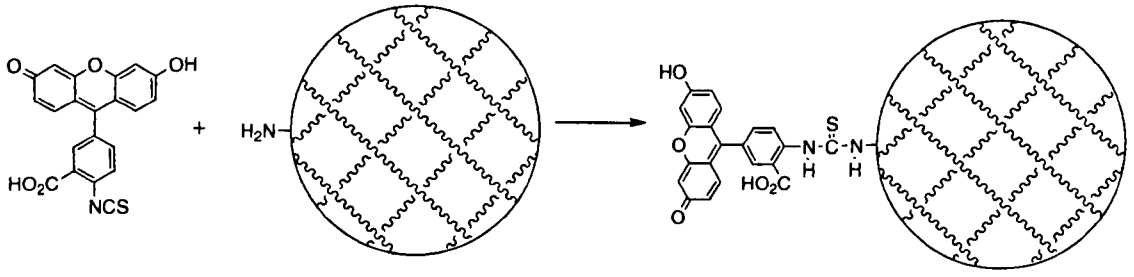

Figure 88 – Simplified FITC Amino-Nanospecies Conjugation Reaction

The attachment protocol chosen was based on a standard procedure routinely used to attach amine reactive compounds to substrates such as antibodies.[330] When the protocol had been optimised for the model system, it was anticipated it could be transferred and, if necessary, modified accordingly for the attachment of the isothiocyanato porphyrin **5** to the amino-nanospecies **7**. Model conjugations (of the amino nanospecies **7**) were attempted prior to investigations regarding the encapsulation of the analyte-sensitive dye; this was to ensure that attachment of the target porphyrin molecules **5** to the nanospecies **7** was viable.

Briefly, aliquots of the amino nanospecies **7** and FITC were individually dispersed/dissolved in a sodium bicarbonate buffer (pH ~9). In order to maintain the primary amino groups of the nanospecies in a non-protonated (reactive form), it is necessary to carry out the coupling reaction in a slightly basic medium (that itself is free from any primary amines). A sodium bicarbonate buffer (pH 9) is therefore recommended for isothiocyanate-amine conjugations. It is also suggested that the success

of the coupling reaction is highly concentration dependent and it is recommended that an amino species concentration of below 2mg/ml will greatly reduce the efficiency of the reaction.[331] The number and position of the primary amines on the periphery of the nanospecies can vary; therefore, it is desirable to investigate several different degrees of labeling, in parallel, using different molar ratios of the amino nanospecies **7** to the FITC dye. With this information in mind, a range of aliquots (table 10) of each of the dispersions/solutions were combined and mixed at room temperature for one hour (protected from sources of light).

AMINO-NANOSPECIES DISPERSION (5mg/ml)/ml	**FITC SOLUTION (1mg/ml)/μl**	**CONJUGATE FORMED**
0.2	12.5	✓
0.2	25.0	✓
0.2	50	✓
0.2	100	✓
0.2	500	✓

Table 10 – Example Nanospecies-FITC Conjugation Ratios

The corresponding conjugated moiety was then recovered by microfiltration and excess FITC removed through washing. The resulting fluorescent conjugates were generated in good yields (≤29 mg). The filtrate was periodically checked *via* fluorescence spectroscopy to ensure all un-bound FITC had been removed from the system (a detailed description of the full procedure is given in section 6.3). The reaction product **10** was then re-dispersed in buffer and analysed *via* fluorescence spectroscopy for the

characteristic FITC excitation ($\lambda_{ex.}$ 492 nm) and emission bands ($\lambda_{em.}$ 520 nm). The spectral data observed (figure 87) suggested that the coupling reactions were successful and that the attachment of the isothiocyanato fluorophore to the amino nanospecies had indeed, been accomplished: a propitious finding for the Project.

It appeared that all three of the amino molar ratios ($1:^1/_{23}$, $1:^1/_{46}$, $1:^1/_{92}$) used allowed significant amounts of the fluorophore (FITC) to be attached to the nanospecies. In addition, the lowest of the three molar ratios ($1:^1/_{92}$) still permitted the attachment of readily identifiable quantities of the FITC fluorophore. These preliminary results were promising since the aim of the desired porphyrin-nanosensing system **14** was to perturb the calcium homeostasis within the cell and **not** to generate such amounts of ROS as to initiate cell death. The lower of these functionalised monomer ratios ($1:^1/_{92}$) was chosen as the one to be used for all further investigations.

To ensure that the fluorophore present in the coupling product was a result of a covalent link between the FITC molecules and the primary amines of the nanospecies, a parallel experiment was run with nanospecies **6** (no primary amino groups) and FITC (figure 89). The resulting nanospecies were analysed (fluorescence spectroscopy) and appeared to be free of any fluorophore molecules (absence of $\lambda_{em.}$ 520 nm (FITC), figure 90); suggesting that FITC **does not** non-covalently bind with the nanospecies, and if this did occur, then none remained once the nanospecies had been thoroughly washed.

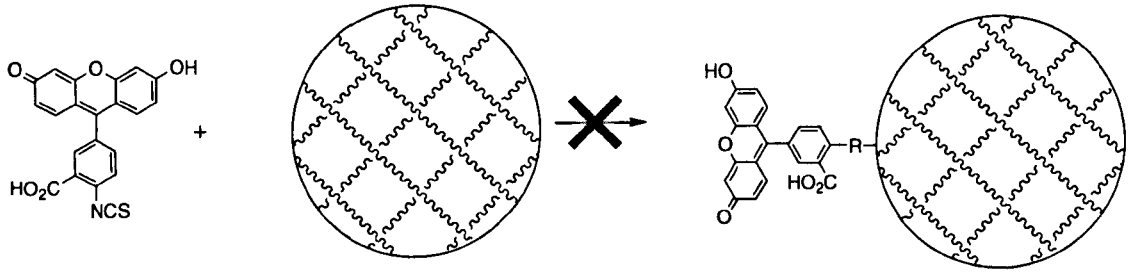

Figure 89 – "Coupling Experiment" with FITC and Polyacrylamide Nanospecies **6**

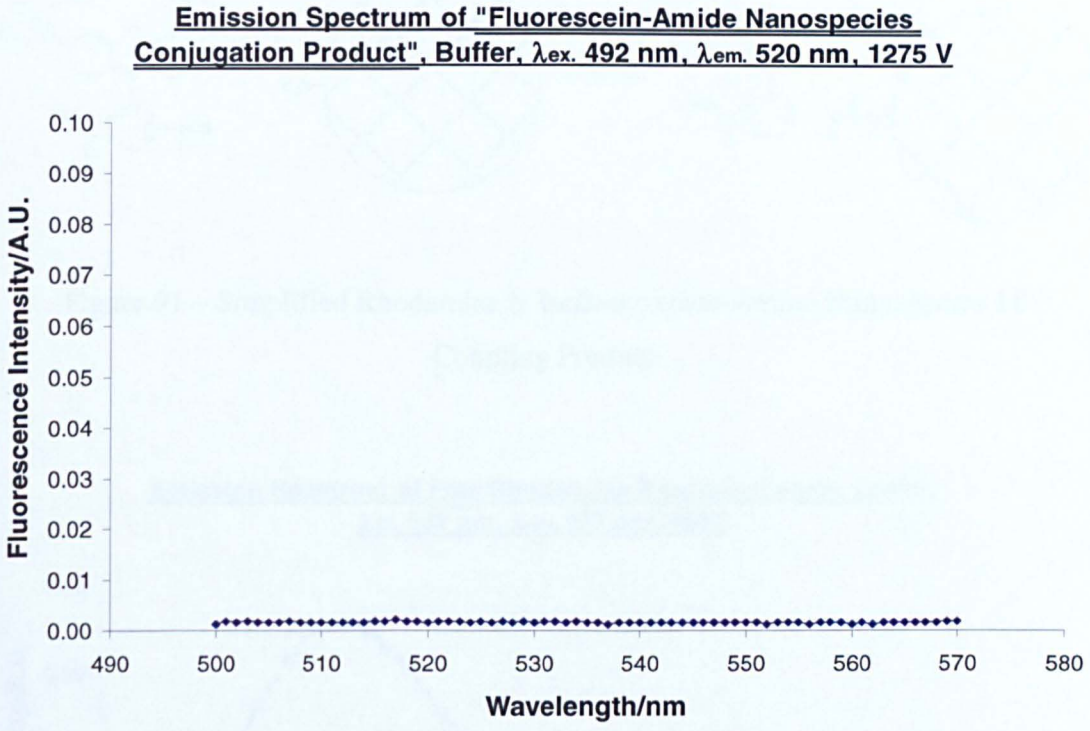

Figure 90 – Emission Spectrum Demonstrating the Absence of a Fluorescein Isothiocyanate Emission Band ($\lambda_{em.}$ 520 nm)

The loading ratio for the FITC fluorophore onto the amino-nanospecies **7** ($1:^{1}/_{92}$) (*via* the above protocol) was determined by fluorescence spectroscopy to be 4.4 mmol/mg, *i.e.* there are 4.4 mmol of FITC coated onto every milligram of FITC-nanospecies conjugate.

Similar success was also achieved using an alternative isothiocyanate bearing fluorophore, rhodamine B isothiocyanate (figures 91 and 92).

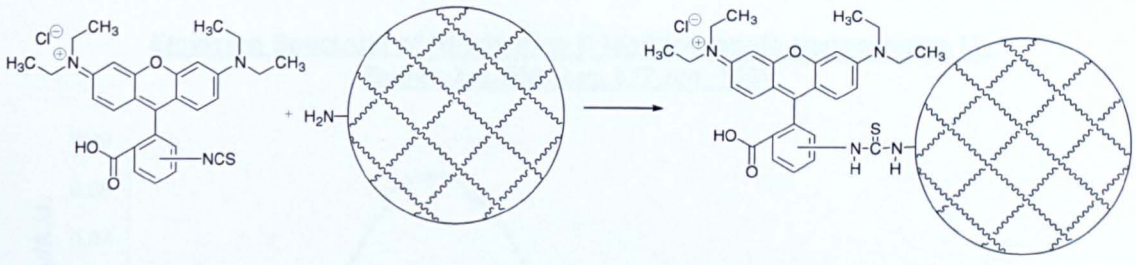

Figure 91 – Simplified Rhodamine B Isothiocyanate-Amino Nanospecies **11** Coupling Product

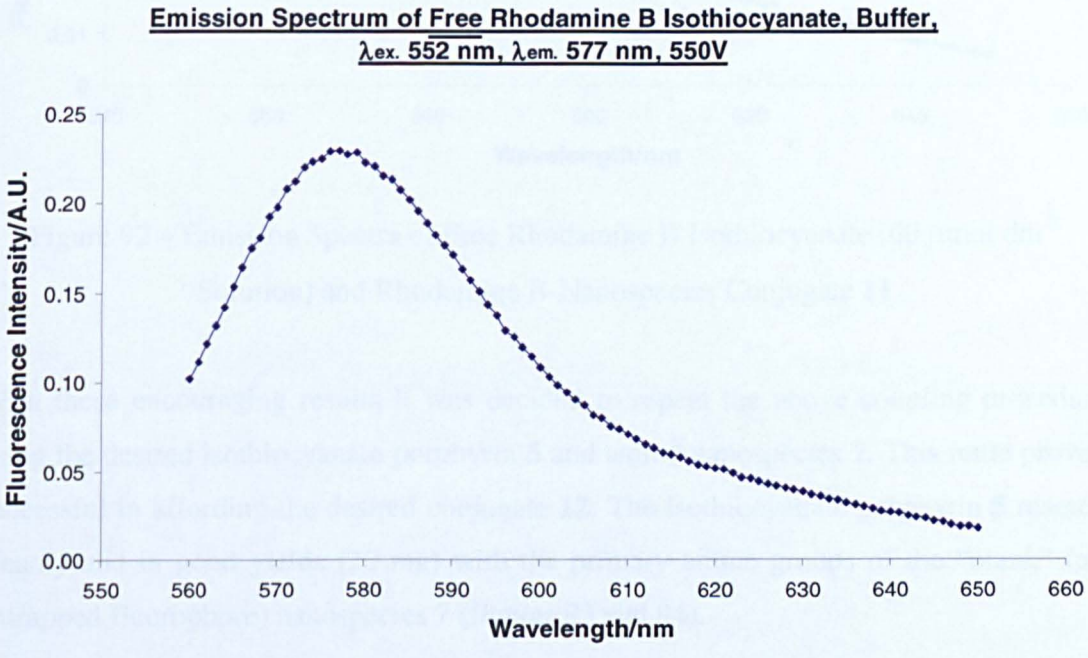

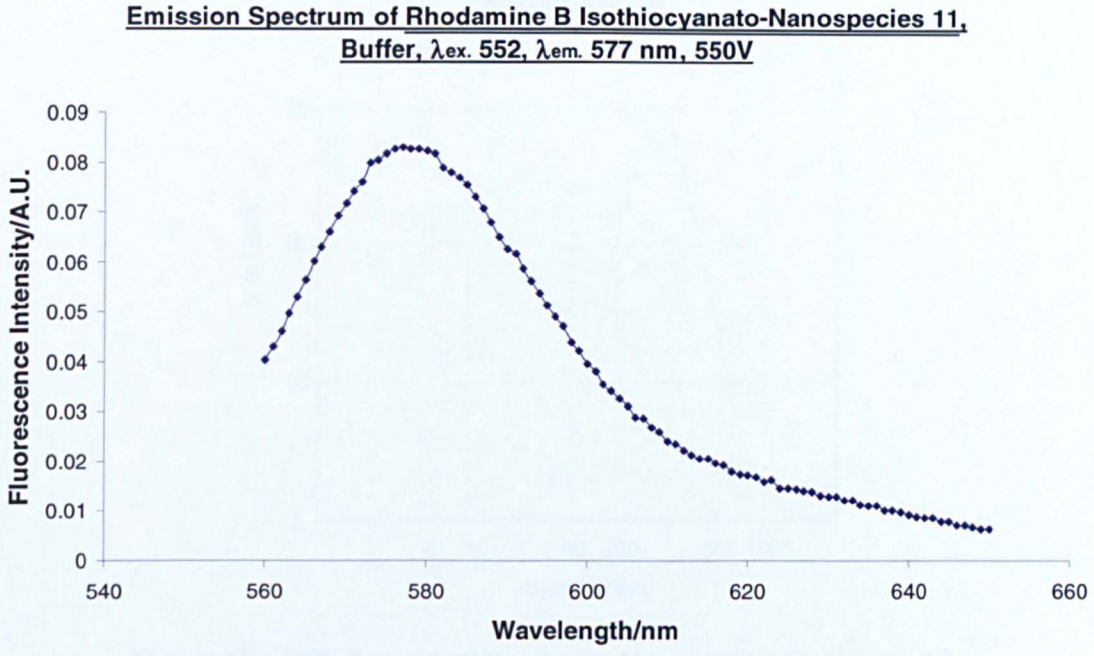

Figure 92 – Emission Spectra of Free Rhodamine B Isothiocyanate (60 μmol dm^{-3} Solution) and Rhodamine B-Nanospecies Conjugate **11**

With these encouraging results it was decided to repeat the above coupling procedure using the desired isothiocyanato porphyrin **5** and amino nanospecies **7**. This route proved successful in affording the desired conjugate **12**. The isothiocyanato porphyrin **5** reacted cleanly and in good yields (20 mg) with the primary amine groups of the "blank" (no entrapped fluorophore) nanospecies **7** (figures 93 and 94).

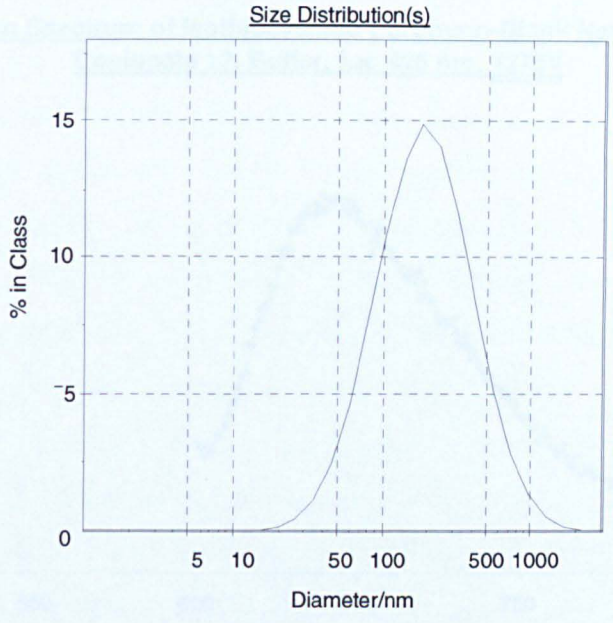

Figure 93 – PCS Spectra of Porphyrin-Nanospecies Conjugate **12**, $z_{ave.}$ 195.6 nm

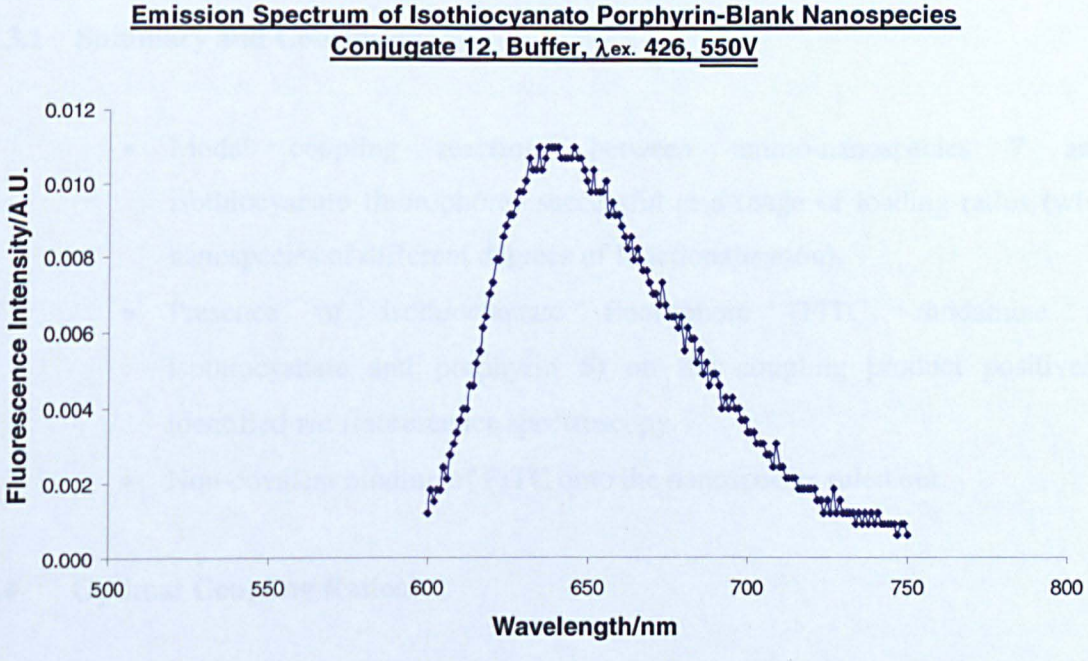

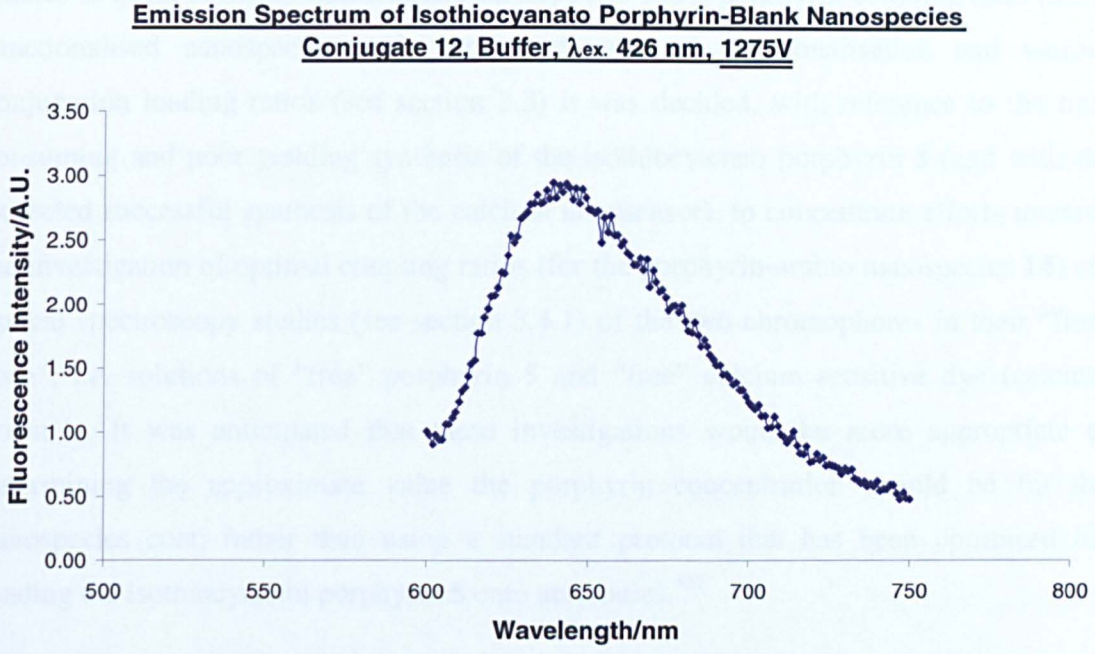

Figure 94– Emission Spectra of Porphyrin-Blank Nanospecies Conjugates **12** (Different Sensitivities)

3.3.1 Summary and Conclusions

- Model coupling reactions between amino-nanospecies **7** and isothiocyanato fluorophores successful at a range of loading ratios (with nanospecies of different degrees of functionalisation).
- Presence of isothiocyanato fluorophore (FITC, rhodamine B isothiocyanate and porphyrin **5**) on the coupling product positively identified *via* fluorescence spectroscopy.
- Non-covalent binding of FITC onto the nanospecies ruled out.

3.4 Optimal Coupling Ratios

Although, the amino species were successfully conjugated to the desired FITC moiety to afford the fluorescein-nanospecies conjugate **10** (see section 3.3); there remained a problem in determining the optimal FITC-coating ratios for the species. After extensive

studies in quest of the optimum amino-nanospecies-FITC/porphyrin coupling ratio (using functionalised nanospecies with varying degrees of functionalisation and various conjugation loading ratios (see section 3.3) it was decided, with reference to the time consuming and poor yielding synthesis of the isothiocyanato porphyrin **5** (and with the expected successful synthesis of the calcium nanosensor), to concentrate efforts towards the investigation of optimal coupling ratios (for the porphyrin-amino nanospecies **14**) *via* optical spectroscopy studies (see section 3.4.1) of the two chromophores in their "free-state", *i.e.* solutions of "free" porphyrin **5** and "free" calcium sensitive dye (calcium green-1). It was anticipated that these investigations would be more appropriate at determining the approximate value the porphyrin concentration should be for the nanospecies coat; rather than using a standard protocol that has been optimised for loading the isothiocyanato porphyrin **5** onto antibodies.[332]

3.4.1 Spectroscopic Investigation (Solution Experiments)

After extensive investigations in the identification of an ideal coupling ratio (varying the ratio of amino monomer in the acrylamide solution and various porphyrin coating-ratios in the coupling reactions) had proven unsuccessful, it was decided that in order to have a good grasp of the "ideal" coating concentration, *i.e.* one which coats the nanospecies with the desired degree of porphyrin **5** and allows both the chromophore individual emission peaks to be observed at almost equal fluorescence intensities, investigations should be moved one step backwards. Both chromophores would be assessed (i) in their free-states and (ii) in the absence of any nanospecies, with the ultimate aim of transferring the spectroscopic results to a conjugated system of porphyrin **5** and nanospecies **13**: the target system **14** to be initially trialed in cellular investigations.

The investigation involved preparing stock solutions at equimolar concentrations of both the activated porphyrin **5** and the calcium green dye. Aliquots of the stock solutions were then added to a fluorescence cuvette, agitated for 30 seconds (1,800 rpm) and the emission spectrum of the resulting solution analysed. Full details of the spectroscopic-solution experiments can be found in Chapter 6 (see section 6.4).

In essence, solutions ranging from 1:1, 2:1, 10:1, 100:1 (porphyrin:calcium green) and 1:2, 1:10 and 1:100 (porphyrin:calcium green), were investigated at the various excitation wavelengths. As a result of the porphyrin **5** and calcium green fluorophores both having different absorption profiles (and therefore different optimal excitation wavelengths), it was important to investigate potential wavelength(s) ideal for mutually exciting both chromophores in the solution (without significantly altering their emission profiles). A range of excitation wavelengths were chosen from those present on the individual chromophore's absorption spectra ($\lambda_{ex.}$ 327, 426 (optimal porphyrin $\lambda_{ex.}$), 488, 493 and 505 (optimal calcium green $\lambda_{ex.}$). It was found that wavelengths 488, 493 and 505 nm mutually excited the two chromophores and generated approximately equal intensity emission peaks in a 100:1 solution of the porphyrin and calcium green dye (figure 95). However, bearing in mind that the nanosensing system **14** is designed to image cellular response(s) to ROS and was anticipated to be transferred to a range of cell lines, the wavelength chosen to sub-optimally excite the porphyrin-calcium green solution was 488nm; conveniently, one of the lasing lines of the argon ion laser used in the confocal microscope (see section 1.1.11).

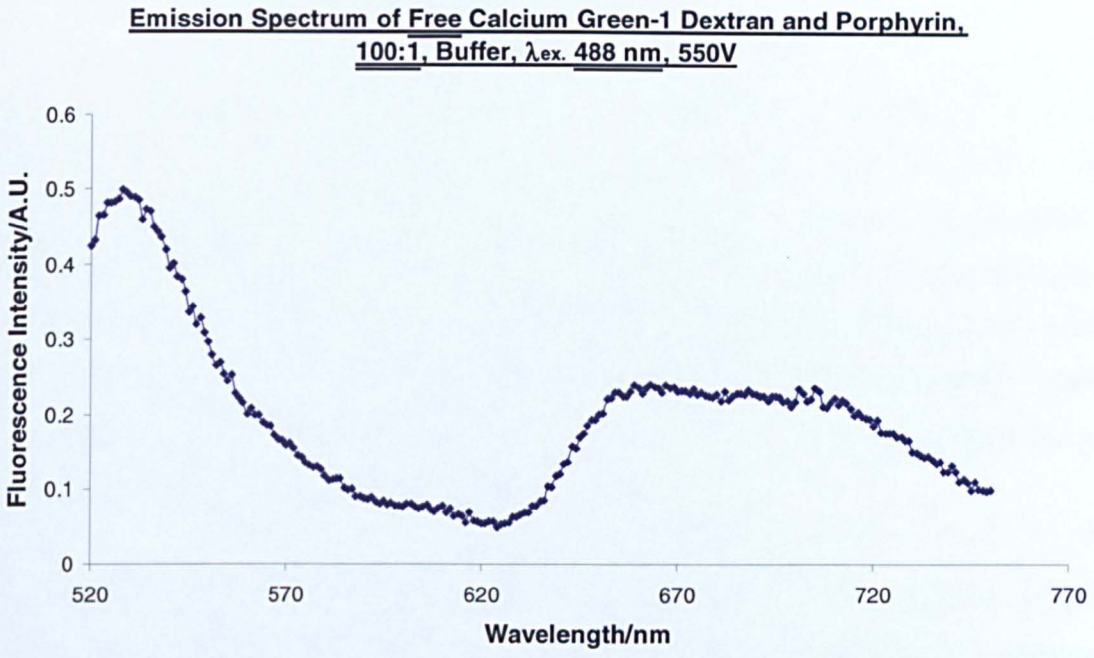

Figure 95 - Luminescence Profile of Free Calcium Green and Free Porphyrin **5**
(Calcium Green and Porphyrin Solutions 37.2 nmol dm^{-3}
and 3.98 nmol dm^{-3} Respectively)

3.4.2 Summary and Conclusions

- At a ratio of 100:1 (porphyrin to calcium green) the two system chromophores are conveniently excited at a mutual sub-optimal wavelength (488 nm).
- Characteristic emission profiles (of porphyrin and calcium green) observed at similar fluorescence intensities.

Having already optimised a methodology which could be used to attach an external fluorescent component to a suitably activated nanospecies, and investigated the optimal loading ratio for the porphyrin-nanosensor coupling reaction, attention was focused onto the entrapment of the required analyte-sensitive fluorophore into the nanospecies matrix.

3.5 Encapsulation – Nanosensor Synthesis

A calcium sensitive system was sought since it is widely believed that ROS, particularly singlet oxygen ($^1O_2$), are directly involved in the instigation of a number of disease states. It is during these processes that fluctuations in the intracellular levels of a major signaling species, calcium, are believed to exist (see section 1.3). Elevated levels of ROS/calcium are especially thought to be implicated in the previously mentioned neurodegenerative diseases, along with certain diseases of the heart (see section 1.3). Unfortunately, current bio-analytical tools are extremely limited with regards to studying ROS-induced fluctuations in the levels of intracellular calcium.

Before attempting the encapsulation of the valuable commercial fluorophore (calcium green), it was decided to undertake the encapsulation procedure using a substrate-sensitive fluorescent dye which was available in the laboratory; a disulphonated ruthenium chloride dye (disulphonated 4,7-diphenyl-1,10-phenanthroline ruthenium(II) chloride) sensitive to molecular oxygen ($^3O_2$). The dye is able to act as an indirect sensor of oxygen, since in the presence of the glucose enzyme, glucose oxidase, and glucose (scheme 19), the fluorescence of the dye is quenched by molecular oxygen.

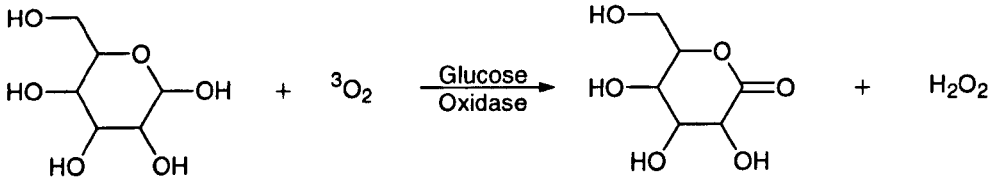

Glucose Gluconolactone

Scheme 19 – The Reaction of Glucose, Oxygen and Glucose Oxidase

The glucose oxidase enzyme is known to oxidise glucose and hence, indirectly decrease the concentration of triplet oxygen present in the sample solution, *i.e.* the fluorescence intensity of the light emitted from the ruthenium dye increases in relation to a decrease in oxygen concentration (figure 96).[333-335]

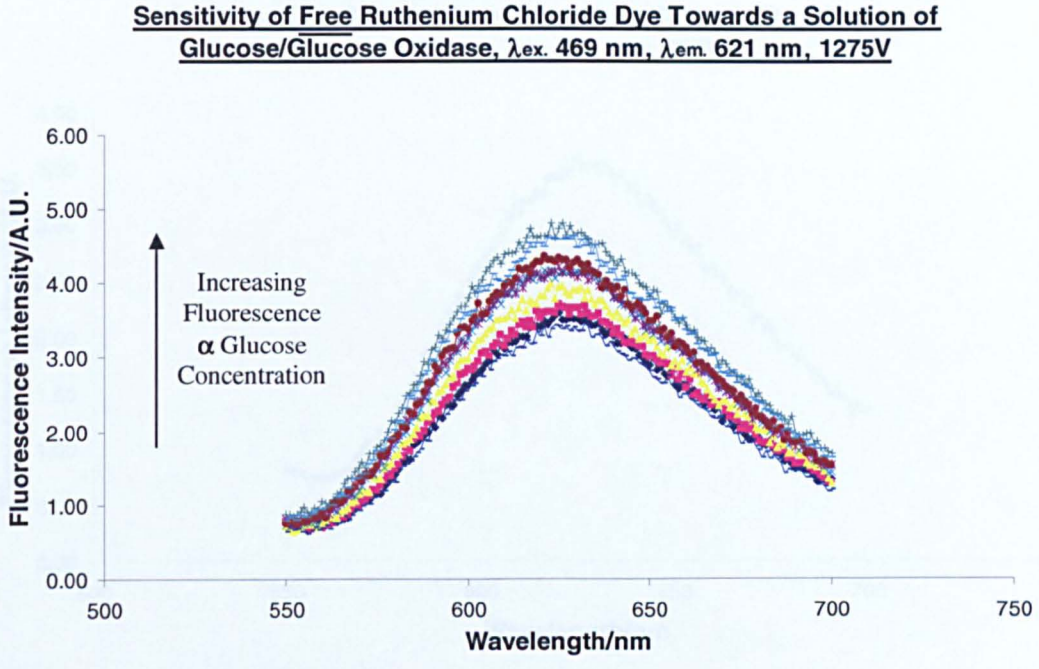

Figure 96 – Sensitivity of Free Ruthenium Chloride Dye (2.4 mmol dm^{-3} Solution) towards Glucose/Glucose Oxidase

The dye was successfully encapsulated into the amine-functionalised nanospecies **9** (figure 97) using the same standard protocol as described for the synthesis of the polyacrylamide based nanospecies **6** and **7** (with the exception of the composition of the aqueous phase).

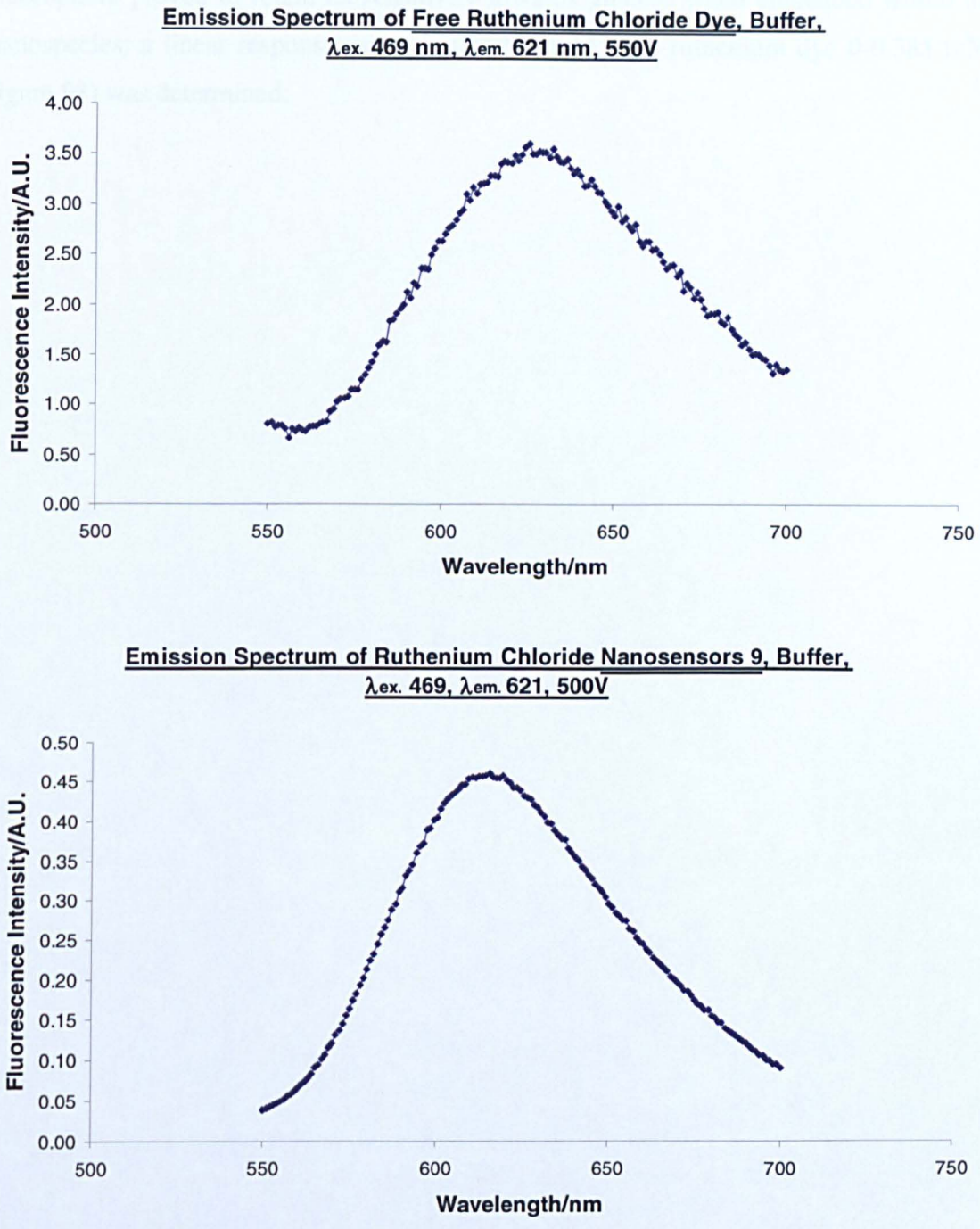

Figure 97 – Emission Spectra of Free Ruthenium Chloride Dye (2.4 mmol dm^{-3} Solution) and Ruthenium Nanosensors **9**

The sensors were briefly analysed *via* fluorescence spectroscopy to assess the effect of the synthetic process on the sensing properties of the dye (see section 6.3). The

fluorophore proved to retain its sensitivity towards glucose when embedded within the nanospecies; a linear response range of 0-0.291 mM (free ruthenium dye 0-0.385 mM, figure 98) was determined.

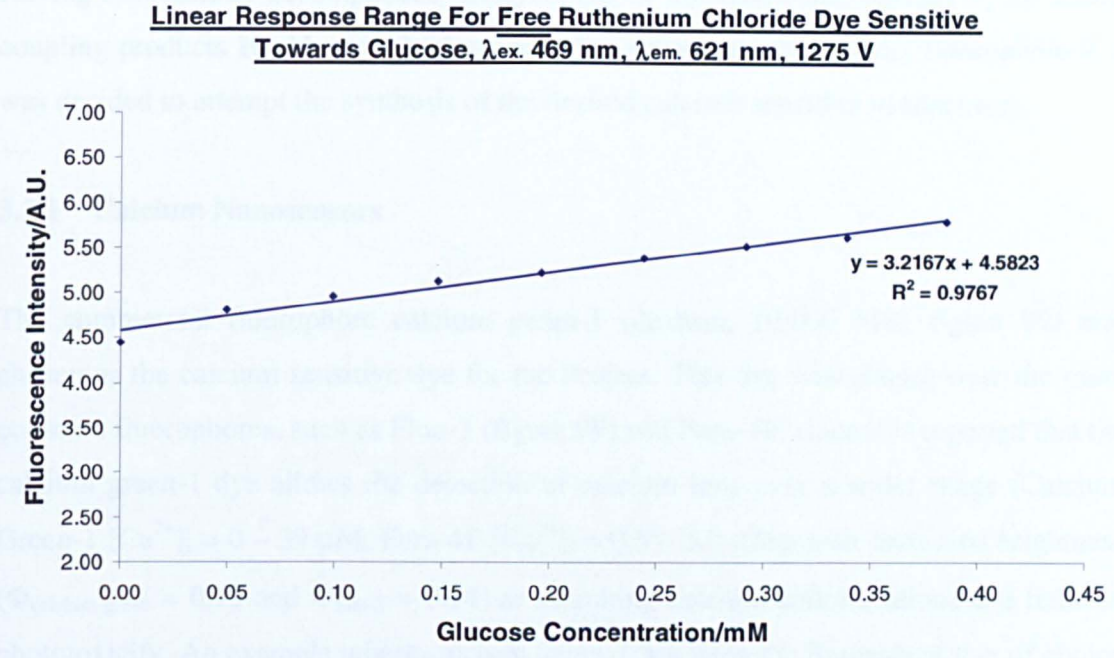

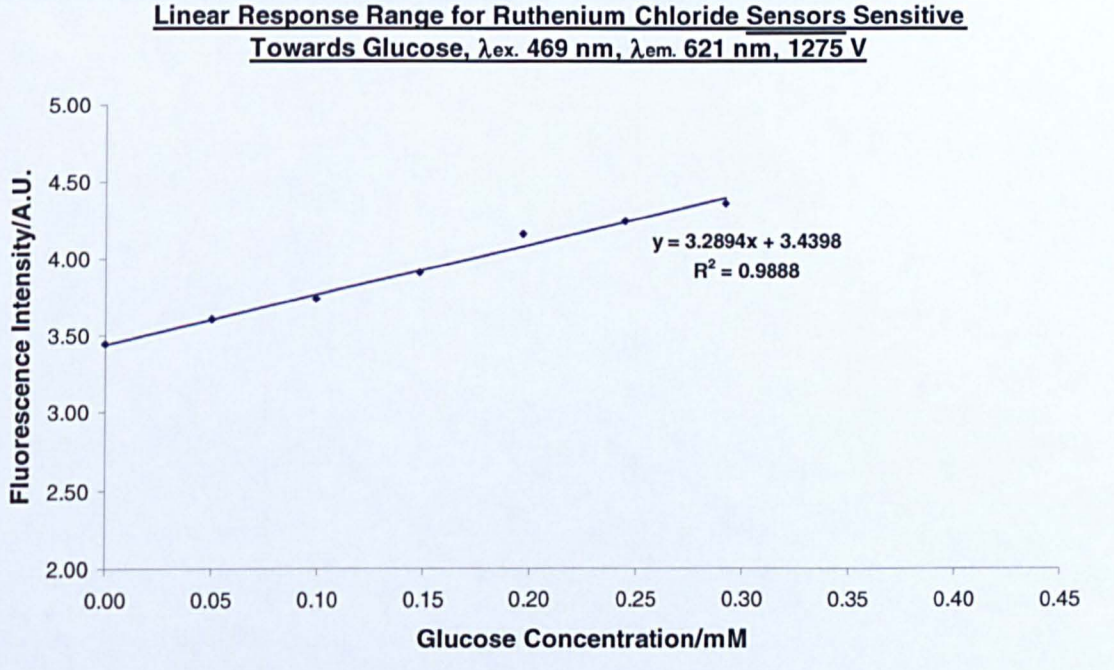

Figure 98 – Linear Response Range of Free Ruthenium Chloride Dye (2.4 mmol dm^{-3} Solution) and Ruthenium Chloride Nanosensors **9** Sensitive towards Glucose/Glucose Oxidase

Having successfully accomplished the synthesis of the amino-nanospecies **7**; the model coupling products **10**, **11** and **12**; along with the entrapment of a model fluorophore **9**, it was decided to attempt the synthesis of the desired calcium sensitive nanosensors.

3.5.1 Calcium Nanosensors

The commercial fluorophore calcium green-1 (dextran, 10,000 Mw, figure 99) was chosen as the calcium sensitive dye for the Project. This dye was chosen over the more common fluorophores, such as Fluo-3 (figure 99) and Fura-4F, since it is reported that the calcium green-1 dye allows the detection of calcium ions over a wider range (Calcium Green-1 $[Ca^{2+}]_i = 0 - 39$ μM, Fura-4F $[Ca^{2+}]_i = 0.5 - 5.0$ μM), with increased brightness ($\Phi_{\text{calcium green}} = 0.75$ and $\Phi_{\text{fluo-3}} = 0.14$) at saturating calcium concentrations and reduced phototoxicity. An example where calcium green-1 has been the fluorescent dye of choice is in the observation of calcium dynamics in brain slice preparations.[336]

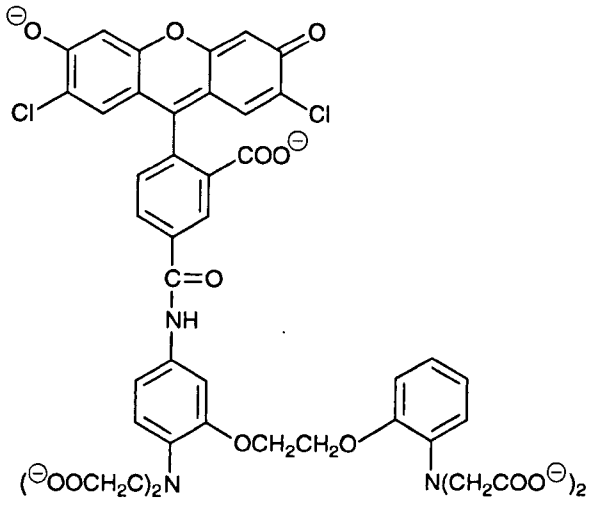

Calcium Green-1

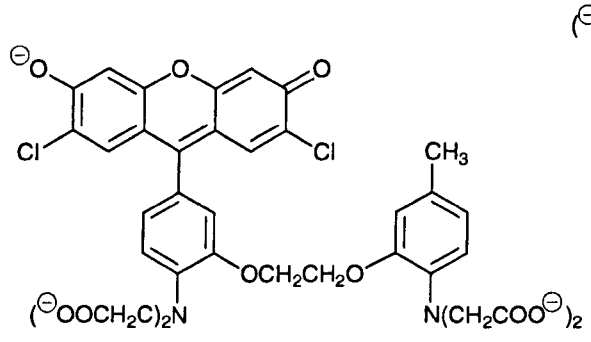

Fluo-3

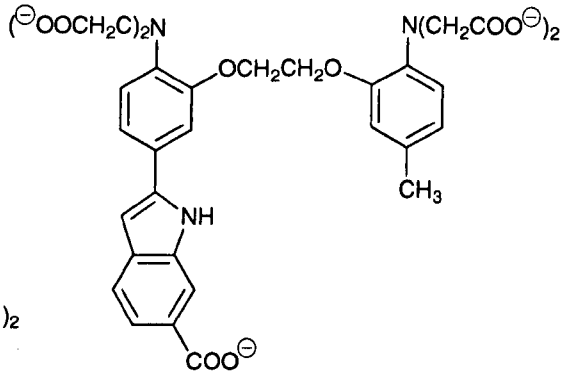

Indo-1

Figure 99 – Structures of Calcium Green-1, Fluo-3 and Indo-1 Fluorophores

Calcium green is excited by visible light as opposed to the dyes Fura-2 and Indo-1 (figure 99), which are UV-excitable. Excitation with visible light is more desirable since it is less damaging to the cell and minimises autofluorescence; a problem which increases at shorter wavelengths. Calcium green-1 also presents a greater affinity (K_d) for free calcium ions (K_d = 190 nM), over fluo-3 or calcium green-2 (K_d = 390 nM and K_d = 550 nM respectively).[337]

It is worthy of mentioning at this point that the dissociation constants for intracellular calcium indicators are different to the corresponding values determined in cell-free

solutions (table 11): a result of the many variables between the two systems including, pH, temperature, ionic strength and the presence of additional ions, such as magnesium.

FLUOROPHORE	K_d *IN VITRO* (nM)	K_d *IN SITU* (nM)	CELL/TISSUE TYPE
Calcium Green -1	**190**	**930**	**HeLa Cells**
Fluo-3	390	2570	Skeletal Muscle
Indo-1	230	844	Cardiac Myocyte

Table 11 – Table of Dissociation Constants for a Selection of Analyte-Sensitive Fluorophores[337]

The calcium green-1 fluorophore is also available in a range of molecular weight dextran conjugates which should, in theory, enhance the retention of the fluorophore within the nanospecies matrix.

3.5.1.1 Calcium Nanosensor Synthesis

The calcium-sensitive dye was encapsulated successfully into the functionalised acrylamide nanospecies following the same reaction protocol as applied to the nanospecies/sensors described earlier (see section 3.1 and 3.5). The stock fluorophore was pre-aliquoted (20 µl x 0.4587 mmol dm^{-3}) and frozen under argon in order to minimise decomposition of the fluorophore and preserve its sensitivity. The dispersible pink calcium-sensitive nanospecies/sensors **13** were repeatedly generated in yields in excess of 80 % (figures 100 and 101 and table 12).

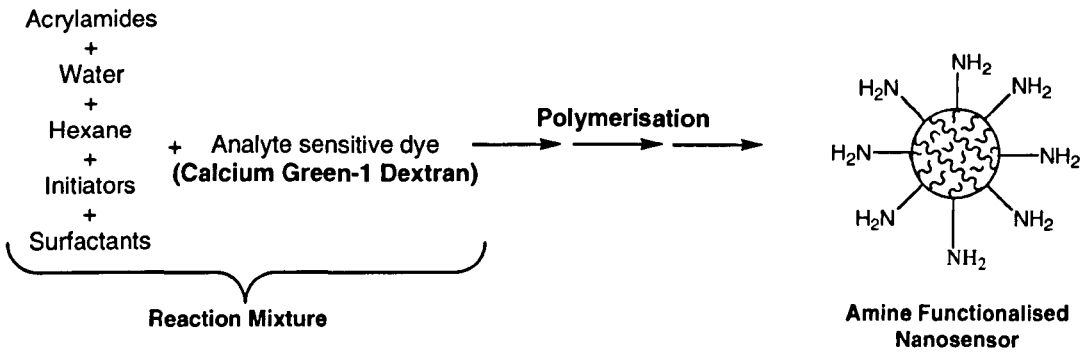

Figure 100 – Synthesis of Calcium Sensitive Nanosensors

NANOSPECIES	SIZE ($z_{ave.}$)/nm	DISPERSE	YIELD/%
Polyacrylamide **6**	37	✓	≥90
Amine-Functionalised Polyacrylamide **7**	38	✓	≥88
Calcium Sensitive Amino-Polyacrylamide **13**	44	✓	≥80

Table 12 – Comparative Size ($z_{ave.}$/nm) and Percentage Yields of the Three Polyacrylamide Type Nanospecies Synthesised

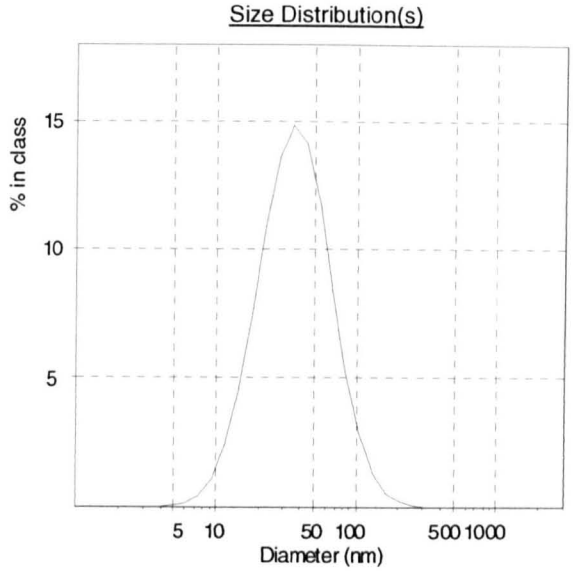

Figure 101 – PCS Spectrum of Calcium Sensitive Nanosensors **13** ($z_{ave.}$ = 44 nm), generated from Optimised Reaction Conditions

To ensure that the polymerisation process did not have a detrimental effect on the calcium green fluorophore, the newly generated nanosensors **13** were analysed *via* fluorescence spectroscopy. The data obtained was then compared to that of the fluorescent dye in its free state, *i.e.* a solution containing only the fluorophore (figures 102 and 103). It was already known, from the optical investigations undertaken (see section 3.4.1 and 6.3), that when the free dye is excited at its optimal ($\lambda_{ex.}$ 505 nm) and sub-optimal ($\lambda_{ex.}$ 488 nm) excitation wavelengths, it has a single emission peak with a $\lambda_{max.}$ of 532 nm (figure 102). Figures 102 and 103 also show that the fluorescence spectrum of the encapsulated fluorescent dye is identical to that of the free dye. This suggests that not only has the dye been successfully embedded into the nanospecies matrix but that its optical properties have not been affected, to any significant degree, by the polymerisation process.

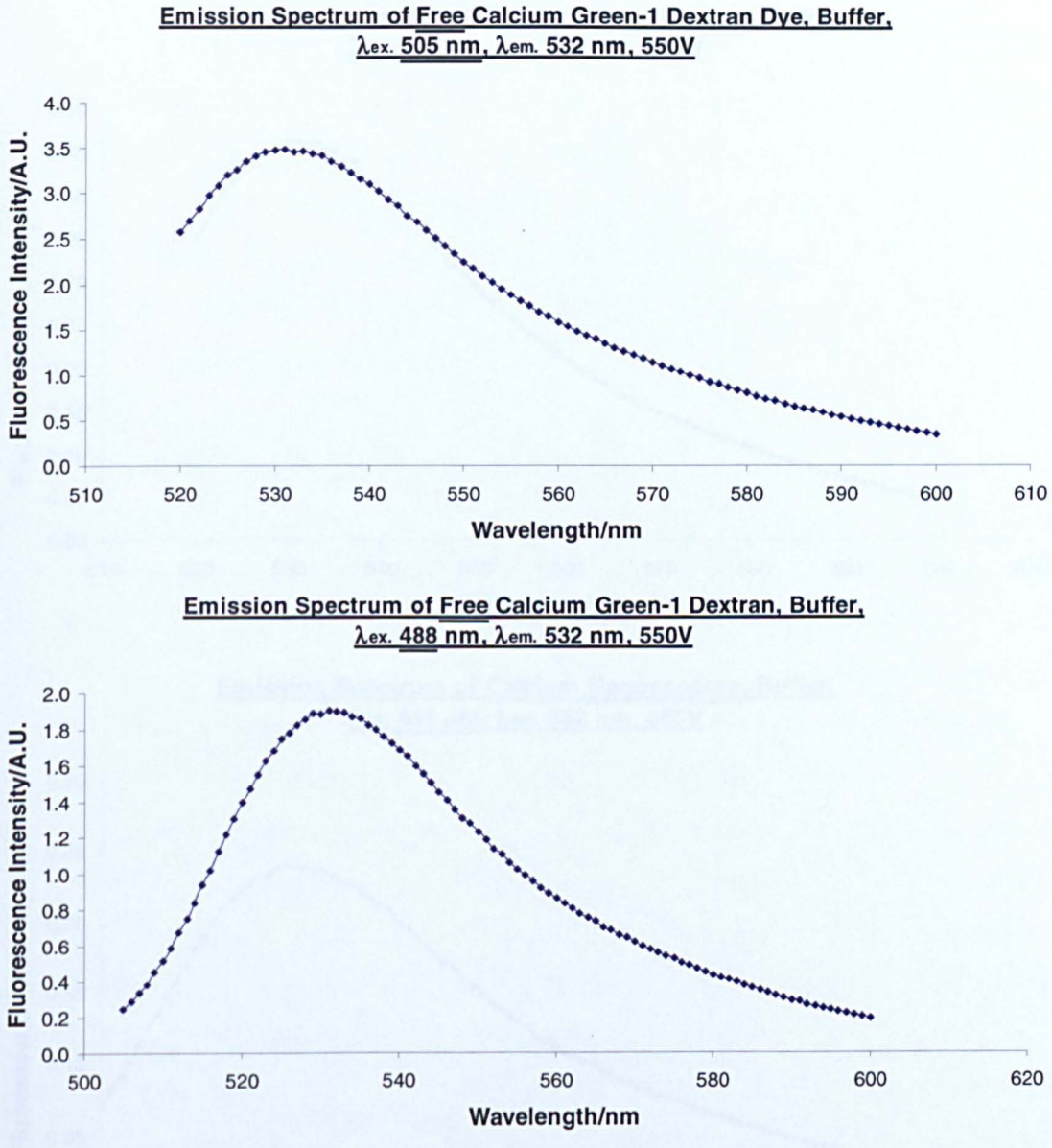

Figure 102 - Emission Spectra of Free Calcium Green ($\lambda_{ex.}$ 505 nm (optimal) and 488 nm (sub-optimal), 1.84 μmol dm^{-3} Solution)

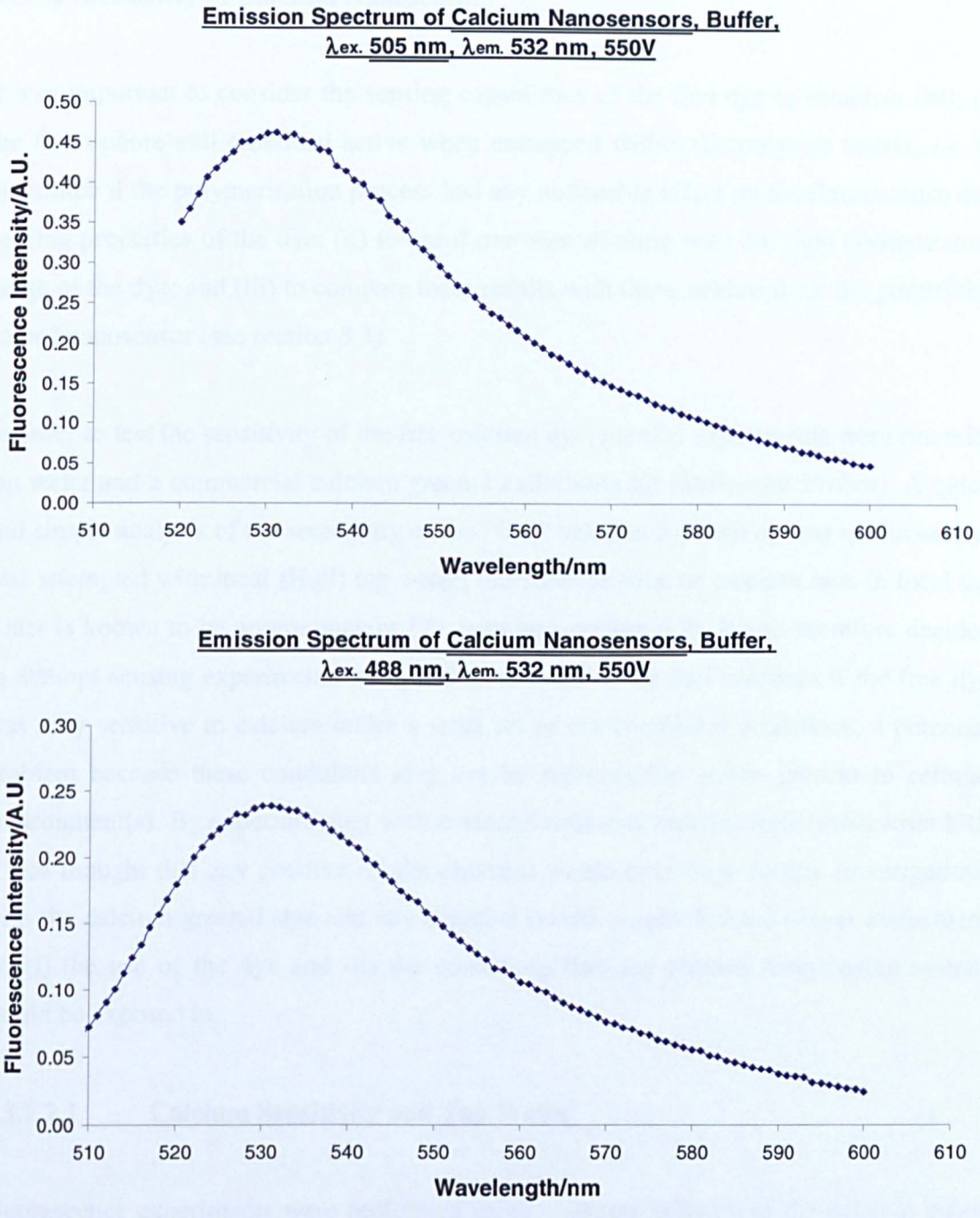

Figure 103 – Emission Spectra of Calcium Nanosensors **13** ($\lambda_{ex.}$ 505 nm (optimal) and 488 nm (sub-optimal))

The next investigative step of the Project was to ensure that the sensing properties of the dye had not been affected by the encapsulation process.

3.5.1.2 Sensitivity of Calcium Nanosensors

It was important to consider the sensing capabilities of the free dye to establish that: (i) the fluorophore still remained active when entrapped within the polymer matrix, *i.e.* to determine if the polymerisation process had any noticeable effect on the fluorescence and sensing properties of the dye; (ii) to see if one was working with the right concentration range of the dye; and (iii) to compare these results with those achieved for the porphyrin-coated nanosensor (see section 3.3).

In order to test the sensitivity of the free calcium dye, parallel experiments were run with tap water and a commercial calcium green-1 calibration kit (Molecular Probes). A quick and simple analysis of the sensitivity of the "free" calcium dye (*via* optical spectroscopy) was attempted with local (Hull) tap water; the concentration of calcium ions in local tap water is known to be approximately 122 ppm (see section 6.3). It was therefore decided to attempt sensing experiments using the local water to try and ascertain if the free dye was only sensitive to calcium under a strict set of environmental conditions: a potential problem because these conditions may not be reproducible and/or present in cellular environment(s). By experimenting with a second source of calcium ions (calibration kit), it was thought that any positive results obtained would encourage further investigations with the calcium green-1 dye and any negative results would demand urgent assessment of: (i) the use of the dye and (ii) the conditions that any formed nanosensing system would be exposed to.

3.5.1.2.1 Calcium Sensitivity and Tap Water

Fluorescence experiments were performed using a sample solution of the calcium green dye in its "free" state, bicarbonate buffer (pH 9.5) and aliquots of the stock tap water (ranging from 1-100 μl). The sample solution was agitated for 30 seconds (1,800 rpm) after each aliquot of water was added (and before further analysis) to ensure through mixing of the component parts. The sample was then excited at 505 nm: the optimal excitation wavelength for the fluorophore. Successive increases in the fluorescence

emission ($\lambda_{em.}$ 532 nm) of the sample, upon addition of water, suggested that the calcium sensitive fluorophore **was** sensitive towards calcium ions present in local tap water (figure 104).

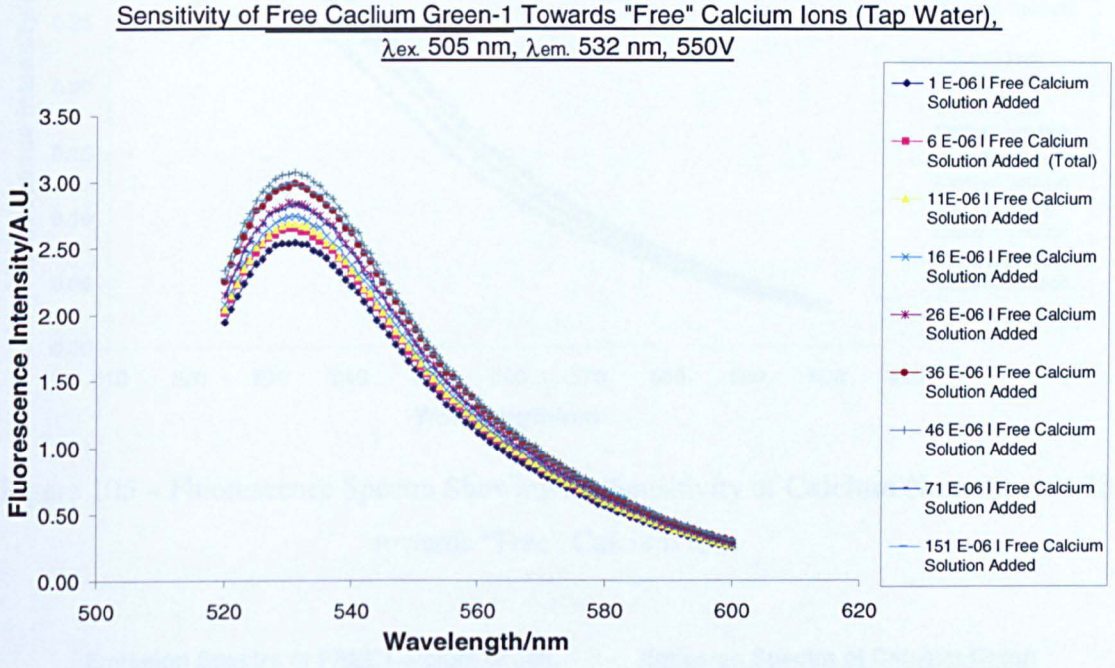

Figure 104 – Fluorescence Spectra Showing the Sensitivity of **Free** Calcium Green-1 (1.84 μmol dm^{-3} Solution) towards "Free" Calcium Ions

The calcium-sensitive nanosensors **13** were then analysed by fluorescence spectroscopy with the same stock solution of local tap water. Experiments were also successfully repeated with local tap water solutions taken on different days (figures 105 and 106) **and** with the commercial calibration buffer kit that was used to determine the linear response range of the nanosensors (see section 6.3).

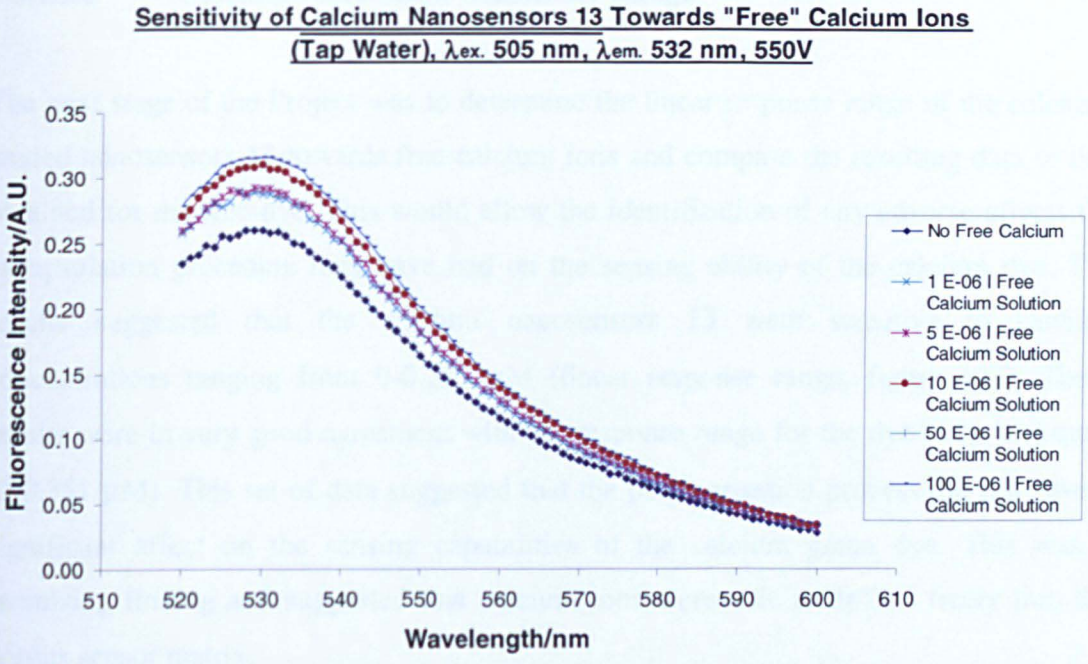

Figure 105 – Fluorescence Spectra Showing the Sensitivity of **Calcium Nanosensors 13** towards "Free" Calcium Ions

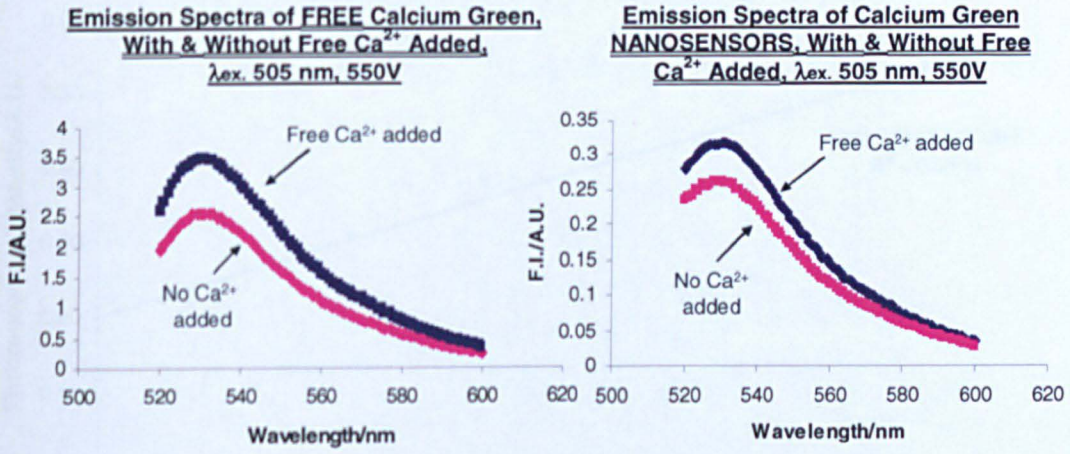

F.I. = Fluorescence Intensity

Figure 106 - Emission Spectra of **Free** Calcium Green-1 Dye and **Calcium Green-1 Nanosensors 13** and Their Response to "Free" Calcium Ions

(Total of 100 µl Calcium added)

3.5.1.2.2 Calcium Nanosensor Sensitivity Range

The next stage of the Project was to determine the linear response range of the calcium-loaded nanosensors **13** towards free calcium ions and compare the resulting data to that obtained for the free-dye. This would allow the identification of any adverse affects the encapsulation procedure may have had on the sensing ability of the calcium dye. The results suggested that the calcium nanosensors **13** were sensitive to calcium concentrations ranging from 0-0.225 μM (linear response range, figure 107). These results were in very good agreement with the response range for the dye in its free-state (0-0.351 μM). This set of data suggested that the polymerisation process did not have a significant affect on the sensing capabilities of the calcium green dye. This was a promising finding and suggested that calcium ions were able to diffuse freely into the porous sensor matrix.

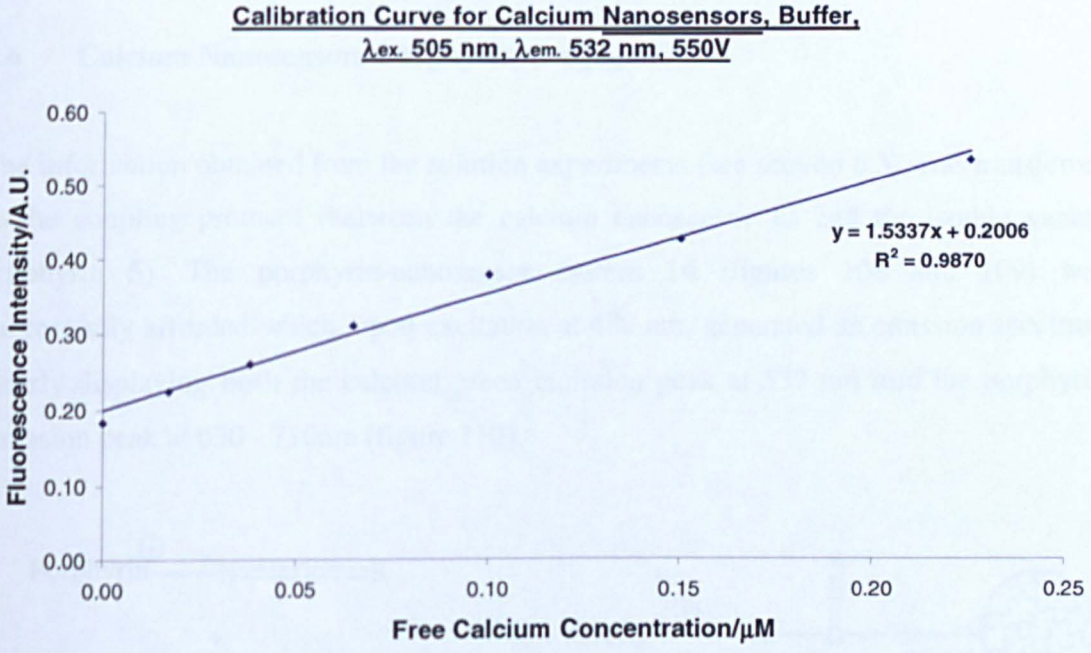

Figure 107 – Linear Response Range of Calcium Green-1 Nanosensors **13**

3.5.2 Summary and Conclusions

- Successful preliminary entrapment of a glucose sensitive fluorophore (ruthenium(II) chloride derivative).
- Resulting nanosensor **9** sensitive towards increasing levels of glucose.
- Target system **14**-sensitive fluorophore (calcium green), successfully incorporated into the nanospecies matrix.
- Sensitivity of entrapped calcium dye (0-0.225 μM) was in good agreement with the dye in its free-state (0-0.351 μM), suggesting that the microemulsion components and polymerisation reaction did not affect (to a significant degree) the sensing ability of the dye or the range it was sensitive over.
- Sensitivity range of the free and entrapped dye identical (0-0.225 μM) when excited optimally (505 nm).

3.6 Calcium Nanosensors-Porphyrin Conjugation

The information obtained from the solution experiments (see section 6.3), was transferred to the coupling protocol (between the calcium nanosensor **13** and the isothiocyanato porphyrin **5**). The porphyrin-nanosensor system **14** (figures 108 and 109) was successfully afforded which, upon excitation at 488 nm, generated an emission spectrum clearly displaying **both** the calcium green emission peak at 532 nm **and** the porphyrin emission peak at 630 - 710nm (figure 110).

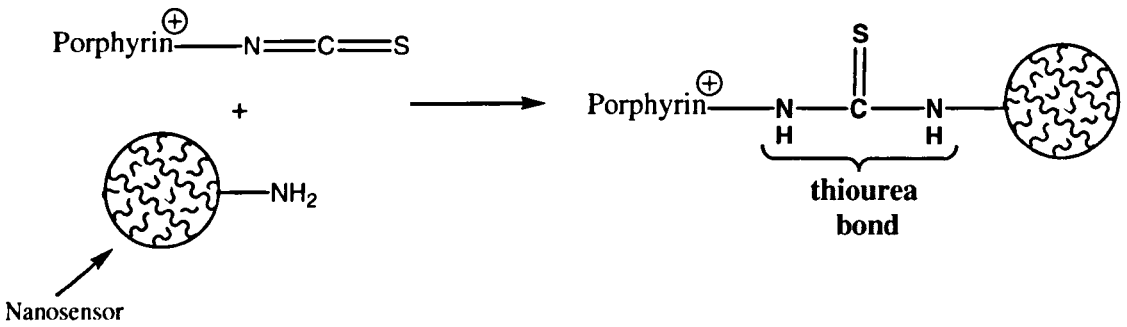

Figure 108 – Target Porphyrin-Nanosensor **14** Conjugation

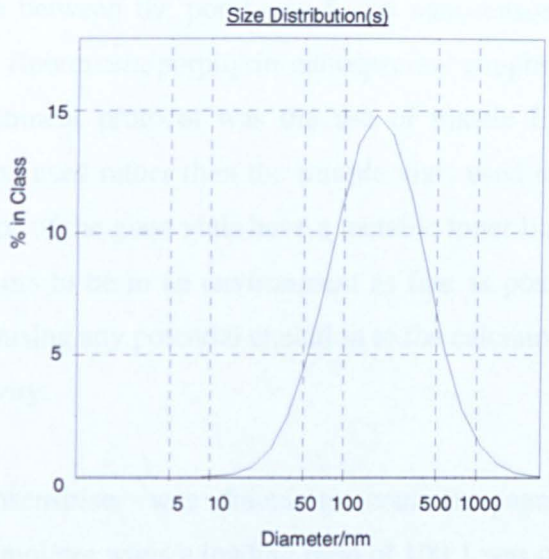

Figure 109 – PCS Spectrum of Porphyrin-Calcium Green Nanosensors **14**, $z_{ave.}$ = 188.6 nm

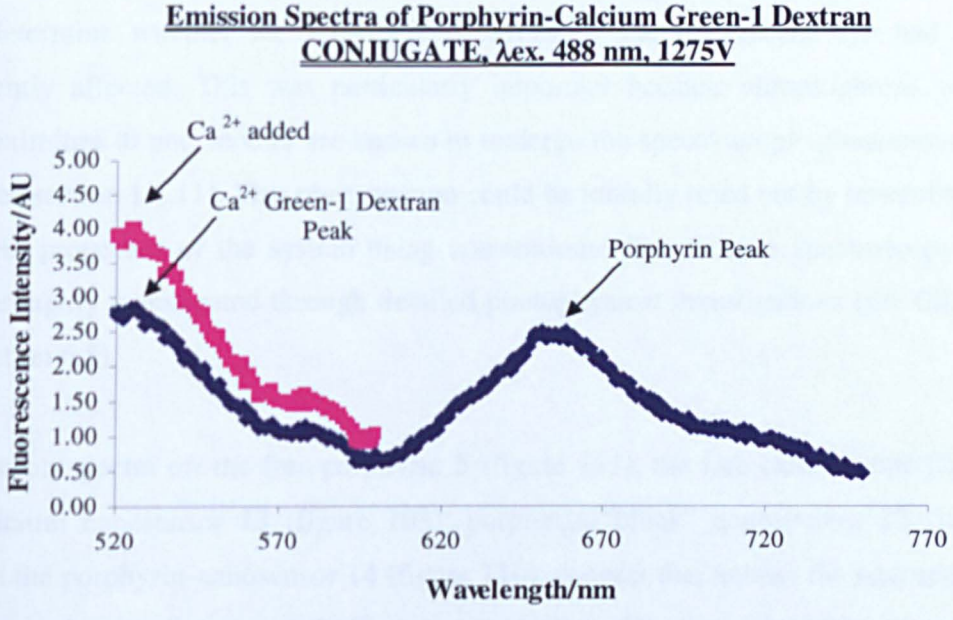

Figure 110 - Emission Spectra of Porphyrin-Calcium Nanosensors **14** and Their Luminescent Response to Free Calcium (Total of 100 µl Calcium added)

The coupling reaction between the porphyrin **5** and nanosensor **13** followed the same protocol as for the fluorescein/porphyrin-nanospecies coupling reaction. The only alteration to the attachment protocol was the use of plastic Eppendorf tubes. It was decided these would be used rather than the sample vials used in the previous coupling reactions, since the caps of the glass vials have a metallic inner lining and one wanted the calcium-sensitive sensors to be in an environment as free as possible from any metallic impurities; thus, minimising any potential chelation to the calcium green dye and hence, a reduction in its sensitivity.

The porphyrin photosensitiser was found to coat the nanospecies/sensors at a concentration of 1.1 mmol/mg when a loading ratio of 100:1 was used.

It was important to ascertain if the individual excited-state properties of the porphyrin **5** and calcium-sensitive dye were affected by (i) the coupling reaction and conditions and, (ii) to determine whether the sensing capabilities of the fluorescent dye had been inadvertently affected. This was particularly important because chromophores within close proximities to one another are known to undergo the spectroscopic phenomenon of FRET (see section 1.1.11). This phenomenon could be initially ruled out by observing the fluorescent properties of the system using conventional fluorescence spectroscopy and more thoroughly investigated through detailed photophysical investigations (see Chapter 4 and section 6.5).

The emission spectra of: the free-porphyrin **5** (figure 111), the free calcium dye (figure 112); calcium nanosensor **13** (figure 103); porphyrin-"blank" nanospecies **12** (figure 113); and the porphyrin-nanosensor **14** (figure 110), suggest that neither the nanosensing synthesis nor the coupling protocol affects the properties of the individual fluorophores in a negative manner: a result which must be further clarified (see section 6.5).

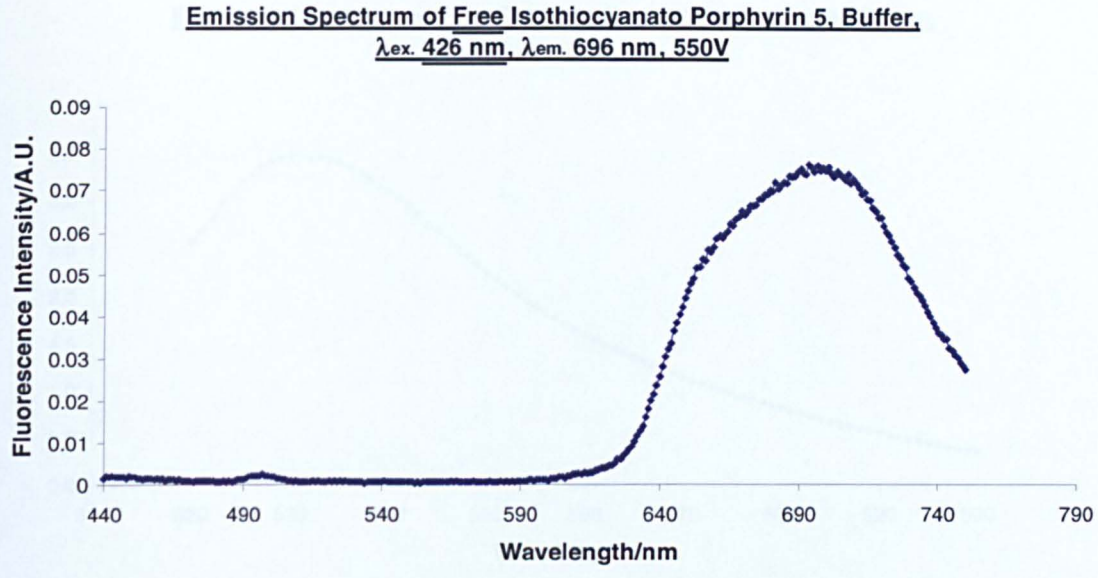

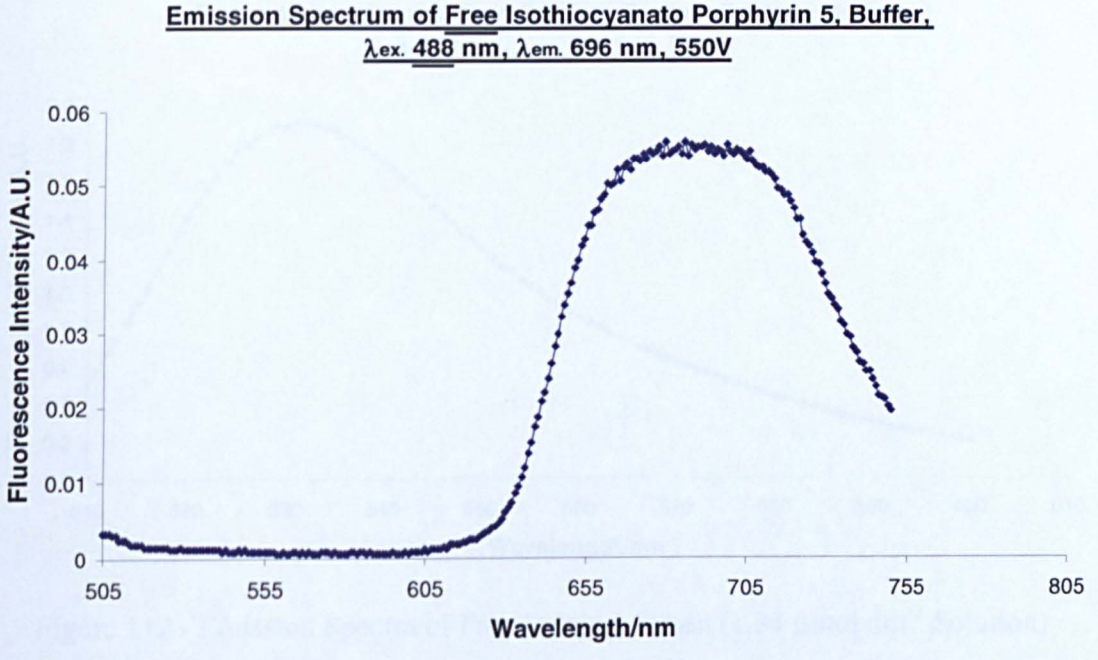

Figure 111 - Emission Spectra of Target Porphyrin **5** Excited (1.94 μmol dm^{-3} Solution) at 426 nm (Soret Band) and 488 nm (sub-optimal)

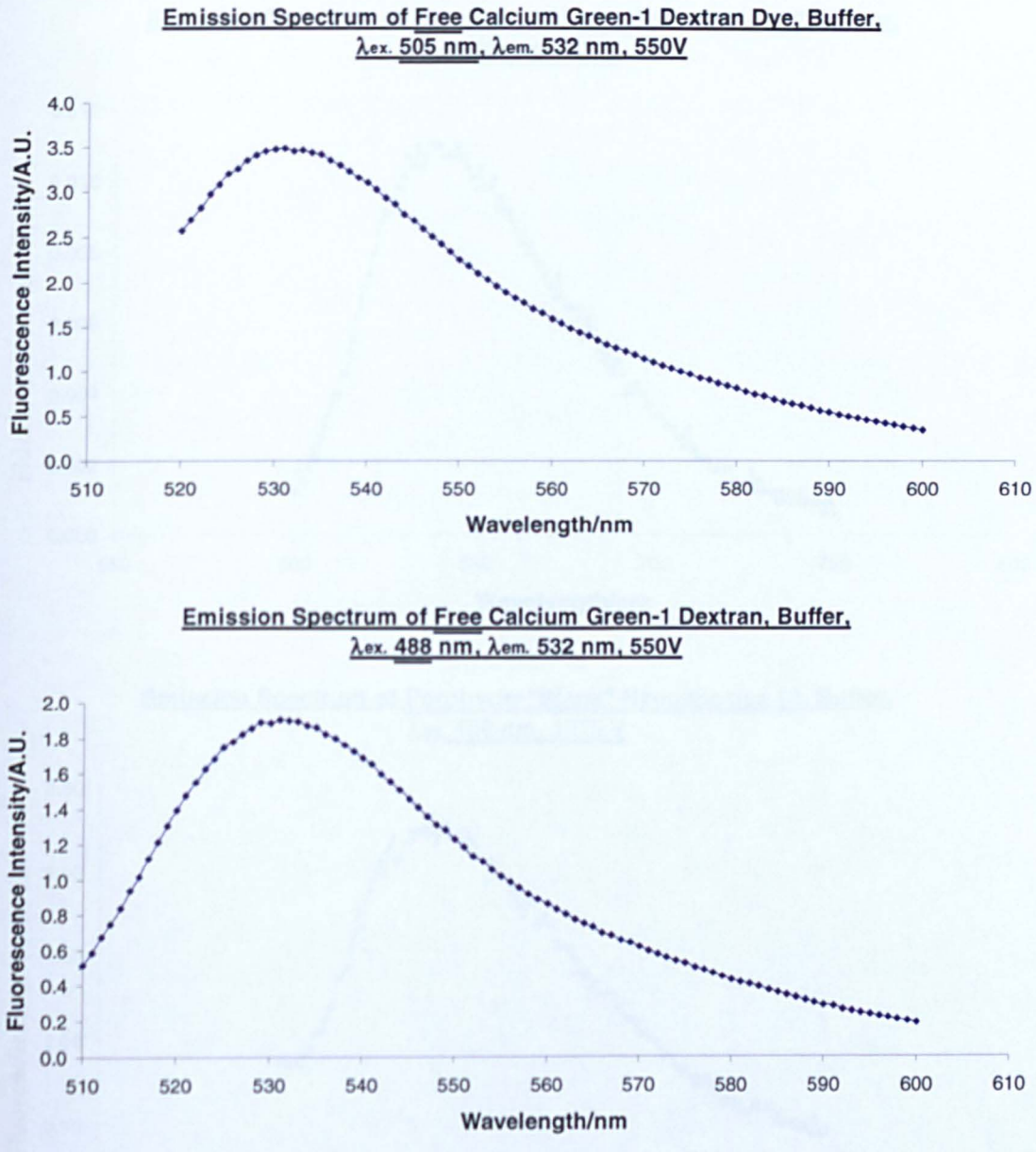

Figure 112 - Emission Spectra of Free Calcium Green (1.84 µmol dm^{-3} Solution) Excited at 505 nm (optimal) and 488 nm (sub-optimal)

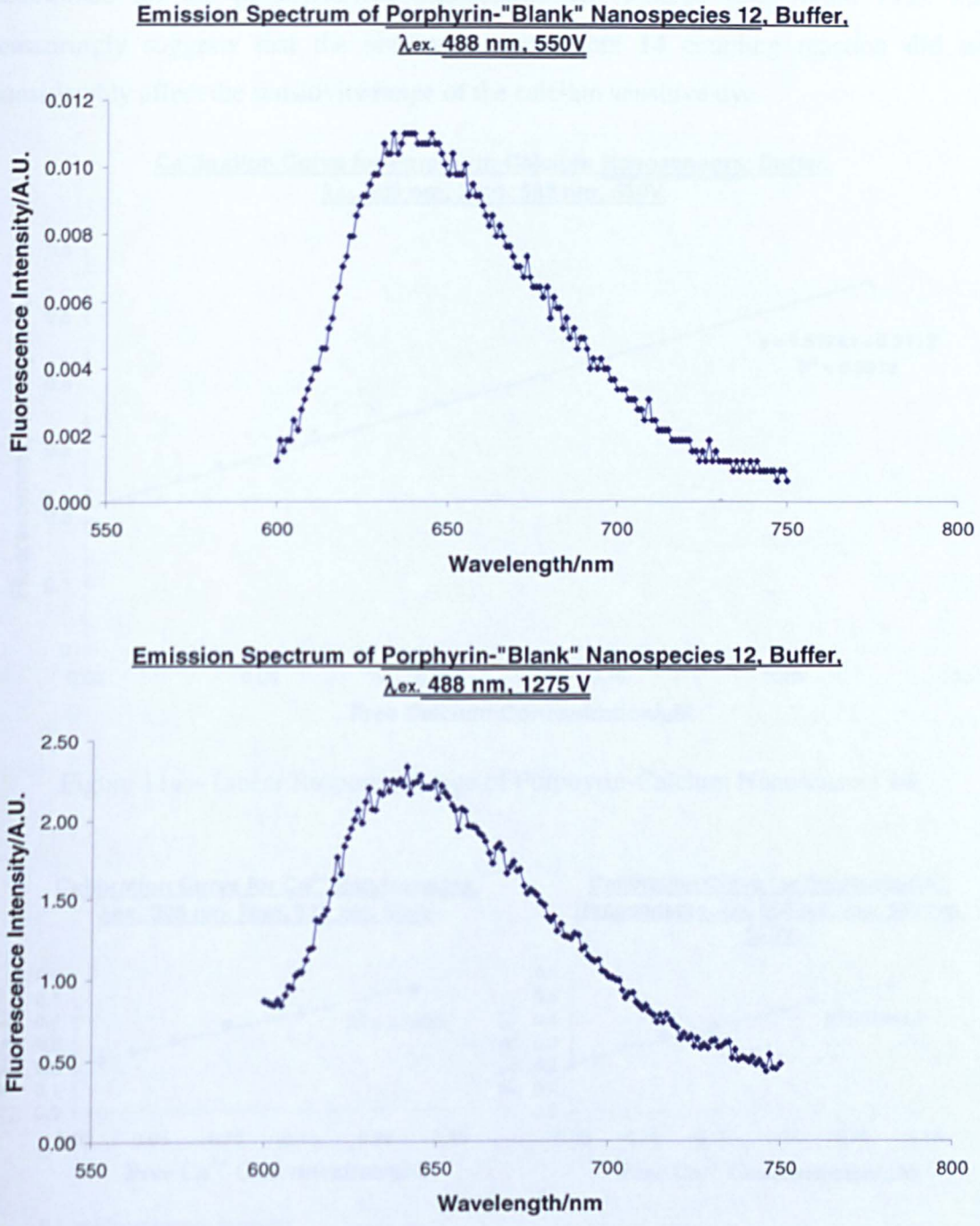

Figure 113 – Emission Spectra of Porphyrin-"Blank" Nanospecies **12** Excited at 488 nm (Sub-optimally) at Different Sensitivities

The porphyrin-coated nanosensors **14** were observed to be sensitive to free calcium ions in the range 0-0.225 μM (figure 114): very good consensus with the linear response range

determined for the porphyrin-free nanosensors **13** (0-0.225 μM, figure 115). This reassuringly suggests that the porphyrin-nanosensors **14** coupling reaction **did not** considerably affect the sensitivity range of the calcium sensitive dye.

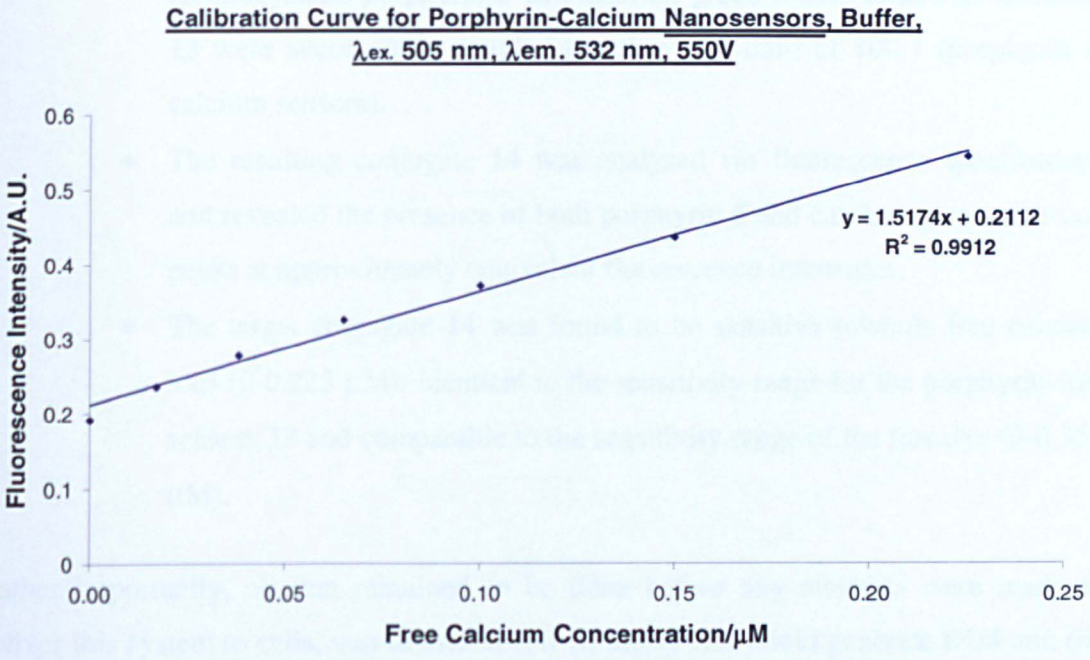

Figure 114 – Linear Response Range of Porphyrin-Calcium Nanosensors **14**

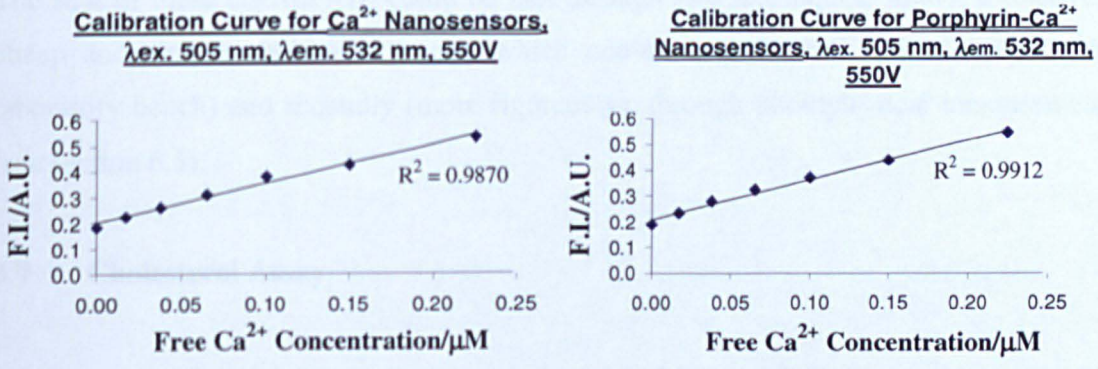

F.I. = Fluorescence Intensity

Figure 115 – Comparison of the Linear Response Range of Calcium Nanosensors **13** and Porphyrin-Coated Nanosensors **14**

3.6.1 Summary and Conclusions

- Using results from the spectroscopic solution experiments, the isothiocyanato porphyrin **5** and calcium green-loaded amino nanosensors **13** were successfully coupled together at a ratio of 100:1 (porphyrin to calcium sensors).
- The resulting conjugate **14** was analysed *via* fluorescence spectroscopy and revealed the presence of both porphyrin **5** and calcium green emission peaks at approximately equivalent fluorescence intensities.
- The target conjugate **14** was found to be sensitive towards free calcium ions (0-0.225 μM): identical to the sensitivity range for the porphyrin-free sensors **13** and comparable to the sensitivity range of the free dye (0-0.351 μM).

Rather importantly, all that remained to be done before any attempts were made to deliver this system to cells, was to establish if (i) the system could generate ROS and (ii) do so without detrimentally affecting the calcium dye.

The first of these criteria ((i)) could be met through two techniques: firstly, a relatively cheap and simple cholesterol assay (which could be performed rather easily at the laboratory bench) and secondly (more rigorously), through photophysical measurements (see section 6.5).

3.7 Cholesterol Assay

Singlet oxygen is known to react with cholesterol *via* an oxidative pathway to give (on reduction of the intermediate peroxide) a dihydroxy sterol product (scheme 20), which can be visualised by thin layer chromatography (TLC). The presence of the dihydroxy product is identified by the appearance of a **blue** coloured spot of a **different** TLC retention factor ($R_f = 0.38$) to the cholesterol starting material ($R_f = 1.0$, figure 116).[31]

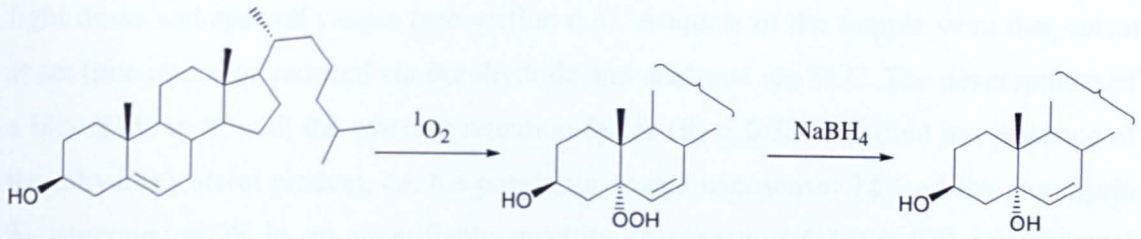

Cholesterol | 5α-Hydroperoxy-3β-cholest-6-ene | Stable Dihydroxy Sterol Product

Scheme 20 – Reaction between Cholesterol and Singlet Oxygen

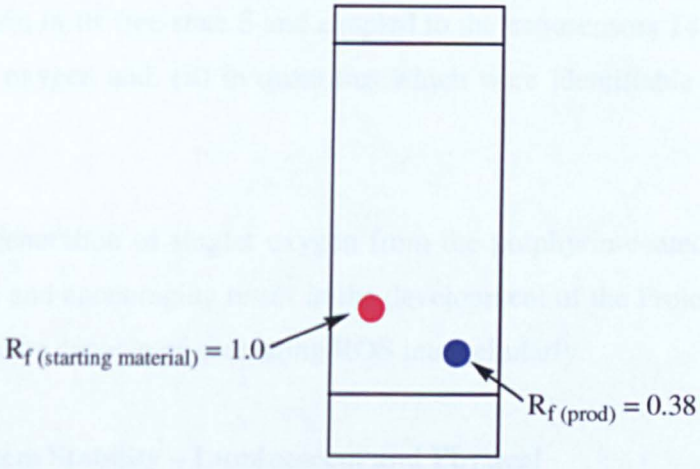

Figure 116 – Cholesterol Assay TLC Plate

Control experiments were run with a free-porphyrin solution to ensure comparable results were achieved between the porphyrin **5** in its free-state and the porphyrin-coated onto the calcium nanosensors, *i.e.* to ensure the nanospecies did not affect the photosensitising properties of the porphyrin. The assay crucially showed that the porphyrin-coated nanosensors **14** produced ROS (including singlet oxygen), capable of oxidising biological substrates, in identifiable quantities.

Briefly, a control porphyrin/cholesterol solution and a nanosensor **14**/cholesterol dispersion were prepared. With a steady stream of air bubbling through them, the samples were then irradiated with a light source. Three different light sources: a filtered xenon arc lamp (Patterson); a LED panel (Omnilux); and an unfiltered tungsten lamp (white light source) were employed to activate the porphyrin **5**, each capable of delivering different

light doses and spectral ranges (see section 6.3). Aliquots of the sample were then taken at set time intervals, reduced *via* borohydride and analysed *via* TLC. The development of a blue-TLC spot, with the relevant retention factor (R_f = 0.38) signified the presence of the dihydroxy sterol product, *i.e.* the porphyrin-coated nanosensor **14** (and free porphyrin **5**) generated ROS in an identifiable quantity (see section 6.3 for full experimental details).

3.7.1 Summary and Conclusions

Both the porphyrin in its free-state **5** and coupled to the nanosensors **14** was shown to (i) generate singlet oxygen and, (ii) in quantities which were identifiable *via* a cholesterol assay.

The successful generation of singlet oxygen from the porphyrin-coated nanosensors **14** was a significant and encouraging result in the development of the Project: signaling that the system should be capable of generating ROS intracellularly.

3.8 Nanosystem Stability – Luminescent and Physical

3.8.1 Leaching Experiments

It was important to assess any possible leaching of the dye molecules out of the nanospecies matrix. Briefly, an aqueous dispersion of the calcium-sensitive nanosensor **13** was prepared (100 mg/100 ml) and allowed to stir at room temperature, protected from light for the duration of the investigation. The fluorescence intensity of an aliquot (3 ml, of filtrate) of the initial dispersion was determined and then every half an hour for 6 hours and after 24, 36 and 92 hours the sampling/analysis process was repeated (section 6.3 for full experimental details).

The percentage of leached fluorophore was determined by dividing the fluorescence intensity of the sample aliquot (at $time_{0+n}$, where n is the time the aliquot is removed) by

the initial fluorescence intensity of the stock solution, *i.e.* the fluorescence intensity of the solution at time zero, and multiplying the ratio by 100.

The fluorescence data obtained suggested that a total of only 1% of the dye molecules leached out of the nanosensors after 4 days (96 hours, table 13). This was a promising result, bearing in mind that the nanosensor-loaded cells were to be used typically 24 hours after the sensing system has been delivered; this low level of leaching was therefore regarded as acceptable.

TIME/HOURS	LEACHED FLUOROPHORE/%
6	≤1
24	≤1
36	≤1
92	≤1 (Total from t_0)

Table 13 – Table Showing Percentage of Entrapped Dye Leaching from the Nanospecies Matrix **13**

The fluorescence of the centrifugation washings (performed during the purification stage of the nanosensors) were also analysed *via* fluorescence spectroscopy to identify if any of the dye molecules leached out of the species during the purification stage. The fluorescence data obtained (absence of the characteristic calcium green emission peak, $\lambda_{em.}$ 532 nm) suggested that the fluorescent dye had not leached out of the nanospecies. Therefore, the fluorophore could be considered as being relatively firmly trapped within the species matrix.

3.8.2 Photobleaching Studies

Simple photobleaching studies were undertaken (section 6.4) of the: fluorescein-coated nanospecies **10**; the calcium nanosensors **13**; the porphyrin-coated nanospecies **14**; and the fluorophores in their free-states, in order to try and ascertain the luminescence stability of the three fluorophores (FITC, calcium green-1 and isothiocyanato porphyrin **5**) in the different environments (free and entrapped). The fluorophores/nanosensors were dissolved/dispersed in a sodium bicarbonate buffer and their fluorescence emission monitored over a period of 3000 seconds (50 minutes, table 14).

FLUORESCENT SPECIES	**λ_{ex}/nm**	**λ_{em}/nm**	**PHOTOSTABLE**
FITC	492	520	×
Fluorescein-Nanospecies Conjugate **10**	492	520	✓
Calcium Green ("free")	488 and 505	532	✓
Calcium Green Nanosensor **13**	488 and 505	532	✓
Porphyrin ("free") **5**	426, 488, 493, 505, 583 and 622	650-750	✓
Porphyrin-Calcium Nanosensor Conjugate 14	**426, 488, 505 and 583**	**655, $710_{shoulder}$**	✓

Table 14 – Table of Fluorophore Photostability

The emission of the free-FITC fluorophore decayed significantly over the time period (figure 117), suggesting it is highly susceptible to the effects of photobleaching. However, when the same fluorophore was attached to the polyacrylamide nanospecies **7** and exposed to identical luminescence conditions, it demonstrated significantly less photobleaching. This set of data/observation suggested that the polymer matrix has a kind of "preservative" effect on the luminescence of the dye. It is possible that the transfer of energy (E_T) between the fluorophore (FITC) molecules is minimised by the steric bulk of the nanospecies in the fluorescein conjugate **10** (figure 118).

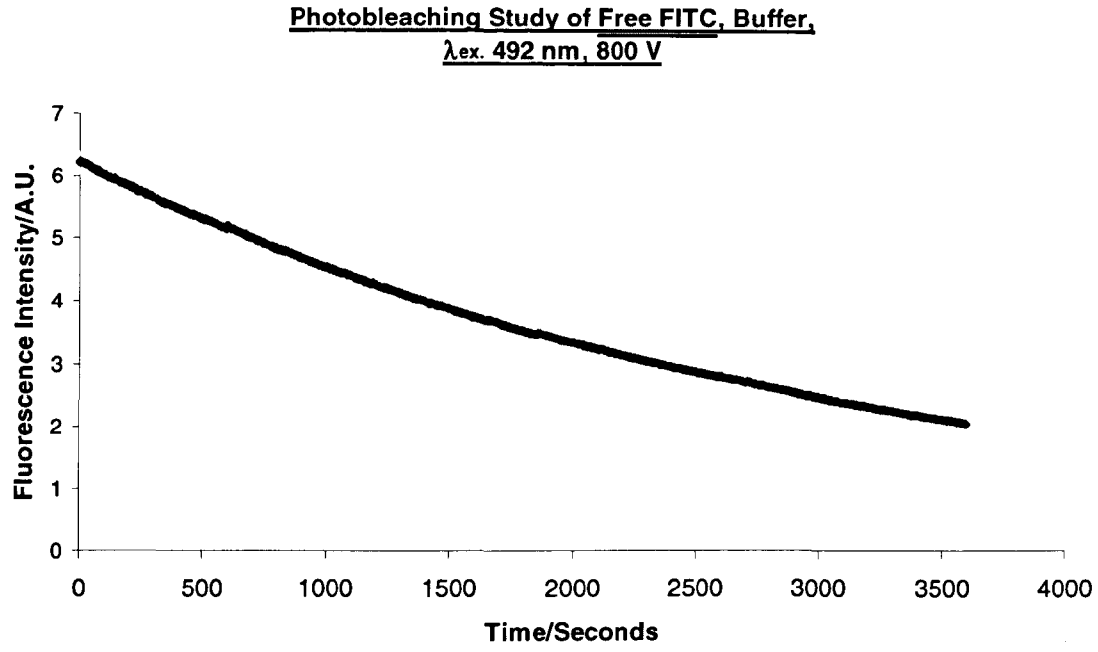

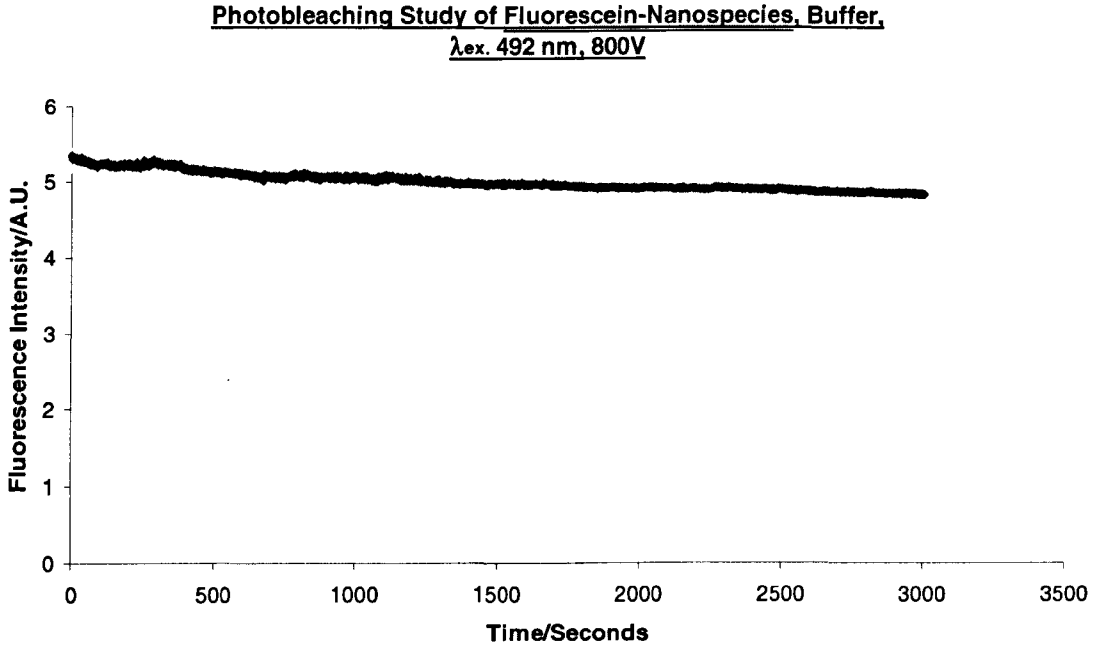

Figure 117 – Photobleaching Spectra of Free FITC (2.5 mmol dm^{-3} Solution) and Fluorescein-Nanospecies **10**

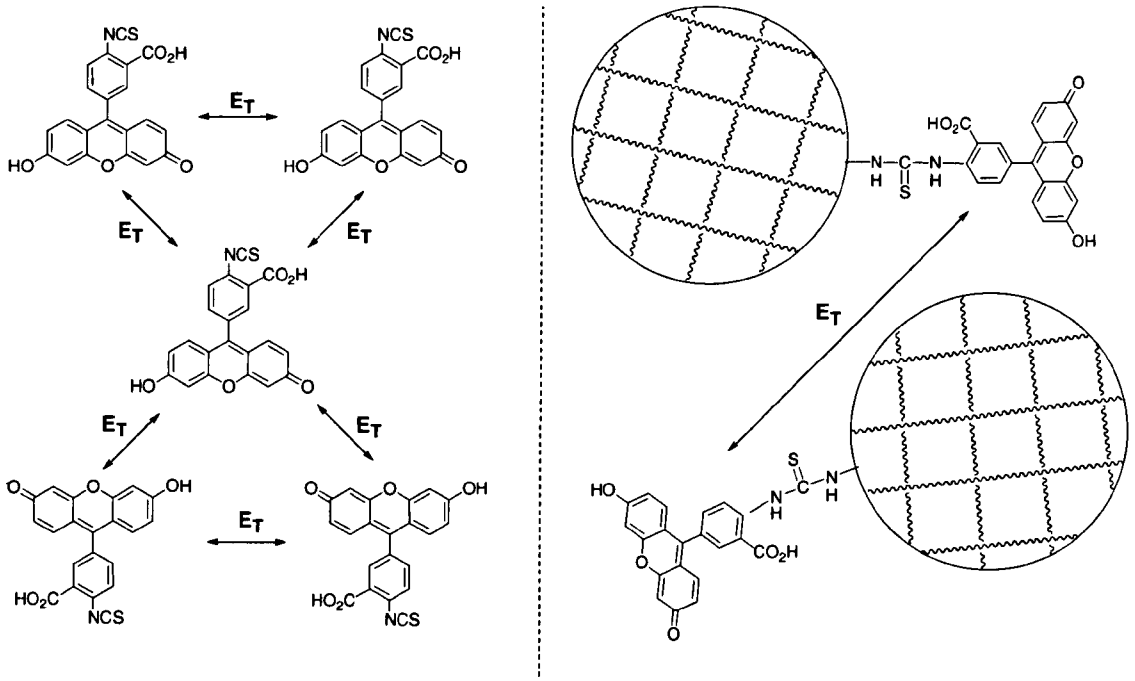

Figure 118 – Simplified Diagram Showing (possible) Energy Transfer between Free FITC Molecules and Fluorescein-Coated Nanospecies **10**

Photobleaching studies undertaken on the free calcium dye and the calcium nanosensors **13** (figure 119) suggest that the calcium green dye is not susceptible to significant photobleaching and is stable over 3000 seconds. In addition, the results for the porphyrin-coated nanospecies **14** (figure 119), mirrored the results for the porphyrin in its free-state (figure 119); supporting the postulation that the polymerisation and conjugation processes **do not** have a noticeable affect on the fluorescence properties of the analyte-sensitive dye or the porphyrin.

Photobleaching Study of Free Calcium Green-1 Dextran, Buffer, $\lambda_{ex.}$ 488 nm, 800V

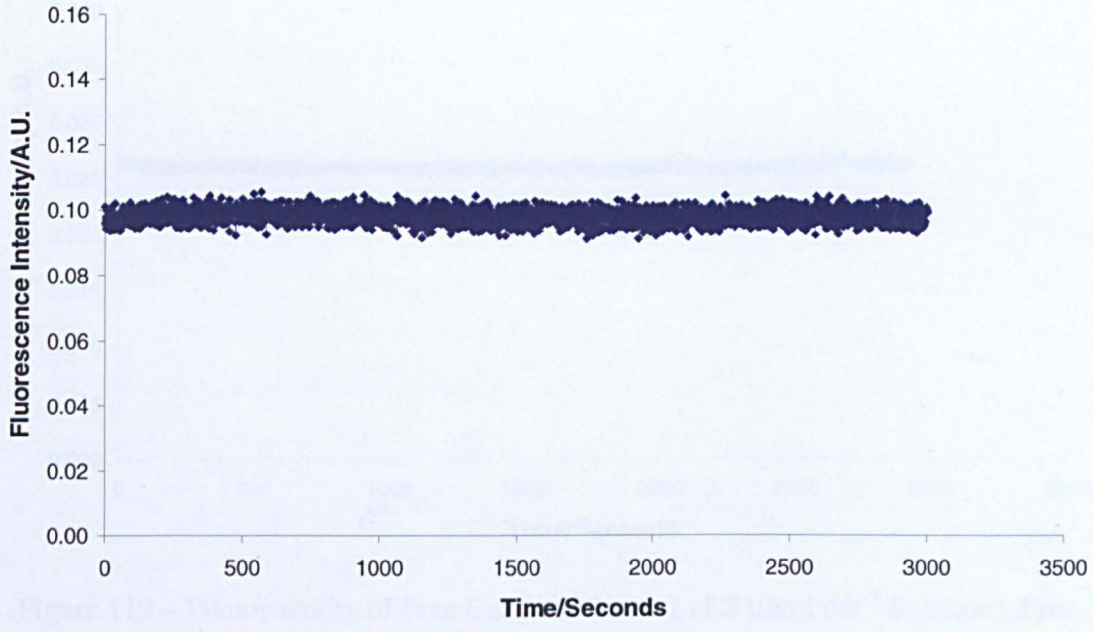

Photobleaching Study of Free Porphyrin, Buffer, $\lambda_{ex.}$ 488 nm, 550V

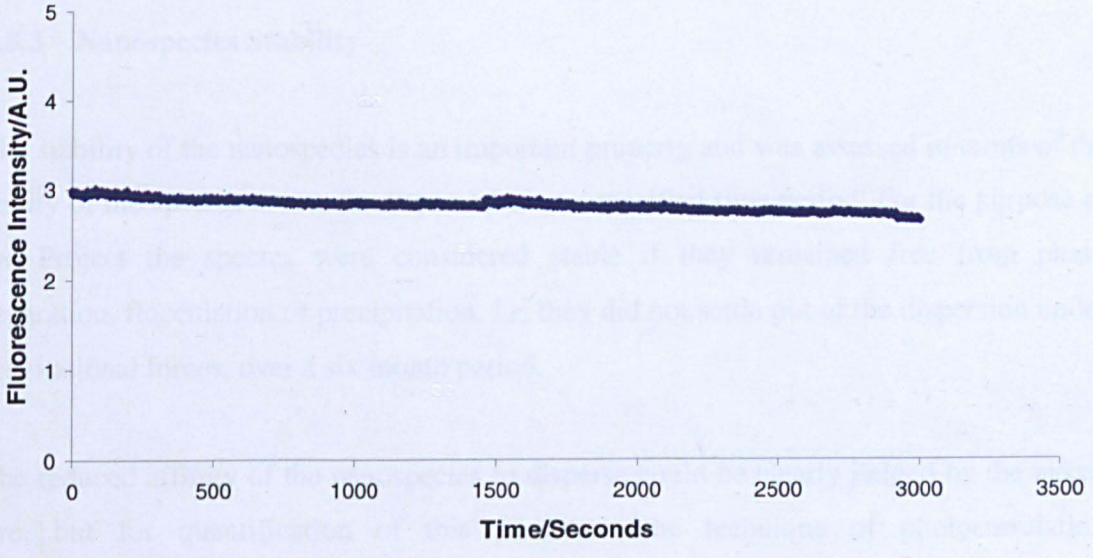

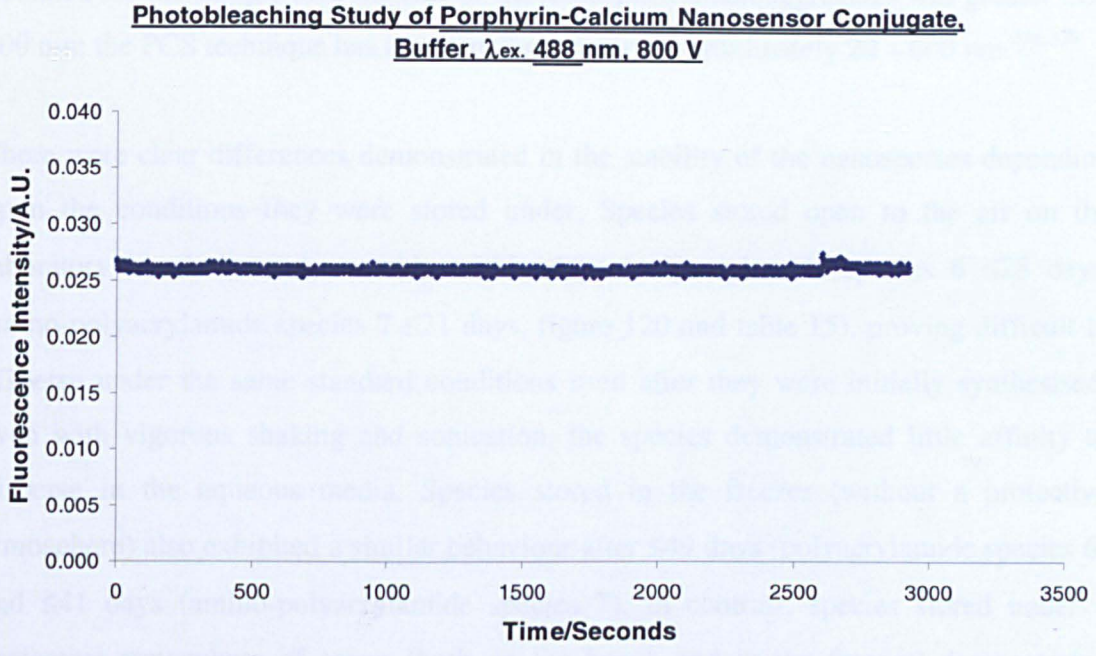

Figure 119 – Photostability of Free Calcium Green-1 (1.8 μmol dm^{-3} Solution), Free Porphyrin **5** (1.94 μmol dm^{-3} Solution) and Porphyrin-Calcium Nanosensors **14**, $\lambda_{ex.}$ 488 nm

3.8.3 Nanospecies Stability

The stability of the nanospecies is an important property and was assessed in terms of the ability of the species to remain dispersed over a specified time period. For the purpose of the Project the species were considered stable if they remained free from phase separation, flocculation or precipitation, *i.e.* they did not settle out of the dispersion under gravitational forces, over a six month period.

The reduced affinity of the nanospecies to disperse could be clearly judged by the naked eye, but for quantification of this parameter the technique of photocorrelation spectroscopy (PCS) was employed. If, size distribution data could be drawn from the "sample" and the sample was optically transparent to the naked eye (with no visible particles "settled" at the bottom of the sample container), the sample was considered to be still dispersed and therefore stable. It was considered that if no PCS data could be

obtained for the sample then the size of the nanospecies/nanoaggregates was greater than 600 nm; the PCS technique has a measuring range of approximately 20 – 600 nm.[338,339]

There were clear differences demonstrated in the stability of the nanospecies depending upon the conditions they were stored under. Species stored open to the air on the laboratory bench became unstable within days (polyacrylamide species **6** ≤28 days, amino-polyacrylamide species **7** ≤21 days, figure 120 and table 15), proving difficult to disperse under the same standard conditions used after they were initially synthesised; even with vigorous shaking and sonication, the species demonstrated little affinity to disperse in the aqueous media. Species stored in the freezer (without a protective atmosphere) also exhibited a similar behaviour after ≤49 days (polyacrylamide species **6**) and ≤41 days (amino-polyacrylamide species **7**). In contrast, species stored under a protective atmosphere of argon (both on the bench and in the freezer) demonstrated significant enhanced stability: those stored on the bench remained stable for ≤69 days (polyacrylamide species **6**), ≤70 days (amino-polyacrylamide species **7**), while those stored in the freezer remained stable for over six months. These results were mirrored for the calcium-sensitive nanosensors **13** and the porphyrin-coated nanosensors **14**. The calcium green sensors **13** and the coupled porphyrin-nanospecies/sensors **14** were always protected from sources of light, regardless of storage conditions.

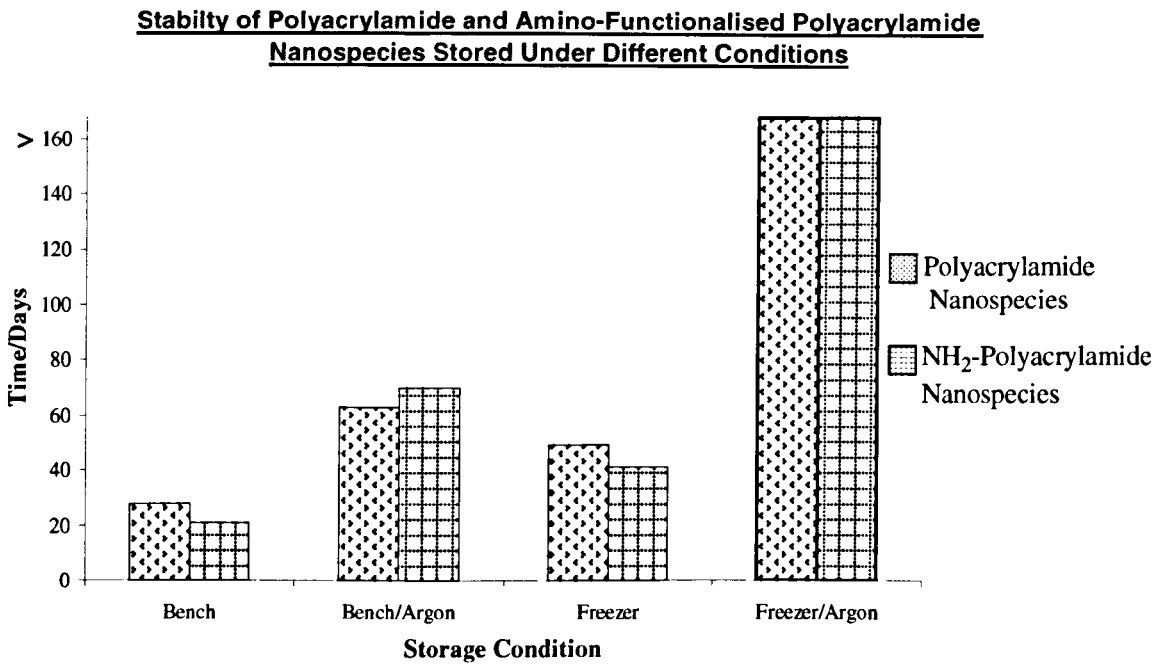

Figure 120 – Stability of Polyacrylamide **6** and Amino-Functionalised Polyacrylamide **7** Nanospecies

ENVIRONMENT/ STORAGE CONDITION	STABLE
Bench	x
Bench/Argon	x
Freezer	x
Freezer/Argon	✓

Table 15 - Table of Storage-Dependent Nanospecies Stability

It is also worthy to note that dispersions of the nanospecies/nanosensors remained stable for up to 3 weeks, showing very little/minimum phase separation, flocculation or precipitation. However, the stability of these dispersions was not investigated further since the desired nanosensing system **14** contains a thiourea bond, which is susceptible to hydrolysis over time. Further, it is anticipated that the system will be used inside the cells well within this time period.

All nanospecies prepared were therefore **always stored under an argon** atmosphere in the **freezer** and remained protected from light until they were required for the appropriate experiments.

3.8.4 Summary and Conclusions

- ≤1% of calcium green leaches out of the porous nanosensors over a 96 hour period.
- Calcium green and porphyrin chromophores photostable in their free, entrapped and coupled forms for 3000 seconds, when illuminated at the optimal and sub-optimal wavelengths.
- Polyacrylamide **6**, amino polyacrylamide **7**, calcium nanosensor **13** and target system **14**, all stable for at least six months when kept under an atmosphere of argon in the freezer, and if appropriate, protected from sources of light.
- Stability of the above nanospecies is severely diminished when storage conditions change; nanospecies stored open to air at room temperature remain stable on average ≤21 and ≤28 days (amino-polyacrylamide **7** and polyacrylamide species respectively **6**).

3.9 Chapter Summary and Conclusions

The synthesis of the polyacrylamide nanospecies **6** (see scheme 21 for structures) was not as straightforward as one may have expected. It was concluded from the experiments, that a number of criteria needed to be rigorously adhered to in order to generate the required nanospecies. It was found that reagents needed to be of a high degree of purity and stored under the correct conditions; and that the reaction components and reaction mixture **must** be **thoroughly** evacuated of any free radical scavenging species. These criteria were considered to be most **vital** steps in the formation of polyacrylamide species dispersible in aqueous media, in good to high yields. Following the identification of these criteria, a range of amino-functionalised nanospecies were (more) readily generated utilising a commercial amino-acrylamide monomer. The presence of free primary amino groups on the nanospecies **7** (see scheme 21 for structures) was subsequently confirmed *via* a non-fluorescent reagent and more appropriately to the Project, through model coupling reactions between two commercial isothiocyanate fluorophores. These findings confirmed the generation of the nanospecies component of the target system; a most encouraging outcome for the Project.

The synthesis of the analyte sensitive nanospecies **13** (see scheme 21 for structures) was readily accomplished following the synthetic route used to afford polyacrylamide nanospecies **6** and **7** (with minor adjustments). The nanosensors generated (ruthenium based glucose **9** and calcium green calcium sensors **13**) were both sensitive to their respective substrates in the same manner and range as the dyes in their free-state; leading to the postulation that the target analyte-sensitive nanosensors (**9** and **13**) could be successfully produced, with minimal affect on the sensing properties of the dye. The outcome of the investigation also led to the hypothesis that the pores in the polymer matrix were within the right size range to accommodate the diffusion of the free substrates (glucose and calcium ions) into the matrix; a further encouraging result.

The calcium nanosensors **13** were successfully coupled to the desired photosensitiser **5** following the protocol optimised for the model coupling reactions. The resulting sensing product **14** (see scheme 21 for structures) was sub-optimally excited (488 nm) to generate

the characteristic emission peaks of the two chromophores at near-equal fluorescence intensities. Further, the system was found to be sensitive towards free calcium ions in the expected manner, with a linear response range comparable to the calcium sensitive dye in its free-state. The same nanosystem **14** also demonstrated the ability to generate ROS when illuminated with a range of light sources. Furthermore, in support of the above findings, the system showed enhanced stability when stored under argon in the freezer (≥6 months); minute leaching of the entrapped fluorophore; and both chromophores demonstrated photostability over 3000 seconds of continuous illumination ($\lambda_{ex.}$ 488 nm). However, one result which was unexpected was the large size of the nanospecies conjugates (195.6 nm for conjugate **12** and 188.6 nm for conjugate **14**). This could be the result of the system components aggregating together, which would generate a "false" PCS reading for the individual porphyrin-nanospecies conjugates. It is unlikely that the values are anomalous measurements since PCS was repeatedly run on different batches of conjugated species. Ideally, the size of the porphyrin-nanospecies conjugate would be clarified by using a more rigorous method, such as electron microscopy; this would allow more accurate size data to be obtained for the conjugates. The experimental findings for the Chapter are summarised in the following tables (tables 16 and 17).

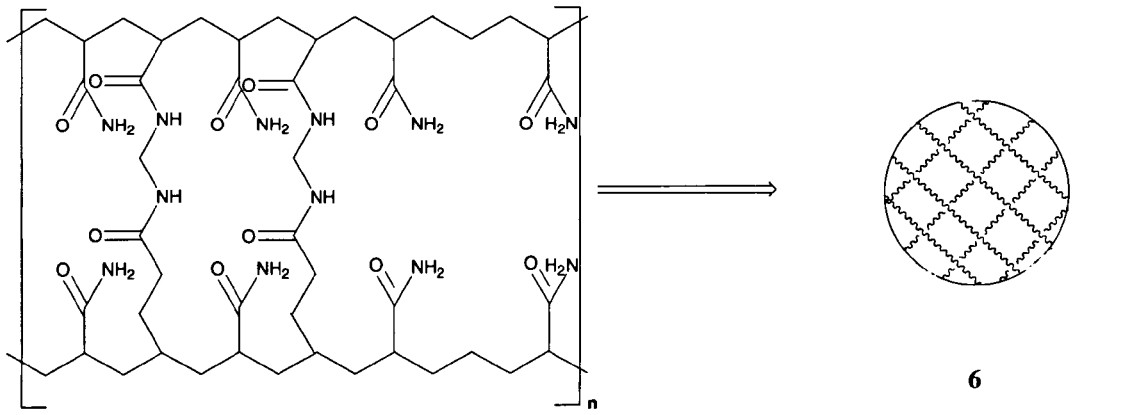

6

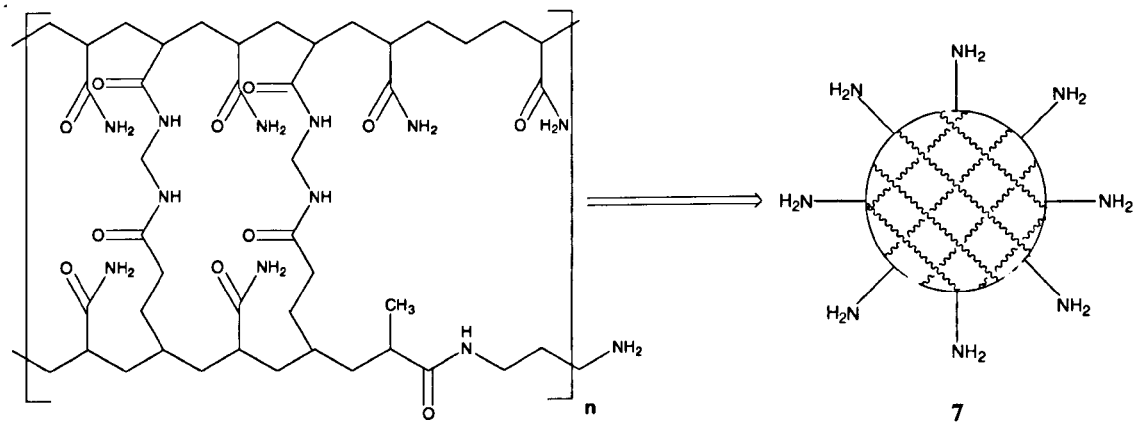

7

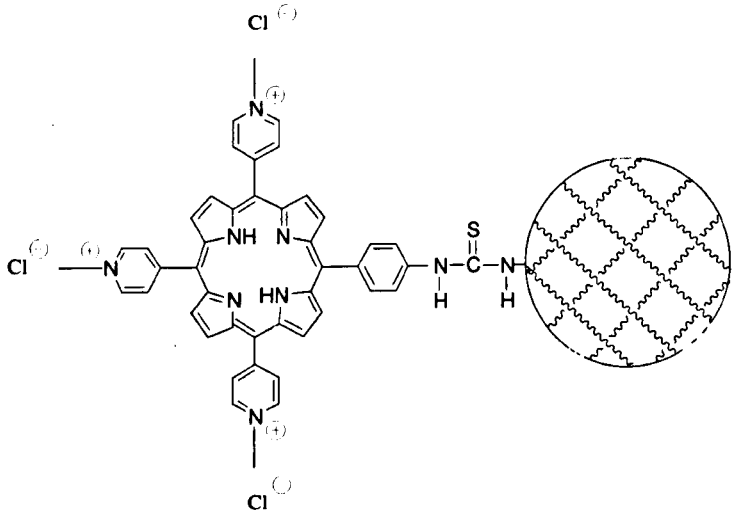

12

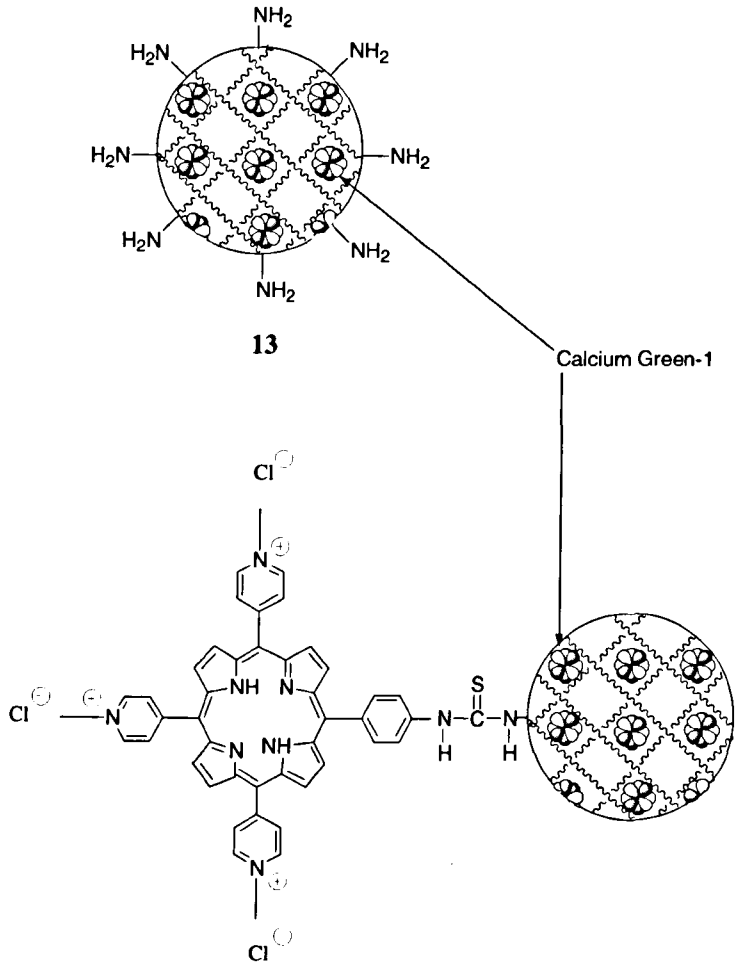

Scheme 21 – Key Nanospecies Components and Conjugates

SPECIES	SIZE ($z_{ave.}$)/nm	PHOTOSTABLE
Polyacrylamide **6**	37	-
Amino-Polyacrylamide **7**	38	-
Amino-Polyacrylamide Calcium Sensors **13**	44	✓
Porphyrin-Nanospecies **12**	195.6	✓
Porphyrin-Nanosensors **14**	188.6	✓

Table 16 – Table of Desired Nanospecies Size and Photostability

SPECIES	"COAT" RATIO/mmol mg^{-1}	RESPONSE RANGE/μM
Calcium Nanosensor **13**	-	0 - 0.225
Porphyrin-Nanospecies **12**	1.1	-
Porphyrin-Nanosensors 14	**1.1**	**0 – 0.225**

Table 17 – Table Showing the Desired Coupling-Product, Their Coating Ratios and Sensitivity Ranges

The Chapter findings (tables 16 and 17) came together and encouraged the hypothesis that: a bifunctional nanosensing system can be created, sensitive to free calcium ions *via* the assembly of the relevant polymeric nanospecies **13** and photosensitising organic molecules **5**.

The flexibility afforded by the nanospecies synthesis highlights the potential for generating nanospecies bearing different functionalities. This flexibility, along with the absence of any significant affect on the sensing capabilities of the entrapped dye, and the photosensitising properties of the external chromophore, are features which demonstrate the potential such a nanosystem has in further and wider bio-sensing/imaging applications.

CHAPTER 4 PHOTOPHYSICS RESULTS AND DISCUSSION

The target system: a bifunctional analyte sensitive nanosystem centred around two independent chromophores has been discussed previously (see Chapters 1, 2 and 3) and is based around the idea that a photosensitiser (in the presence of molecular oxygen ($^3O_2$)) can generate ROS when illuminated at a selective wavelength. It is widely believed that such cytotoxic species cause a disturbance to the homeostasis of free calcium ions present in the cell and, that these divalent ions are implicated in the disease pathways leading to neurodegenerative disorders and heart disease (see section 1.3). By selectively monitoring this kind of response to the toxic oxygen species, it should be possible to make advancements in understanding the labyrinth of pathways behind cell signaling and disease states.

4.1 Aims

In order for an efficient target nanosystem to be generated a number of criteria need to be met: (i) the photosensitiser must be efficient at undergoing intersystem crossing (ISC); for a photosensitiser to be able to generate ROS, particularly singlet oxygen, the excited photosensitiser must be efficacious at undergoing spin-inversion and populating the triplet state (T_1), *i.e.* the photosensitiser should have a high quantum yield of formation (Φ_T) and a relatively long triplet-state lifetime (τ_T) that molecular oxygen ($^3O_2$) can quench (see figures 14 and 19, and section 1.1.6). Singlet oxygen is known to have a short radius of action and therefore elicit change close to their site of generation (Chapter 1); (ii) accordingly, it is key that the analyte-sensitive dye must be within close proximity to the site of singlet oxygen generation; achieved by attaching the sensing component directly to the photosensitiser; in addition, (iii) it is desirable that the analyte sensitive portion of the target system has a high quantum yield of fluorescence ($\Phi_{fl.}$) - its response to free calcium ions is detected *via* luminescence spectroscopy; (iv) it is also **crucial** that the two chromophores work simultaneous and independent of each other with regard to their photophysical parameters; the two will, through the nature of the target system, be located within very close proximities to one another; a primary concern therefore is

luminescence interaction (energy transfer, E_T) between the two species, hence, it is important to ascertain if the phenomenon of FRET occurs between the two. It is also important to identify if the luminescence of the species are affected by: (i) the entrapment process/matrix; (ii) the coupling protocol; and/or (ii) the chelating process, *i.e.* do the nanospecies matrix and respective reactions have any detrimental affect on the photophysical properties of the entrapped dye.

These questions can all be addressed by determining the quantum yield (Φ) and lifetime (τ) data for the chromophores in their entrapped, conjugated and free-states; thereby, facilitating the assessment of the imaging/sensing potential of the target nanosystem **14**.

All of the above criteria can be accomplished using time resolved single photon counting spectroscopy (see section 1.1.12) and will be discussed in the following section, both with respect to the individual/free luminescence parameters (Φ_Δ (porphyrin), τ_T (porphyrin), $\Phi_{fl.}$ (calcium green), $\tau_{fl.}$ (calcium green)) and the effect of coupling the two chromophore "systems" together. The effect of calcium ion complexation on their respective parameters will also be investigated.

In summary, questions to be addressed:

- Does the porphyrin generate singlet oxygen; vital as the target system is based on the response of intracellular calcium to *in situ* generated ROS?
- What are the quantum yields of formation and lifetime of singlet oxygen/what is the triplet lifetime of the excited photosensitiser?
- Are these values comparable to those for the coupling product?
- Does the quantum yield of fluorescence of the calcium-sensitive dye change upon/with calcium binding?
- Does the calcium green quantum yield change upon encapsulation and conjugation?
- Is there significant energy transfer (E_T) between the two fluorophores?

4.2 Time Correlated Spectroscopy Data Analysis

Data from time resolved spectroscopic measurements can be used to extract the excited-state lifetime(s) of species from the respective excitation and emission data. However, the interpretation and analysis of this data is not a straightforward task. If the fluorescence lifetime ($\tau_{fl.}$) of a species is much longer than the laser excitation pulse, then the log of the decay curve must be plotted and the excited lifetime of the species determined from the slope of the resulting line. If, on the other hand, the fluorescence lifetime of the species is shorter than the excitation flash, the radiative decay must be deconvolved from the excitation pulse. This can be accomplished by using the least squares iterative deconvolution algorithm (see section 1.1.12): the excitation pulse is convolved with exponential decay functions of different lifetimes until a lifetime which matches the emission data is found.

4.3 Porphyrin Photophysics

In order for a photosensitiser to be efficient at generating singlet oxygen it must be efficient at undergoing spin inversion and populating the excited triplet state (see figures 14 and 19, and section 1.1.6). Therefore, the main aim of the porphyrin **5** photophysical investigations was to ascertain if they generated singlet oxygen upon illumination.

The experimental set-up used to determine the singlet oxygen lifetime (τ_{Δ}) of the porphyrin photosensitiser **5** was as described in Chapter 1 (see section 1.1.12). Briefly, sample solutions of the porphyrin **5** in deuterated water (D_2O is known to enhance singlet oxygen lifetimes) were held in a 1 cm path-length quartz cuvette. The samples were excited using the third harmonic (355 nm) of the diode-pumped, Q-switched Nd:YAG laser guided through a refractive prism. The phosphorescence of the sample was collected at a 90° angle to the excitation beam, passed through an interference filter centred at 1270 nm and, *via* an elliptical mirror, focused onto the active area of the liquid nitrogen-cooled germanium photodiode. The resulting output from the diode was then amplified and AC coupled to a digital oscilloscope where the emission transients were digitised and

averaged before being relayed to a PC for analysis. The evaluation of the data at increasing time intervals revealed the pattern of decay which the excited state species followed. The lifetime of the species was determined by mathematical analysis of the decay curves through the least squares iterative method. The data was χ^2 fitted to the decay curve using deconvolution software (see section 1.1.12 and 6.5). χ^2 values approaching unity were desired.

4.4 Results

All photophysical data were obtained as a result of collaboration with Dr Andy Beeby at The University of Durham, U.K. The experiments were all repeated with different batches of the corresponding species (porphyrin, sensors and conjugate) to yield comparable (±5 μs) data/results.

To ensure the weak luminescence signal observed at 1270 nm was from the phosphorescence of singlet oxygen, the porphyrin **5** sample solution was evaluated with the inert gas nitrogen. Nitrogen was purged through the aqueous solution for five minutes and the cell/cuvette covered with an air tight Teflon® stopper to prevent re-oxygenation of the solution. The luminescence of the sample was then recorded under identical conditions to the "aerated" solution (ambient).

Data acquired (figure 121), clearly demonstrates that the decay curve observed when the porphyrin sample was illuminated sub-optimally at 355 nm, is that of singlet oxygen. A control experiment was run with naphthalene as a standard reference to ensure that the singlet oxygen detector was working correctly.

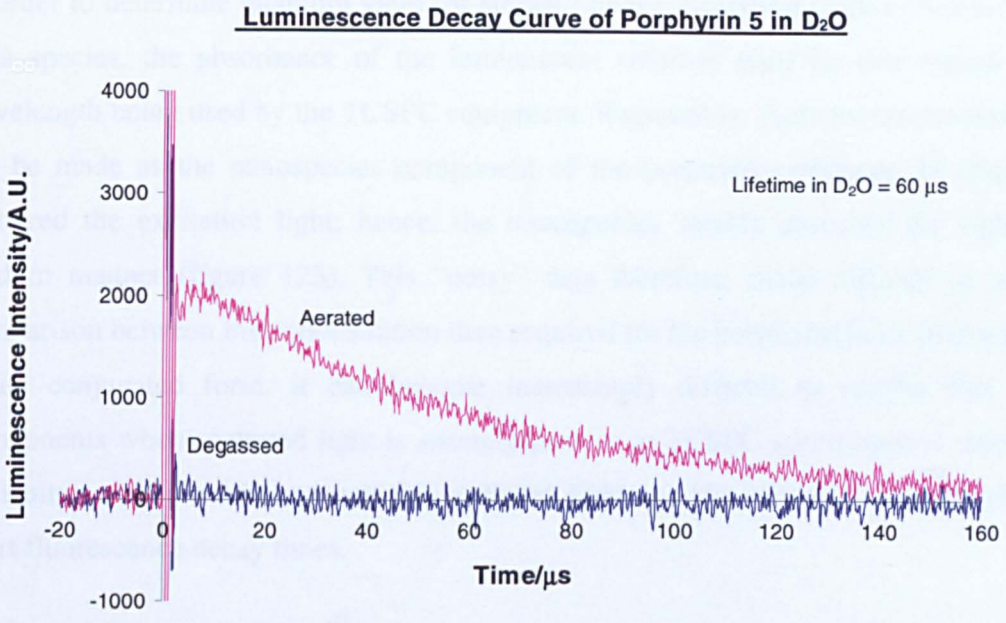

Figure 121 – Porphyrin **5** Decay Curve Showing Presence of Singlet Oxygen (1.95 µmol dm^{-3} Solution)

The lifetime calculated for the free porphyrin solution 60 µs (figures 121 and 122) is in good agreement with published literature values (55-60 µs); further supporting the evidence that singlet oxygen is indeed generated by porphyrin **5**.[30] In order to ascertain if the porphyrin coupled to the nanospecies was still able to generate singlet oxygen (*i.e.* did the coupling protocol have a negative effect of the photosensitising capacity of the porphyrin) the above experiments were repeated with the porphyrin-fluorophore free ("blank") nanospecies **12** and the nanosensor conjugates **14**. The singlet oxygen lifetimes determined (55 and 63.40 µs) were in good agreement with the porphyrin in its free-state, suggesting that the coupling protocol would appear not to have had a detrimental affect on the photosensitiser. These findings are in good correlation with those from the cholesterol assay study in section 3.7 (also see section 6.4). Further clarification would ideally have been achieved through the determination of quantum yields of singlet oxygen formation. Unfortunately, these measurements could not be made (see below).

In order to determine quantum yield (of singlet oxygen formation (and/or fluorescence)) of a species, the absorbance of the luminescent solution must be determined at the wavelength being used by the TCSPC equipment. Regrettably, these measurements could not be made as the nanospecies component of the porphyrin-conjugate **14** dispersion scattered the excitation light; hence, the nanospecies weakly absorbed the light in a random manner (figure 123). This "noisy" data therefore, made difficult to make a comparison between the concentration data acquired for the porphyrin in its free-state and in its conjugated form. It can become increasingly difficult to resolve fast decay components when scattered light is strongly present in TCSPC spectrometry: since, it is difficult to differentiate between the scattered light and the presence of multiple very short fluorescence decay times.

It can also be seen (figures 122 and 123) that the intensity of the luminescence signals from the nanospecies-containing samples were reduced; thus, further complicating the collection of reliable and comparable data.

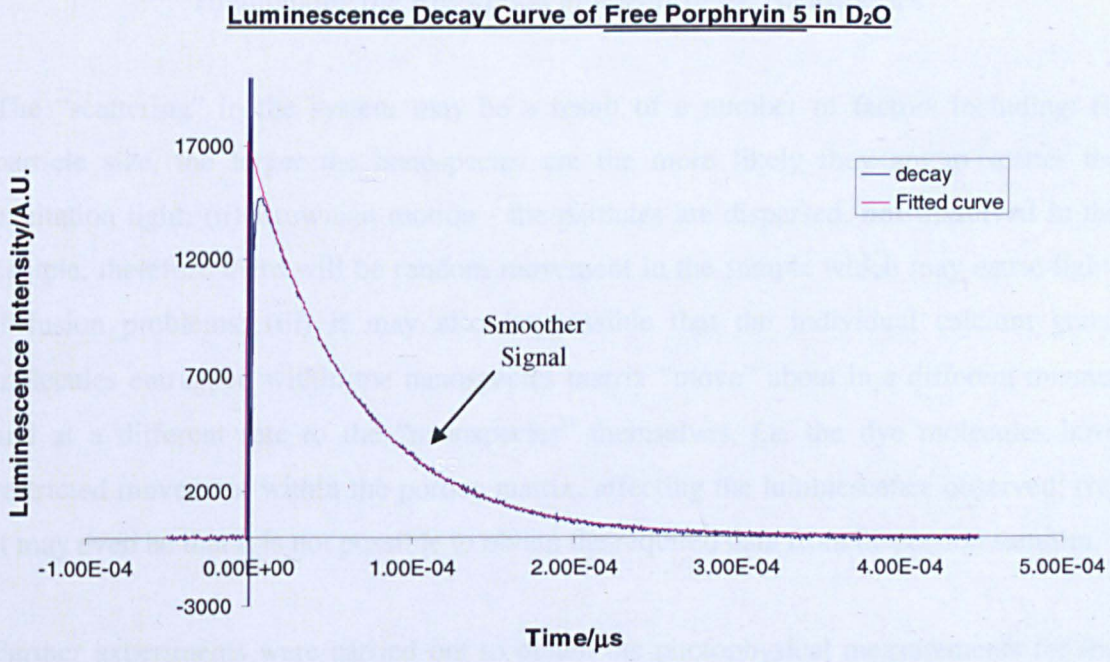

Figure 122 – Time-Resolved Emission Decay Curve of Porphyrin **5** (1.94 µmol dm^{-3} Solution) Showing Experimental Data Curve Overlaid with the Fitted Decay Curve

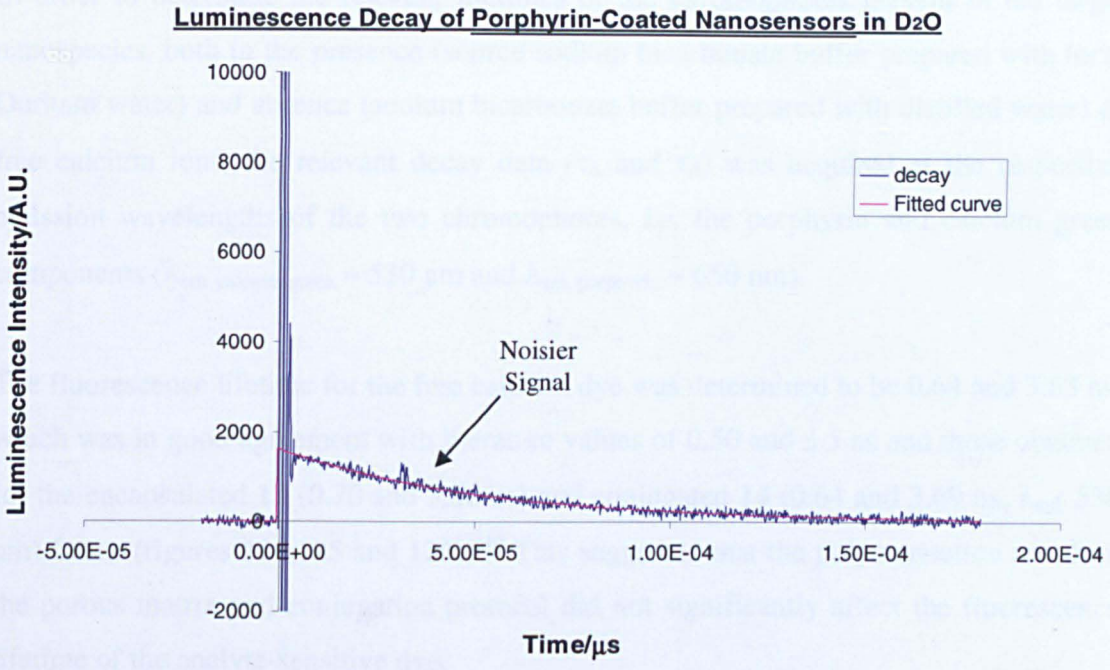

Figure 123 – Decay Curve of Porphyrin-Coated Nanosensors **14** Showing an Intensity Decrease of Nearly Fifteen Times Difference Compared to Figure 122 (Porphyrin), Highlighting the Absorption Problems of the Nanospecies

The "scattering" in the system may be a result of a number of factors including: (i) particle size, the larger the nanospecies are the more likely they are to scatter the excitation light; (ii) Brownian motion - the particles are dispersed, **not dissolved** in the sample, therefore there will be random movement in the sample which may cause light-diffusion problems; (iii) it may also be possible that the individual calcium green molecules entrapped within the nanospecies matrix "move" about in a different manner and at a different rate to the "nanospecies" themselves, *i.e.* the dye molecules have restricted movement within the porous matrix, affecting the luminescence observed; (iv) it may even be that it is not possible to obtain the required data from dispersion samples.

Further experiments were carried out to obtain the photophysical measurements for the calcium sensitive dye in its free, entrapped and coupled forms. The experiments were carried out as described for the above porphyrin investigations.

In order to determine the relevant lifetimes of the chromophores present in the target nanospecies, both in the presence (source sodium bicarbonate buffer prepared with local Durham water) and absence (sodium bicarbonate buffer prepared with distilled water) of free calcium ions, the relevant decay data (τ_{Δ} and τ_{fl}) was acquired at the respective emission wavelengths of the two chromophores, *i.e.* the porphyrin and calcium green components ($\lambda_{em.\ calcium\ green} \approx 530$ nm and $\lambda_{em.\ porphyrin} \approx 650$ nm).

The fluorescence lifetime for the free calcium dye was determined to be 0.64 and 3.63 ns, which was in good agreement with literature values of 0.50 and 3.5 ns and those obtained for the encapsulated **13** (0.70 and 3.50 ns) and conjugated **14** (0.64 and 3.69 ns, $\lambda_{em.}$ 530 nm) forms (figures 124,125 and 126).[340] This suggested that the polymerisation reaction, the porous matrix and conjugation protocol did not significantly affect the fluorescence lifetime of the analyte-sensitive dye.

It was also necessary to determine the same set of data ($\tau_{fl.}$) when the dye was in the presence of/chelated to free calcium ions. A fluorescence lifetime of 0.65 and 3.65 ns for the chelated "free dye", 0.50 and 3.54 ns for the sensors **13** and 0.55 and 3.77 ns for the target system **14**, agrees with the formed hypothesis (see section 3.9) that the calcium dye is "stable" to the polymerisation reaction, coupling protocol, with minimum effect on its "sensing ability". Further support would have been given to the hypothesis had it been possible to determine the quantum yield of fluorescence ($\Phi_{fl.}$) for the dye. Unfortunately, this was not possible as the nanospecies were scattering the excitation light and therefore, absorbing the laser energy in an inefficient manner (as demonstrated in figure 123); thus, hindering the collection of reliable data.

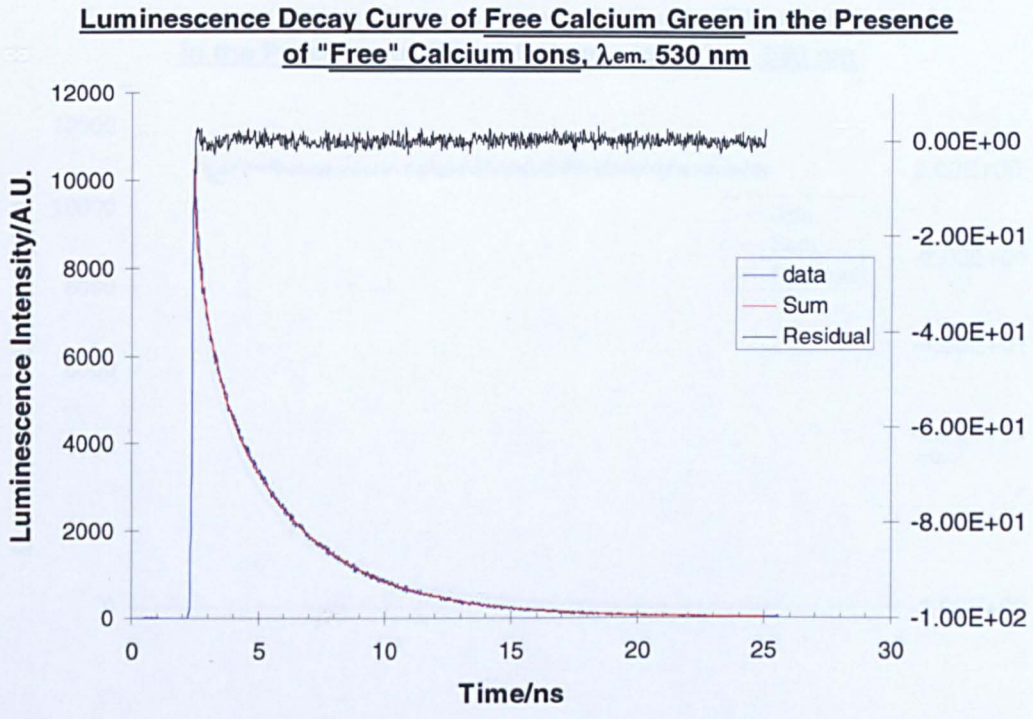

Figure 124 – Decay of Free Calcium Green (1.84 μmol dm^{-3} Solution) in the Presence of Free Calcium Ions, $\lambda_{em.}$ **530 nm**, Showing the Residual Centred About 0 (Offset on a Linear Scale)

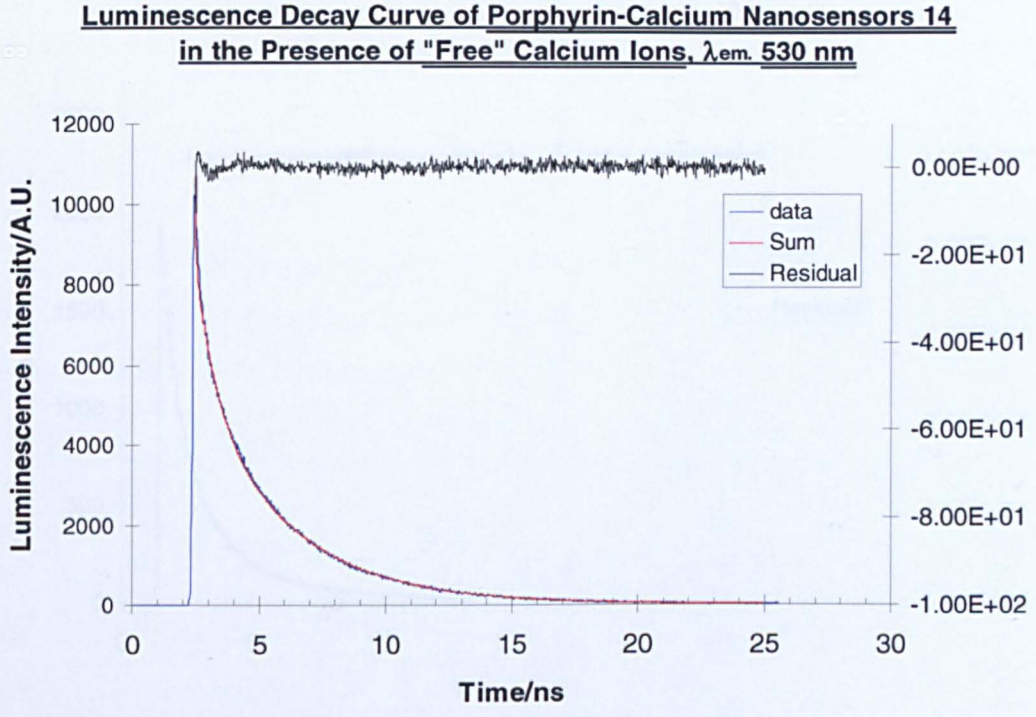

Figure 125 – Decay Curve of Porphyrin-Calcium Nanosensors **14** in the Presence of Free Calcium Ions, Luminescence Collected around Calcium Green $\lambda_{em.}$ **530 nm** Showing a Residual Centred about 0 (Offset on a Linear Scale)

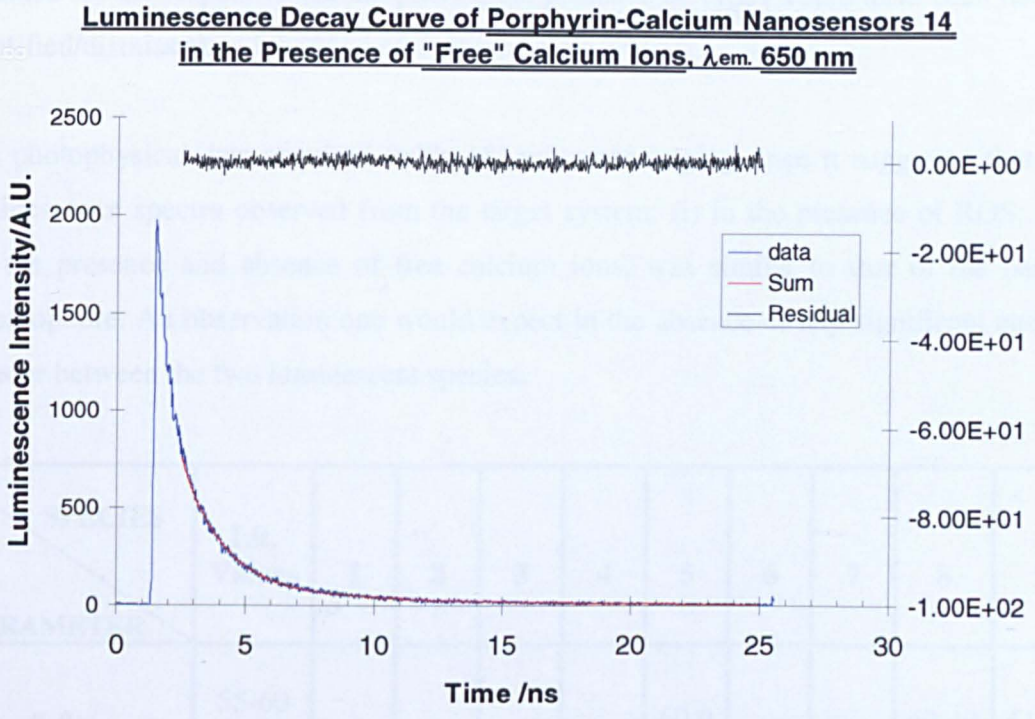

Figure 126 – Decay Curve of Porphyrin-Calcium Nanosensors **14** in the Presence of Free Calcium Ions, Luminescence Collected around Porphyrin $\lambda_{em.}$ **650 nm**, Residual Centred About 0 (Offset on a Linear Scale)

4.3.1 Energy Transfer

The final scenario that needed to be addressed was the presence of any significant energy transfer (E_T) between the two species. If a significant amount of energy was being transferred from one chromophore to the other, then the fluorescence lifetime of calcium green in its free-state would be greater than that for the fluorescence lifetime of the dye (calcium green) in the porphyrin-coated nanosensors **14**: k_{ET} reduces the fluorescence lifetime of a species (and the fluorescence quantum yield). This phenomenon could be easily ruled out since; the previously described experiments generated data within acceptable deviation ranges (±5 μs) for the different forms/states of the chromophore components, suggesting that their luminescent properties are not subject to interference from their neighbouring chromophore.[341] Had the fluorescence quantum yield data been

obtained for the respective chromophores, the presence of FRET could have been further identified/dismissed.

The photophysical data acquired (table 18) was encouraging since it suggested that the luminescence spectra observed from the target system: (i) in the presence of ROS; and (ii) the presence and absence of free calcium ions, was similar to that of the parent chromophore. An observation one would expect in the absence of any significant energy transfer between the two luminescent species.

SPECIES / PARAMETER	Lit. Values	1	2	3	4	5	6	7	8	9
$\tau_{\Delta}/\mu s$	55-60 (D_2O)	-	-	-	-	60.0	-	-	63.40	61.83
τ_{fl}/ns	0.50 and 3.5[337]	0.64 and 3.63	0.65 and 3.65	0.70 and 3.50	0.50 and 3.54	-	0.64 and 3.69	0.55 and 3.77	-	-
FRET	-	-	-	-	-	-	N	N	N	N

1 = free calcium green, 2 = free calcium green in the presence of free calcium ions, 3 = calcium green nanosensors **13**, 4 = calcium green nanosensors **13** in the presence of free calcium ions, 5 = free porphyrin **5**, 6 = porphyrin-coated nanosensors **14** ($\lambda_{em.}$ 530 nm), 7 = porphyrin-coated nanosensors **14** in the presence of free calcium ions ($\lambda_{em.}$ 530 nm), 8 = porphyrin-coated nanosensors **14** ($\lambda_{em.}$ 650 nm), 9 = porphyrin-coated nanosensors **14** in the presence of free calcium ions ($\lambda_{em.}$ 650 nm).

Table 18 - Table Comparing the Luminescence Lifetimes of the Calcium Green and Porphyrin Chromophores in Different States

Thus, all that remained to be accomplished was the successful delivery of the system into cells and the observation of their anticipated response to (*in situ* generated) ROS. Investigations regarding the intracellular nanospecies experiments are described in the following Chapter.

4.5 Summary and Conclusions

- Target porphyrin **5** generates singlet oxygen.
- Lifetime of singlet oxygen (60 ± 5 μs) generated from porphyrin **5** comparable to that from the porphyrin-nanospecies/nanosensor conjugates **12** and **14**; both consistent with published limits (55-60 μs).
- Fluorescence lifetimes for free-calcium sensitive dye (0.64 and 3.63 ns, ± 5 μs) correlated to those for the entrapped dye **13** (0.70 and 3.50 ns) and porphyrin-coated nanosensors **14** (0.64 and 3.69 ns). Also in agreement with the calcium-chelated nanosensors (0.5 and 3.5 ns) and literature values.
- No significant energy transfer observed between the two luminescent species.

The findings from the TCSPC spectroscopy measurements supported the postulation formed from the cholesterol assay (see sections 3.7 and 6.3) that singlet oxygen is produced by porphyrin **5**. Along with the lifetime data, it can be concluded that the coupling of the two luminescent species does not affect: the ability of the photosensitiser to form excited singlet/triplet states and hence, the generation of singlet oxygen; or the fluorescence properties of the calcium green dye. Minimal energy transfer between the two target system chromophores was also observed, supporting the theory that the two chromophores behave independently towards each other, with respect to luminescence.

4.6 Final Remarks

The results from this Chapter were encouraging in the realisation of the target nanosystem **14**.

Whilst the relative measurements of singlet oxygen-luminescence decay curves can be typically used to measure quantum yields of formation, in this Project, difficulties were encountered in determining the parameter for singlet oxygen generation and in determining the fluorescence quantum yield for calcium green (with regard to the target nanosystem). This was believed to be a result of the light scattering exhibited by the nanospecies. Had these data sets been available they would have given further evidence in support of the above findings; alternatively, they may have highlighted luminescent weaknesses present in the target system.

A number of variables may be attempted to try and remedy this shortfall. These potentially include: (i) reducing the size of the species; and/or (ii) by using a weaker, *i.e.* a lower "total/final" concentration of nanosystem that has a greater concentration of the calcium green entrapped within the nanospecies and is coated in a higher concentration of the target porphyrin, *i.e.* a weaker sample dispersion composed of a nanoconjugate which has an increased concentration of both chromophores. The latter method is not as desirable because the optimised ratio of porphyrin to calcium green for the system had been identified: it may not be possible to increase these components in the system by simply scaling their relative concentrations up, without inadvertently increasing the size of the nanospecies, *i.e.* the calcium green dye molecules may already be at a saturation level within the porous nanospecies matrix used. Also, increasing the size of the nanospecies would increase the problem of light scattering further. Another possibility may be to use a more sensitive detector/PMT, such as an infra-red PMT. Although, this would not have removed the light scattering issue, it may have been possible to obtain an increased luminescence signal from which the relevant quantum yields could be derived.

CHAPTER 5 CELLULAR STUDIES RESULTS AND DISCUSSION

5.1 Aims

The aim of developing a bifunctional sensing device, capable of selectively generating **small bursts** of reactive oxygen species (ROS), whilst simultaneously monitoring an intracellular response, has been described in the preceding Chapters. A high concentration of singlet oxygen/ROS is not desired since the cells under study may enter (unwanted) into late-stage apoptosis; a response similar to that reported by Oleinick for photodynamic photosensitisers.[52]

The major concern of this Project was the primary effect the cytotoxic species singlet oxygen has on the homeostasis of intracellular calcium ions: perturbations in calcium signaling pathways have been linked to a number of serious diseases (see section 1.3 particularly, 1.3.6). If the correlation between the altered calcium pathway(s) and ROS can be elucidated further, then one day, it may be possible to identify and control "mal-functioning" signaling pathways, potentially allowing the early detection, intervention and treatment of distressed, damaged and/or diseased cells.

The first step of such an endeavour would be to artificially recreate the distressed/diseased state in the cellular environment. One way in which this could be accomplished is through the use of photosensitisers (see sections 1.1.5, 1.1.6, particularly, 1.1.7 and 1.1.8). Delivering a photosensitiser to a cell and stimulating it to undergo electronic ISC and form singlet oxygen, is alone not sufficient to increase the knowledge surrounding the relationship between (i) cell behaviour and signaling pathways; and (ii) cellular damage and death.

These responses need to be observed almost instantaneous to the generation of ROS and this is where the target nanosensing system **14** comes into play: by attaching a luminescent sensing system directly to a photosensitiser it should be possible to simultaneously image select intracellular variations whilst generating the cytotoxic species *in situ*. The delivery of this system to the cells must be done in a manner which:

(i) primarily does not kill the cell or cause significant perturbations to the cellular environment (in its neutral non-excited form); this is a **key** requirement since it is most preferable that any cellular responses/changes come from the ROS stimuli and not a secondary effect; in addition (ii) the delivery of the system needs to be *via* a method which does not alter the sensing system itself.

There are a number of possibilities which can be explored to accomplish this delivery criterion (see section 1.4.7.9); two of which are highlighted in this Chapter (see section 5.2). Cellular localisation of the porphyrin-nanosensor system **14** and cellular response(s) to the device are also discussed.

All cellular investigations were generously undertaken at the Institute for Cardiovascular Research at The University of Leeds, U.K., in collaboration with Professor Chris Peers and Dr John Boyle.

5.2 Delivery Methods

The two key methods which were used to deliver the sensing system to the cells during the cellular investigations were the gene gun method and lipofection (see section 1.4.7.9). The lipofection method was the preferred technique since it is somewhat more "friendly" to the cells than the gene gun process. Nevertheless, the gene gun technique was attempted, with some success, as a second comparative delivery method.

5.2.1 Gene Gun Delivery

Although, it had appeared a considerable amount of the nanosystem **14** had been delivered inside the cells (human neuroblastoma cells, (SHSY5Y)), progress was not positive: a degree of the porphyrin-coated sensors **14** appeared to be located on the outer surface of the cells; an unexpected result since the technique essentially "fires" the sensing system into the cells *via* a release of high pressure. In addition to this anomaly, the expected positive (luminescent) response was not detected in relation to an additional calcium stimulus; the viability of the cells was also brought into question. Questions over

the health of the cells were not particularly surprising since the gene gun technique was developed for use with thick plant leaves/cells and by no means was it a delicate or "cell-friendly" method. It was therefore decided to concentrate on the lipofection protocol from which encouraging results were beginning to develop.

5.2.2 Lipofection Delivery

Lipofection essentially involves incubating liposomes with the target nanosystem **14**. The porphyrin-nanosystem **14** loaded liposomes then pass through a further incubation protocol with the cell-line of choice, through which the liposomes fuse with the cell membrane and release their contents (nanosystem) into the cytoplasmic fluid (cytosol).

A range of lipofection agents are commercially available, including Cellfectin®, Lipofectin® and Oligiofectamine™. Some of these are more specific to certain cell-lines, while others are more generalised (broad-spectrum reagents) with respect to the cell ranges they are compatible with.[342] Two of the commercially available lipofection reagents, Lipofectamine™ and *Trans*IT® 293, were utilised in the delivery of the target nanosystem **14** into the cells. The Lipofectamine™ reagent is the more general lipofection media, while TransIT® 293 is selective towards human embryonic kidney (HEK 293) cells.

5.3 Nanosensor Delivery

The porphyrin-coated nanosensors **14** were trialed with two different cell-lines: human neuroblastoma cells (SHSY5Y) and human embryonic kidney cells (HEK 293) with differing results. The sensors were successfully delivered into the human neuroblastoma cells *via* the Lipofectamine™ reagent (see section 6.6.1 for experimental protocol). The cells were imaged on a confocal scanning laser microscope (CLSM) and illuminated using the 488 nm argon-ion lasing line. The nanosystem **14** could be clearly observed (both the calcium green and porphyrin emissions were identified); they appeared to be located **within** the cells (figure 127). This was confirmed by producing "*z*-stack" images whereby, the nanosystem **did** indeed appear to be present inside the cells, *i.e.* the absence

of target system **14** protruding at the cell surface. This was an encouraging finding since it implied that both the target system and the cells were amenable to: (i) liposomes and (ii) cellular internalisation of the nanosystem, without significant alteration to the "health" of the cell or nanosystem. *Z*-stacks are images formed by "slicing" through the cell and recording the cellular image in a single focal plane (*z*-plane), these images are subsequently built-up generating a 3D image of the cell.

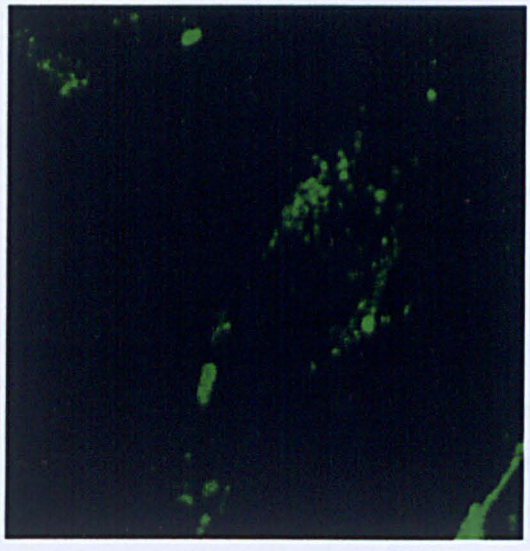

Green Channel –
Calcium Green Emission

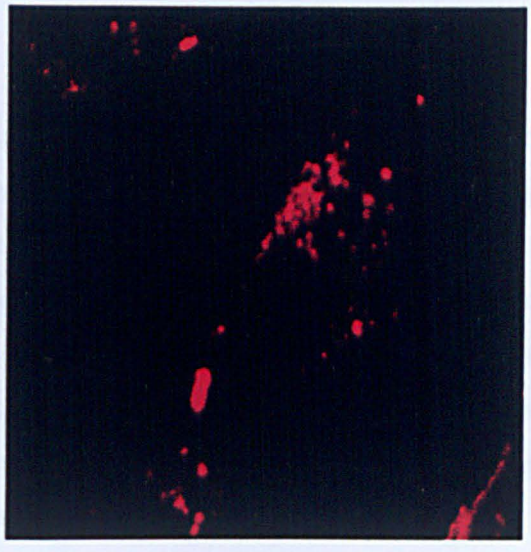

Red Channel –
Porphyrin Emission

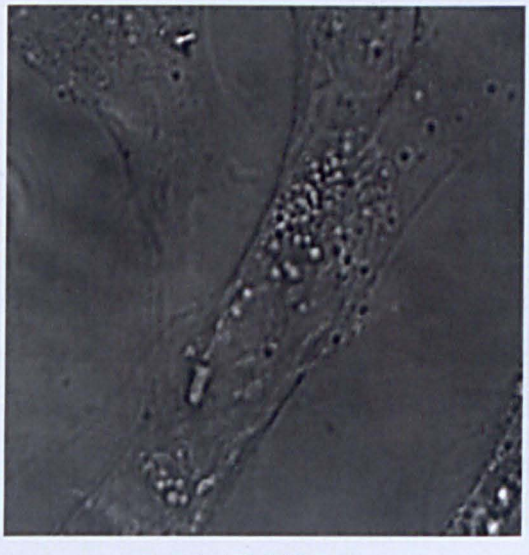

Bright Field View

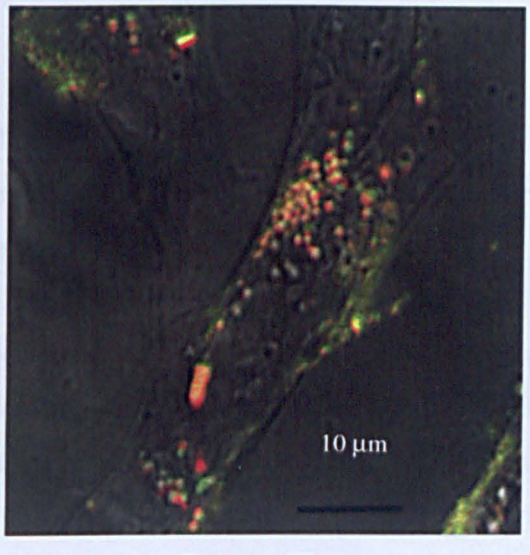

Overlay View

Figure 127 – Confocal Images of Human Neuroblastoma Cells Showing Internalised Porphyrin-Coated Nanosensors **14** Delivered *via* Lipofectamine™

5.4 Cellular Localisation

The cellular localisation of the sensing system **14** is potentially a very important property; different sub-cellular organelles are believed to be involved in the pathways leading to cell death at different times and with different levels of contribution (see section 1.2). To be able to image these organelles during the diverse stages and mechanisms involved in diseased and dying cells would be a major breakthrough in understanding the role these organelles play in cell disease and death. These sub-cellular organelles also present different susceptibilities towards death-promoting mechanisms and species. For example, mitochondria are thought to have a significant role in apoptosis (see sections 1.2 and 1.3 particularly, 1.2.2); thus, if the target nanosystem were to selectively localise in one sub-cellular region, further insight could be gained into the role that organelle and alterations to its calcium homeostasis play in cell death mechanisms.

The subcellular localisation of the nanosystem **14** can be investigated with commercial agents such as Lysotracker® and Mitotracker®. These are luminescent compounds which exhibit a specificity/affinity for lysosomes and mitochondria respectively. Cells are treated with the fluorescent markers and their subcellular localisation observed *via* CLSM. Through the use of these dyes the localisation properties of the target nanosystem **14** were investigated. Spectral data obtained suggested that the porphyrin-nanosensor conjugate **14** appeared to show no preference for either the lysosomes or mitochondria (figures 128 and 129). This was a little surprising since the porphyrin moiety **5** attached to the nanosensor was polycationic and it has previously been postulated that cationic species demonstrate a greater affinity for mitochondrial uptake/localisation (see section 1.1.8). It can be seen however, that the porphyrin-nanosystem **14** does appear to show some selective localisation, repeatedly accumulating around the inner membrane of the cells and not in the expected life-sustaining mitochondria (figures 127 and 129). A similar response for cationic nanoparticles has been reported by Euliss.[206,241]

Blue Channel –
Lysotracker® Emission

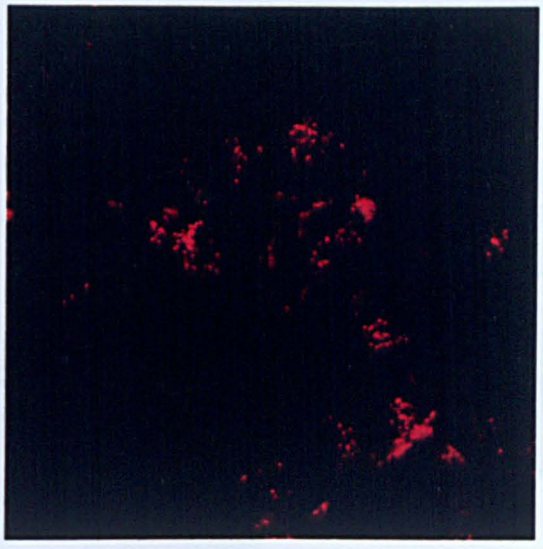

Red Channel – Porphyrin-Nanosensors **14**
Porphyrin Emission

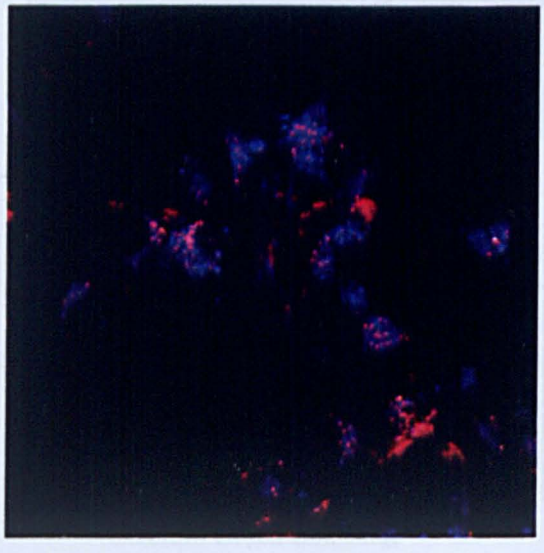

Overlay – No Light

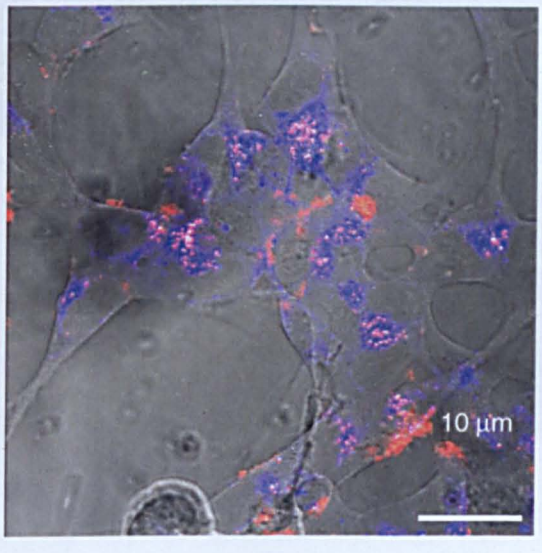

Overlay – Light

Figure 128 - Cells Loaded with Lysotracker® and Porphyrin-Calcium Nanosensors **14**

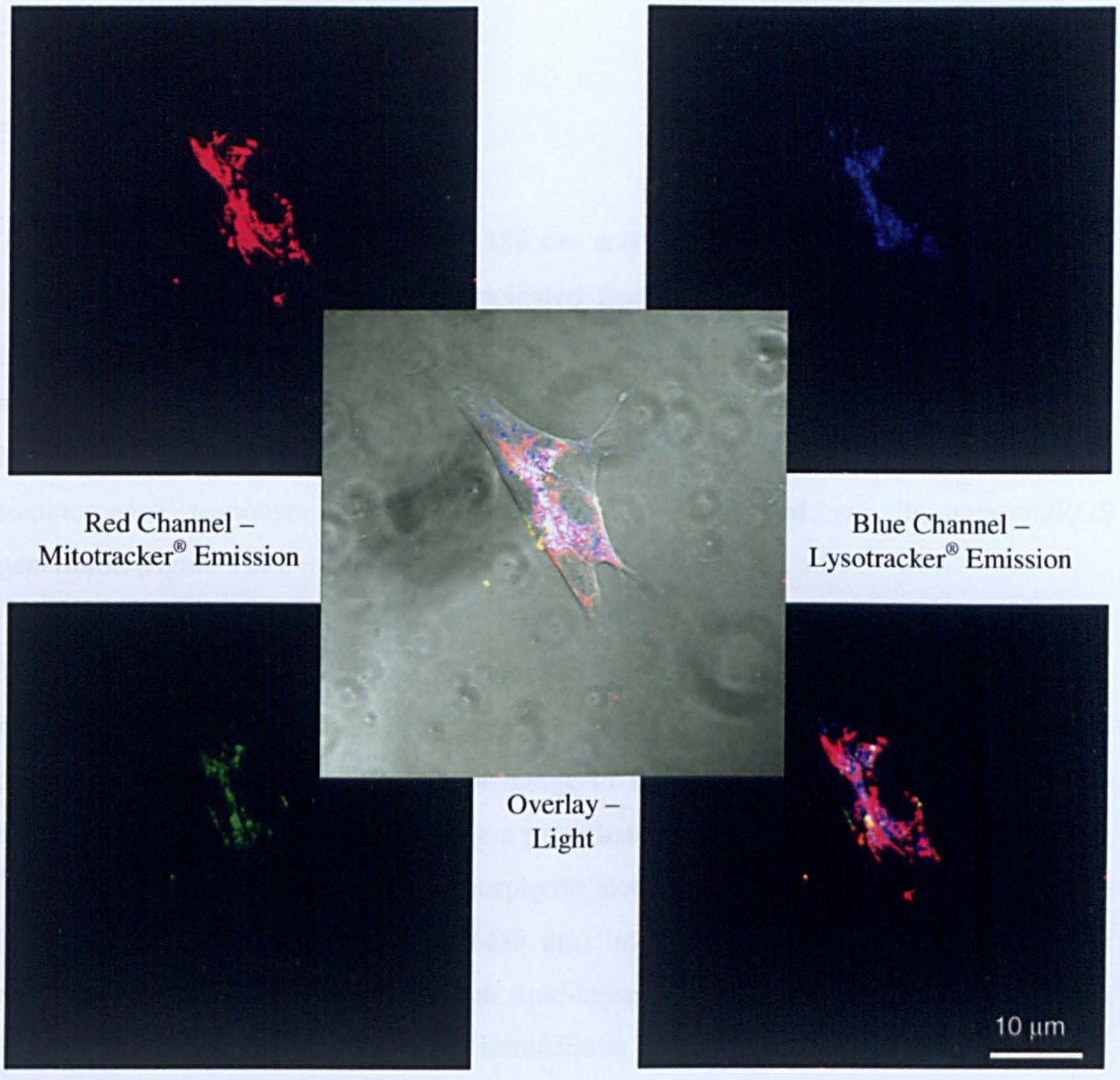

Figure 129 – Cells Loaded with Lysotracker®, Mitotracker® and Porphyrin-Calcium Nanosensors **14**

5.5 Cellular Response

5.5.1 Lipofectamine™

The nanosensors were illuminated at 488 nm and the green confocal channel (calcium green emission) observed. It was anticipated that if upon illumination, the porphyrin generated amounts of ROS sufficient to perturb the intracellular homeostasis of calcium, an increase in the fluorescence intensity of the calcium green fluorophore would be seen. However, it appeared for the human neuroblastoma cell-line, that there was no additional luminescence response from the sensors when stimulated *via* illumination/ROS generation (figure 127).

This raised a number of questions: (i) had the system degraded; (ii) had the sensors been inadvertently affected by the Lipofectamine™ reagent; (iii) were the sensors capable of detecting the appropriate concentration range of **intracellular** calcium ions; (iv) were enough ROS being generated to induce a perturbation in the intracellular calcium levels, *i.e.* was there significant amounts of porphyrin loaded onto the nanosensors and was the (porphyrin) sub-optimal wavelength (488 nm) intense enough to suitably activate the porphyrin; (v) was there a long enough time-lapse between irradiating the sensors/cells and imaging the system; and (vi) can intracellular calcium levels be elevated by singlet oxygen? Questions (i) to (v) were addressed in a number of ways.

Firstly, a porphyrin-nanosensor **14** aqueous solution was prepared and imaged under the CLSM. It was observed that the calcium green emission from the sensors/solution increased tremendously when tap water (Leeds) was added *in situ* to the solution; therefore, ruling out any degradation issues. Secondly, the sensor-loaded cells were irradiated (i) for a longer time period (10 seconds, 1 minute and 10 minutes) at 633 nm and (ii) with a greater laser power, to identify if ROS were being generated by the porphyrin, for which no real increase in calcium green fluorescence intensity was being observed in the sensors. Thirdly, the sensors/cells were observed post-illumination for a longer period of time (up to 10 minutes), to establish if there was a problem with the calcium ions permeating through into the polymeric matrix: this should not have

presented a significant problem since the calcium ions appeared to traverse the matrix quite readily when the sensors were investigated in solution; nevertheless, this remained a feasible problem *in vitro* since cells are a complex and heterogeneous environment.

Positive results were still not observed, therefore the second cell-line, human embryonic kidney cells (HEK 293), was investigated. It was anticipated that if similar results were observed for these cells, then the sensing system **14** as a whole may have needed re-addressing, *i.e.* (i) was there sufficient porphyrin loaded onto the sensors to generate ROS under the experimental (confocal) conditions employed and (ii) was the calcium sensitive fluorophore capable of detecting changes in **intracellular** calcium ions. However, if positive results were to be achieved with this second cell-line, suggestions would point to either a problem with (i) the lipofection agent and/or (ii) the cell-line investigated.

Transfection of the Lipofectamine™ media takes place at 90% confluence: this is not ideal since cells are not in their linear phase of growth at this range. Although, Lipofectamine™ is a relatively successful broad-spectrum transfection agent, it carries with it the issue of high cell-death rates; hence 90% confluence is preferable when using the reagent.

5.5.2 *Trans*It®

The porphyrin-nanosensor conjugates **14** were delivered to the human embryonic kidney cell-line using the lipofection reagent TransIT® 293. The protocol for the reagent is essentially the same as for the broad-spectrum Lipofectamine™ reagent. The main difference between the two routes is the selectivity of the TransIT® 293 media for the human embryonic kidney cell-line. This selectivity should increase the efficiency of nanosystem delivery into the cells with minimal affects to cell health.

The nanosensor-loaded cells were imaged on the confocal microscope under the same parameters as used with the human neuroblastoma cells. Once again, the sensor conjugates could be identified within the cell, with calcium green and porphyrin luminescence both clearly visible (figure 130). This observation was consistent with that

of the neuroblastoma cells, suggesting that both the target-nanosystem and the two cell-lines were amenable to lipofection delivery methods, without an undesirable affect on either the porphyrin or calcium green emission profiles, or more crucially, on the viability of the cells under study.

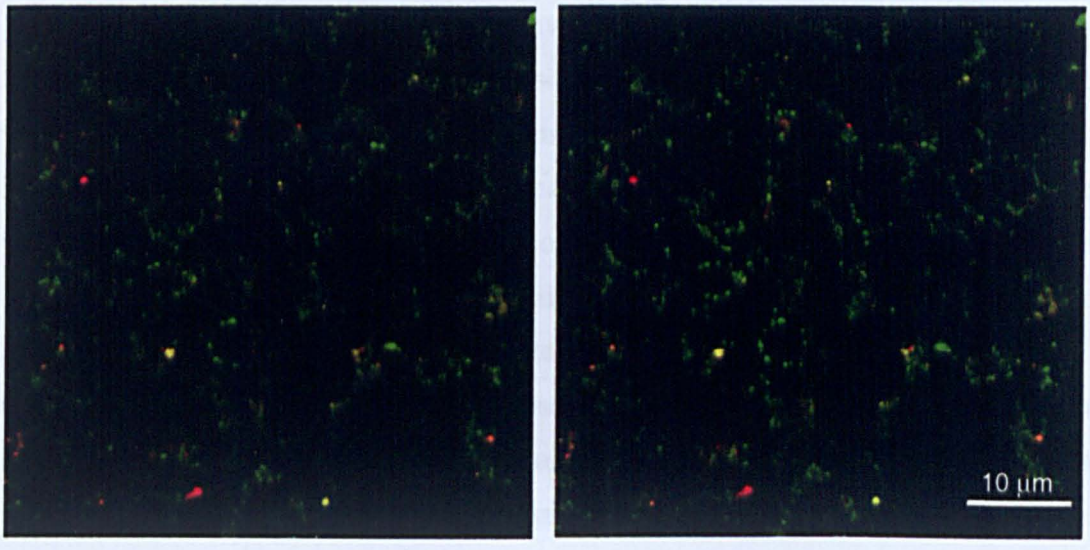

Overlay View - Control

Overlay View - 4 minutes Post-Stimulation

Figure 130 – Confocal Images of HEK 293 Cells Demonstrating Intracellular Localisation and a Calcium Response Four Minutes After Stimulation (Ionomycin)

The sensors were illuminated at 488 nm in anticipation of a ROS-stimulated calcium response. Unfortunately, like the neuroblastoma cells, a response was not observed in the embryonic kidney cell-line.

The response of the sensors was also tested *via* alternative calcium sources. A calcium ionophore (ionomycin) in a buffer (Kreb's) that is known to have free calcium ions present was used. These experiments were run in parallel to those using only the laser energy to stimulate the porphyrin, *i.e.* generate ROS. Hence, additional data could be gathered regarding the response of the calcium sensitive fluorophore. Results from these investigations differed from the observations of the "singlet oxygen-stimulated calcium

response" in a positive manner: an **increase** in fluorescence intensity of the calcium green dye was observed in response to **increasing** levels of **free calcium ions** (ionomycin, figure 130). The intensity of the luminescence increased further over a ten minute observation period (figure 131 and 132), following irradiation. This was a most encouraging result since it suggested that the nanosystem **14** was capable (through the luminescence signal of the calcium-sensitive dye) of "sensing" free calcium ions. These findings led to the hypothesis that the sensing device afforded **14**, was indeed capable of monitoring an analyte-specific variation intracellularly. This result supported the findings proffered by Kopelman - that changes in calcium levels can be monitored intracellularly by nanospecies.[306,309] Kopelman reported observing a fluorescence intensity increase of approximately five-fold from calcium crimson nanosensor-loaded cells (rat alveolar macrophages), which he had stimulated with the mitogen Concanavalin A.[309] Concanavalin A stimulates a cell to release calcium from its internal stores. Kopelman has also reported a similar result from nanosensors loaded with calcium green. These sensors were localised in human C6 glioma cells and the cells were stimulated to release calcium *via* the toxin *m*-dinitrobenzene. The increase in intracellular calcium ions was successfully observed through an increase in the fluorescence intensity of calcium green, monitored over a ten minute period.[306,309]

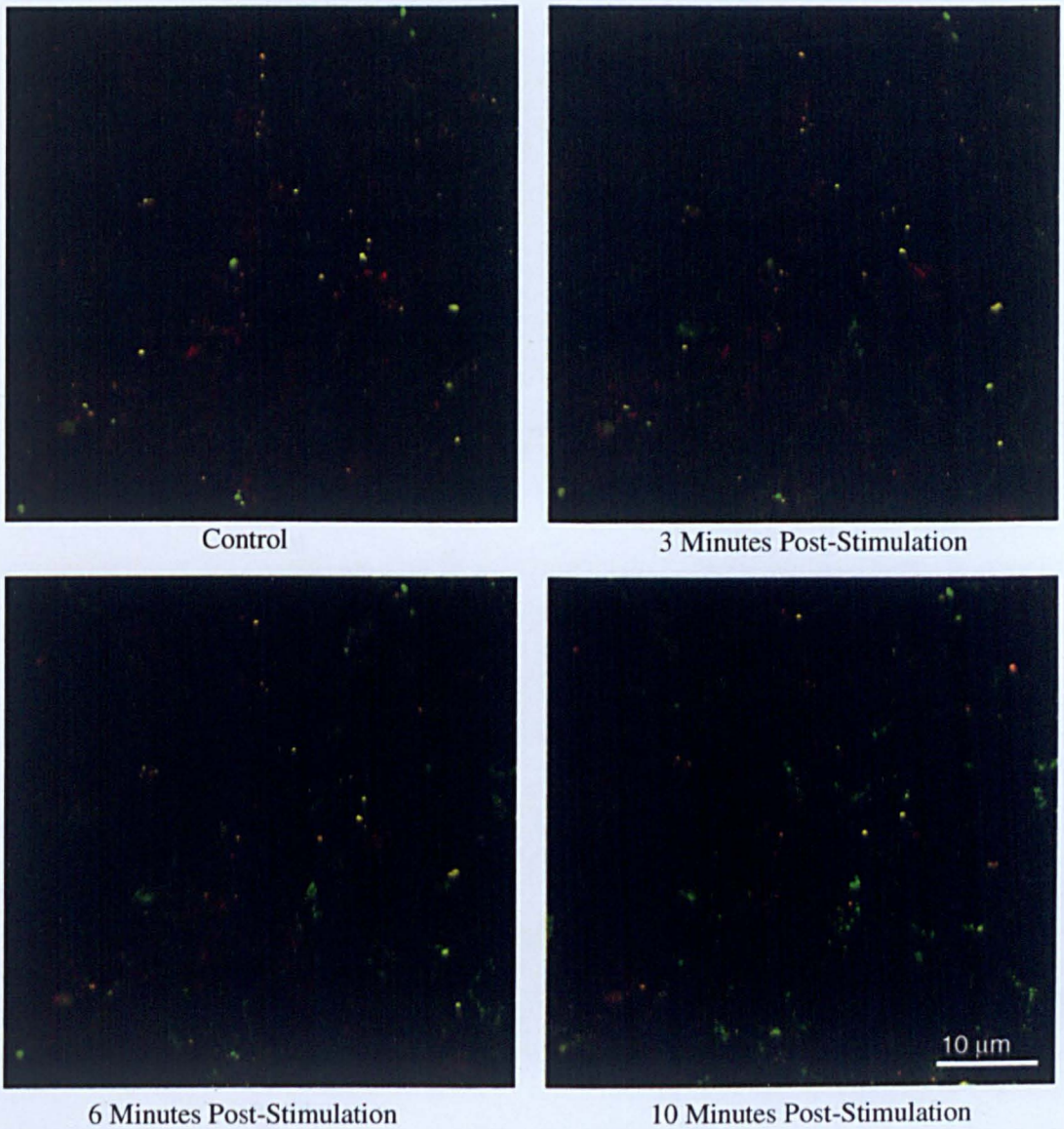

Figure 131 – Confocal Images (Overlay View) of Porphyrin-Nanosensor **14** Loaded HEK 293 Cells Post-Calcium Stimulation (Ionomycin), Showing Increasing Calcium Green (Green) Luminescence

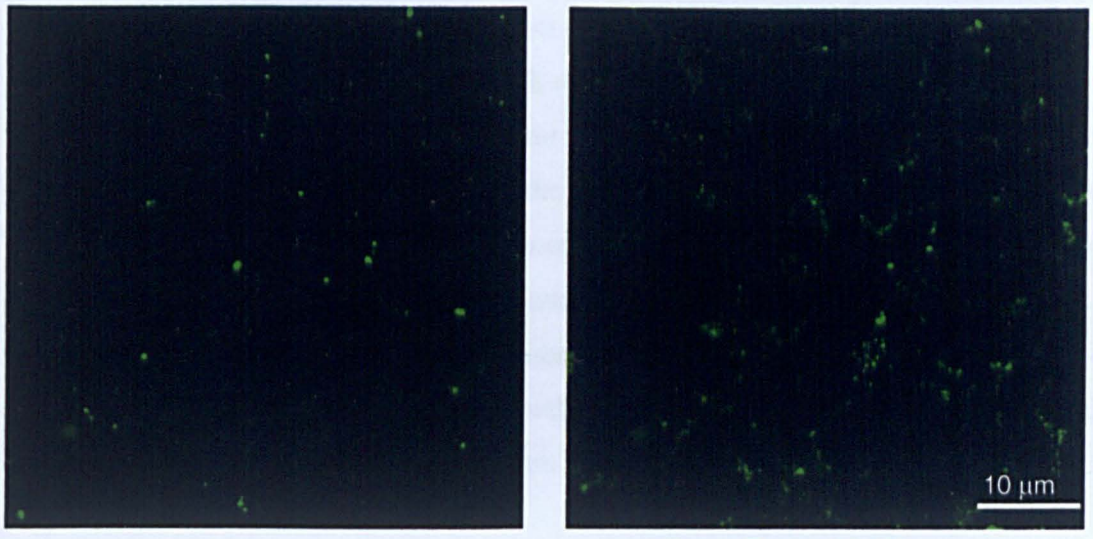

Control

Green Channel 10 Minutes Post-Stimulation

Figure 132 – Green Channel View (Overlay) of Figure 131 Confocal Images 10 Minutes Post-"Calcium" Stimulation

5.6 Summary and Conclusions

- Absence of positive results from gene gun delivery.
- Lipofection route repeatedly afforded viable nanosystem-loaded cells.
- Cell viability therefore appears dependent upon nanosystem delivery route.
- Successful nanosystem response appears to be dependent upon cell-line.
- Positive response detected/observed for porphyrin-nanosensor **14** loaded cells (*via* ionomycin).

The response of the porphyrin-nanosensor **14** to free calcium ions from an "artificial" stimulus was an encouraging result. However, further investigations must be conducted into the intracellular sensitivity range of the sensing system, along with the reproducibility of these findings for different cell lines and transfection reagents.

Investigations into the different ROS concentration ranges and their effect on cell death pathways may also prove informative with regard to the ROS "tolerance" levels of a cell. Such investigations could be conducted through: (i) varying the level of porphyrin-coat present on the nanosensors; (ii) varying the fluence rate; and (iii) the irradiation power. These variables would allow different concentrations and durations of ROS bursts to be generated, *i.e.* a system could be fine-tuned to induce (i) **minimal** perturbations to intracellular signaling pathways/mechanisms which could be further increased to (ii) more **rapidly** induce the cell death pathways apoptosis and necrosis; potentially, affording a multi-functional sensing system.

OVERALL CONCLUSION FOR THE PROJECT

The aim of this Project was to create a tool capable of selectively monitoring/observing intracellular signaling ions in response to oxidative stress. It was postulated that this could be achieved through the use of a fluorescence dye and a species (a photosensitiser) capable of generating *in situ* reactive oxygen species (ROS).

Although, fluorescent probes and photosensitiser species have been used in their free-states to image physiologically relevant ions/molecules, they carry with them a number of problems. In particular, difficulties associated with controlling their subcellular localisation and concentration. It was hypothesised that through the use of nanotechnology and photosensitiser chemistry these drawbacks could be minimised/removed.

This Project was particularly concerned with monitoring the effect ROS/oxidative stress has on the intracellular homeostasis of the major cellular signaling ion calcium; believed to be involved in a number of diseased states. In this respect, it was envisaged that through ROS-induced oxidative stress, a perturbation to the intracellular homeostasis of calcium could be accomplished. This was achieved synthetically by generating and coupling an amino-functionalised nanospecies **13** (loaded with a calcium sensitive fluorophore) to a tricationic isothiocyanato-porphyrin **5**.

The main difficulties encountered in this Project were in relation to the generation of the polymeric nanospecies. These problems were resolved by ensuring that the microemulsion/polymerisation reaction system was completely free from (any unwanted) free radical scavengers. This was achieved through the thorough and repeated deaeration of the reaction mixture.

Photophysical studies of the optimised porphyrin-nanosensor conjugate **14** suggested that: (i) the porphyrin component **5** of the sensing system was indeed capable of generating singlet oxygen; and (ii) that the two system chromophores were both stable with respect to their individual luminescent properties and the target system. It was also

(importantly) determined that there was no energy transfer between the two chromophores in the target nanosensor. These findings gave support to the successful formation of a porphyrin-nanosensor conjugate **14**, capable of generating ROS and reporting variations in free calcium ion concentration, with minimum energy transfer between the analyte sensitive fluorophore and the photosensitiser (in solution).

Having established the ability of the target nanosystem to generate ROS and chelate free calcium ions in solution, the target system was evaluated *in vitro*. The cellular studies undertaken suggested that the porphyrin-nanosensor conjugate **14** had been successfully loaded into two cell-lines and was sensitive towards intracellular calcium dyshomeostasis (evoked by ionomycin). Unfortunately, the target nanosystem did not appear to generate (*via* changes in intracellular calcium concentrations) identifiable levels of ROS *in situ*, under the experimental conditions used. Clearly, the *in situ* generation of ROS is a crucial element of the target nanosystem; therefore, before any significant progress can be made in developing the target sensing system (as a bifunctional intracellular nanosensor) a number of questions must be considered. These include: (i) the possibility that 10 minutes is insufficient time to monitor changes in intracellular calcium levels – the intracellular calcium storage organelles are stimulated *via* global signals and therefore there may be a time delay before any (significant) release of calcium ions is observed; (ii) is singlet oxygen generated when the photosensitiser is irradiated at 488 nm? Singlet oxygen is detected when the photosensitiser is illuminated with a red or white light source (see section 3.7) and when excited at 355 nm (see section 4.3); however, it may be that no/very little singlet oxygen is generated when the photosensitiser is irradiated at 488 nm; and finally, (iii) perhaps the photosensitiser is indeed generating singlet oxygen *in situ* but the case may be that singlet oxygen does **not** have an observable effect on intracellular calcium levels.

However, despite the "lack" of intracellular/*in situ* generation of ROS, the target system generated may still have potential as a cellular sensing tool. The findings from the photophysics and solution investigations suggested the target nanosensor does generate singlet oxygen and is capable of detecting free calcium ions; the latter finding was further supported by evidence from the cellular studies. One potential solution could be to vary

the concentration of the porphyrin coat loaded onto the nanosensor. Therefore, by modifying the chromophore(s) concentration(s) and/or the cellular experimental parameters, it may be possible to "fully" achieve the desired target system.

Since oxidative stress can initiate cell death and the concentration of the photosensitiser (porphyrin) coat on the nanosensor can be varied, there is a potential to create a tool capable of generating a variety of ROS concentrations, *i.e.* the ability to elicit a wide range of disturbances to the homeostasis of intracellular calcium (ranging from a slight disturbance to a lethal disruption) is possible. Should the generation of intracellular/*in situ* ROS, from the target system developed in this Project, be optimised (with regards to generating intracellular calcium dyshomeostasis), the development of an "effective" bifunctional intracellular sensing device could be close to realisation. Such an event could potentially help to highlight/identify key markers involved in disease states.

CHAPTER 6 EXPERIMENTAL

6.1 Materials and Methods

- All reagents were purchased from Sigma-Aldrich, Lancaster, Avocado or Polymer Sciences unless otherwise stated. Solvents were obtained in house, both the reagents and solvents were of the highest purity grades available.
- The calcium green dextran dye used was a 10,000 Da dextran conjugate, purchased from Invitrogen, Paisley, U.K..
- Lipofectamine™ and *Trans*It® were all purchased from Invitrogen, Paisley, U.K..
- All water used was deionised, ELGASTAT Prima Reverse Osmosis unless otherwise stated.
- Analytical thin layer chromatography was carried out using Merck kGaA, Germany, aluminium backed silica-coated plates, silica gel 60 F_{254}, which were visualised using ultra-violet light 365 nm or iodine vapour.
- Column chromatography was carried using EcoChrom, MP silica 32-63, 60Å silica gel.
- ^{1}H NMR and ^{13}C NMR spectra were recorded on a JEOL JNM-LA400 FT NMR spectrometer. ^{1}H NMR were acquired at 400 MHz and ^{13}C NMR at 100 MHz. All NMR were acquired in solvents as indicated and chemical shifts (δ) are quoted in parts per million (ppm), measured downfield relative to tetramethylsilane (TMS). Coupling constants are quoted in hertz (Hz).
- Mass spectra were recorded using either a Brucker Reflex IV MALDI-TOF, a Shimadzu QP5050A GC/MS, 70 eV, EI or a Thermo-Finnigan LCQ Classic electrospray mass spectrometer system. Samples were run in the absence of a matrix unless otherwise stated.
- Ultra-violet visible spectra were recorded on a Agilent 8453 diode array spectrophotometer, uv-vis Chemstation software, Agilent Technologies, Cheshire, U.K., in solvents as indicated.
- High performance liquid chromatography analysis was performed using a high pressure liquid chromatography system with an MD-1515 ultra-violet visible

multi-wavelength detector, PU-1580 intelligent HPLC pump, HG-1580-32 dynamic mixer and an AS-1555 intelligent autosampler all from Jasco Limited, Essex, U.K..

- Fluorescence spectra were recorded on a SLM Aminco-Bowman Series 2 Luminescence Spectrometer with a continuous wave xenon lamp, SLM AB2 software, in solvents as indicated and a band-pass setting of 4 nm, SLM Instruments, Illinois, U.S.A..
- Cuvettes used were a Starna optiglass 2, type 23, optical glass, 10 mm and a VWR International, uv-vis. Optical glass, 10 mm, from Starna, Hainault and VWR International, Leicestershire, U.K.
- Ultra-violet lamp, CAMAG, UVLS-28, long/short wave assembly (254 nm and 365 nm), 230 V, ~50 Hz, 0.16 A, 95-0201-02, UVP, Upland, CA 91786, U.S.A..
- Autoclavable Nichiryo Nichipet Ex Plus micropipettes (Japan) were used for measuring/pipetting small volumes.
- Centrifugation was carried out using a P Selecta Centronic S-577 centrifuge, Lab-Plant, Laboratory Instruments and Equipment, Huddersfield, U.K..
- A Millipore filter unit (fritted glass) with 0.02 μm, 25 mm, Whatman Anodisc 25 filters were used to recover the nanospecies.
- A MS 2 Minishaker was used for mixing fluorescence solutions, 1,800 revolutions per minute (rpm) for 20 seconds, IKA, Staufen, Germany.
- Photocorrelation spectra were recorded on a Malvern Zetasizer 1000/2000/3000, Malvern Instruments Limited, Worcestershire, U.K..
- The rotator used for the coupling reactions was a Stuart Scientific Blood Tube Rotator SB1, Wolf Laboratories Limited, York, U.K..
- The pump used in the cholesterol assays was a Fisherbrand® dry vacuum pump/compressor, FB70150, Leicestershire, U.K..
- The white light source was a 3M Overhead Projector, 1700 A4, Visual Systems Division, Austin, Texas, U.S.A..
- The Paterson Pdt Lamp, BL1000A, Glens 100 367 0134 filter and Omnilux EL1000A light sources were from Phototherapeutics Limited, Altrincham, U.K..

- The power meter used to determine the light does with the different light sources used in the cholesterol assay was a portable radiometer, model R203 from Macam Photometrics Limited, Livingston, U.K..
- Tubes used in preparation of liposomes/lipofection medium-nanospecies complexes were B D Falcon round bottomed polystyrene tubes, BDB Biosciences, Erembodegem, Belgium.
- All cell images were obtained with a C-Apochromat x40 oil immersion lens on a Zeiss (U.K.) Axiovert 200 M inverted microscope fitted with a Zeiss LSM 510 laser-scanning module.

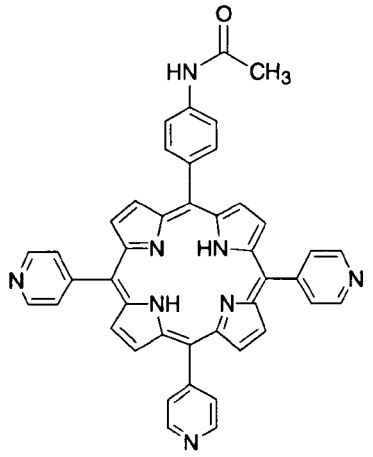

1

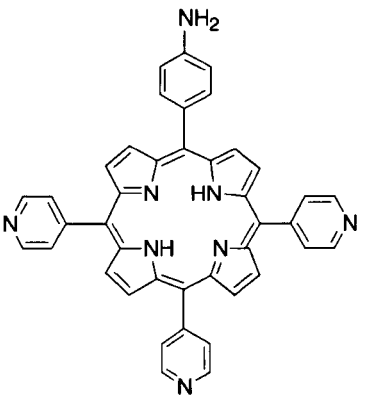

2

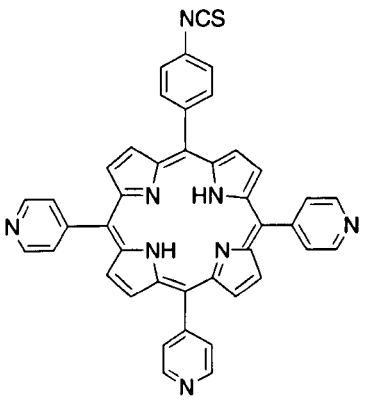

3

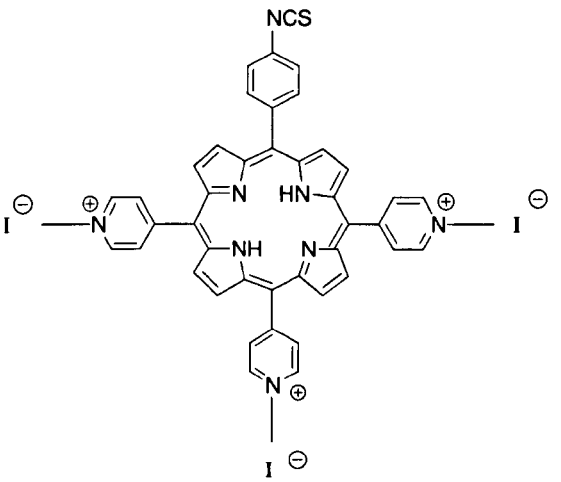

4

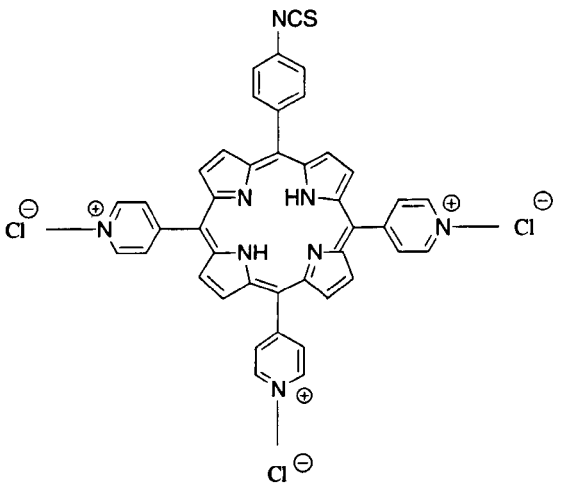

5

Scheme 22 - Porphyrin Molecules **1-5**

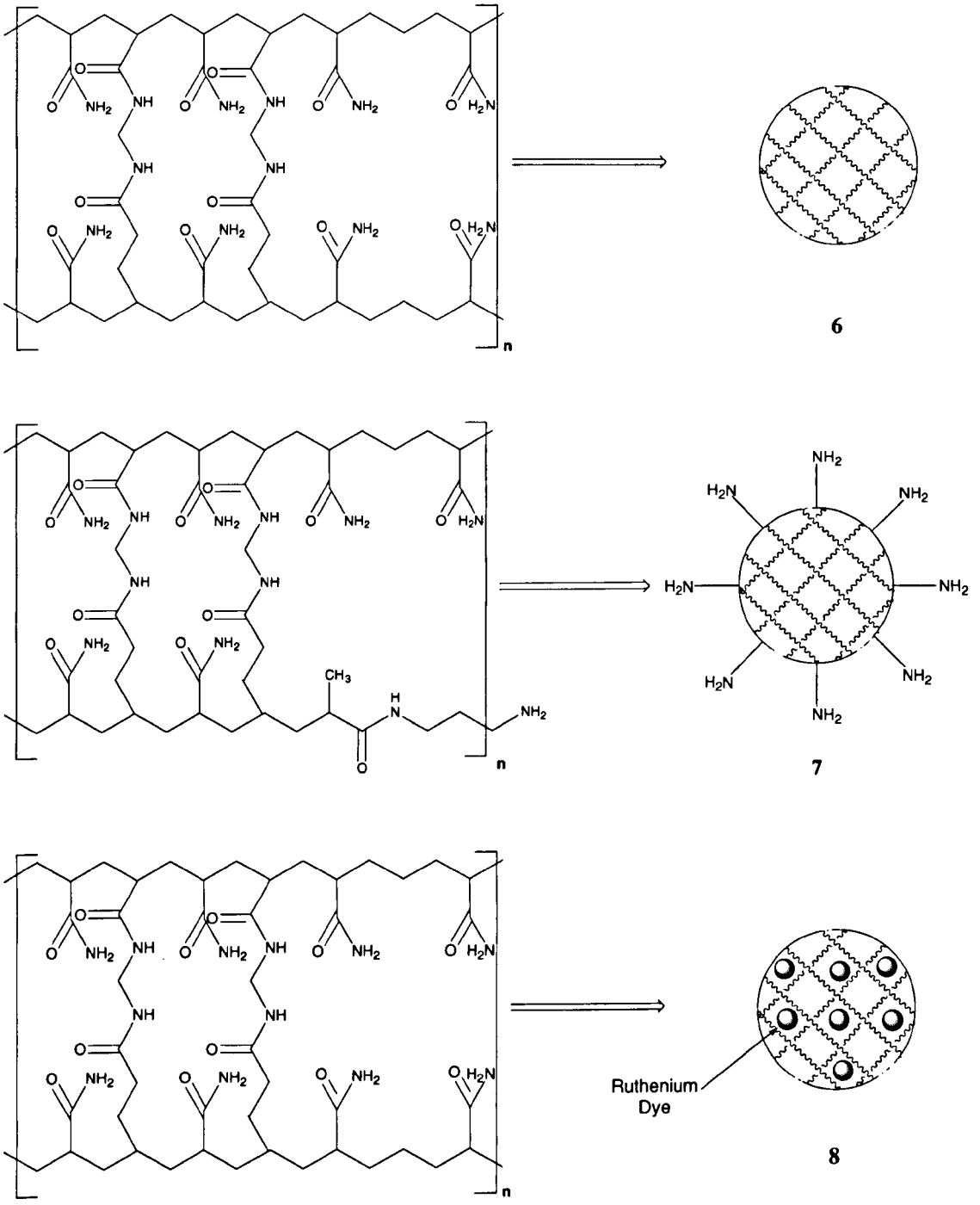

Scheme 23 – Nanospecies/sensors **6-8**

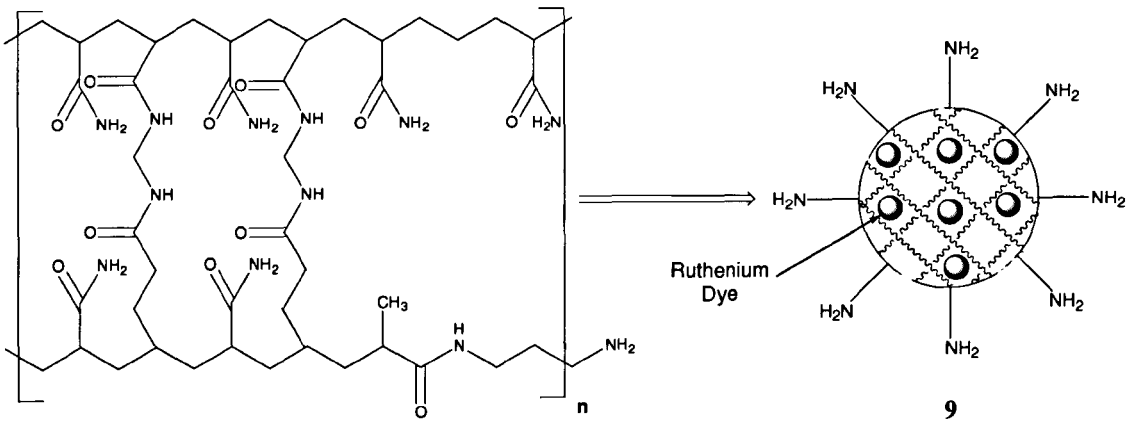

9

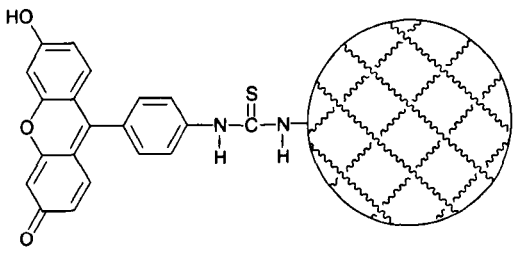

10

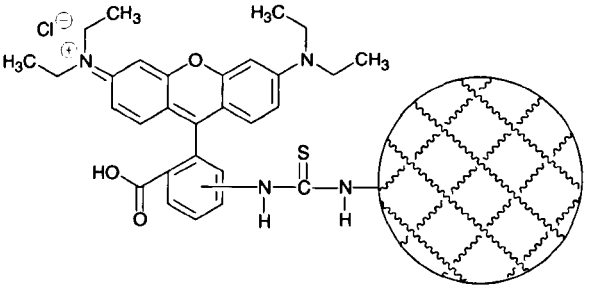

11

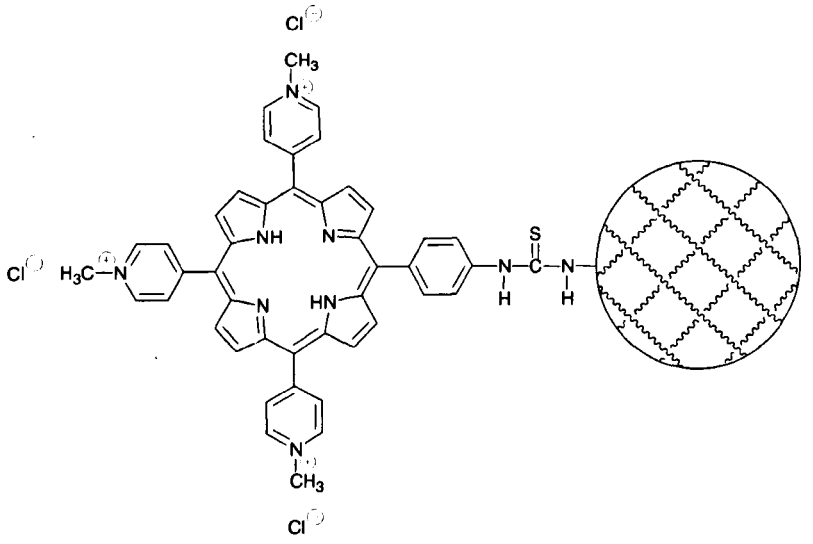

12

Scheme 24 – Nanosensors/species **9-12**

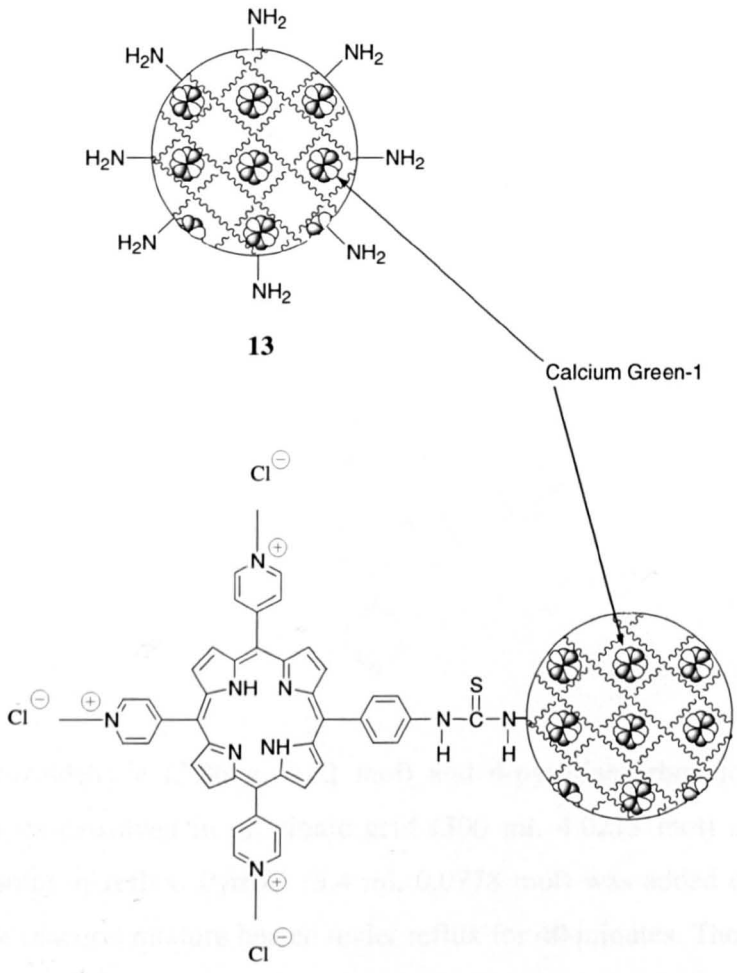

Figure 25 – Nanosensors **13-14**

6.2 Organic Synthesis

5-(4-Acetamidophenyl)-10,15,20-tri-(4-pyridyl)porphyrin 1

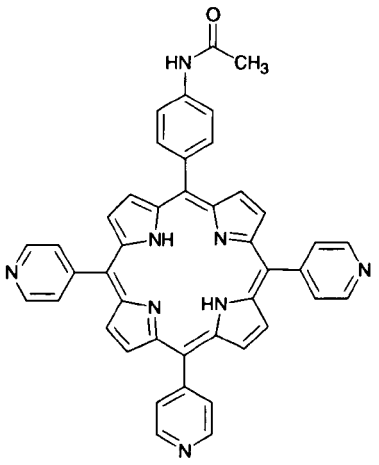

4-Acetamidobenzaldehyde (3.26 g, 0.02 mol) and 4-pyridinecarboxaldyhyde (5.7 ml, 0.0605 mol) were dissolved in propionic acid (300 ml, 4.0213 mol) and the solution heated to the point of reflux. Pyrrole (5.4 ml, 0.0778 mol) was added drop wise to the solution and the reaction mixture heated under reflux for 40 minutes. The cooled reaction mixture was then concentrated *in vacuo* to yield a dark purple solid. The crude purple solid was purified by column chromatography on silica (50 g) using a chloroform/methanol mixture (18:2) as the eluent. The relevant fractions were combined, dried (Na_2SO_4) and concentrated *in vacuo* to yield the desired porphyrin **1** (980 mg, 7%) as a purple solid.

Mp >350°C (decomp.); R_f = 0.56 (silica, $CHCl_3$/MeOH, 18:2); λ_{max}($CHCl_3$)/nm 419, 515, 550, 583 and 646; δ_H(400 MHz; $CDCl_3$; TMS) -2.8912 (2H, br, s, N*H*), 2.3835 (3H, s, $COCH_3$), 7.1489-7.1692 (2H, d, $^3J_{HH}$ = 8.1, 5-*m*-Ar*H*), 7.9362-7.9566 (2H, d, $^3J_{HH}$ = 8.1, 5-*o*-Ar*H*), 8.1462-8.1609 (6H, m, 10+15+20-*o*-pyr*H*), 8.8520 (6H, s, β*H*) and 9.0332-9.0479 (6H, m (overlapping), 10+15+20-*m*-pyr*H* and 2H, β*H*); *m/z*(MALDI, no matrix) 675.67 (M + 1, 100%).

5-(4-Aminophenyl)-10,15,20-tri-(4-pyridyl)porphyrin 2

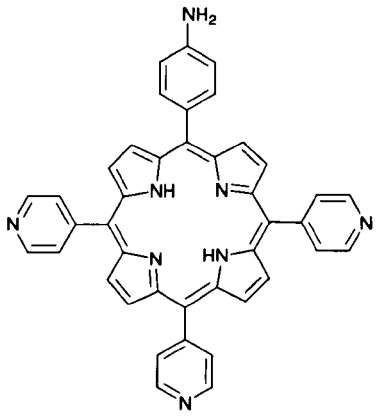

Porphyrin **1** (500 mg, 0.7410 mmol) was dissolved in 18% hydrochloric acid (100 ml) and the solution heated under reflux for 2 hours. The hot reaction mixture was concentrated *in vacuo* to yield a crude green solid. The solid was dissolved in a mixture of dichloromethane/triethylamine (9:1, 180:20 ml) and stirred for 10 minutes at room temperature. The solution was then washed with water (3 x 200 ml) and saturated brine (200 ml), the organic layer was separated, dried (Na_2SO_4) and concentrated *in vacuo* to yield a crude purple solid. The solid was purified by column chromatography on silica using a chloroform/methanol mixture (18.5:1.5) as the eluent. Relevant fractions were combined, dried (Na_2SO_4) and concentrated *in vacuo* to yield the desired amine functionalised porphyrin **2** (314.30 mg, 67%) as a purple solid.

Mp >350°C (decomp.); R_f = 0.31 (silica, $CHCl_3$/MeOH, 18.5:1.5); λ_{max}($CHCl_3$)/nm 419, 517, 554, 591 and 648; δ_H(400 MHz; $CDCl_3$/MeOD; TMS) -2.8652 (2H, br, s, N*H*), 4.301 (2H, br, s, NH_2), 7.1140-7.1341 (2H, d, $^3J_{HH}$ = 8.0, 5-*m*-Ar*H*), 7.9806-8.0007 (2H, d, $^3J_{HH}$ = 8.0, 5-*o*-Ar*H*), 8.2123-8.2219 (6H, d, $^3J_{HH}$ = 3.8, 10+15+20-*o*-pyr*H*), 8.8000-8.8442 (6H, m, β*H*) and 9.0037-9.0134 (6H, dd (overlapping), $^3J_{HH}$ = 3.8, 10+15+20-*m*-pyr*H* and 2H, β*H*); δ_C(100 MHz; $CDCl_3$/MeOD) 113.5 (5-*m*-Ar*C*), 116.0 (β*C*), 116.7 (β*C*), 120.3 (*mesoC*), 122.8 (*mesoC*), 129.5 (10+15+20-*o*-pyr*C*), 131.1 (5-Ar*C*), 135.6 (5-*o*-Ar*C*), 146.6 (α*C*), 147.4 (α*C*), 149.1 (10+15+20-*m*-pyr*C*), 150.6 (10+15+20-pyr*C*) and 150.7 (5-*p*-Ar*C*); *m/z*(MALDI, no matrix) 632.30 (M^+, 100%).

5-(4-Isothiocyanatophenyl)-10,15,20-tri-(4-pyridyl)porphyrin 3

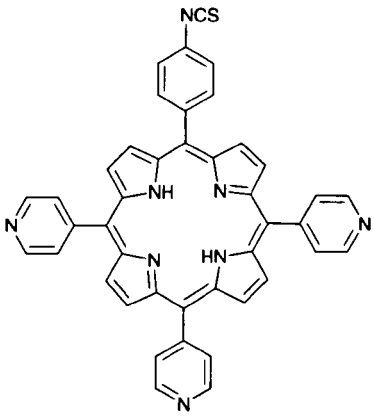

1,1'-Thiocarbonyldi-2(1H)-pyridone (117.20 mg, 0.5046 mmol) was added to a stirred solution of porphyrin **2** (160 mg, 0.2529 mmol) dissolved in freshly distilled dichloromethane (32 ml). The reaction mixture was allowed to stir under argon for 6 hours at room temperature and upon completion was concentrated *in vacuo* to yield a dark purple solid. The crude solid was purified by column chromatography on silica using a chloroform/methanol mixture (49:1) as the eluent. Relevant fractions were combined, dried (Na_2SO_4) and concentrated *in vacuo* to yield the desired isothiocyanato functionalised porphyrin **3** (158.69 mg, 93%) as a purple solid.

Mp >350°C (decomp.); R_f = 0.56 (silica, $CHCl_3$/MeOH, 49:1); λ_{max}($CHCl_3$)/nm 419, 517, 554, 591 and 648; δ_H(400 MHz; $CDCl_3$; TMS) -2.9048 (2H, br, s, N*H*), 7.6436-7.6646 (2H, m, 5-*m*-Ar*H*), 8.1536-8.1644 (6H, m, 10 + 15 + 20-*o*-pyr*H*), 8.1660-8.1870 (2H, m, 5-*o*-Ar*H*), 8.8429-8.8771 (8H, br, s, β*H*) and 9.0593-9.0701 (6H, m, 10+15+20-*m*-pyr*H*); *m/z*(MALDI, DCTB matrix) 675.20 (M + 1, 100%).

5-(4-Isothiocyanatophenyl)-10,15,20-(4-*N*-methylpyridiniumyl)porphyrin triiodide 4

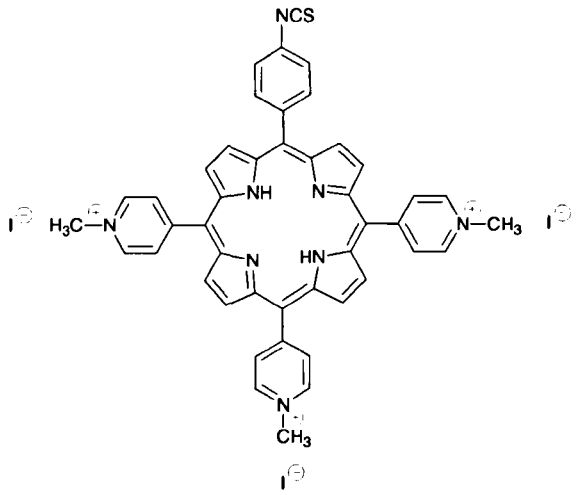

Iodomethane (1.94 ml, 0.0312 mol) was added to a stirred solution of porphyrin **3** (97 mg, 0.1437 mmol) in anhydrous dimethylformamide (19.4 ml). The reaction mixture was allowed to stir under argon for 3½ hours at room temperature and was monitored by thin layer chromatography (TLC) using a water/saturated aqueous potassium nitrate/acetonitrile mixture (1:1:8) as the solvent system. Upon completion the reaction mixture was concentrated *in vacuo* to yield the desired triiodide porphyrin **4** (143.90 mg, 91%) as a purple solid.

Mp >350°C (decomp.); R_f = 0.20 (silica, H_2O/saturated $KNO_3^-{}_{(aq)}$/MeCN, 1:1:8); *HPLC* t_R = 12.10 minutes, 97% (flow rate 1 min ml^{-1}; eluent A H_2O plus 0.1% trifluoroacetic acid (TFA); eluent B MeOH; gradient 0 min. 0% B; 10 min. 75% B; 15 min. 75% B and 19 min. 0% B); λ_{max}(MeOH)/nm 426, 518, 554, 592 and 648; δ_H(400 MHz; $CDCl_3$; TMS) -3.0430 (2H, br, s, N*H*), 4.6069 (9H, br, s, CH_3-pyr), 7.6919-7.7130 (2H, m, 5-*m*-Ar*H*), 7.7846-7.8008 (6H, d, $^3J_{HH}$ = 6.5, 10+15+20-*o*-pyr*H*), 8.2678-8.2889 (2H, d, $^3J_{HH}$ = 8.4, 5-*o*-Ar*H*), 8.9497-8.9664 (8H, br, s, β*H*) and 9.3696-9.3858 (6H, d, $^3J_{HH}$ = 6.5, 10+15+20-*m*-pyr*H*); *m/z*(MALDI, no matrix) 719.69 (M + 1, 100%), 704.64 (12, M-CH_3), 689.58 (7, M-2CH_3) and 676.76 (3, M-3CH_3); (ES) 719.30 (100%).

5-(4-Isothiocyanatophenyl)-10,15,20-(4-*N*-methylpyridiniumyl)porphyrin trichloride 5

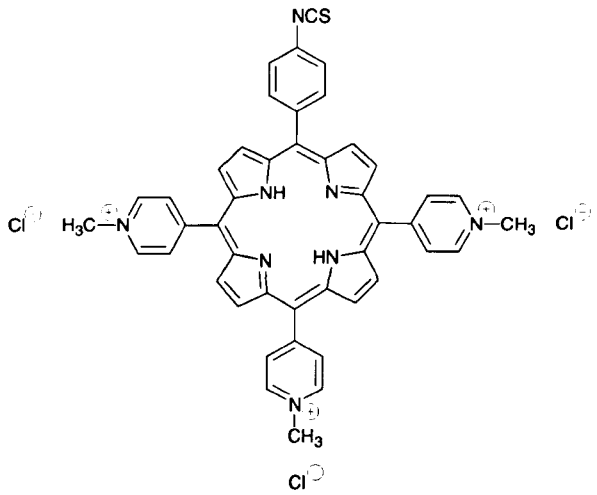

Amberlite® IRA 400 (Cl^- form, 2.3 g) was added to a stirred solution of porphyrin **4** (69 mg, 0.0627 mmol) in anhydrous methanol (69 ml, 1.7035 mol). The reaction mixture was allowed to stir under argon for 1 hour at room temperature. The Amberlite® IRA 400 resin was removed under vacuum filtration and washed with a small amount of anhydrous methanol. The porphyrin filtrate was recovered, dried (Na_2SO_4) and concentrated *in vacuo* to yield the desired trichloride porphyrin **5** (47.14 mg, 91%) as a water soluble purple solid. Porphyrin **4** and porphyrin **5** were distinguished from one other only by their differing water solubilities and HPLC R_f.

Mp >350°C (decomp.); *HPLC* t_R = 10.30 minutes, 95% (flow rate 1 min ml^{-1}; eluent A H_2O plus 0.1% TFA; eluent B MeOH; gradient 0 min. 0% B; 10 min. 75% B; 15 min. 75% B and 19 min. 0% B); $\lambda_{max}(H_2O)$/nm 424, 521, 581 and 642; λ_{ex}(550 V, sodium bicarbonate buffer, pH 9.5)/nm 426 (λ_{em} br, 650-750), 488 (br, 650-750), (br, 650-750) 493 (br, 650-750), 505 (br, 650-750), 517 (br, 650-750), 583 (br, 650-750) and 622 (br, 650-750); λ_{em}(550 V, sodium bicarbonate buffer, pH 9.5)/nm 397 (λ_{ex} 683), 445 (683), 522 (683), 561 (683) and 587 (683); *standard curve linear range*(λ_{ex}/nm 583, λ_{em} 683, 550 V, sodium bicarbonate buffer, pH 9.5)/μM 0 – 0.14, R^2 = 0.9834, y = $2.57x10^5x$ + 0.0029.

It is noted here that the porphyrin was excluded from light during all reactions and kept stored under a blanket of argon in the freezer (protected from light). The target porphyrin **5** was also stable to storage under defined conditions (argon and freezer) for ≤12 months.

6.3 Nanospecies Synthesis and Conjugations

Polyacrylamide Nanospecies 6

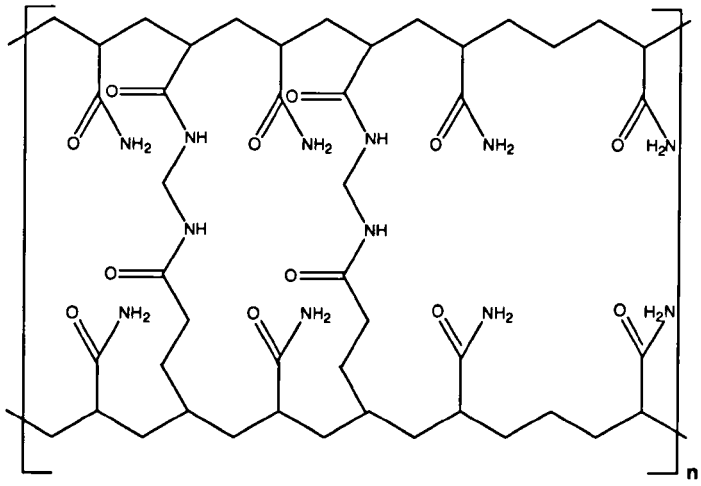

Degassed hexane (42 ml) was added to a stirred solution of Brij 30 (3.08 g, 8.5 mmol) and dioctyl sulfosuccinate sodium salt (1.59 g, 3.6 mmol). The mixture was allowed to stir under argon until the sodium salt had fully dissolved. A solution (2 ml) of acrylamide (540 mg, 7.6 mmol) and N,N'-methylenebisacrylamide (160 mg, 1.0 mmol) in water (2 ml) was added to the hexane mixture. An ice cold solution (30 μl, 0.4382 mol dm^{-3}) of ammonium persulphate (100 mg, 0.4382 mmol) in water (1 ml), followed by N,N,N',N'-tetramethylethylenediamine (TEMED, 15 μl, 0.1 μmol), were then added to the reaction flask and the reaction mixture allowed to stir under a positive argon pressure for two hours at room temperature. Excess hexane was removed *in vacuo* and the resulting white viscous liquid was washed with ethanol and centrifuged (8 x 50 ml, 10 minutes, 4,500 revolutions per minute (rpm)). The solid was recovered by microfiltration (Whatman® Anodisc 25, 0.02 μm, 25 mm filters) to yield the desired amide functionalised nanospecies **6** (576 mg, 82%) as a white solid. These gave an optically clear dispersion upon addition to aqueous media (water or sodium bicarbonate buffer).

PCS mean(z_{ave}, sodium chloride solution, 0.25 mmol, 1 mmol dm^{-3})/nm 37; *fluorescamine test*(λ_{ex}/nm 366) negative.

Amino-Functionalised Polyacrylamide Nanospecies 7

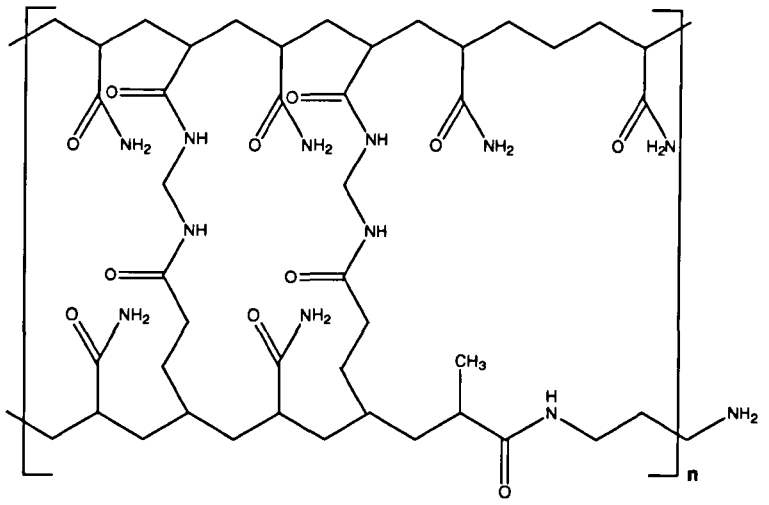

Degassed hexane (42 ml) was added to a stirred solution of Brij 30 (3.08 g, 8.5 mmol) and dioctyl sulfosuccinate sodium salt (1.59 g, 3.6 mmol). The mixture was allowed to stir under argon until the sodium salt had fully dissolved. A solution (2 ml) of acrylamide (527 mg, 7.4 mmol), N,N'-methylenebisacrylamide (160 mg, 1.0 mmol) and N-(3-aminopropyl)methacrylamide hydrochloride (13 mg, 0.073 mmol) in water (2 ml) was added to the hexane mixture. An ice cold solution (30 µl, 0.4382 mol dm^{-3}) of ammonium persulphate (100 mg, 0.4382 mmol) in water (1 ml), followed by TEMED (15 µl, 0.1 µmol), were then added to the reaction flask and the reaction mixture allowed to stir under a positive argon pressure, for two hours at room temperature. Excess hexane was removed *in vacuo* and the resulting white viscous liquid was washed with ethanol and centrifuged (8 x 50 ml, 10 minutes, 4,500 rpm). The solid was recovered by microfiltration (Whatman® Anodisc 25, 0.02 µm, 25 mm filters) to yield the desired amine functionalised nanospecies **7** (617 mg, 88%) as a white solid. These gave an optically clear dispersion upon addition to aqueous media (water or sodium bicarbonate buffer).

PCS mean(z_{ave}, sodium chloride solution, 0.25 mmol, 1 mmol dm^{-3})/nm 38; *fluorescamine test*(λ_{ex}/nm 366) positive.

Disulphonated 4,7-diphenyl-1,10-phenanthroline Ruthenium(II) Chloride Polyacrylamide Glucose (Oxygen) Nanosensors 8

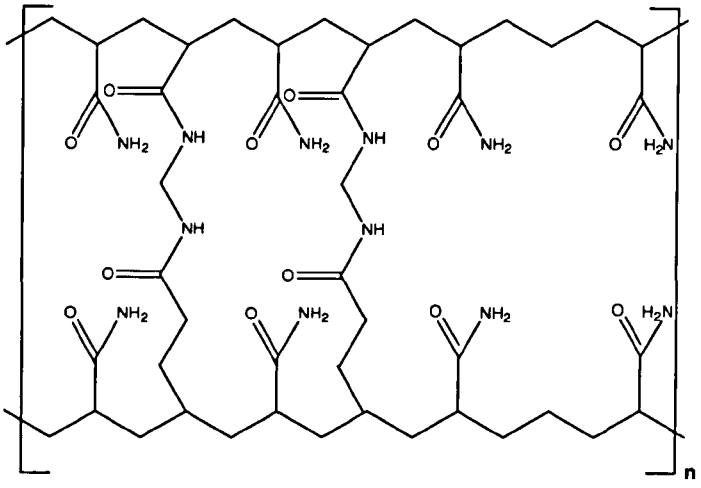

Degassed hexane (42 ml) was added to a stirred solution of Brij 30 (3.08 g, 8.5 mmol) and dioctyl sulfosuccinate sodium salt (1.59 g, 3.6 mmol). The mixture was allowed to stir under argon until the sodium salt had fully dissolved. A solution (1.960 ml) of acrylamide (540 mg, 7.6 mmol) and N,N'-methylenebisacrylamide (160 mg, 1.0 mmol), followed by the disulphonated 4,7-diphenyl-1,10-phenanthroline ruthenium(II) chloride dye (20 µl, 2.8 mmol dm^{-3}), were added to the hexane mixture. An ice cold solution (30 µl, 0.4382 mol dm^{-3}) of ammonium persulphate (100 mg, 0.4382 mmol) in water (1 ml), followed by TEMED (15 µl, 0.1 µmol) were then added to the reaction flask and the reaction mixture allowed to stir under a positive argon pressure, for two hours at room temperature. Excess hexane was removed *in vacuo* and the resulting orange viscous liquid was washed with ethanol and centrifuged (8 x 50 ml, 10 minutes, 4,500 rpm). The solid was recovered by microfiltration (Whatman® Anodisc 25, 0.02 µm, 25 mm filters) to yield the desired amide functionalised oxygen sensitive nanosensors **8** (576 mg, 82%) as an orange solid, which upon addition to aqueous media (water or sodium bicarbonate buffer) gave an optically clear dispersion.

PCS mean(z_{ave}, sodium chloride solution, 0.25 mmol, 1 mmol dm^{-3})/nm 53; *fluorescamine test*(λ_{ex}/nm 366) negative; λ_{ex}(800 V, sodium bicarbonate buffer, pH 9.5)/nm 469 (λ_{em} 621).

Disulphonated 4,7-diphenyl-1,10-phenanthroline Ruthenium(II) Chloride Amino-Functionalised Polyacrylamide Glucose (Oxygen) Nanosensors 9

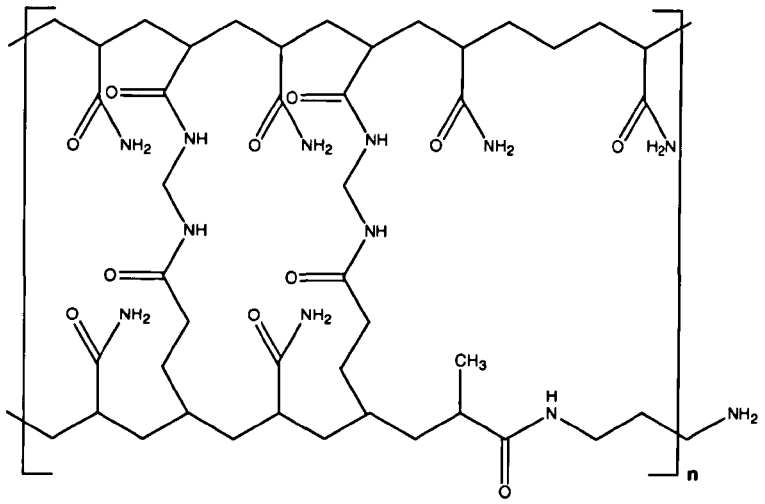

Degassed hexane (42 ml) was added to a stirred solution of Brij 30 (3.08 g, 8.5 mmol) and dioctyl sulfosuccinate sodium salt (1.59 g, 3.6 mmol). The mixture was allowed to stir under argon until the sodium salt had fully dissolved. A solution (1.960 ml) of acrylamide (527 mg, 7.4 mmol), N,N'-methylenebisacrylamide (160 mg, 1.0 mmol) and N-(3-aminopropyl)methacrylamide hydrochloride (13 mg, 0.0730 mmol) in water (2 ml), followed by the disulphonated 4,7-diphenyl-1,10-phenanthroline ruthenium(II) chloride dye (20 µl, 2.8 mmol dm^{-3}), were added to the hexane mixture. An ice cold solution (30 µl, 0.4382 mol dm^{-3}) of ammonium persulphate (100 mg, 0.4382 mmol) in water (1 ml), followed by TEMED (15 µl, 0.1 µmol) were then added to the reaction flask and the reaction mixture allowed to stir under a positive argon pressure, for two hours at room temperature. Excess hexane was removed *in vacuo* and the resulting orange viscous liquid was washed with ethanol and centrifuged (8 x 50 ml, 10 minutes, 4,500 rpm). The solid was recovered by microfiltration (Whatman® Anodisc 25, 0.02 µm, 25 mm filters) to yield the desired amino functionalised oxygen sensitive nanosensors **9** (391 mg, 56%) as an orange solid, which upon addition to aqueous media (water or sodium bicarbonate buffer) gave an optically clear dispersion.

PCS mean(z_{ave}, sodium chloride solution, 0.25 mmol, 1 mmol dm^{-3})/nm 46; *fluorescamine test*(λ_{ex}/nm 366) positive; λ_{ex}(800 V, sodium bicarbonate buffer, pH 9.5)/nm 469 (λ_{em} 621); *linear free glucose response range*(λ_{ex}/nm 469, λ_{em} 621, 1275 V)/μM 0 - 291, $R^2 = 0.9812$, $y = 0.0159x + 3.4458$.

Free Ruthenium(II) Chloride Dye and Ruthenium(II) Chloride Nanosensor Response Range

Stock solutions of phosphate buffer (0.01 mol dm^{-3}, pH 7.0), the disulphonated 4,7-diphenyl-1,10-phenanthroline ruthenium (II) chloride dye (5 mg, 0.003 mmol) in phosphate buffer (1 ml, pH 7.0), the amine functionalised disulphonated 4,7-diphenyl-1,10-phenanthroline ruthenium(II) chloride nanosensors **9** (20 mg) in phosphate buffer (2 ml, pH 7.0) and glucose oxidase from *Aspergillus niger* (unit activity of 15,000 – 50,000 units per gram) (10 mg) in phosphate buffer (1ml, pH 7.0) were prepared. Aliquots of the ruthenium dye solution (0.5 ml, 2.8 mmol dm^{-3}) and the glucose oxidase solution (0.5 ml) were added to the phosphate buffer (1 ml) and an emission spectrum then run on the sample (λ_{ex}/nm 469). Aliquots (from 10-90 µl) of a D-(+)-glucose monohydrate solution (10 mmol dm^{-3}, Fluka Chemicals, U.K.) were then added to the ruthenium/glucose oxidase solution and the emission spectra of the samples run.

Linear free glucose response range(λ_{ex}/nm 469, λ_{em} 621, 1275 V)/µl 0 - 80, $R^2 = 0.9957$, $y = 0.0139x + 4.6769$.

A parallel fluorescence experiment was run using the ruthenium(II) chloride nanosensor dispersion. Experimental conditions were as described above. Successive increases in fluorescence intensity were observed for both the free ruthenium dye solution and the ruthenium nanosensors, upon addition of the glucose solution to the respective solutions.

Linear free glucose response range(λ_{ex}/nm 469, λ_{em} 621, 1275 V)/µM 0 – 291, $R^2 = 0.9812$, $y = 0.0159x + 3.4458$.

Fluorescein-Amino Functionalised Nanospecies Conjugation 10

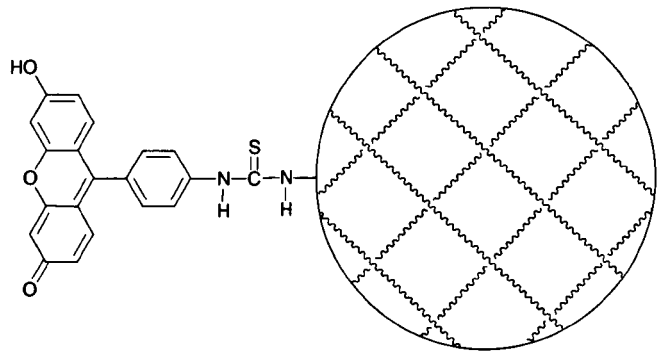

An aliquot (50 µl, 0.0026 mol dm^{-3}) of a solution of fluorescein isothiocyanate (isomer I) (1 mg, 0.0026 mmol) in sodium bicarbonate buffer (1 ml. pH 9.5) was added to a dispersion (0.2 ml) of amino functionalised nanospecies **7** (5 mg) in sodium bicarbonate buffer (1 ml, pH 9.5). The mixture was spun in Eppendorf tubes, for 1 hour on a spinning rotator, at room temperature and protected from light. The fluorescein-nanoparticle conjugate was recovered by microfiltration (Whatman® Anodisc 25, 0.02 µm, 25 mm filters) and washed with ethanol to remove excess fluorescein isothiocyanate and yield the desired conjugated nanoparticle **10** as a yellow solid, which upon addition to aqueous media (water or sodium bicarbonate buffer) gave an optically clear dispersion. The filtrate was periodically checked via fluorescence to ensure all the excess fluorescein isothiocyanate had been removed.

PCS mean(z_{ave}, sodium chloride solution, 0.25 mmol, 1 mmol dm^{-3})/nm 48; λ_{max}(sodium bicarbonate buffer, pH 9.5)/nm 494; λ_{ex}(550 V, sodium bicarbonate buffer, pH 9.5)/nm 492 (λ_{em} 520); *photobleaching*(λ_{ex}/nm 492, 550 V, sodium bicarbonate buffer, pH 9.5, 1 second intervals for 3000 seconds) stable; *loading ratio* of fluorescein to nanoparticle ~ 0.0044 mol/mg, $R^2 = 0.9983$, $y = 7.0 \times 10^6 x + 0.171$ (~ 4.4 mmol of fluorescein per mg of fluorescein-nanospecies conjugate).

Rhodamine B Isothiocyanato-Amino Functionalised Nanospecies Conjugation 11

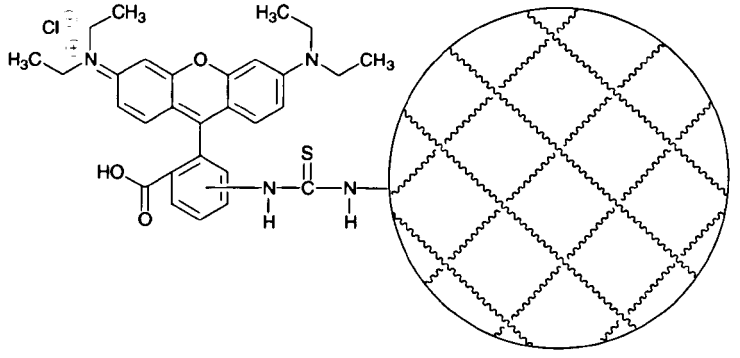

An aliquot (50 μl, 0.0019 mol dm^{-3}) of a solution of rhodamine B isothiocyanate (1 mg, 0.0019 mmol) in sodium bicarbonate buffer (1 ml, pH 9.5) was added to a dispersion (0.2 ml) of amine functionalised nanospecies **7** (5 mg) in sodium bicarbonate buffer (1 ml, pH 9.5). The mixture was spun in Eppendorf tubes, for 1 hour on a spinning rotator, at room temperature and protected from light. The rhodamine-nanoparticle conjugate was recovered by microfiltration (Whatman® Anodisc 25, 0.02 μm, 25 mm filters) and washed with ethanol to remove excess rhodamine B isothiocyanate and yield the desired conjugated nanospecies **11** as a purple solid, which upon addition to aqueous media (water or sodium bicarbonate buffer) gave an optically clear dispersion. The filtrate was periodically checked via fluorescence to ensure all the excess rhodamine B isothiocyanate had been removed.

PCS mean(z_{ave}, sodium chloride solution, 0.25 mmol, 1 mmol dm^{-3})/nm 52; λ_{max}(sodium bicarbonate buffer, pH 9.5)/nm 552; λ_{ex}(550 V, sodium bicarbonate buffer, pH 9.5)/nm 552 (λ_{em} 579).

Porphyrin-Amino Functionalised Nanospecies Conjugation 12

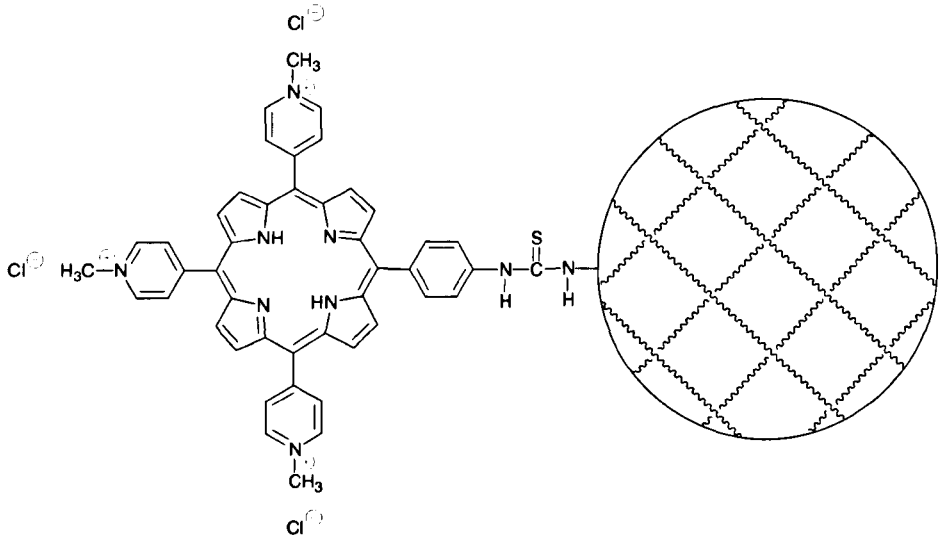

An aliquot (0.6 ml, 0.1704 mmol dm^{-3}) of a solution of porphyrin **5** (1 mg, 0.0012 mmol) in sodium bicarbonate buffer (7.1 ml, pH 9.5) was added to a dispersion (0.6 ml, 0.0017 mmol dm^{-3}) of the amino functionalised nanospecies **7** (15 mg) in sodium bicarbonate buffer (3 ml, pH 9.5). The mixture was spun in Eppendorf tubes, for 1 hour on a spinning rotator, at room temperature and protected from light. The porphyrin-nanoparticle conjugate was recovered by microfiltration (Whatman® Anodisc 25, 0.02 μm, 25 mm filters) and washed with ethanol to remove excess porphyrin and yield the desired conjugated nanospecies **12**, as a yellow solid, which upon addition to aqueous media (water and sodium bicarbonate buffer, pH 9.5) gave an optically clear dispersion. The filtrate was periodically checked via fluorescence to ensure all the excess porphyrin had been removed.

PCS mean(z_{ave}, sodium chloride solution, 0.25 mmol, 1 mmol dm^{-3})/nm 195.6; λ_{max}(sodium bicarbonate buffer, pH 9.5)/nm 425, 522, 561, 582 and 642; λ_{ex}(1275 V, sodium bicarbonate buffer)/nm 426 (λ_{em} 655 and 710sh), 505 (655 and 710sh) and 583 (655 and 710sh); *photobleaching*(λ_{ex}/nm 488, 800 V, sodium bicarbonate buffer, pH 9.5, 1 second intervals for 3000 seconds) stable; *loading ratio* of trichloride porphyrin to

nanoparticle ~ 0.0011 mol/mg, R^2 = 0.9878, y = 1.62x105x + 0.0012 (~ 1.1 mmol of trichloride porphyrin per mg of trichloride porphyrin-nanoparticle conjugate).

Calcium Green-1 Dextran 10,000 Amino-Functionalised Polyacrylamide Nanosensors 13

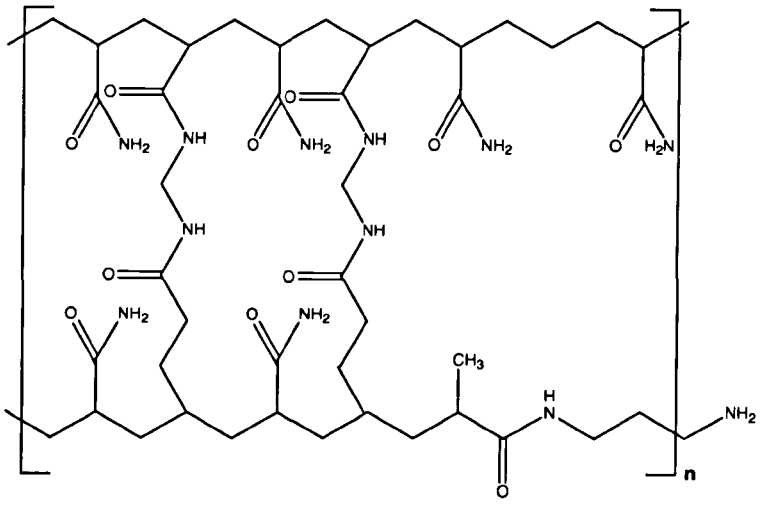

Degassed hexane (42 ml) was added to a stirred solution of Brij 30 (3.08 g, 8.5 mmol) and dioctyl sulfosuccinate sodium salt (1.59 g, 3.6 mmol). The mixture was allowed to stir under argon until the sodium salt had fully dissolved. A solution (1.960 ml) of acrylamide (527 mg, 7.4 mmol), N,N'-methylenebisacrylamide (160 mg, 1.0 mmol) and N-(3-aminopropyl)methacrylamide hydrochloride (13 mg, 0.0730 mmol) in water (2 ml), along with calcium green-1 dextran (10,000 Da, 40 µl, 0.4587 mmol dm^{-3}) were added to the hexane mixture. An ice cold solution (30 µl, 0.4382 mol dm^{-3}) of ammonium persulphate (100 mg, 0.4382 mmol) in water (1 ml), followed by TEMED (15 µl, 0.1 µmol), were then added to the reaction flask and the reaction mixture allowed to stir under a positive argon pressure, for two hours at room temperature. Excess hexane was removed *in vacuo* and the resulting pink viscous liquid was washed with ethanol and centrifuged (8 x 50 ml, 10 minutes, 4,500 rpm). The solid was recovered by microfiltration (Whatman® Anodisc 25, 0.02 µm, 25 mm filters) to yield the desired amino functionalised calcium sensitive nanosensors **13** (632 mg, 90%) as a pink solid, which upon addition to aqueous media (water or sodium bicarbonate buffer) gave an optically clear dispersion.

PCS mean(z_{ave}, sodium chloride solution, 0.25 mmol, 1 mmol dm^{-3})/nm 44; *fluorescamine test*(λ_{ex}/nm 366) positive; λ_{ex}(550 V, sodium bicarbonate buffer, pH

9.5)/nm 505 (λ_{em} 532), 426 (532), 488 (532) and 493 (532); *photobleaching*(λ_{ex}/nm 488, 800 V, sodium bicarbonate buffer, pH 9.5, 1 second intervals for 3000 seconds) stable; *leaching*(λ_{ex}/nm 488, λ_{em} 532, 500 V, sodium bicarbonate buffer, pH 9.5)/% 1 (6 hours), ~1 (24) and ~1 (96), total leaching after 4 days ~1%; *linear free calcium response range*(λ_{ex}/nm 505, λ_{em} 532, 550 V, sodium bicarbonate buffer, pH 9.5)/μM 0 - 0.225, R^2 = 0.9870, $y = 1.5337x + 0.2006$.

Porphyrin-Amino Functionalised Calcium Green-1 Nanosensor Conjugation 14

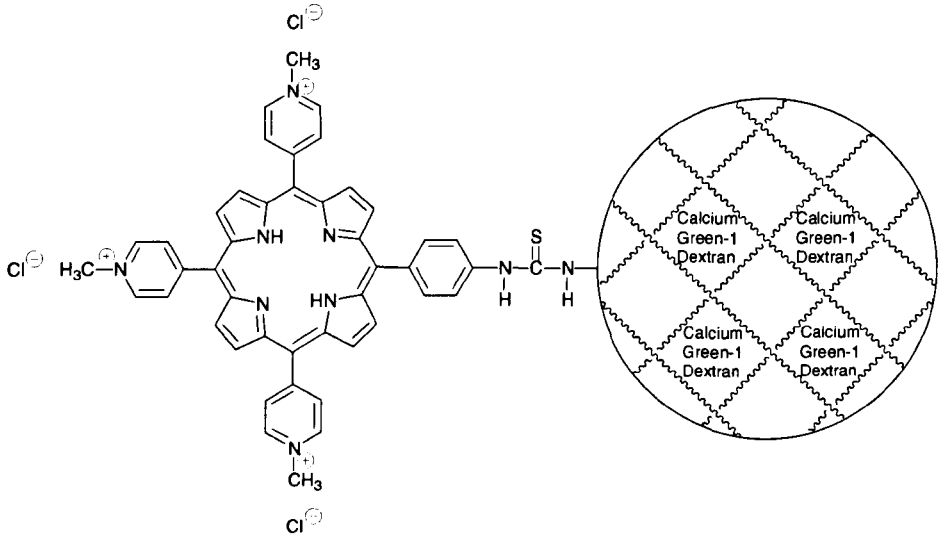

An aliquot (0.6 ml, 0.1704 mmol dm^{-3}) of a solution of porphyrin **5** (1 mg, 0.0012 mmol) in sodium bicarbonate buffer (7.1 ml, pH 9.5) was added to a dispersion (0.6 ml, 0.0017 mmol dm^{-3}) of the amino functionalised calcium sensitive nanosensors **13** (15 mg) in sodium bicarbonate buffer (3 ml, pH 9.5). The mixture was spun in Eppendorf tubes, for 1 hour on a spinning rotator, at room temperature and protected from light. The porphyrin-nanosensor conjugate was recovered by microfiltration (Whatman® Anodisc 25, 0.02 μm, 25 mm filters) and washed with ethanol to remove excess porphyrin and yield the desired calcium sensitive nanosystem **14** as a yellow solid, which upon addition to aqueous media (water or sodium bicarbonate buffer) gave an optically clear dispersion. The filtrate was periodically checked via fluorescence to ensure all the excess porphyrin had been removed.

PCS mean(z_{ave}, sodium chloride solution, 0.25 mmol, 1 mmol dm^{-3})/nm 188.6; λ_{max}(sodium bicarbonate buffer, pH 9.5)/nm 436, 524, 563, 583 and 641; λ_{ex}(1275 V, sodium bicarbonate buffer, pH 9.5)/nm 426 (λ_{em} 532, 650 and 705sh) and 488 (532, 650 and 705sh); *photobleaching*(λ_{ex}/nm 488, 800 V, sodium bicarbonate buffer, pH 9.5, 1 second intervals for 3000 seconds) stable; *linear free calcium response range*(λ_{ex}/nm

505, λ_{em} 532, 550 V, sodium bicarbonate buffer, pH 9.5)/μM 0 - 0.225, $R^2 = 0.9912$, $y = 1.5174x + 0.2112$.

6.4 Chromophore and Target System Investigations

Porphyrin-Calcium Geeen-1 Dextran Solution Experiments

Stock solutions of porphyrin **5** (1 mg, 0.0012 mmol, 1.21 mmol dm^{-3}) in a sodium bicarbonate buffer (1 ml, pH 9.5), further diluted by taking 10 μl of porphyrin solution and adding to 1 ml of buffer, and calcium green-1 dextran (25 μl, 0.011 mmol dm^{-3}) in a sodium bicarbonate buffer (1 ml, pH 9.5) were prepared. Aliquots of the porphyrin stock solution (10 μl) and calcium green-1 dextran stock solution (10 μl) were then added to the bicarbonate buffer (2 ml). The porphyrin-calcium green-1 dextran solution was then excited at a number of wavelengths (λ_{ex}/nm 327, 426, 488, 493 and 505) and the emission spectra recorded.

λ_{ex}(1:1, porphyrin/calcium green-1 dextran, 550 V, sodium bicarbonate buffer, pH 9.5)/nm 327 (λ_{em} 532 and 655), 426 (532 and br, 640-740sh), 488 (532), 493 (532) and 505 (532).

Parallel fluorescence experiments were run, with fresh fluorescence solutions, varying the porphyrin to calcium green-1 dextran ratios from 1:1 (above) to 2:1 (porphyrin/calcium green-1 dextran), 10:1 and 100:1 and then 1:2 (porphyrin/calcium green-1 dextran), 1:10 and 1:100. Experimental conditions were as described above.

λ_{ex}(2:1, 550 V, sodium bicarbonate buffer, pH 9.5)/nm 327 (λ_{em} 532 and 655), 426 (532 and br, 640-740sh), 488 (532), 493 (532) and 505 (532); λ_{ex}(10:1, 550 V, sodium bicarbonate buffer, pH 9.5)/nm 327 (λ_{em} 532 and 655), 426 (532 and br, 640-740sh), 488 (532), 493 (532) and 505 (532); λ_{ex}(100:1, 550 V, sodium bicarbonate buffer, pH 9.5)/nm 327 (λ_{em} 655), 426 (br, 640-740sh), 488 (532 and br, 640-740sh), 493 (532 and br, 640-740sh) and 505 (532 and 640-740sh); λ_{ex}(1:2, 550 V, sodium bicarbonate buffer, pH 9.5)/nm 327 (λ_{em} 532 and 655), 426 (532 and br, 640-740sh), 488 (532), 493 (532) and 505 (532); λ_{ex}(1:10, 550 V, sodium bicarbonate buffer, pH 9.5)/nm 327 (λ_{em} 532 and 655), 426 (532), 488 (532), 493 (532) and 505 (532); λ_{ex}(1:100, 550 V, sodium

bicarbonate buffer, pH 9.5)/nm 327 (λ_{em} 532 and 655), 426 (532), 488 (532), 493 (532) and 505 (532).

Tap Water Experiment (Calcium Response)

Stock solutions of sodium bicarbonate buffer (pH 9.5), calcium green-1 dextran (5 mg, 0.4587 μmol) in sodium bicarbonate buffer (1 ml, pH 9.5) and calcium green-1 dextran nanosensors **13** (10 mg) in sodium bicarbonate buffer (2 ml, pH 9.5) were prepared. A control experiment was run using a mixture of the free calcium green-1 dextran dye (5 μl, 0.4587 mmol dm^{-3}) and sodium bicarbonate buffer (2 ml, pH 9.5). Aliquots of tap water (from 1-100 μl) were added to the calcium green-1 dextran/sodium bicarbonate buffer solution and the emission spectra of the samples run (λ_{ex}/nm 505, 550 V).

A parallel experiment was run using the calcium green-1 dextran nanosensor dispersion. Experimental conditions were as described above. Successive increases in fluorescence intensity upon addition of tap water were observed for both the free calcium green-1 dextran dye and the calcium green-1 dextran nanosensors.

To determine the amount of calcium ions present in tap water, a titration was performed using an ethylenediaminetetra-acetic acid (EDTA) solution and tap water.

A stock solution of EDTA was prepared (0.9977 g, 3.4 mmol, 0.01 mol dm^{-3}) in water (250 ml). The solution was then titrated against a solution of tap water (100 ml), with a few drops of murexide indicator added and sodium hydroxide (5 ml). The solution was titrated with EDTA until a colour change (pink to purple) was observed. The titration was repeated three times (average titre 28.53 ml). There were 122 mg (122 ppm) of calcium per litre of tap water.

Calcium Green-1 Dextran Linear Response Range (Calibration Curve)

Stock solutions of calcium green-1 dextran (5 mg, 0.0005 mmol) in a sodium bicarbonate buffer (1 ml, pH 9.5), the calcium green-1 dextran nanosensors **13** (5mg) in a sodium bicarbonate buffer (1 ml, pH 9.5) and the porphyrin-calcium green-1 dextran conjugated nanosystem **14** (5 mg) in the sodium bicarbonate buffer (1 ml, pH 9.5) were prepared. An aliquot of the calcium green-1 dextran solution (10 μl, 0.0112 mmol dm^{-3}) was added to the zero free calcium buffer (calcium calibration buffer kit number 2, Invitrogen, C-3009) (2 ml) and the emission spectrum recorded for the sample.

Parallel fluorescence experiments were run, with fresh solutions, varying the concentration of the calcium in the calcium buffer from 0 μM (above) to 0.017, 0.038, 0.065, 0.100, 0.150, 0.225, 0.351, 0.602, 1.35 and 39, allowing the creation of a calibration curve for the free calcium green-1 dextran dye.

Linear free calcium response range(λ_{ex}/nm 505, λ_{em} 532, 550 V, sodium bicarbonate buffer, pH 9.5)/μM 0 - 0.351, $R^2 = 0.9904$, $y = 5.331x + 1.5362$.

Parallel experiments were repeated using the calcium green-1 dextran nanosensor dispersion and the porphyrin-calcium green-1 dextran conjugated nanosystem dispersion. Experimental conditions as above.

Linear free calcium response range(λ_{ex}/nm 505, λ_{em} 532, 550 V, sodium bicarbonate buffer, pH 9.5)/μM 0 - 0.225, $R^2 = 0.9870$, $y = 1.5337x + 0.2006$ and *linear free calcium response range*(λ_{ex}/nm 505, λ_{em} 532, 550 V, sodium bicarbonate buffer, pH 9.5)/μM 0 - 0.225, $R^2 = 0.9912$, $y = 1.5174x + 0.2112$, respectively.

Calcium Green-1 Dextran Nanosensor 13 Leaching Experiment

Stock solutions of the calcium green-1 dextran nanosensors **13** (100 mg) in a sodium bicarbonate buffer (100 ml, pH 9.5) and of a blank sodium bicarbonate buffer (pH 9.5) were prepared. The solutions were allowed to continuously stir in sealed flasks at room temperature whilst protected from light. Every thirty minutes an aliquot (5 ml) of the calcium green-1 dextran buffer solution was taken and filtered. An aliquot (3 ml) of the filtrate was taken and an emission spectrum run. Parallel spectra were run on the blank buffer (3 ml) and an aliquot (3ml) of the nanospecies-sample buffer which had been passed through the filter unit base. Samples were taken and run every thirty minutes for 6 hours, after 24 hours and finally after 4 days. Photocorrelation spectroscopy (PCS) was run on every alternate sample.

Leaching(λ_{ex}/nm 488, λ_{em} 532, 500 V, sodium bicarbonate buffer, pH 9.5)/% 1 (6 hours), ~1 (24) and ~1 (96), total leaching after 4 days ~1%.

Cholesterol Assay

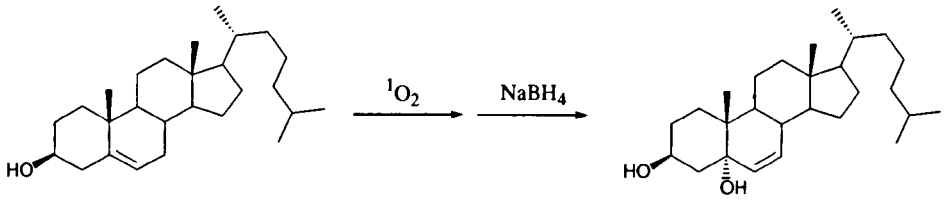

Stock solutions of cholesterol (38.70 mg, 0.1 mmol, 0.01 mol dm^{-3}) in a methanol/ethyl acetate mixture (1:1, 10 ml), porphyrin **5** (1 mg, 0.0012 mmol, 1.21 mmol dm^{-3}) in methanol (1ml) and porphyrin-calcium sensitive nanosystem **14** (10 mg) in methanol (2 ml) were prepared. A control experiment was run using a mixture of the cholesterol solution (2 ml) and the porphyrin solution (2 ml). The cholesterol/porphyrin solution was continuously irradiated with red (634 ± 15 nm, Patterson light source, ~ 230 Wm^{-2}, 8 $Jcm^{-2}W^{-1}$ or 633 ± 3 nm, Omnilux light source, ~ 800 Wm^{-2}, 80 Jcm^{-2}) or white light (broad band white light source, 3M OHP Overhead Projector, 1700 A4, ~ 651.80 Wm^{-2}) and air slowly bubbled through the system using a Fisherbrand® dry vacuum pump/compressor. The reaction was monitored by thin layer chromatography (TLC) using silica and a hexane/ethyl acetate mixture (1:1) as the solvent system. Small aliquots of the solution were taken every thirty minutes and reacted with a few crystals of sodium borohydride (reduction <1 minute). The aliquot solvent was then replaced with dichloromethane and a TLC run. The solvent was allowed to run $^2/_3$ of the way up the silica plate before the plate was removed from the solvent chamber and allowed to air dry. Once dry, the plate was replaced inside the chamber and the solvent allowed to run to the designated solvent front. The plate was then air dried, exposed to a 5% sulphuric acid/ethanol solution and heated on a hotplate (120°C) to allow the development of the cholesterol and dihydroxy sterol coloured spots.

$R_{f(cholesterol)}$ = 1.0 (red, silica, C_6H_{14}/EtOH, 1:1); $R_{f(product)}$ = 0.38 (blue, silica, C_6H_{14}/EtOH, 1:1).

A parallel experiment was run using the cholesterol solution (2 ml) and the porphyrin-calcium sensitive nanosystem solution (2 ml). Experimental conditions were as described above.

$R_{f(cholesterol)}$ = 1.0 (red, silica, C_6H_{14}/EtOH, 1:1); $R_{f(product)}$ = 0.38 (blue, silica, C_6H_{14}/EtOH, 1:1).

6.5 Photophysical Investigations - Time Correlated Single Photon Counting

The third harmonics (355 nm) of a Q-witched Nd:YAG laser was used to excite the luminescent samples held in a 1 x 1 cm Quartz cuvette. The laser light was passed through cobalt sulphate and neutral density filters to remove the 532 nm excitation wavelength from the laser output and focused onto the sample. The pulse duration was <10 ns, with a pulse energy of 0.1-5 mJ at the sample and a pulse repetition frequency of 10 Hz. Light from the sample was collected at a 90° angle to the excitation beam and passed through a band-pass interference filter (Infra-Red Engineering Limited) centred at 270 nm. The detector was a liquid nitrogen cooled germanium photodiode (North Coast E0-817P) with a spectral response from 800-1700 nm, enabling sensitive detection in the 1200-1300 nm range. Its rapid response allowed photon counting of the singlet oxygen luminescence. The system operating voltage was set at -1500 kV and the detector output amplified by an analogue to digital converter (ADC) and relayed to a personal computer. The luminescence signal was summed over many laser pulses (10 Hz) giving data collection times of 25 ps per channel. Measurements were made in the time-resolved mode, yielding a time-integrated spectrum of the light emitted from the sample. The complete time curve was measured at 1270 nm and the background subtracted. Emission wavelengths of 530 and 650 nm were used for studies with the conjugated species respectively. In order to confirm that the singlet oxygen detector was working a standard reference of naphthalene in dichloromethane was run. All experiments performed were repeated to yield results within (± 5 μs).

All samples were prepared using a sodium bicarbonate buffer (pH 9.5) with distilled water. Exceptions were made for the samples where free calcium ions were sought in which cases the buffer was prepared with tap water (Durham). Nanosensors and porphyrin-nanosensor conjugate samples were prepared at a concentration of 5mg/ml. Time resolved luminescence at 1270 nm was recorded following laser excitation, and at each laser intensity the recorded luminescence trace was obtained by averaging 20-50 single laser shots. The averaged traces were fitted with a single exponential (singlet oxygen, first order kinetics) or multiexponential (calcium green dye, bimolecular

kinetics) function, which was extrapolated to t=0. Plots of I_0 *versus* laser intensity were then made and the data χ^2 fitted (non-linear least squares curve fitting) using software (written by Dr Andy Beeby and his group from the University of Durham, U.K.) from which the average luminescent lifetimes of the species were determined.

Calcium green: $\tau_{fl.}$/ns = 0.64 and 3.63, χ^2 = 1.41, $\lambda_{ex.}$/nm = 355, $\lambda_{em.}$/nm = 530; calcium green and free calcium ions: $\tau_{fl.}$/ns = 0.65 and 3.65, χ^2 = 1.05, $\lambda_{ex.}$/nm = 355, $\lambda_{em.}$/nm = 530; calcium green nanosensors **13**: $\tau_{fl.}$/ns = 0.70 and 3.50, χ^2 = 1.40, $\lambda_{ex.}$/nm = 355, $\lambda_{em.}$/nm = 530; calcium green nanosensors and free calcium ions: $\tau_{fl.}$/ns = 0.50 and 3.54, χ^2 = 1.17, $\lambda_{ex.}$/nm = 355, $\lambda_{em.}$/nm = 530; porphyrin **5**: τ_{Δ}/μs = 60.00, χ^2 = 1.02, $\lambda_{ex.}$/nm = 355, $\lambda_{em.}$/nm = 650; porphyrin-calcium nanosensors **14**: $\tau_{fl.}$/ns = 0.64 and 3.69, χ^2 = 1.21, $\lambda_{ex.}$/nm = 355, $\lambda_{em.}$/nm = 530; porphyrin-calcium nanosensors **14** and free calcium ions: $\tau_{fl.}$/ns = 0.55 and 3.77, χ^2 = 1.21, $\lambda_{ex.}$/nm = 355, $\lambda_{em.}$/nm = 530; porphyrin-calcium nanosensors **14**: τ_{Δ}/μs = 63.40, χ^2 = 1.20, $\lambda_{ex.}$/nm = 355, $\lambda_{em.}$/nm = 650; porphyrin-calcium nanosensors **14** and free calcium ions: τ_{Δ}/μs = 61.83, χ^2 = 1.08, $\lambda_{ex.}$/nm = 355, $\lambda_{em.}$/nm = 650.

6.6 Cellular Investigations

6.6.1 Lipofectamine Delivery Route

The day before transfection/lipofection human neuroblastoma cells (SHSY5Y) were plated in 9 ml of serum-free and antibiotic-free growth medium. After 4-6 hours the medium was replaced with normal growth medium and allowed to reach ~90% confluence before transfection was attempted. The Lipofectamine™ reagent (45 µl) was diluted down by the Opti-MEM® serum-free medium (900 µl) and the resulting solution mixed and incubated for five minutes at room temperature before the porphyrin-nanosensor conjugates **14** were added. The Lipofectamine™-nanosystem conjugate solution was further mixed and allowed to incubate for twenty minutes at room temperature. 100 µl of the nanosystem-Lipofectamine™ complexes were added to each cell-containing well of the culture vessel and mixed gently. The cells were allowed to incubate with the Lipofectamine™-nanosystem solution at 37°C in a 5% carbon dioxide incubator for 24 hours until they were ready for assay, after which chamberslides were prepared.

6.6.2 *Trans*It® Delivery Route

The day before transfection/lipofection human embryonic kidney cells (HEK 293) were plated in 800 µl of growth medium and allowed to reach ~60% confluence before transfection was attempted. The *Trans*It® 293 reagent (47 µl) was diluted down by Opti-MEM® MEDIUM (800 µl) and the resulting solution mixed and incubated for 5-20 minutes at room temperature before the porphyrin-nanosensor conjugates were added. The *Trans*It®-nanosystem conjugate solution was further mixed and allowed to incubate for 15-30 minutes at room temperature. The nanosystem-*Trans*It® complexes were added dropwise to each cell-containing well of the culture vessel and mixed gently. The cells were allowed to incubate with the *Trans*It®-nanosystem solution at 37°C in a 5% carbon dioxide incubator for 24 hours until they were ready for assay.

All images were obtained with a C-Apochromat x40 oil immersion lens on a Zeiss Axiovert 200 M inverted microscope fitted with a Zeiss LSM 510 laser-scanning module.

REFERENCES

1. H. L. Anderson, *Chem. Commun.*, 1999, 2323-2330.
2. L. R. Milgrom, in *The Colours of Life: An Introduction to the Chemistry of Porphyrins and Related Compounds*, Oxford University Press, Oxford, 1997, ch. 1, pp. 1 and 16; ch. 2, pp 48-57; and ch. 3, pp. 70, 71, 78-80,84 and 85.
3. E. D. Sternberg, D. Dolphin and C. Brückner, *Tetrahedron*, 1998, **54**, 4151-4202.
4. W. M. Sharman, C. M. Allen and J. E. van Lier, *Drug Disc. Today*, 1999, **4**, 507-517.
5. A. P. Castano, T. N. Demidova and M. R. Hamblin, *Photodiagnosis Photodynamic Ther.*, 2004, **1**, 279-293.
6. A. P. Castano, T. N. Demidova and M. R. Hamblin, *Photodiagnosis Photodynamic Ther.*, 2005, **2**, 1-23.
7. A. J. Rest, in *Light, Chemical Change and Life: Porphyrins and Phthalocyanines*, OUPC, Milton Keynes, 1982, ch. 2.3, pp. 43-51.
8. www.washburn.edu/cas/chemistry/sleung/porphyrin/properties_frame.html, 08/08/06.
9. E. S .Nyman and P. H. Hynninen, *J. Photochem. Photobiol., B: Biol.*, 2004, **73**, 1-28.
10. www.chem.ucdavis.edu/groups/smith/chime/porph_struc/lots_of_files/intro.html, 28/05/04.
11. C. Rimmington, *J. Biochem.*, 1960, **75**, 620-623.
12. I. J. MacDonald and T. J. Dougherty, *J. Porphyrins Phthalocyanines*, 2001, **5**, 105-129.
13. http://chemdept.chem.ncsu.edu/~franzen/CH795Z/lecture/aromatics/aromatics.html, 01/12/06.
14. P. Rothemund, *J. Am. Chem. Soc.*, 1936, **58**, 625-627.

15. S. Shanmugathasan, C. Edwards and R. W. Boyle, *Tetrahedron*, 2000, **56**, 1025-1046.

16. A. D. Adler, F. R. Longo, J. D. Finarelli, J. Goldmacher, J. Assour and L. Korsakoff, *J. Org. Chem.*, 1967, **32**, 476.

17. J. S. Lindsey, I. C. Schreiman, H. C. Hsu, P. C. Kearney and A. M. Marguerettaz, *J. Org. Chem.*, 1987, **52**, 827-836.

18. R. A. Sheldon, in *Metalloporphyrins in Catalytic Oxidations*, ed. R. A. Sheldon, Marcel Dekker Inc., New York, ch. 1, pp. 4.

19. www.ipac.caltech.edu/Outreach/Edu/Regions/irregions.html, 10/03/07.

20. S. Brown, G. Gregory, S. Montan, S. Anderson-Engels and S. Svanberg, *Acta Radiol.*, 1998, **39**, 2-9.

21. R. Bonnett and G. Martinez, *Tetrahedron*, 2001, **57**, 9513-9547.

22. C. A. Rebeiz, C. A. Reddy, U. B. Nandihalli and J. Velu, *Photochem. Photobiol.*, 1990, **52**, 1099.

23. T. BenAmor, M. Tronchin, L. Bortolotto, R. Verdiglione and G. Jori, *Photochem. Photobiol.*, 1998, **67**, 206-211.

24. R. Bonnett, *Chem. Soc. Rev.*, 1995, **24**, 19-33.

25. P. B. Keating, M. F. Hinds and S. J. Davis, *The Proceedings of the International Congress on Applications of Lasers and Laser-Optics*, 2000.

26. http://class.fst.ohio-state.edu/fst821/Lect/Singlet1.pdf, 03/02/04.

27. www.uni-frankfurt.de/~rsch/1O2-english.html, 03/02/04.

28. www.photobiology.com/educational/len2/singox.html, 12/04/04.

29. I. E. Kochevar and R. W. Redmond, *Methods Enzymol.*, 2000, **319**, 20-28.

30. K. Lang, J. Mosinger and D. M. Wagnerová, *Coord. Chem. Rev.*, 2004, **248**, 321-350.

31. J. E. van Lier, in *Photobiological Techniques, Photosensitisation: Reaction Pathways*, ed. D.P Valenzeno, R.H. Pottier, P. Mathis and R. H. Douglas, NATO

ASI Series, Series A: Life Sciences, Plenum Press, New York and London, 1991, vol. 216, ch. 7, pp. 85-98.

32. T. J. Dougherty, C. J. Gomer, B. W. Henerderson, G. Jori, D. Kessel, M. Korbelik, J. Moan and Q. Peng, *J. Natl. Cancer Inst.*, 1998, **90**, 889-905.

33. M. R. Detty, S. L. Gibson and S. J. Wagner, *J. Med. Chem.*, 2004, **47**, 3897-3915.

34. F. Wilkinson, W. P. Helman and A. B. Ross, *J. Phys. Chem. Ref. Data*, 1993, **22**, 113-262.

35. M. Oschner, *J. Photochem. Photobiol. B: Biol.*, 1997, **39**, 1-18.

36. E. Weizman, C. Rothmann, L. Greenbaum, A. Shainberg, A. Adamek, B. Ehrenberg and Z. Malik, *J. Photochem. Photobiol. B: Biol.*, 2000, **59**, 92-102.

37. http://www.chem.ucla.edu/dept/Organic/CSF_Brochure.html, 24/08/06.

38. K. See Lee, I. K. Forbes and W. H. Betts, *Photochem. Photobiol.*, 1984, **39**, 631-634.

39. L. Ma, J. Moan and K. Berg, *Int. J. Cancer*, 1994, **57**, 883-888.

40. T. Hasan and A. U. Khan, *Proc. Natl. Acad. Sci. U.S.A.*, 1986, **83**, 4604-4606.

41. J. Morgan and A. R. Oseroff, *Adv. Drug Delivery Rev.*, 2001, **49**, 71-86.

42. R. Bonnett, P. Charlesworth, B. D. Djelal, S. Foley, D. J. McGarvey and T. G. Truscott, *J. Chem. Soc. Perkin Trans. II*, 1999, **2**, 325-328.

43. M. F. Edelson, *Sci. Am.*, 1988, **259**, 68-75.

44. R. R. Allison, H. C. Mota and C. H. Sibata, *Photodiagnosis Photodynamic Ther.*, 2004, **1**, 263-277.

45. Z. Smetana, E. Ben-Hur, E. Mendelson, S. Salzberg, P. Wagner and Z. Malik, *J. Photochem. Photobiol. B: Biol.*, 1998, **44**, 77-83.

46. www.urbanfischer.de/journals/lasermed, 10/10/06.

47. G. Jori, *J. Photochem. Photobiol. B: Biol.*, 1996, **36**, 87-93.

48. R. Decreau, M. J. Richard P. Verrando, M. Chanon and M. Julliard, *J. Photochem. Photobiol. B: Biol.*, 1999, **48**, 48-56.

49. R. Hudson, M. Carcenac, K. Smith, L. Madden, O. J. Clarke, A. Pèlegrin, J. Greenman and R. W. Boyle, *Br. J. Cancer*, 2005, **92**, 1442-1449.

50. N. Malatesti, K. Smith, H. Savoie, J. Greenman and R. W. Boyle, *Int. J. Oncol.* 2006, **28**, 1561-1569.

51. I. F. Patito, C. Rothmann and Z. Malik, *Biol. Cell*, 2001, **93**, 285-291.

52. M. L. Agarwal, M. E. Clay, E. J. Harvey, H. H. Evans, A. R. Antunez and N. L. Oleinick, *Cancer Res.*, 1991, **51**, 5993-5996.

53. C. V. Coulter, G. F. Kelso, T-K. Lin, R. A. J. Smith and M. P. Murphy, *Free Radical Biol. Med.*, 2000, **28**, 1547-1554.

54. D. Kessel, *Photochem. Photobiol.*, 1986, **39**, 851-859.

55. A. P. Castano, T. N. Demidova and M. R. Hamblin, *Photodiagnosis Photodynamic Ther.*, 2005, **2**, 91-106.

56. G. F. Kelso, C. M. Porteous, C. V. Coulter, G. Hughes, W. F. Porteous, E. C. Ledgerwood, R. A. J. Smith and M. P. Murphy, *J. Biol. Chem.*, 2001, **276**, 4588-4596.

57. D. A. Bellnier, B. W. Henderson, R. K. Pandey, W. R. Potter and T. J. Dougherty, *Photochem. Photobiol.*, 1993, **20**, 55-61.

58. A. Villanueva and G. Jori, *Cancer Lett.*, 1993, **73**, 59-64.

59. M. Del Governatore, M. R. Hamblin, C. R. Shea, I. Rizvi, K. G. Molpus, K. K. Tanabe and T. Hasan, *Cancer Res.*, 2000, **60**, 4200-4205.

60. A. Graham, G. Li, Y. Chen, J. Morgan, A. Oseroff, T. J. Dougherty and R. K. Pandey, *Photochem. Photobiol.*, 2003, **77**, 561-566.

61. P. Peng, J. M. Nesland, J. Moan, J. Evenson, M. Konshaug and C. Rimmington, *Int. J. Cancer*, 1990, **46**, 719-726.

62. A. Ruck and R. Steiner, *Minimally Invasive Ther. Allied Technol.*, 1998, **7**, 503-509.

63. P. Peng, J. M. Nesland, J. Moan, J. Evenson, M. Konshaug and C. Rimmington, *Int. J. Cancer*, 1990, **45**, 972-979.

64. I. Freitas, *J. Photochem. Photobiol. B: Biol.*, 1990, **7**, 359-361.

65. P. J. Bugelski, C. W. Porter and T. J. Dougherty, *Cancer Res.*, 1981, **41**, 4606-4612.

66. L. Milas, J. Wike, N. Hinter, J. Volpe and I. Basic, *Cancer Res.*, 1987, **47**, 1069-1075.

67. M. Korbelik, G. Krosi, P. L. Olive and D. J. Chaplin, *Br. J. Cancer*, 1991, **64**, 508-512.

68. W. Beyer, *J. Photochem. Photobiol. B: Biol.*, 1996, **36**, 153-156.

69. A. C. Kübler, *Med. Laser Appl.*, 2005, **20**, 37-45.

70. www.dermatology.org/laser/pdt.html, 08/09/06.

71. M. G. Alvarez, N. B. R. Vittar, F. Principe, J. Bergesse, M. C. Romanini, S. Romanini, M. Bertuzzi, E. N. Durantini and V. Rivarola, *Photodiagnosis Photodynamic Ther.*, 2004, **1**, 335-344.

72. L. Collins-Gold, N. Feichtinger and T. Wärnheim, *Mod. Drug Discovery*, 2000, **3**, 44-46, 48.

73. H. M. El-Laithy, *AAPS Pharm. Sci. Tech.*, 2003, **4**, 1-10.

74. T. M. Fahmy, P. M. Fong, A. Coyal and W. M. Saltzman, *Nanotoday*, 2005, 18-26.

75. R. W. Boyle and D. Dolphin, *Photochem. Photobiol.*, 1996, **64**, 469-485.

76. www.chemheritage.org/EducationalServices/pharm/chemo/readings/ehrlich.htm, 10/09/06.

77. R. J. Collier and D. A. Kapplan, *Sci. Am.* 1994, **251**, 56-64.

78. P. Collard, in *The Development of Microbiology*, Cambridge University Press, Cambridge, 1976, ch. 5, pp. 52-58.

79. K. D. Bagshawe, *Br. J. Cancer*, 1989, **60**, 275-281.

80. S. K. Sharma, *Adv. Drug Delivery Rev.*, 1996, **22**, 369-376.

81. G. Winter and C. Milstein, *Nature*, 1991, **349**, 293-299.

82. I. Niculescu-Duvaz and C. J. Springer, *Adv. Drug Delivery Rev.*, 1997, **26**, 151-172.

83. L. M. Jungheim and T. A. Shepherd, *Chem. Rev.*, 1994, **94**, 1553-1566.

84. K. N. Syrigos and A. A. Epenetos, *Anticancer Res.*, 1999, **19**, 605-613.

85. L. A. Wolfe, R. J. Mullin, R. Laethem, T. A. Blumenkopf, M. Cory, J. F. Miller, B. R. Keith, J. Humphries and G. K. Smith, *Bioconjugate Chem.*, 1999, **10**, 38-48.

86. P. Wentworth, A. Datta, D. Blakey, T. Boyle, L. Partridge and G. M. Blackburn, *Proc. Natl. Acad. Sci. U.S.A.*, 1996, **93**, 799-803.

87. G. X. B. Ma, R. A. Batey, S. D. Taylor, G. Hum and J. B. Jones, *Synth. Commun.*, 1997, **27**, 2445-2453.

88. I. A. McNeish, P. F. Searle, L. S. Young, D. J. Kerr, *Adv. Drug Delivery Rev.*, 1997, **26**, 173-184.

89. T. A. Connors, *Gene Ther.*, 1995, **2**, 702-709.

90. S. M. Freeman, C. N. Abboud, K. A. Whartenby, C. H. Packman, D. S. Koeplin, F. L. Moolten and G. N. Abraham, *Cancer Res.*, 1993, **53**, 5274-5283.

91. www.teo.com.cn/eWebEdit/uploadfile/20061027191120803.pdf, 01/02/07.

92. www.dur.ac.uk/andrew.beeby/Equipment5.html, 01/02/07.

93. D. B. Papkovsky, A. N. Ovchinnikov, V. I. Ogurtsov, G. V. Ponomarev and T. Korpela, *Sens. Actuators, B*, 1998, **51**, 137-145.

94. P. Borrell, in *Photochemistry: A Primer*, ed. B. J. Stokes and A. J. Malpas, Edward Arnold Limited, London, 1973, ch. 4, pp. 27-31.

95. R. P. Wayne, in *Principles and Applications of Photochemistry*, Oxford Science Publications, Oxford University Press, Oxford, 1991, ch. 7. pp. 157-159 and 172-175.

96. www.astbury.leeds.ac.uk/facil/spectros/time.html, 01/02/07.

97. C. E. Wayne and R. P Wayne, in *Photochemistry*, Oxford Chemistry Primers, Oxford Science Publications, Oxford University Press, Oxford, 1996, vol. 39, ch. 1, pp. 11,16 and 17; and ch. 4., pp. 61-63.

98. www.physics.princeton.edu/~austin/hf_book/chapter20.pdf, 01/05/04.

99. R. Schmidt and H. D. Brauer, *J. Am. Chem. Soc.*, 1987, **109**, 6976-6981.

100. M. Kreitner, R. Ebermann and G. Alth, *J. Photochem. Photobiol. B: Biol.*, 1996, **36**, 109-111.

101. M. Niedre, M. S. Patterson and B. C. Wilson, *Photochem. Photobiol.*, 2002, **75**, 382-391.

102. D. V. O'Conner and D. Phillips, in *Time Correlated Single Photon Counting*, ed. H. Kume, Academic Press, 1984, ch. 6, pp. 158-209.

103. K. Eaton, B. Douglas and P. Douglas, *Sens. Actuators, B*, 2004, **97**, 2-12.

104. M. vande Ven, M. Ameloot, B. Valeur and N. Boens, *J. Fluorescence*, 2005, **15**, 377-413.

105. P. Rothemund, *J. Am. Chem. Soc.*, 1935, **57**, 2010-2011.

106. P. Rothemund and A. R. Mentotti, *J. Am. Chem. Soc.*, 1941, **63**, 267-270.

107. J. L. Sessler, A. Mozaffari and M. R. Johnson, *Org. Synth.*, 1992, **70**, 68-78.

108. C. Brückner, J. J. Posakony, C. K. Johnson, R. W. Boyle, B. R. James and D. Dolphin, *J. Porphyrins Phthalocyanines*, 1998, **2**, 455-465.

109. R. W. Boyle, C. Brückner, J. Posakony, B. R. James and D. Dolphin, *Org. Synth.*, 2004, Coll. Vol. **10**, 370; 1999, **76**, 287.

110. C. Brückner, V. Karunaratne, S. J. Rettig and D. Dolphin, *Can. J. Chem.*, 1996, **74**, 2182-2193.

111. J. E. Baldwin, M. J. Crossley, T. Klose, E. A. O'Rear III and M. K. Peters, *Tetrahedron*, 1982, **38**, 27-39.

112. G. P. Arsenault, E. Bullock and S. F. MacDonald, *J. Am. Chem. Soc.*, 1960, **82**, 4384-4395.

113. J. M. Sutton, O. J. Clarke, N. Fernandez and R. W. Boyle, *Bioconjugate Chem.*, 2002, **13**, 249-263

114. O. J. Clarke and R. W. Boyle, *Chem. Commun.*, 1999, 2231-2232.

115. R. F. Pasternack, P. R. Huber, P. Boyd, G. Engasser, L. Francesconi, E. Gibbs, P. Fasella, G. Cerio Venutro and L. deC. Hinds, *J. Am. Chem. Soc.*, 1972, **94**, 4511-4517.

116. K. Kano, K. Fukuda, H. Wakami, R. Nishiyabu and R. F. Pasternack, *J. Am. Chem. Soc.*, 2000, **122**, 7494-7502.

117. S. Orrenius, *Toxicol. Lett.*, 2004, **149**, 19-23.

118. I. I. Kruman and M. P. Mattson, *J. Neurochem.*, 1999, **72**, 529-540.

119. A. G. Renehan, C. Booth and C. S. Potten, *Brit. Med. J.*, 2001, **322**, 1536-1538.

120. J. S. Isenberg and J. E. Klaunig, *Toxicol. Sci.*, 2000, **53**, 340-351.

121. J. Krebs, *Biomet.*, 1998, **11**, 375-382.

122. www.celldeath.de/encyclo/aporev/apointro.pdf, 10/11/06.

123. S. H. Kaufmann, M. O. Hengartner, *Trends Cell Biol*, 2001, **11**, 526-534.

124. http://www.sghms.ac.uk/depts/immunology/~dash/apoptosis/, 25/09/06.

125. http://www.geocities.com/CollegePark/Lab/1580/apoptosis.html, 28/05/04.

126. http://users.rcn.com/jkimball.ma.ultranet/BiologyPages/A/Apoptosis.html, 22/09/06.

127. http://www.neuro.wustl.edu/neuromuscular/mother/apoptosis.htm, 25/05/04.

128. http://www.acs.ucalgary.ca/~browder/apoptosis.html, 25/05/04.

129. http://www.cellsalive.com/apop.htm, 01/05/06.

130. K. L. King, J. A. Cidlowski, *Annu. Rev. Physiol.*, 1998, **60**, 601-617.

131. T. H. Landowski, C. J. Megli, K. D. Nullmeyer, R. M. Lynch and R. T Dorr, *Cancer Res.*, 2005, **65**, 3828-3836.

132. K. F. Ferri and G. Kroemer, *Nat. Cell Biol.*, 2001, **3**, E225-E263.

133. C. Adrian, S. J. Martin, *Trends Biochem. Sci.*, 2001, **26**, 390-397.

134. E.G. Jeong, J. W. Lee, Y. H. Soung, S. W. Nam, S. H. Kim, N. J. Yoo and S. H. Lee, *Acta Pathologic, Microbiologica et Immunilogica Scandinavica*, 2006, **114**, 867.

135. www.onderzoekinformatie.nl/en/oi/nod/onderzoek/OND1289059/, 01/08/06.

136. J. M. Adams. S. Cory, *Trends Biochem. Sci.*, 2001, **26**, 61-66.

137. S. Desagher and J-C. Martinou, *Trends Cell Biol.*, 2000, **10**, 369-377.

138. J. F. Curtin, T. G. Cotter, *Cell. Signaling*, 2003, **15**, 983-992.

139. R. D. Almeida, B. J. Manadas, A. P. Carvalho and C. B. Duarte, *Biochim. Biophys. Acta*, 2004, **1704**, 59-86.

140. http://medweb.bham.ac.uk/research/calcium/Functions/ApopNec.html, 25/09/06.

141. http://www.ucihs.uci.edu/anaotomy/histo/Old_Files_2005/corenotes/celldeath2004.pdf#search, 20/06/05.

142. E. Sun and Y. Shi, in *Molecular Mechanisms of Programmed Cell Death*, ed. Y. Shi, J. A. Cidlowski, D. Scott, J-R. Wu and Y-B. Shi, Kluwer Academic/Plenum Publishers, New York, 2003, ch. 1, pp. 10 and 11.

143. L. D. Tomai and F. O. Cope, in *Apoptosis: The Molecular Biology of Programmed Cell Death*, ed. M. D. Jacobson and N. McCarthy, Oxford University Press, New York, 2002, ch. 1. pp. 2-3.

144. R. A. Lockshin and Z. Zakeri, in *When Cells Die II*, ed. R. A. Lockshin and Z. Zakeri, Wiley and Sons, New Jersey, 2004, ch. 1, pp. 10-11; and ch. 2, pp. 36-37.

145. D. Kessel, *Photochem. Photobiol. Sci.*, 2002, **1**, 837-840.

146. C. Fabris, G. Valduga, G. Miotto, L. Borsetto, G. Jori, S. Garbisa and E. Reddi, *Cancer Res.*, 2001, **61**, 7495-7500.

147. www.oscal.com/calcium.asp, 27/10/05.

148. www.faqs.org/nutrition/Calcium-De/Calcium.html, 08/08/06.

149. www.calciuminfo.com/osteoporosis/calciumdeficiency.aspx, 08/08/06.

150. W. Chang and D. Shoback, *Cell Calcium*, 2004, **35**, 183-196.

151. C. Montell, *Cell*, 2005, **122**, 157-163.

152. www.chemsoc.org/chembytes/ezine/2002/east_mar02.htm, 29/09/06.

153. http://users.rcn.com/jkimball.ma.ultranet/BiologyPages/S/second_messengers.htm l, 30/11/05.

154. M. R. Duchen, *J. of Physiol.*, 2000, **529**, 57-68.

155. S. Zhou, A. Starkov, M. Kent. Froberg, R. L. Leino and K. B. Wallace, *Cancer Res.*, 2001, **61**, 771-777.

156. W. Paschen, *Cell Calcium*, 2003, **34**, 305-310.

157. www.hhmi.org/research/investigators/clapham.html, 08/08/06.

158. www.chelationtherapyonline/articles/p185.htm, 20/10/06.

159. A. Takahashi, P. Camacho, J. D. Lechleiter and B. Herman, *Physiol. Rev.*, 1999, **79**, 1089-1125.

160. www.ebi.ac.uk/interpro/potm/2004_3/Page1.htm, 27/10/05.

161. www.chemistry.emory.edu/justice/seminar/second.htm, 05/10/06.

162. M. Brini, *Cell Calcium*, 2003, **34**, 399-405.

163. B. F. Trump, I. K. Berezesky, T. Sato, K. U. Laiho, P. C. Phelps and N. DeClaris, *Environ. Health Perspect.*, 1984, **57**, 281-287.

164. I. Splawski, K. W. Timothy, L. M. Sharpe, N. Decher, P. Kumar, R. Bloise, C. Napoliano, P. J. Schwartz, R. M. Joseph, K. Consouris, H. Tager-Flusberg, S.G. priori, M. C. Sangunietti and M. T. Keating, *Cell*, 2004, **119**, 19-31.

165. E. Ben-Hur and T. M. A. R. Dubbelman, *Photochem. Photobiol.*, 1993, **58**, 890-894.

166. J. L. Farber, *Chem. Res. Toxicol.*, 1990, **3**, 503-508.

167. I. Schnurra, H. G. Bernstein, P. Reiderer and K. H. Braunewell, *Neurobiol. Disease*, 2001, **8**, 900-909.

168. T. E. Gunter, D. I. Yule, K. K. Gunter, R. A. Eliseev and J. D. Salter, *FEBS Lett.*, 2004, **567**, 96-102.

169. A. R. Marks, *J. Clin. Invest.*, 2003, **111**, 597-600.

170. M. E. Johnson, G. J. Gores, C. B. Uhl and J. C. Still, *J. Neurosci.*, 1994, **14**, 4040-4049.

171. T. Kristian, B. K. Siesjö, *Stroke*, 1998, **29**, 705-718.

172. www.celldeath.de/encylo/misc/pt.htm, 29/10/06.

173. www.cvphysiology.com, 01/10/06.

174. D. Lindholm, H. Wootz and L. Korhonnen, *Cell Death Differ.*, 2006, **13**, 385-392.

175. M. P. Mattson, *Nature*, 2004, **430**, 630-639.

176. E. R. Kokoska, G. S. Smith, A. B. Wolff, Y. Deshpande, C. L. Rieckenberg, A. Banan and T. A. Miller, *Am. J. Physiol. – Gastr. Liver Physiol.*, 1998, **275**, 322-330.

177. S. P. Yu, L. M. T. Canzoniero and D. W. Choi, *Curr. Opin. Cell Biol.*, 2001, **13**, 405-411.

178. L. S. Jouvaville, F. Ichas and J-P. Mazat, *Mol. Cell. Biochem.*, 1998, **184**, 371-376.

179. L. Schild, G. Keilhoff, W. Augustin, G. Reiser and F. Striggow, *FASEB J.*, 2001, **15**, 565-567.

180. N. Brustovetsky, T. Brustovetsky, K. J. Purl, M. Capano, M. Crompton and J. M. Dubinsky, *J. Neurosci.*, 2003, **23**, 4858-4867.

181. P. Bernardi, *Physiol. Rev.*, 1999, **79**, 1127-1155.1

182. M. C. Beatrice, J. W. Palmer and D. R. Pfeiffer, *J. Biol. Chem.*, 1980, **255**, 8663-8671.

183. A. W. Harman and M. J. Maxwell, *Annu. Rev. Pharmacol. Toxicol.*, 1995, **35**, 129-144.

184. E. Fontaine, F. Ichas and P. Bernardi, *J. Biol. Chem.*, 1998, **273**, 25734-25740.

185. I. G. Stavrovskaya and B. S. Kristal, *Free Radical Biol. Med.*, 2005, **8**, 687-697.

186. A. K. Lee and A. Tse, *Endocrinology*, 2005, **146**, 4985-4993.

187. G. Szalai, R. Krishnamurthy and G. Hajnóczky, *Eur. Molec. Bio. J*, 1999, **18**, 6349-6361.

188. J. S. Armstrong, H. Yang, W. Duan and M. Whiteman, *J. Biol. Chem.*, 2004, **279**, 50420-50428.

189. M. G. Vander Heiden, N. S. Chandel, X. X. Li, P. T. Schumacker, M. Colombini and C. B. Thompson, *Proc. Natl. Acad. Sci. USA*, 2000, **97**, 4666-4671.

190. www.sciencedaily.com/releases/2006/09/060911105059.htm, 01/09/06.

191. M. Boyce and J. Yuan, *Cell Death Differ.*, 2006, **13**, 363-373.

192. S. V. Lennon, S. A. Kilfeather and T. G. Cotter, *Biochem. Soc. Trans*, 1991, **20**, 77S.

193. T. Flynn and C. Wei, *Nanomed.: Nanotechnol., Biol. Med.*, 2005, **1**, 47-51.

194. I. Roy, T. Y. Ohulchanskyy, D. J. Bharali, H. E. Pudavar, R. A. Mistretta, N. Kaur and P. N. Prasad, *Proc. Natl. Acad. Sci. U. S. A*, 2005, **102**, 279-284.

195. G-P. Wang, E-Q. Song, H-Y. Xie, Z-L. Zhang, Z-Q. Tian, C. Zuo, D-W. Pang, D-C. Wu and Y-B. Shi, *Chem. Commun.*, 2005, **34**, 4276-4278.

196. L. Levy, Y. Sahoo, K-S. Kim, E. J. Bergey and P. N. Prasad, *Chem. Mater.*, 2002, **14**, 3715-3721.

197. R. A. Freitas Jr., *Nanomed.: Nanotechnol., Biol. Med.*, 2005, **1**, 2-9.

198. http://archives.sensorsmag.com/articles/1103/22/, 10/10/06.

199. Y-M. Huh, Y-W. Jun, H-T. Song, S. Kim, J-S. Choi, J-H. Lee, S. Yoon, K-S. Kim, J-S. Shin, J-S. Suh and J. Cheon, *J. Am. Chem. Soc.*, 2005, **127**, 12387-12391.

200. B. A. Moffat, G. R. Reddy, P. McConville, D. E. Hall, T. L. Chenevert, R. R. Kopelman, M. Philbert, R. Weissleder, A. Rehemtulla and B. D. Ross, *Mol. Imaging*, 2003, **2**, 324-332.

201. J. W. Aylott, *Analyst*, 2003, **128**, 309-312.

202. P. Tartaj, M. del Puerto Morales, S. Veintemillas-Verdauger, T. González-Carreño and C. J. Serna, *J. Phys. D: Appl. Phys.*, 2003, **36**, R182-R197.

203. A. S. Zahr, M. de Villiers and M. V. Pishko, *Langmuir*, 2005, **21**, 403-410.

204. M. Arduini, S. Marcuz, M. Montolli, E. Rampazzo, F. Mancin, S. Gross, L. Armelao, P. Tecilla and U. Tonellato, *Langmuir*, 2005, **21**, 9314-9321.

205. B. M. Cullum and T. Vo-Dinh, *TIBTECH*, 2000, **18**, 388-393.

206. A. Burns, H. Ow and U. Weisner, *Chem. Soc. Rev.*, 2006, **35**, 1028-1042.

207. B. Pegaz, E. Debefve, F. Borle, J. P. Ballini, H. van den Burgh and Y. N. Kouakou-Konan, *J. Photochem. Photobiol., B: Biol.*, 2005, **80**, 19-27.

208. H. Zhu and M. J. McShane, *J. Am. Chem. Soc.*, 2005, **127**, 13448-13449.

209. I. Roy, T. Y. Ohulchanskyy, H. E. Pudavar, E. J. Bergey, A. R. Oseroff, J. Morgan, T. J. Dougherty and P. N. Prasad, *J. Am. Chem. Soc.*, 2003, **125**, 7860-7865.

210. D. J. Maxwell, J. R. Taylor and S. Nie, *J. Am. Chem. Soc.*, 2002, **124**, 9606-9612.

211. H. Zhang, Y. Sun, K. Ye, P. Zhang and Y. Wang, *J. Mater. Chem.*, 2005, **15**, 3181-3186.

212. C. O'Donovan, J. Hynes, D. Yashunski and D. Papkovsky, *J. Mater. Chem.*, 2005, **15**, 2946-2951.

213. D. J. Bharali, I. Klejbor, E. K. Stachowiak, P. Dutta, I. Roy, N. Kaur, E. J. Bergey, P. N. Prasad and M. K. Stachowiak, *Proc. Natl. Acad. Sci. U. S. A*, 2005, **102**, 11539-11544.

214. P. Couvreur, G. Barratt, E. Fattal, P. Legrand and C. Vauthier, *Crit. Rev. Ther. Drug.*, 2002, **19**, 99-134.

215. L. R. Hirsch, R. J. Stafford, J. A. Bankson, S. R. Sershen, B. Rivera, R. E. Price, J. D. Hazle, N. J. Halas and J. L. West, *Proc. Nat. Acad. Sci. U.S.A.*, 2003, **100**, 13549-13554

216. X. Zhao, L. R. Hilliard, S. J. Mechery, Y. Wang, R. P. Bagwe, S. Jin and W. Tan, *Proc. Natl. Acad. Sci. U. S. A*, 2004, **101**, 15027-15032.

217. Y. N. Konan, R. Cerny, J. Favet, M. Berton, R. Gurny and E. Allémann, *Eur. J. Pharm. Biopharm.*, 2003, **55**, 115-124.

218. Y. Bae, W-D. Jang, N. Nishiyama, S. Fukushima and K. Kataoka, *Mol. Biosyst.*, 2005, **1**, 242-250.

219. Y. Bae, N. Nishiyama, S. Fukushima, H. Koyama, M. Yasuhiro and K. Kataoka, *Bioconjugate Chem.*, 2005, **16**, 122-130.

220. H Gu, K. Xu, Z. Yang, C. K. Chang and B. Xu, *Chem. Commun.*, 2005, 4270-4272.

221. K. Kikuchi, K. Komatsu and T. Nagano, *Curr. Opin. Chem. Biol.*, 2004, **8**, 182-191.

222. A. G. Howard and N. H. Khdary, *Analyst*, 2005, **130**, 1432-1438.

223. T. Balaji, M. Sasidharan and H. Matsunaga, *Analyst*, 2005, **130**, 1162-1167.

224. D. B. Papkovsky and C. O'Riordan, *J. Fluorescence*, 2005, **15**, 569-584.

225. J. H. Shin and M. H. Schoenfisch, *Analyst*, 2006, **13**, 609-615.

226. C-Y. Li, X-B. Zhang, Z-X. Han, B. Åkermark, L. Sun, G-L. Shen and R-Q. Yu, *Analyst*, 2006, **131**, 388-393.

227. T. Nakanishi, S. Fukushima, K. Okamoto, M. Suzuki, Y. Matsumura, M. Yokoyama, T. Okano, Y. Sakurai and K. Kataoka, *J. Control. Release*, 2001, **74**, 295-302.

228. A. Vargas, B. Pegaz, E. Debefve, Y. K-Kouakou, N. Lange, J-P. Ballini, H. van den Bergh, R. Gurny and F. Delie, *Int. J. Pharm.*, 2004, **286**, 131-145.

229. J. C. Zguris, L. J. Itle, W-G. Koh and M. V. Pishko, *Langmuir*, 2005, **21**, 4168-4174.

230. A. J. Thote and R. B. Gupta, *Nanomed.: Nanotechnol., Biol. Med.*, 2005, **1**, 85-90.

231. M. Kullberg, K. Mann and J. L. Owens, *Med. Hypotheses*, 2005, **64**, 468-470.

232. G. A. Hughes, *Nanomed.*, 2005, **1**, 22-30.

233. http://news.bbc.co.uk/go/pr/fr/-/1/hi/health/4734507.stm, 20/11/06.

234. V. N. Paunov, G. MacKenzie and S. D. Stoyanov, *J. Mater. Chem.*, 2007, **17**, 609-612.

235. K. Almdal, H. Sun, A. K. Poulsen, L. Arleth, I. Jakobsen, H. Gu, A-M. Scharff-Poulsen, *Polym. Adv. Technol.*, 2006, **17**, 790-793.

236. O. Crespo-Biel, B. J. Ravoo, J. Huskens and D. N. Reinhoudt, *Dalton Trans.*, 2006, 2737-2741.

237. R. Duncan, *Nanotoday*, 2005, 16-17.

238. T. Vo-Dinh, *The 1st International Symposium on Micro and Nanotechnology*, Honolulu, Hawaii, U.S.A., 2004.

239. J. J. Gomm, P. J. Browne, R. C. Coope, Q-Y. Liu, L. Buluwela and R. Charles Coombes, *Anal. Biochem.*, 1995, **226**, 91-99.8

240. S-J. Cho, B. R. Jarrett, A. Y. Louie and S. M. Kauzlarich, *Nanotechnology*, 2006, **17**, 640-644.

241. L. E. Euliss, J. A. DuPont, S. Gratton and J. DeSimone, *Chem. Soc. Rev.*, 2006, **35**, 1095-1104.

242. R. K. O'Reilly, C. J. Hawker and K. L. Wooley, *Chem. Soc. Rev.*, 2006, **35**, 1068-1083.

243. T. Vo-Dinh, B. M. Cullum and D. L. Stokes, *Sens. Actuators, B*, 2001, **74**, 2-11.

244. W. Tan, Z-Y. Shi and R. Kopelman, *Sens. Actuators, B*, 1995, **28**, 157-163.

245. R. Voss, A. Thomas, M. Antonietti and G. A. Ozin, *J. Mater. Chem.*, 2005, **15**, 4010-4014.

246. J. C. Peck, C. Bezold, M. Kaushal and R. H. Smith, *Business Briefing: Pharmatech*, 2003.

247. O. Birkert, H-M. Haake, A. Schütz, J. Mack, A. Brecht, G. Jung and G. Gauglitz, *Anal. Biochem.*, 2000, **282**, 200-208.

248. E. K. F. Yim and K. W Leong, *Nanomed.*, 2005, **1**, 10-21.

249. S. W. Metzger, M. Natesan, C. Yanavich, J. Schneider and G. U. Lee, *J. Vac. Sci. Technol., A*, 1999, **17**, 2623-2628.

250. P. A. Dresco, V. S. Zaitsev, R. J. Gambino and B. Chu, *Langmuir*, 1999, **15**, 1945-1951.

251. J. Jang, J. H. Oh and X. L. Li, *J. Mater. Chem.*, 2004, **14**, 2872-2880.

252. G. Barratt, *Cell. Mol. Life Sci.*, 2003, **60**, 21-37.

253. C. Daubresse, C. Grandfils, R. Jérome and P. Teyssié, *J. Colloid Interface Sci.*, 1994, **168**, 222-229.

254. R. Gref, P. Couvreur, G. Barratt and E. Mysiakine, *Biomaterials*, 2003, **24**, 4529-4537.

255. G. J. Kim and S. Nie, *Nanotoday*, 2005, 28-33.

256. F. Candau and J. Selb, *Adv. Colloid Interface Sci.*, 1999, **79**, 149-172.

257. M. E. Wieder, D. C. Hone, M. J. Cook, M. M. Handsley, J. Gavrilovic and D. A. Russell, *Photochem. Photobiol. Sci.*, 2006, **5**, 727-734.

258. http://www.newscientisttech.com/article.ns?id=dn8938&print=true, 17/07/07.

259. http://news.bbc.co.uk/1/hi/technology/4872188.stm, 17/07/07.

260. http://engineering.princeton.edu/news/prudhomme, 10/04/07.

261. E. Kawasaki and A. Player, *Nanomed.: Nanotechnol., Biol. Med.*, 2005, **1**, 101-109.

262. L. Josephson, C-H Tung, A. Moore and R. Weissleder, *Bioconjugate Chem.* 1999, **10**, 186-191.

263. H-R. Choi Kim, Y. Luo, G. Li and D. Kessel, *Cancer Res.*, 1999, **59**, 3429-3432.

264. www.resins.com/resins/eu/pdf/vv-2-0.pdf, 22/12/06.

265. J. Fossey, D. Leforts and J. Sorba, in *Free Radicals in Organic Chemistry*, Wiley, England, 2nd edn., 1995, ch. 5, pp. 40-43; ch. 7, pp. 73-77; and ch. 9, pp. 109-110.

266. P. B. O'Donnell and J. W. McGinity, *Adv. Drug Del. Rev.*, 1997, **28**, 25-42.

267. www.microteklabs.com/technical_overview.pdf, 01/01/07.

268. www.chm.bris.ac.uk/pt/eastoe/surf_chem/1%20Surfactant%20chemistry%20and%20general%20phase%20behaviour.pdf, 09/10/06.

269. T. P. Hoar and J. H. Schulman, *Nature*, 1943, **152**, 102-103.

270. D. O. Shah, in *Macro- and Microemulsions Theory and Applications*, ed. D. O. Shah, American Chemical Society, Washington D.C., ACS Symposium Series 272, 1985, ch. 1, pp. 10-11; ch. 6, pp. 75-77; ch. 8, pp. 105-108; and ch. 9, pp. 119-124.

271. www.pnl.gov/supercriticalfluid/tech_mic.stm, 24/02/06.

272. F. Candau, M. Pabon and J-Y. Anquetil, *Colloids Surf. A*, 1999, **153**, 47-59.

273. F. Candau, *Macromol. Symp.*, 1995, **92**, 169-178.

274. www.fisica.unam.mx/liquids/tutorials/microemulsions.htm, 24/02/06.

275. J. Tabony, *Nature (Letts. Nature)*, 1986, **319**, 400.

276. I. Capek, *Adv. Colloid Interface Sci.*, 2004, **110**, 49-74.

277. A. K. Poulsen, L. Arleth, K. Almdal and A. M. Scharff-Poulsen, *J. Colloid Interface Sci.*, 2007, **306**, 143-153.

278. C. Kumar and D. Balasubramanian, *J. Phys. Chem.*, 1980, **84**, 1895-1899.

279. B. K. Paul and S. P. Moulik, *Curr. Sci.*, 2001, **80**, 990-1001.

280. http://channels.crienglish.com/wp/?p=108, 22/01/07.

281. www.psrc.usm.edu/macrog/emulsion.htm, 20/01/05.

282. www.sigmaaldrich.com/Brand/Fluka_Riedel_Home/Bioscience/BioChemik, 24/02/06.

283. www.chemistry.co.nz/surfactants.htm, 24/02/06.

284. J. Jang, X. Li-Li and J. Hak-Oh, *Chem. Commun.*, 2004, 794-795.

285. B. Ekman, C. Lofter and I. Sjöholm, *Biochem.*, 1976, **15**, 5115-5120.

286. http://web.umr.edu/~wlf/CHEM381/Chap12.html, 10/02/04.

287. http://plc.cwru.edu/tutorial/enhanced/files/polymers/synth/synth.htm, 16/12/06.

288. M. Pabon, J. Selb, F. Candau and R. G. Gilbert, *Polymer*, 1999, **40**, 3101-3106.

289. www.stanford.edu/class/cheme160/lectures/lecture6.pdf, 20/10/06.

290. N. A. Peppas, *Adv. Drug Delivery Rev.*, 2004, **56**, 1529-1531.

291. J. Barton, *Prog. Polymer Sci.*, 1996, **21**, 399-438.

292. J. P. Wilcoxon and B. L. Abrams, *Chem. Soc. Rev.*, 2006, **35**, 1162-194.

293. D. J. Cebula, R. H. Ottewill, J. Ralston and P. N. Pusey, *J. Chem. Soc., Faraday Trans. I*, 1981, **77**, 2585-2612.

294. C-S. Chern and C-H. Lin, *Polymer*, 2000, **41**, 4473-4481.

295. B. Liao, Y. Huang, G. Cong and S. Zhao, *J. App. Polym. Sci.*, 1998, **70**, 2075-2079.

296. S. Slomkowski, *Prog. Polym. Sci.*, 1998, **23**, 815-874.

297. F. J. Arriagada and K. Osseo-Asare, *J. Colloid Interface Sci.*, 1999, **211**, 210-220.

298. K. Ishizu and N. Tahara, *Polymer*, 1996, **37**, 1729-1734.

299. www.unl.edu/CMRAcfem/em.htm, 18/01/07.

300. www.sintef.no, 18/01/07.

301. M. Kruk, M. Jaroniec and K. P. Gadkaree, *J. Colloids Interface Sci.*, 1997, **192**, 250-256.

302. www.jhu.edu/~chem/fairbr/derive.html, 18/01/07.

303. S. Brunauer, P. H. Emmett and E. Teller, *J. Am. Chem. Soc.*, 1938, **60**, 309-319.

304. N. W-S-Kam, M. O'Connell, J. A. Wisdom and H. Dai, *Proc. Natl. Acad. Sci. U. S. A*, 2005, **102**, 11600-11605.

305. L. Rabinovich-Guilatt, P. Couvreur, G. Lambert and C. Dubernet, *J. Drug Target.*, 2004, **12**, 623-633.

306. H. A. Clark, R. Kopelman, R. Tjalkens and M. A. Philbert, *Anal. Chem.*, 1999, **71**, 4837-4843.

307. E. J. Park, M. Brasuel, C. Behrend, M. A. Philbert and R. Kopelman, *Anal. Chem.*, 2003, **75**, 3784-3791.

308. H. Xu, J. W. Aylott and R. Kopelman, *Analyst*, 2002, **127**, 1471-1477.

309. S. M. Buck, H. Xu, M. Brasuel, M. A. Philbert and R. Kopelman, *Talanta*, 2004, **63**, 41-59.

310. S. M. Buck, Y-E. Lee Koo, E. Park, H. Xu, M. A. Philbert, M. A. Brasuel and R. Kopelman, *Curr. Opin. Chem. Biol.*, 2004, **8**, 540-546.

311. I. F. Smith, J. P. Boyle, L. D. Plant, H. A. Pearson and C. Peers, *J. Biol. Chem.*, 2003, **278**, 4875-4881.

312. J. P. Sumner, N. M. Westerberg, A. K. Stoddard, C. A. Fierke and R. Kopelman, *Sens. Actuators, B*, 2006, **113**, 760-767.

313. D. H. P. Hedges, D. J. Richardson and D. A. Russell, *Langmuir*, 2004, **20**, 1901-1908.

314. T. Fusai, R. Durand, Y. Boulard, M. Paul, C. Bories, D. Rivollet, R. Houin and M. Deniau, *Med. Trop. (Mars)*, 1995, **55**, 73-78.

315. K. G. Nelson, J. V. Bishop, R. O. Ryan and R. Titus, *Antimicrob. Agents Chemother.*, 2006, **50**, 1238-1244.

316. J. Wang and M. J. Lenardo, *J. Cell Sci.*, 2000, **113**, 753-757.

317. M. Brasuel, R. Kopelman, M. A. Philbert, J. W. Aylott, H. Clark, I. Kasman, M. King, E. Monson, J. Sumner, H. Xu, M. Hoyer, T. J. Miller and R. Tjalkens, in *Optical Biosensors: Present and Future*, ed. F. S. Ligler and C. A. Rowe, Elsevier Science, BV, 2002, ch. 16, pp. 497-533.

318. G. T. Hermanson, in *Bioconjugate Techniques*, Academic Press, London, 1996, ch. 2, pp. 137-166.

319. G. Woltmann, R. J. Ward, F. A. Symon, D. A. Rew, I. D. Pavord and A. J. Wardlaw, *Thorax*, 1999, **54**, 224-130.

320. R. F. Pasternack, L. Francesconi, D. Raff and E. Spiro, *Inorg. Chem.*, 1973, **12**, 2606-11.

321. L. Ding, G. Eternad-Moghadar, S. Cros, C. Auclair and B. Meunier, *J. Med. Chem.*, 1991, **34**, 900-906.

322. G. G. Meng, B. R. James and K. A. Skov, *Can. J. Chem.*, 1994, **72**, 1894-1909.

323. I. Batinic-Haberle, R. D. Stevens and I. Fridovich, *J. Porphyrins Phthalocyanines.*, 2000, **4**, 217-227.

324. www.biocompare.com/technicalarticle/1089/Acrylamide-Polymerization, 04/12/06.

325. www.polysciences.com/shop/assests/datasheets/522.pdf, 08/07/04.

326. S. Udenfriend, S. Stein, P. Böhlen, W. Dairman, W. Leimgruber and M. Weigele, *Science*, 1972, **178**, 871-872.

327. M. Weigele, J. F. Blount, J. P. Tengi, R. C, Czajkowski and W. Leimgruber, *J. Am. Chem. Soc.*, 1972, **94**, 4052-4054.

328. E. E. Snyder, B. W. Buoscio and J. J. Falke, *Biochemistry*, 1990, **29**, 3937-3943.

329. D. Cheng and Q-H. Xu, *Chem. Commun.*, 2007, 248-250.

330. www.sigmaaldrich.com/sigma/bulletin/fitc1bul.pdf, 10/11/06.

331. http://probes.invitrogen.com/media/pis/mp00143.pdf, 12/12/06.

332. Personal Communication with Dr K. Smith, Medical Research Laboratory, Department of Biology, University of Hull, U.K., 2003.

333. K. P. McNamara and Z. Rosenzweig, *Anal. Chem.*, 1998, **70**, 4853-4859.

334. M. Schäferling, M. Wu and O. S. Wolfbeis, *J. Fluorescence,* 2004, **14**, 561-568.

335. L. Rossi, A. Quach and Z. Rosenzweig, *Anal. Bioanal. Chem.*, 2004, **380**, 606-613.

336. F. Helmchen, K. Svoboda, W. Denk and D. W. Tank, *Nat. Neurosci.*, 1999, **2**, 989-996.

337. D. Thomas, S. C. Tovey, T. J. Collins, M. D. Bootman, M. J. Berridge and P. Lipp, *Cell Calcium*, 2000, **28**, 213-223.

338. www.dukescientific.com, 15/05/00.

339. www.lab.hii.horiba.com/products/particle_characterization/lb550.html, 12/12/06.

340. L. Schoutteten, P. Denjean, J. Faure and R. B. Pansu, *Phys. Chem. Chem. Phys.*, 1999, **1**, 2463-2469.

341. Personal Communication with Dr. A. Beeby, Department of Chemistry, University of Durham, U.K., 2006 and 2007.

342. http://catalog.invitrogen.com/index.cfm?fuseaction=viewCatalog.viewCategories &pc=2791&npc=388&nc=413&, 01/03/07.